**DANIEL CARREIRA BATALHA**

# CESIUM HETEROPOLYACID SALTS, NIOBIUM, AND DYSPROSIUM COMPOUNDS AS SOLID CATALYSTS IN OXIDATION REACTIONS OF TERPENIC ALCOHOLS WITH HYDROGEN PEROXIDE AND FURFURAL ACETALIZATION

Thesis submitted to the Multicenter Chemistry Post-Graduate Program of Minas Gerais State of the Universidade Federal de Viçosa in part of fulfillment of the requirements for the degree of *Doctor Scientiae*.

Adviser: Márcio José da Silva

**VIÇOSA - MINAS GERAIS**
**2021**

**Ficha catalográfica elaborada pela Biblioteca Central da Universidade Federal de Viçosa - Campus Viçosa**

T

B328c
2021

Batalha, Daniel Carreira, 1990-

Cesium heteropolyacid salts, Niobium, and Dysprosium compounds as solid catalysts in oxidation reactions of terpenic alcohols with Hydrogen peroxide and furfural acetalization / Daniel Carreira Batalha. – Viçosa, MG, 2021.

1 tese eletrônica (160 f.): il. (algumas color.).

Orientador: Márcio José da Silva.

Tese (doutorado) - Universidade Federal de Viçosa, Departamento de Química, 2021.

Inclui bibliografia.

DOI: https://doi.org/10.47328/ufvbbt.2021.224

Modo de acesso: World Wide Web.

1. Catálise heterogênea. 2. Catálise. 3. Catalisadores. 4. Nióbio - Oxidação. 5. Césio. 6. Peróxido de hidrogênio. I. Silva, Márcio José da, 1965-. II. Universidade Federal de Viçosa. Departamento de Química. Programa de Pós-Graduação em Química. III. Título.

CDD 22. ed. 541.395

Bibliotecário(a) responsável: Renata de Fátima Alves CRB6/2578

**DANIEL CARREIRA BATALHA**

# CESIUM HETEROPOLYACID SALTS, NIOBIUM, AND DYSPROSIUM COMPOUNDS AS SOLID CATALYSTS IN OXIDATION REACTIONS OF TERPENIC ALCOHOLS WITH HYDROGEN PEROXIDE AND FURFURAL ACETALIZATION

Thesis submitted to the Multicenter Chemistry Post-Graduate Program of Minas Gerais State of the Universidade Federal de Viçosa in part of fulfillment of the requirements for the degree of *Doctor Scientiae*.

APPROVED: October 27, 2021.

Assent:

Daniel Carreira Batalha
Author

Márcio José da Silva
Adviser

## ACKNOWLEDGMENT

Firstly, I thank God, because without Him I would not have come this far. For having given me strength, intelligence, wisdom, discipline and discernment to get where I could.

To my parents who always educated me and made efforts so that I had the best possible teaching opportunities.

To my sister who always supported me and valued all my achievements.

To my beautiful wife, for her encouragement, which helped me to grow even more and to overcome all the difficulties along the way.

To my grandmother who was always present in my life, worrying about my commitments and always willing to help in whatever she needed.

To my great friends who were always present in my academic life. People I could always trust.

To my friends and research colleagues, especially Carlos “materias”, Alana “miguxa”, César, Diêgo and Castelo, who contributed directly with my research and they also became great friendships outside the lab.

To my advisor Márcio who always helped me not only to complete this project, but also for all the teachings shared, for the incentives of always looking for the best, making me grow in my academic life.

To Professors Dr. Neftalí, from the Federal University of Pelotas, Dr. Humberto, from the Federal University of Ouro Preto, Dr. Mário, from Federal University of Catalão, and Dr. Luiz, from Federal University of Minas Gerais, for kindly providing materials for analysis and catalytic testing in addition to their time for important discussions.

To all those professors from the Department of Chemistry at the Federal University of Viçosa who contributed to make this work possible.

To the FAPEMIG, CNPq and CAPES for the financial support.

## ABSTRACT

BATALHA, Daniel Carreira, D.Sc., Universidade Federal de Viçosa, October, 2021. **Cesium heteropolyacid salts, Niobium, and Dysprosium compounds as solid catalysts in oxidation reactions of terpenic alcohols with Hydrogen peroxide and furfural acetalization.** Adviser: Márcio José da Silva.

Catalysis is an area of science whose advances brings important throughput in industrial processes, because simplify conditions of operation, reduces energy consumption, improves the yield of target products, and minimize environmental impact. Particularly, when renewable raw materials are involved, a catalyst can play a key role. On this sense, the development of catalysts for converting renewable origin substrates to fine chemical using environmentally benign oxidants such as $H_2O_2$ has attracted interest due to environmental and economic reasons. Also, solid heterogeneous catalysts are easily recoverable and reusable at the end of the processes, reducing their cost and environmental impacts. In this work, four classes of solid catalysts were synthesized and evaluated: Cesium heteropolyacid salts (HPAs) with lacunar anions, Niobium oxides, Dysprosium-doped Zinc tungstate, and Niobium compounds treated and non-treated with Hydrogen peroxide. Synthesis methodologies for the four types of catalysts were established: precipitation processes to synthesize the HPA salts, microwave-assisted hydrothermal method to obtain the Niobium oxides that were used in the oxidation processes, coprecipitation method followed by microwave hydrothermal heating to produce the Zinc tungstate and finally, a treatment with Hydrogen peroxide of the commercial samples of Niobium compounds. These catalysts were evaluated in oxidation reactions of terpene alcohols with $H_2O_2$, a non-polluting oxidant that have only water as byproduct. Besides that, the commercial Nb catalysts were also evaluated in the furfural acetalization reactions. The catalysts were characterized by porosimetry analysis, determination of the strength and quantity of acid sites, infrared and Raman spectroscopies, powder X-rays diffraction, X-ray fluorescence analysis, thermogravimetry analysis, and electronic scanning and transmission microscopies. The effects of the main reaction parameters were assessed such as temperature, type of substrate, amount of oxidant, catalyst load, and reaction time. A review was published highlighting the properties and applicability of Niobium solids in esterification and transesterification reactions and another one is in preparation standing out the use of Niobium catalysts in different reactions.

**Keywords:** Heterogeneous catalysts. Nerol oxidation. Cesium salts. Niobium catalysts. Hydrogen peroxide. Furfural acetalization.

## RESUMO

BATALHA, Daniel Carreira, D.Sc., Universidade Federal de Viçosa, outubro de 2021. **Sais heteropoliácidos de Césio, e compostos de Nióbio e Disprósio como catalisadores sólidos em reações de oxidação de álcoois terpênicos com peróxido de hidrogênio e acetalização do furfural.** Orientador: Márcio José da Silva.

Catálise é uma área da ciência cujos avanços trazem importantes rendimentos nos processos industriais, pois simplificam as condições de operação, reduzem o consumo de energia, melhoram o rendimento dos produtos alvo e minimizam o impacto ambiental. Particularmente, quando as matérias-primas renováveis estão envolvidas, um catalisador pode desempenhar um papel fundamental. Neste sentido, o desenvolvimento de catalisadores para conversão de substratos de origem renovável em química fina utilizando oxidantes ambientalmente benignos como o $H_2O_2$ tem despertado interesse devido à razões ambientais e econômicas. Também, catalisadores sólidos heterogêneos são facilmente recuperáveis e reutilizáveis no final dos processos, reduzindo seu custo e impactos ambientais. Neste trabalho, quatro classes de catalisadores sólidos foram sintetizados e avaliados: sais heteropoliácido de Césio (HPAs) com ânions lacunares, óxidos de Nióbio, tungstato de Zinco dopado com Disprósio e compostos de Nióbio tratados e não tratados com peróxido de hidrogênio. Metodologias de síntese para os quatro tipos de catalisadores foram estabelecidas: processos de precipitação para sintetizar sais de HPAs, método hidrotérmico assistido por micro-ondas para obter óxidos de Nióbio que foram aplicados nos processos de oxidação, método de coprecipitação seguido de método hidrotérmico de micro-ondas para produzir o tungstato de Zinco e finalmente, um tratamento com peróxido de Hidrogênio das amostras comerciais dos compostos de Nióbio. Estes catalisadores foram avaliados em reações de oxidação de álcoois terpênicos com $H_2O_2$, um oxidante não poluente tendo água como subproduto. Além disso, os catalisadores Nb comerciais também foram avaliados nas reações de acetalização do furfural. Os catalisadores foram caracterizados por análise de porosimetria, determinação da força e quantidade de sítios ácidos, espectroscopias de infravermelho e Raman, difração de raios-X de pós, análise de fluorescência de raios-X, análise termogravimétrica e microscopias eletrônica de varredura e transmissão. Os efeitos dos principais parâmetros de reação foram avaliados como temperatura, tipo de substrato, quantidade de oxidante, carga de catalisador e tempo de reação. Foi publicada uma revisão destacando as propriedades e aplicabilidades dos sólidos de Nióbio em reações de

esterificação e transesterificação e outra revisão está em elaboração destacando o uso de catalisadores de Nióbio em reações diferentes.

**Palavras-chave:** Catalisadores heterogêneos. Oxidação do nerol. Sais de Césio. Catalisadores de Nióbio. Peróxido de Hidrogênio. Acetalização do furfural.

## LIST OF FIGURES

### MAIN TEXT



### PAPER 1

**PAPER 2**

**PAPER 3**

**PAPER 4**

## LIST OF TABLES

### MAIN TEXT



### PAPER 1



### PAPER 2



### PAPER 3



### PAPER 4

## LIST OF SCHEMES

### MAIN TEXT



### PAPER 1



### PAPER 2



### PAPER 3

**SUMMARY**

# 1. GENERAL INTRODUCTION

The processes for obtaining compounds with high added value from abundant and low-cost raw materials preferably require catalytic reaction conditions which are favorable to make the process economically viable. The oxidation of terpenic alcohols is of interest to the perfume and fragrance industries because it can generate compounds that are ingredients to synthesize various high added value products, which may have attractive organoleptic properties. Furthermore, drug intermediates can also be obtained from such compounds. In this sense, terpenic alcohols such as nerol and geraniol stand out for being abundant, renewable, and attractive origin feedstocks to synthesize fine chemicals (DA SILVA et al., 2018; MONTEIRO; VELOSO, 2004).

In the same way, furfural is also originated from renewable sources, being a platform-molecule that can be used as building blocks for the production of many chemicals and biofuel components, as well as to be used in different types of industries to produce medicines, polymers and flavors (LANGE et al., 2012; RASPOLLI GALLETTI et al., 2020).

The oxidation of terpenic alcohols can be carried out in either homogeneous or heterogeneous media. However, the success of the process will depend on the oxidizing agent, the design of the catalyst, the operating conditions such as temperature and pressure used. Different types of catalysts have been used, including transition metal complexes, polyoxometalates, oxides, molecular sieves, and zeolites (ALIZADEH; TAYEBEE, 2005; TUMMA; NAGARAJU; REDDY, 2009). Generally, it is desirable that the reactions take place under mild conditions, under atmospheric pressure, and temperatures below 373 K to avoid polymerization processes.

Oxidation reactions have been carried out with several oxidants, such as peracetic acid, *tert*-butyl hydroperoxide, molecular Oxygen and Hydrogen peroxide. In particular, Hydrogen peroxide is noteworthy for being low cost, atom-efficient, liquid, safe to handle and environmentally friendly, as it only generates water as a by-product (ALIZADEH; TAYEBEE, 2005; TUMMA; NAGARAJU; REDDY, 2009). In addition, when used with heterogeneous catalysts, it can bind to the catalyst surface, resulting in the cleavage of the O–O bonds and giving different species of active Oxygen (ZIOLEK et al., 2015). These species can be generated through the interaction with Hydrogen peroxide as illustrated in the Scheme 1.

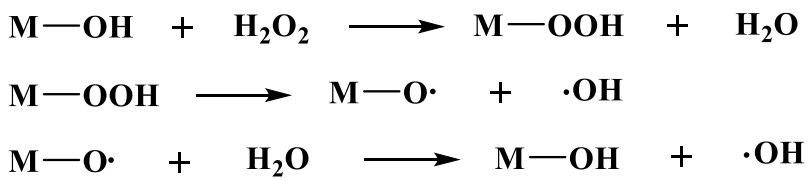


**Scheme 1.** Possible reactive species that can be generated through the interaction between metallic catalyst and Hydrogen peroxide

Keggin HPAs are highly active catalysts in oxyfunctionalization reactions, due to their redox and acidity properties. However, they are solids with low surface area and are soluble in polar organic solvents, a property that hamper their recovery and subsequent reuse in heterogeneous systems (DA SILVA; LIBERTO, 2016). A common strategy has been reported to support Keggin HPAs in solids with high surface area and porosity (DA SILVA; LIBERTO, 2016). However, in addition to the laborious synthesis, such catalysts can be leached due to the high polarity of the reaction medium. Alternatively, soluble HPAs can be converted to solid salts by replacing their protons with large monovalent cations such as $Cs^+$, $NH_4^+$, $Rb^+$, which have a radius greater than 1.30 Å. Such modifications can reduce the HPA solubility in organic solvents, allowing their use as a heterogeneous catalyst, in addition to improving surface properties such as surface area, and pore size (SANTOS et al., 2011).

In addition to the protons exchanges, a change that can improve the catalytic activity of Keggin HPAs in oxidation reactions is the removal of an MO unit (i.e., MoO, WO) from its heteropolyanion, generating lacunar catalysts which can be highly active in oxidation reactions with $H_2O_2$ (DA SILVA et al., 2018).

Niobium compounds are well known catalysts widely explored in many types of reactions such as esterification and transesterification processes (ie., acid-catalyzed reactions), epoxidation of cyclohexene, oxidation of organic compounds and hydrogenation of $CO_2$ (BATALHA; DA SILVA, 2021; CHAGAS et al., 2013; DA SILVA; MOTA, 2019). Due to their acidic properties and high thermal stability, they are promising materials to be used in acetalization of furfural. Moreover, they have Lewis and Brønsted acid sites, which are active sites responsible for the generation of the alkyl furfuryl acetal (CARNITI et al., 2016).

Terpenic alcohols and furfural are substrates frequently used for the generation of products which have high commercial value, besides numerous applications in different industries. In this work, our main intension was to obtain solid catalysts that could be used to converting terpenic alcohol to oxidation products, in more efficient and environmentally benign processes, as well as develop potential materials to be more explored in the furfural acetalization under mild conditions. Therefore, initially, Cesium-substituted Keggin lacunar

salts were synthesized, characterized, and evaluated in terpenic alcohol oxidation reactions with Hydrogen peroxide as an oxidant. Cesium HPA salts were easily synthesized from the precursor salts (i.e., $Na_2SiO_3$, $Na_2WO_4.2H_2O$, $Na_2HPO_4.7H_2O$ and $Na_2MoO_4$).

In a second step, Niobium oxide catalysts were evaluated, which were provided by Prof. Dr. Neftalí Lenin Villarreal Carreño. These catalysts were synthesized at the Federal University of Pelotas from the precursor ammoniacal Niobium oxalate; afterward, they were evaluated in oxidation reactions of terpenic alcohols with Hydrogen peroxide.

For the same oxidation reactions, Dysprosium-doped Zinc tungstate nanospheres were synthesized by the research group of Prof. Dr. Mário Júnior Godinho at Federal University of Catalão. These catalysts were obtained through the coprecipitation step followed by microwave hydrothermal method, originating different catalysts with distinct Dy loads.

Finally, oxides and phosphates Niobium were synthesized and characterized by the research group of the Prof. Dr. Luiz Carlos A. Oliveira at the Federal University of Minas Gerais. These solids were tested as catalysts in the acetalization of furfural.

All the catalysts were characterized by infrared spectroscopy (IR-FT), X-ray diffraction (DRX), physical adsorption/desorption of $N_2$, thermogravimetry (TG-DSC), spectroscopic analysis of X-ray fluorescence energy, Raman spectroscopy, scanning electron microscopy (SEM), and transmission electron microscopy (TEM). Acidity properties (i.e., strength and number of total acid sites) were determined by potentiometric titration with n-butylamine, ammonia temperature-programed desorption ($NH_3$-TPD), and pyridine chemisorption to identify the nature of the acid sites.

In alcohol oxidation reactions, Nerol was the model molecule used to study the effects of the main reaction variables (i.e., catalyst load, temperature, and reaction time). The oxidation of other terpenic alcohols was also evaluated, such as geraniol, linalool, β-citronellol and α-terpineol.

Two review articles were elaborated, to carefully describe the impacts of the structural, morphological, and acidic properties of the Nb-containing catalysts, as well as their application in a plethora of reactions, contributing to the describe the state-of-art of Niobium catalyzed reactions.

## 2. LITERATURE REVIEW

### 2.1. Catalysis: a brief introduction

Catalysis is so important that today it becomes an indispensable issue to improving the quality of human life. It is estimated that at least 85% of all chemical processes are carried out by means of catalysts, and about 80% of these processes are performed over heterogeneous catalysts (DE JONG, 2009). Heterogenous catalysts are predominant in industrial processes because they are easier to manipulate and recovery than homogenous counterparts, contributing to reduce the cost and environmental impact of the processes.

Actually, catalysts are increasingly used in reactions of industrial interest due to environmental and economic aspects (SCHMAL, 2016). Catalysts make faster the reactions, allowing that the process becomes economically viable when they are carried out at mild conditions; it is possible because catalysts act lowering the activation energy, and increasing the selectivity of the target products.

The main properties of a catalyst (i.e., activity, selectivity, stability) are closely linked to its physicochemical composition and the preparation technology. In recent decades, the theoretical bases for preparing heterogeneous catalysts have been widely studied. The number of publications involving different methodologies for obtaining catalysts, ranging from the simplest to the most elaborate, is so high that nowadays it can be considered a science (LI; WANG; GONG, 2009; LIOTTA, 2010; SCIRÈ; LIOTTA, 2012).

The morphology of the particles is an important parameter to explain the catalytic properties presented by a material, and it can be controlled during the synthesis process. Some of the important parameters that must be observed when choosing the synthesis method are those that lead to a better control of surface area, porosity, size, shape, and spatial orientation of the particles.

## 2.2. Keggin Heteropolyacids (HPAs)

Keggin HPAs belong to the class of polyoxometalates (POMs), metal-Oxygen clusters, which have gained increasing emphasis not only in the field of inorganic chemistry but also in medicine, materials science, electrochemistry and catalysis (PATEL et al., 2016).

Keggin HPAs have a strong Brønsted acid character, which makes them interesting catalysts for various reactions (ZHOU et al., 2014), and they are widely used in many acid-catalyzed reactions (DA SILVA; TEIXEIRA, 2017; ZHENG et al., 2016). These solid POMs have great variety in their composition, structure, and electronic properties, which make them versatile catalysts in different reactions (GAURAV; NG; REMPEL, 2016).

There are HPAs with anions of different structures, but the most studied is that with Keggin type anion, which has the general formula $[X^{n+}M_{12}O_{40}]^{(8-n)-}$, where M are transition metals (W, Mo, V, Nb, etc.). and X represents a p-block heteroatom. This central unit is composed of an $XO_4$ tetrahedron bonded at the edges by twelve $MO_6$ octahedra arranged in $M_3O_{13}$ groups (DA SILVA; DE OLIVEIRA, 2018). Figure 1 below illustrates a Keggin anion.

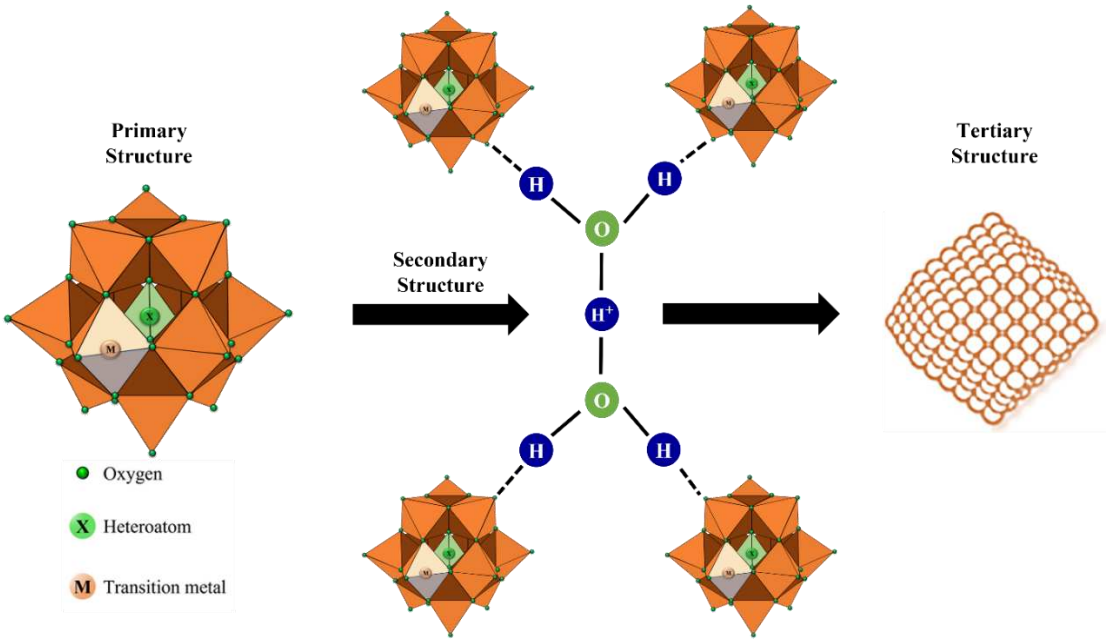


**Figure 1.** Primary, secondary and tertiary structure representations of the Keggin anion

HPAs have three distinct crystal structures: the primary structure, the heteropolyanion; the secondary, resulting from the union of primary structures interconnected by Hydrogen bonds to dihydronium cations ($H_5O_2^+$); and the tertiary structure, which is the final crystal structure of the HPAs, formed by the arrangement of secondary ones. The fundamental textural properties, such as surface area, porosity and crystallite size, are consequence of different arrangement and composition of these heteropolyanions (DA SILVA; DE OLIVEIRA, 2018).

In addition to being active in acid-catalyzed reactions, Keggin HPAs are effective catalysts in oxidation processes of different substrates such alcohols, olefins, and aldehydes (CAVANI, 1998). However, they have a low surface area and are soluble in organic solvents, which makes their recovery and reuse difficult, hampering their use as heterogeneous catalysts when “in nature”.

To try to circumvent their low surface area and solubility in polar solvents, HPAs have been immobilized in matrices such as silica, activated Carbon, zeolites, alumina and zirconia (ESTRADA et al., 2011a; KOZHEVNIKOV, 2007). However, the great challenge becomes to avoid problems such as leaching due to the high polarity of the reaction medium, and thus,

preserve its intrinsic activity (DA SILVA; LIBERTO, 2016; SHRINGARPURE; PATEL, 2011).

### 2.3. Keggin Heteropolyacid salts: saturated vs lacunars

There are two alternative approaches to get around the low surface area problems of Keggin's HPAs and convert them into insoluble salts: the first, the removal of Hydrogen atoms, keeping the Keggin anion intact (saturated salts); and the second one, beside the protons exchange, the removal of one or more MO units of the anion generating vacancies (lacunary salts), made by the appropriate adjustment of the pH.

Exchanging the protons of the HPAs by cations with larger radii, they become insoluble (DA SILVA; DE OLIVEIRA, 2018). This transformation results in efficient catalysts, such as the Cesium silicotungstate salt. The addition of Cesium as a countercation in HPAs improves thermal stability and increases both surface area and porosity (INUMARU et al., 1996; OKUHARA; NISHIMURA; MISONO, 1995).

According to the literature, phosphotungstic acid is the most acidic Keggin HPA, and the partial exchange of their protons by Cesium cations results in very active solid catalysts. When this transformation is carried out, mesoporous are generated which enables the increase of the surface area and consequently, the availability of the surface acid sites (IWASE et al., 2014; KAMIYA et al., 2010; KOZHEVNIKOV, 1998; PARK et al., 2010).

On the other hand, there is an aspect still little explored in the literature, the vacancy created in the coordination sphere of the Tungsten or Molybdenum into Keggin heteropolyanion. Such lacunar salts are potentially active catalysts, even without the introduction of transition metal cations in the vacancy, which is also a strategy used to improve the catalytic activity of these salts (LI et al., 2015). Recently, lacunar salts of Potassium-substituted HPAs have been shown to be highly active in the oxidation reactions of borneol, a saturated and secondary terpenic alcohol (DA SILVA et al., 2018).

Therefore, the creation of a vacancy in the Keggin heteropolyanion and the replacement of protons by metallic cations of larger radii lead to lacunar Keggin salts that can be suitable catalysts for oxidation reactions with Hydrogen peroxide under heterogeneous conditions (CORONEL; DA SILVA, 2018).

However, the lacunary structure of the heteropolyanion has a high nucleophilicity that favors the formation of coordination compounds with metallic cations, which in turn, can be introduced into the octahedral lacuna (MIZUNO; YAMAGUCHI; KAMATA, 2005).

Consequently, lacunar anions can be coordinated to transition metals and are potentially active catalysts in redox transformations (CHOI et al., 2013; KARCZ et al., 2017).

Recently, transition metal substituted Keggin polyoxometalates salts have been used in many successful oxidation reactions, such as desulfurization or oxidative amination, oxidation of alkanes, cycloalkanes, aromatic hydrocarbons, polyaromatics and methacrolein, where Hydrogen peroxide is generally used as an oxidant (ESTRADA et al., 2009, 2010, 2011b; PATEL; SHRINGARPURE; PATEL, 2011; SANTOS et al., 2008; ZHOU et al., 2017).

## 2.4. Niobium compounds

Brazil is the country with the largest reserves of Niobium in the world, and responsible by more than 90% of Niobium world production (DNPM (DEPARTAMENTO NACIONAL DE PRODUÇÃO MINERAL), 2019). Its use has been very extensive and covers several industrial sectors and research fields. Niobium has interesting catalytic properties, and it can be used both as an active phase and as a support (LOPES et al., 2014). Also, Niobium oxide has interesting characteristics for its use as a heterogeneous catalyst.

Niobium oxide and phosphate have Brønsted and Lewis sites in its structure, with high acidity. Brønsted acidity is related to proton donor groups represented by $OH^-$ clusters attached to the solid material surface. On the other hand, Lewis acid sites are related to metallic atoms capable of receiving electrons due to the electron deficiency of their incomplete *d* orbitals. (MORENO; RAJAGOPAL, 2009).

These acidic characteristics can favor the use of Nb catalysts in many reactions, such as benzylation of anisole (KITANO et al., 2012), oxidation of *n*-butane (TANABE, 2003), furfural production from sugarcane bagasse (CATRINCK et al., 2020), hydration of alkynes (RATHNAYAKE et al., 2020), methylene blue degradation (DO PRADO; OLIVEIRA, 2017), acetalization of glycerol to solketal (SOUZA et al., 2015), conversion of furfuryl alcohol and α-angelica lactone (SKRODCZKY et al., 2019) and conversion of biomass to biofuels (GAO et al., 2018; KUMARI et al., 2019; XIA et al., 2015).

$Nb_2O_5$ has a high structural complexity due to its characteristic polymorphism, and can form many distinct crystalline phases, among them, we can mention monoclinic, orthorhombic, tetragonal, and pseudohexagonal phases (NICO; MONTEIRO; GRAÇA, 2016). However, two main crystalline phases are more studied, the T phase, orthorhombic and the H phase, monoclinic (LOPES et al., 2014).

Besides the intrinsic acidic properties and good stability to high temperatures, the Niobium phosphate has been also an excellent choice in reactions where the water is present. The high-water tolerance can be attributed to the Lewis acid sites in tetrahedral units. These units can interact with the water molecule and preserve the tetrahedral positive charges (MEJÍA; VERBART; DE JONG, 2021; VIEIRA et al., 2021).

## 2.5. Dysprosium-doped Zinc tungstate

Zinc tungstate ($ZnWO_4$) is a solid has been explored in the photocatalysis field to decompose undesirable compounds. Many different synthesis methodologies can be applied to the preparation of this catalyst like hydrothermal procedure, sol-gel, electrodeposition, and mechanochemical synthesis (RAHIMI-NASRABADI et al., 2015; WEN et al., 2019). As example, in an experiment simulating the solar light irradiation, Huang and co-authors (2016) synthesized different Zinc tungstate microspheres which were applied in the NOx degradation (HUANG et al., 2016). This solid has the monoclinic wolframite structure ($AWO_4$) and possesses high chemical stability and low cost (DKHILALLI et al., 2018).

The potential exploration of the luminescence characteristics of Zinc tungstates are well described in the literature in different reactions. However, they can be modified by a variety of elements to make possible the application in new processes. A good example is the interaction between tungstate and rare earths. The doping of the $ZnWO_4$ structure with earth rare metals bring benefits in the fluorescence properties, besides the improvements in its structural and electronic properties (CHAI et al., 2017; GONÇALVES et al., 2017; LIU et al., 2017).

Furthermore, in some organic reactions, lanthanides have been used as a source of Lewis acid sites. These composites can present low toxicity, good stability, and low price. These characteristics have motivate the use of Dysprosium compounds as catalysts in oxidation procedures (HAJIASHRAFI; SALEHI, 2020; MOLAEI; GHADERMAZI, 2020).

## 2.6. Oxidation of terpenic alcohols

Terpenes represent the most diversified class of secondary plant metabolites, and today they are widely exploited by various industrial sectors. These compounds are valued in the production of medicines, pesticides, cosmetics, fine chemicals, and the food industry (SCHWAB; FUCHS; HUANG, 2013).

Among the various processes to convert terpenic alcohols into high added value products, hydrogenation/ dehydrogenation, alkylation, isomerization, and oxidation/ epoxidation reactions deserves to be highlighted. The oxidation, as well as the epoxidation of terpenic alcohols, has great industrial importance due to the generation of products which are intermediates in pharmaceuticals, perfumes, and food industry (GUO et al., 2014).

Two different approaches to the oxidation of terpenic alcohols can basically take place through two sites: the hydroxyl group and the double bond. The alcohol group can be oxidized to an aldehyde group, generating compounds that have attractive organoleptic properties for industries (GUO et al., 2014). In addition, olefinic double bonds can be epoxidized, generating chiral compounds that are important intermediates as building blocks to originate potential compounds for the synthesis of drugs and agrochemicals (BAHOU et al., 2019; NICOLAOU et al., 1989; SERRA; DE SIMEIS, 2018). Thus, the synthesis of catalysts that can act on these sites and produce compounds with high selectivity becomes a matter of extreme importance (MONTEIRO; VELOSO, 2004; SWIFT, 2004).

Nerol is a monoterpene found in several essential oils and is also widely used as an input in different industrial sectors. Figure 2 below illustrates two important products obtained from the oxidation of nerol.

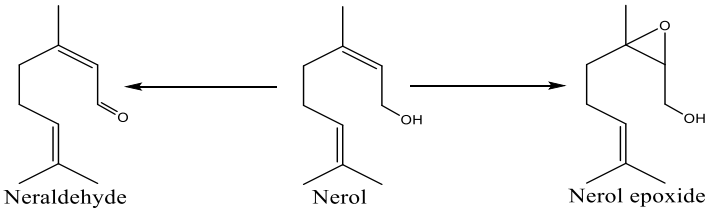


**Figure 2**. Structural formulas of nerol and two important products obtained by the oxidation process

The mechanistic proposal for the epoxidation of nerol is summarized below (Scheme 2). The Brønsted and Lewis acid sites, on the metallic catalyst, act together, interacting both with the oxidant and the nerol.

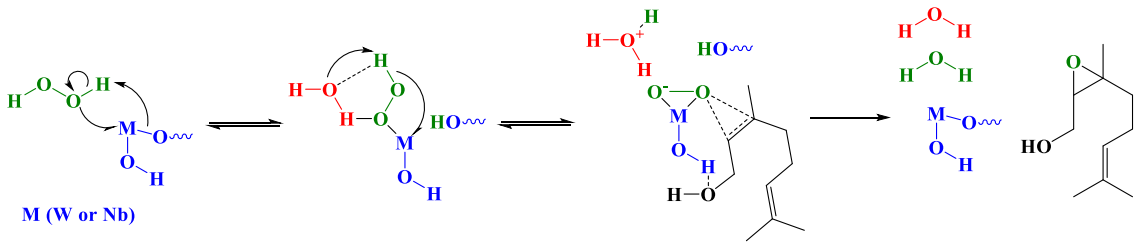


**Scheme 2.** Proposal of nerol epoxidation over acid sites. The reduced representation of the catalyst was chosen to simplify the visualization (BATALHA et al., 2020a, 2020b; CLAYDEN; GREEVES; WARREN, 2012; SHIMA et al., 2009)

Firstly, the metallic *d* orbitals are responsible for the activation of the Hydrogen peroxide, leading to the formation of metal-hydroperoxo complex. Next, the metallic specie is responsible for the electron abstraction from the other peroxidic Oxygen, being possible the formation of the oxirane ring which, throw the assisted Hydrogen interaction with the alcohol hydroxyl group, will enable the interaction between the doble bond with the peroxidic Oxygen. This is possible due to the attack from the HOMO (highest occupied molecular orbital) of the olefine to the LUMO (lowest occupied molecular orbital) of the Oxygen bonded with the metal specie (AMINI; HAGHDOOST; BAGHERZADEH, 2014; BECK; MALLAT; BAIKER, 2003; CLAYDEN; GREEVES; WARREN, 2012; KUMAR et al., 1995; SHIMA et al., 2009; VILANCULO; DA SILVA, 2021; YAN et al., 2018).

## 2.7. Acetalization of furfural

Furfural is another natural feedstock derived from dehydration of xylan, present in the lignocellulose residues. It is an important key platform molecule to produce a range of chemicals, such as furan, furfuryl alcohol, furoic acid, furfural dimethyl acetal, etc (BERNAL et al., 2015). Besides that, the acetalization process can make possible the generation of high added value products, which can be used in fuel, perfumes, medicines and polymers industries (RASPOLLI GALLETTI et al., 2020).

Common routes of acetalization have been performed using homogeneous acid catalysts. However, there are many problems related with the catalyst recovery, besides the high corrosiveness of these acids. Notwithstanding, acidic solid catalysts, like Niobium compounds, can solve these problems (CORMA; GARCÍA, 2003).

The furfural acetalization can be done over two different ways: via carbonyl activation by the Brønsted acid sites (Scheme 3); or alternatively, being mediated by the carbonyl polarization over Lewis acid sites coordination (Scheme 4). In Brønsted acid-catalyzed reactions, the catalyst is responsible by the increase in the electrophilicity of the carbonyl Carbon. Next, this Carbon suffers a nucleophilic attack from the alcohol, generating a tetrahedral intermediary. Following the reaction, this intermediary loses a proton, and the hemiacetal is formed. Afterwards, a carbocation is obtained after a loss of a water molecule what makes possible other nucleophilic attack by one alcohol molecule, generating the acetal (DU et al., 2018; TEIXEIRA; NATALINO; DA SILVA, 2020).

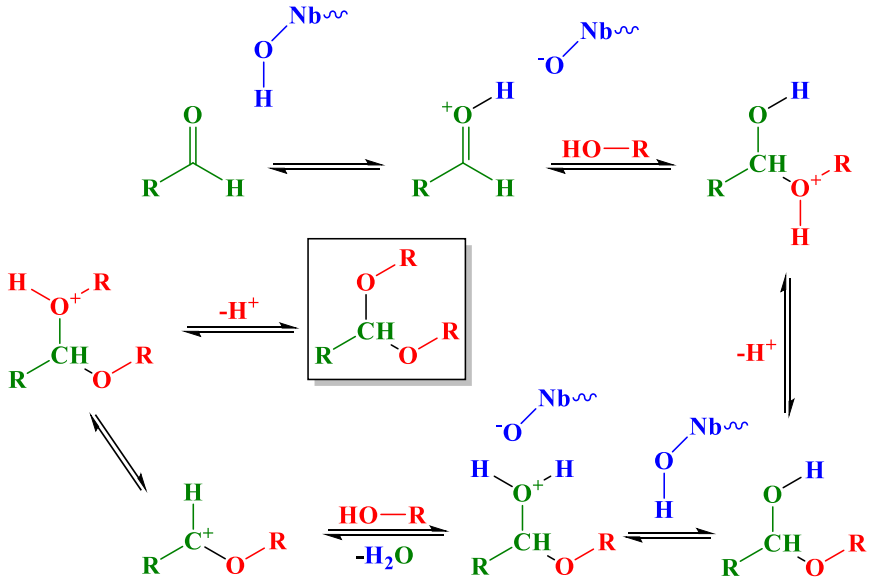

**Scheme 3.** Proposed mechanism through activation of furfural carbonyl by Niobium catalysts through Brønsted acid protonation (DU et al., 2018; TEIXEIRA; NATALINO; DA SILVA, 2020)

Via Lewis acid sites (Scheme 4), the metallic specie is the electron acceptor, where the furfural activation involves a HOMO/LUMO interaction. The π electrons of the carbonyl Oxygen (HOMO) interact with the *d* orbitals of the Niobium cation (LUMO). This interaction makes the carbonyl Carbon more electrophilic and makes it susceptible to an alcohol attack to form the hemiacetal intermediate and later acetal, together with the loss of a water molecule (DA SILVA; TEIXEIRA, 2018; DA SILVA; TEIXEIRA; NATALINO, 2019).

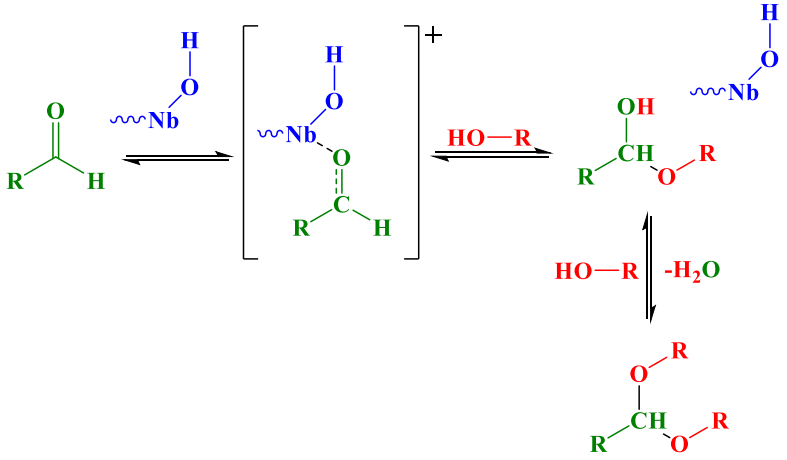

**Scheme 4.** Proposed summarized mechanism through activation of furfural carbonyl by metallic catalyst through binding to Lewis sites (DA SILVA; TEIXEIRA, 2018; DA SILVA; TEIXEIRA; NATALINO, 2019)

This reaction has been explored by different researchers with a diversity of catalysts for the acetal production. Table 1 gathers some experiments from the literature of furfural acetalization.

**Table 1.** Summarized results of furfural acetalization into acetal from the literature

| Entry | Catalyst | Alcohol | Conditions | Conversion % | References |
|---|---|---|---|---|---|
| **1** | NbP | Methanol | Furfural (2.5 mmol)<br>Cat. (15 mg)<br>Temp. (25 ºC)<br>Time (3 h) | 95% | This work |
| **2** | $H_3PW_{12}O_{40}$ | Methanol | Furfural (0.62 mmol)<br>Cat. (0.5% of $H^+$ cations)<br>Temp. (25 ºC)<br>Time (30 min) | 93% | (TEIXEIRA; NATALINO; DA SILVA, 2020) |
| **3** | $FeCl_3.6H_2O$ | Methanol | Furfural (5 mmol)<br>Cat. (2.0 mol%)<br>Temp. (25 ºC)<br>Time (2 h) | 94% | (DA SILVA; TEIXEIRA, 2018) |
| **4** | $SnCl_2$ | Ethanol | Furfural (0.62 mmol)<br>Cat. (4.0 mol%)<br>Temp. (25 ºC)<br>Time (4 h) | 80% | (DA SILVA; TEIXEIRA; NATALINO, 2019) |
| **5** | Zeolite H-USY | Ethanol | Furfural (0.8 mmol)<br>Cat. (75 mg)<br>Temp. (25 ºC)<br>Time (1 h) | 79% | (RUBIO-CABALLERO et al., 2014) |

## 3. OBJECTIVES

### 3.1. General Objectives

The general objectives were to synthesize, characterize, and evaluate heterogeneous catalysts (i.e., Keggin Cesium-exchanged Keggin HPAs lacunar salts, Niobium oxides, and Dysprosium-doped Zinc tungstate), in terpenic alcohols oxidation reactions by Hydrogen peroxide. Niobium oxides and phosphates were also evaluated in acetalization reactions of furfural in the presence of alkyl alcohols.

### 3.2. Specific Objectives

- Synthesize Cesium-exchanged heteropoly salt catalysts from the $Na_2SiO_3$, $Na_2WO_4.2H_2O$, $Na_2HPO_4.7H_2O$ and $Na_2MoO_4$ precursors, characterize, and evaluate their activity in the oxidation reactions of terpenic alcohols;
- Study the activity of Niobium oxides synthesized from Niobium ammoniacal oxalate and evaluate its activity in the oxidation reactions of terpenic alcohols;
- Study the activity of Dysprosium-doped Zinc tungstate synthesized from $Na_2WO_4.2H_2O$, $Zn(NO_3)_2.6H_2O$ and $Dy(NO_3)_3.6H_2O$ in the oxidation reactions of terpenic alcohols;
- Study the activity of commercial Niobia and Niobium phosphate catalysts treated with Hydrogen peroxide in the acetalization of furfural;
- Correlate all the characterization data of the catalysts with their catalytic activity.

## 4. GENERAL METHODOLOGY

The methodology used in the project includes the following steps:
- Bibliographic survey;
- Preparation of the catalysts;
- Physical-chemical characterization of the catalysts;
- Catalytic tests;
- Analysis and discussion of results;
- Preparation of materials for presentation and participation in technical-scientific events;
- Writing of scientific articles and other distribution materials;
- Qualification presentation;
- Thesis defense.

### 4.1. Catalyst syntheses

The precipitation method was used for the synthesis of Cesium heteropolyacid salts. The catalysts were synthesized and applied at LabCat from Federal University of Viçosa in the terpenic alcohols oxidation.

The Niobium oxides used in the terpenic alcohols oxidation were prepared by microwave-assisted hydrothermal synthesis in the Novonano laboratory - Advanced Materials Applied Technologies Group - coordinated by Prof. Dr. Neftalí Lenin Villarreal Carreño from

the Federal University of Pelotas and the materials were kindly provided for the experiments. The work also counts on collaboration for complementary analysis of the catalysts by the Heterogeneous Catalysis laboratory, coordinated by Prof. Dr. Humberto Vieira Fajardo from the Federal University of Ouro Preto. Thus, this project relies on part of the collaborative work maintained between the UFV-UFOP-UFPel research groups.

The Dysprosium catalysts, also used for the conversion of terpenic alcohols, were synthesized by a mixed methodology, coprecipitation and microwave hydrothermal method, which were kindly provided by the Prof. Dr. Mário Júnior Godinho group from the Federal University of Catalão. Also, the work had the collaboration between the researchers from four universities, UFV-UFCAT-UFOP-UFMG, to provide all the necessary characterizations.

Finally, to convert furfural in the respective acetals, the niobia and Niobium phosphates were kindly provided and characterized by the Prof. Dr. Luiz Carlos A. Oliveira group from Federal University of Minas Gerais, a collaborative work between UFV-UFMG.

### *4.1.1. Synthesis of the Cesium salts*

$Cs_yXM_{11}O_{39}$ Cesium salts (Y = 7 or 8; X = Si or P; M = W or Mo) were synthesized by precipitation according to the methodology adapted from the literature (DA SILVA et al., 2018). Unlike most processes in the literature (DA SILVA; LIBERTO, 2016), which started from the HPAs to synthesize the salts, herein all the catalysts were synthesized from their precursor salts: $Na_2SiO_3$ (2.5 mmol) for the $Cs_8SiW_{11}O_{39}$ salt; $Na_2WO_4.2H_2O$ (0.028 mol) for the salts $Cs_8SiW_{11}O_{39}$ and $Cs_7PW_{11}O_{39}$; $Na_2HPO_4.7H_2O$ (2.5 mmol) for the $Cs_7PW_{11}O_{39}$ and $Cs_7PMo_{11}O_{39}$ salts; and $Na_2MoO_4$ (0.028 mol) for the $Cs_7PMo_{11}O_{39}$ salt.

Typically, an aqueous solution (approximately 353 K) containing the precursor of Tungsten or Molybdenum ($Na_2WO_4$ or $Na_2MoO_4$) was added to 8.25 mL of 4.0 $molL^{-1}$ HCl for 30 minutes, where hydrated tungstic and molybdic acid are formed. Another solution containing Silicon or Phosphorus precursor salt ($Na_2SiO_3$ or $Na_2HPO_4$) was prepared, depending on the target heteropolyanion ($SiW_{12}O_{40}^{4-}$, $PW_{12}O_{40}^{3-}$ or $PW_{12}O_{40}^{3-}$). These solutions were then mixed and stirred for 60 minutes at approximately 353 K resulting in the saturated Sodium HPA salts ($Na_3PW_{12}O_{40}$, $Na_3PMo_{12}O_{40}$ and $Na_4SiW_{12}O_{40}$). For this, an addition of 4.0 $molL^{-1}$ HCl is necessary to adjust the pH to the proper range (pH = 5.4, $SiW_{11}O_{39}^{8-}$ and $PW_{11}O_{39}^{7-}$; pH = 4.5, $PMo_{11}O_{39}^{7-}$), converting the saturated anions into lacunar anions. Then, the solution was cooled to room temperature and 0.1 mol of $CsCl_{(s)}$ was added to precipitate the Cesium salt. The solid salt obtained was washed twice (50 mL, 1.0 $molL^{-1}$ of $CsCl_{(aq)}$) and once with 50 mL of cold

distilled water, then air-dried. After this step, the Cesium salts were dried in an oven at 423 K / 5 h. Figure 3 illustrates a scheme of the preparation methodology.

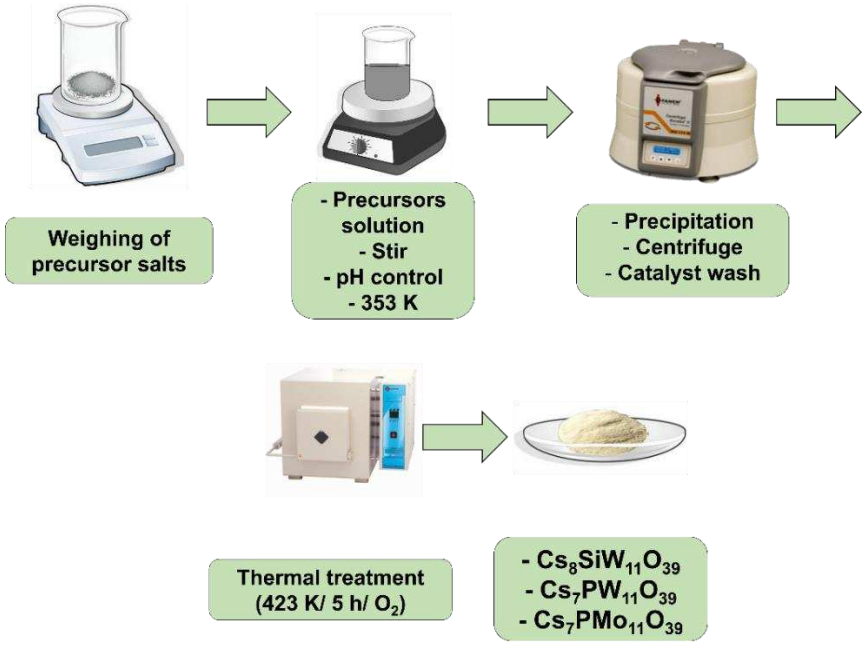


**Figure 3.** Simplified scheme of the precipitation synthesis method of the three different Cesium heteropoly salts

*4.1.2. Synthesis of Niobium oxides by microwave-assisted hydrothermal method*

$Nb_2O_5$ particles were synthesized by the microwave-assisted hydrothermal synthesis method (Figure 4) as described in the literature (MARINS et al., 2018). Niobium ammonia oxalate was dispersed in distilled water and the mixture sonicated for 120 minutes. Then aqueous $H_2O_2$ was added dropwise to the solution which was then sonicated again for another 30 minutes. The final solution was placed in a Teflon container, and later in a sealed autoclave and placed in a microwave (Electrolux, MEF41, Brazil). The temperature was adjusted to 433 K and the synthesis was carried out at different times (2, 4 and 8 h) under a constant pressure of 85 psi. After cooling, the precipitate was washed with absolute ethanol (LabSynth, Brazil) and dried in an oven (DeLeo, A5SE, Brazil) at 323 K for 24 h under atmospheric air. The three different materials were obtained: $Nb_2O_5$ 2 h, $Nb_2O_5$ 4 h and $Nb_2O_5$ 8 h.

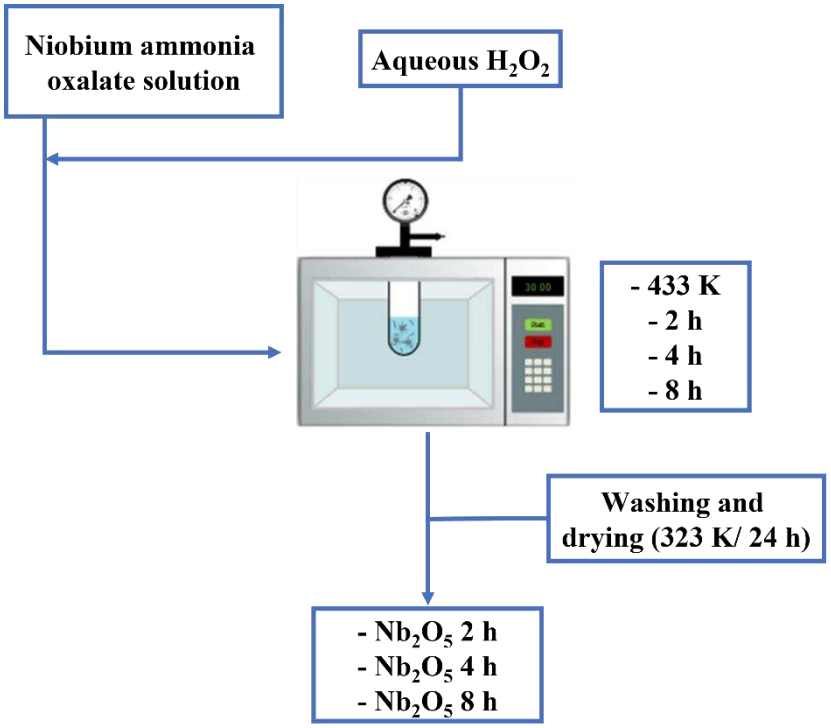


**Figure 4.** Simplified scheme of the microwave-assisted hydrothermal synthesis of the three different Niobium oxide catalysts

*4.1.3. Coprecipitation followed by the microwave hydrothermal method for the Dysprosium-doped Zinc tungstate synthesis*

To synthesize the Dysprosium-doped Zinc tungstate catalysts, two methodologies was adopted. First of them, the coprecipitation started with the dissolution of the precursor $Na_2WO_4.2H_2O$ (ca. $5x10^{-3}$ mol) in 50 mL of deionized water and in constant stirring. Similarly, $5x10^{-3}$ mol of $Zn(NO_3)_2.6H_2O$ was dissolved and it was kept at pH=6. To this solution, specific amounts of the dopant $Dy(NO_3)_3.6H_2O$ were added (0.5, 1.0 and 2.0 mol%) followed by the addition of the tungstate solution. After that, the final solution was kept at 363 K and under stirring for 30 min, generating a white suspension. For the last step, this white suspension was placed in a Teflon autoclave and heated in a microwave system at 413 K for 1 h, with the heat rate of 25 $Kmin^{-1}$. The pressure of the system was stabilized at 245 kPa. The final suspension was washed with deionized water until the neutralization of the solution. The white precipitate was dried at 333 K to obtain the catalyst. The Figure 5 below illustrates the summarized synthesis.

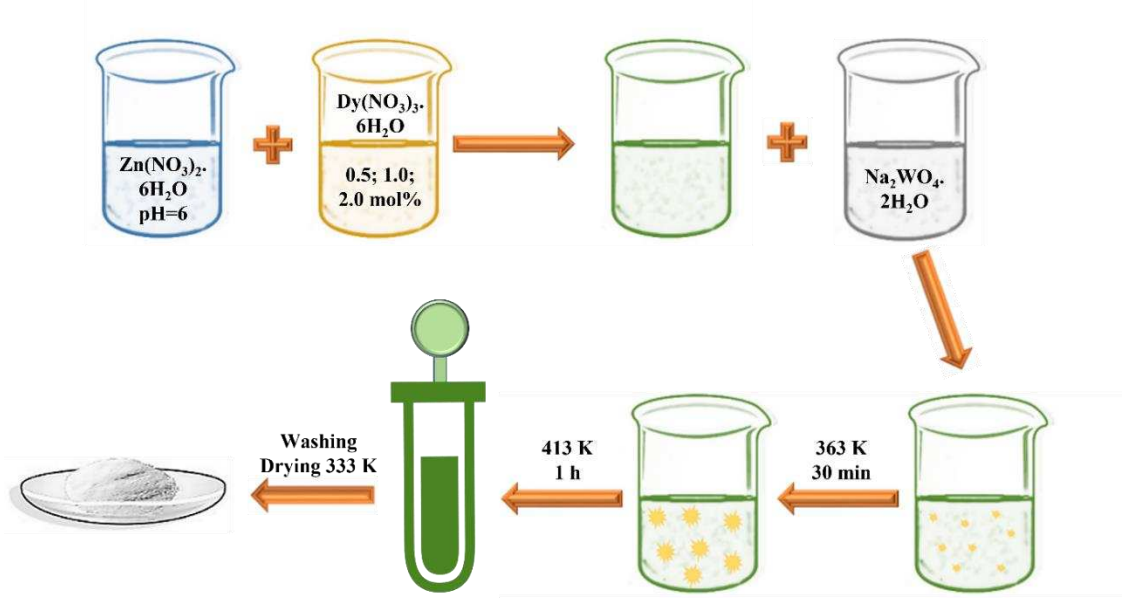


**Figure 5.** Simplified scheme of the coprecipitation followed by microwave-assisted hydrothermal synthesis of the Dysprosium tungstate catalysts

*4.1.4. Treated Niobium oxide and phosphate*

To generate more active surface sites on the Niobium oxide and Niobium phosphate, these materials were treated with Hydrogen peroxide, leading to the materials named T-NA and T-NbP, Niobium oxide and Niobium phosphate treated, respectively (Figure 6). To the treatment of 5 g of the material, 100 mL of deionized water and 8 mL of $H_2O_2$ (50 %. wt) were kept under stirring for 10 min. After an aging about 12 h, the material was centrifuged, washed with distilled water e dried at 353 K in an oven overnight.

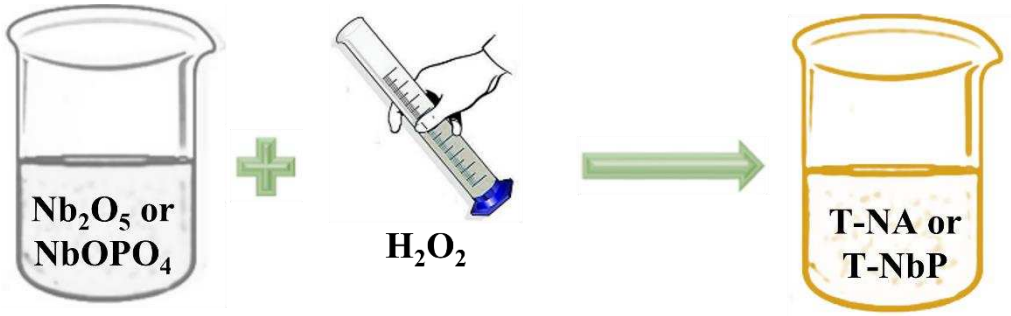


**Figure 6.** Simplified scheme of the Hydrogen peroxide treatment of the Niobium oxide and phosphate catalysts

**4.2. Physicochemical characterizations of the catalysts**

To evaluate the surface properties of prepared catalytic materials, physicochemical characterizations were proposed using available techniques. At first, the solids were subjected to the following processes:

*4.2.1. Physical adsorption of Nitrogen (BET/DFT)*

The methods used to determine the surface areas and distribution of mean diameter and pore volume of the Cesium salts, Niobium oxides (2 h, 4 h and 8 h) and Dysprosium catalysts were Brunauer-Emmett-Teller (BET) and Functional Density Theory (DFT) respectively. The analyzes were carried out in the NOVA 1200 Quantachrome equipment, through the physical adsorption/desorption isotherms of $N_2$, at 77 K, at Federal University of Viçosa.

The textural properties of the samples used in the acetalization reactions of the furfural, such as specific surface area, average pore diameter and pore volume were obtained by $N_2$ physical adsorption-desorption assays at 77 K using Quantachrome Autosorb IQ2, at Federal University of Minas Gerais. Previously, the materials were preheated at 120 °C under the vacuum of $2.0x10^{-9}$ atm.

*4.2.2. Fourier transform infrared spectroscopy (IR-FT)*

The FT-IR spectra of the synthesized Cesium catalysts were recorded in Varian 660-IR equipment coupled to the attenuated total reflectance technique (FT-IR / ATR), in the spectral range from 400 to 4000 $cm^{-1}$, at Federal University of Viçosa.

Infrared spectroscopy analyses were performed in KBr pellets using an ABB Bomen MB 3000 FTIR spectrometer (Quebec, Canada) equipped with ZnSe optics and a deuterated triglycine sulfate (DTGS) detector set at a 4 $cm^{-1}$ resolution and wavenumber range of 400-4000 $cm^{-1}$ for the Niobium catalysts applied in the alcohol oxidation processes, at Federal University of Pelotas.

*4.2.3. Raman spectroscopy*

For the Niobium oxides used in the nerol oxidations, Raman analyzes were performed on a Horiba / Jobin-Yvon LABRAM-HR spectrometer equipped with a He-Ne laser (632.8 nm laser excitation lines and 18 mW power) and an Olympus microscope, at Federal University of Ouro Preto. Measurement acquisition time was 5 s, with 10 accumulations in the region of 60 to 1200 $cm^{-1}$, using a 100x objective.

The Raman spectra of the catalysts applied to convert furfural in acetals were recorded on a Witec Alpha 300 equipped with an EMCCD detector. The Raman spectroscopy were excited at 532 nm operated at 150 mW, at Federal University of Minas Gerais.

*4.2.4. Powder X-ray diffraction (DRX)*

The identification of the crystal structures of the Cesium catalysts was carried out using the X-ray diffraction (XRD) technique. Cesium salts powder diffraction patterns were obtained by X-ray diffraction (XRD) in a Bruker D8 Discover diffractometer, operating at 40 kV accelerating voltage, 40 mA current in the copper emission line (Cu- Kα, λ = 1.5418 Å), with a scan rate of 0.3°/min for a 2θ angle of 5-80°, at Federal University of Viçosa.

The $Nb_2O_5$ powders used in the alcohol oxidation reactions were analyzed by X-Ray diffraction by the Shimadzu equipment, XRD 6000, Japan, using a CuKa radiation diffractometer (λ = 1.5418 Å) with a scan rate of 0.5 °/min scan for an angle 2θ 20-70°, at Federal University of Pelotas.

All Dy catalytic materials were characterized by X-ray diffraction (XRD) using a D/Max-2500PC diffractometer (Rigaku, Japan), (Cu–Kα radiation λ = 1.5406 Å) in the 2θ range from 10° to 70° at a scanning rate of 0.02° $min^{-1}$, at Federal University of Catalão.

Powder X-ray data for the Niobium catalysts applied in the acetalization processes were collected using a SHIMADZU XRD-7000 diffractometer with $CuK_\alpha$ (λ=1.5406 Å) as radiation source from 2θ=10-80°, at a 1.0s step and the generator setting is 30 kV and 30 mA, at Federal University of Minas Gerais.

*4.2.5. Thermogravimetric analysis (ATG)*

Thermal analysis makes it possible to monitor the temperatures at which the salt anions degrade and to make an approximate calculation of the amount of coordination water present. Characterization (ATG – DSC) was performed on a Perkin Elmer (STA) 6000 Simultaneous Thermal Analyzer. Approximately 10 mg of sample was heated from 298 to 973 K at a rate of 10 $Kmin^{-1}$ under Nitrogen flow, at Federal University of Viçosa.

*4.2.6. Potentiometric Titration*

The number and strength of the acidic sites of the Cesium salts and Niobium oxides, both applied in the nerol oxidations, were determined by potentiometric titration by n-butylamine using a BEL potentiometer, model W3B, with a glass electrode. Typically, a solid sample of the catalytic material (50 mg) was suspended in $CH_3CN$ (30 mL) and stirred by a magnetic bar for 3 h. Subsequently, the suspension was slowly titrated with n-butylamine solution (100 μL portions; 0.025 $molL^{-1}$), until the electrode potential remained stable after the addition of the titrant, at Federal University of Viçosa.

*4.2.7. X-ray energy dispersion spectroscopy*

Technique used to verify the chemical composition of the obtained catalysts and compare with what was predicted in theory and visualization of the microstructure of the catalysts, being able to predict certain properties. SEM images of lacunar Cesium salts were obtained on a JEOL JSM – 6010 / LA microscope equipped with an energy dispersion spectrometry (EDS) system, at Federal University of Viçosa.

*4.2.8. $NH_3$ temperature-programmed desorption ($NH_3$-TPD)*

The acid sites strength of the commercial Niobium oxide and Niobium phosphate and the Dysprosium catalysts was measured by the $NH_3$ temperature-programmed desorption technique ($NH_3$-TPD), at Federal University of Minas Gerais. The samples were placed in a U-shaped quartz tube and exposed to the flow of He (40 $mL.min^{-1}$ for Niobium catalysts and 80 $mL.min^{-1}$ for Dy solids) at 120 °C for 1 hour. The flux of ammonia occurred for 10 min to the chemisorption through the acid-base reaction. Once again, a flow of He was passed through the sample to remove any amount of physically adsorbed ammonia. CHEMBET-3000 TPR/TPD detector Chemisorption analyzer (Quantachrome instrument) coupled with the TCD detector under heating 200-900 °C (10 °C/min) recorded the amount of chemosorbed $NH_3$.

*4.2.9. Pyridine chemisorbed FT-IR spectroscopy*

Pyridine chemisorbed FT-IR spectroscopy was used to identify the nature of the acid sites of the Niobium catalysts used in the acetalization reactions, at Federal University of Minas Gerais. First, the catalyst surface was cleaned at 200 °C/ 3 h, to eliminate chemi or physisorbed water molecules. Later, dry pyridine was spread into the samples to the chemisorption.

Physisorbed pyridine was driven off by heating the sample at 120 °C for 2 h. Tablets containing 10 mg of the sample and 80 mg of KBr were pressing under vacuum for 3 minutes. Pyr-FTIR spectra of the catalysts were recorded at room temperature using a Spectrum PerkinElmer FT-IR RXI equipment in the range of 1700-1400 $cm^{-1}$.

*4.2.10. Scanning electron microscopy (SEM)*

For Niobium solids applied in the nerol oxidation reactions, microscopy images were generated by an SSX-550 microscope, SHIMADZU, Japan, at Federal University of Pelotas.

The morphology of the materials used in the acetalization reactions was investigated by scanning electron microscopy (SEM) Hitachi TM 400 Plus, at Federal University of Minas Gerais.

*4.2.11. High-resolution transmission electron microscopy (HR-TEM)*

The shape, size, and form of the nanocrystals of the Dysprosium materials were analyzed using a high-resolution transmission electron microscopy (HR-TEM) with a Tecnai G2-F20 microscope (200 kV), at Federal University of Catalão.

**4.3. Catalytic tests**

The tests were carried out in liquid phase, under atmospheric pressure, using a reaction system composed of batch reactors (50 mL round bottom balloon) coupled to a condenser, with monitored reaction temperature, under agitation. The reaction medium consisted of predetermined amounts of organic solvent (acetonitrile for oxidation reactions and allylic alcohols for acetalization processes), oxidizing agent (for the oxidation reactions), heterogeneous catalysts, and terpene or furfural substrate. This process is illustrated in the Figure 7.

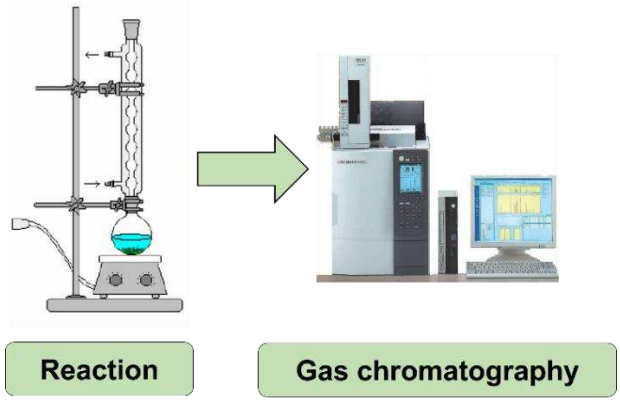


**Figure 7.** Illustrative scheme of the reaction system and GC analyses

Reaction tests were performed at different times, with a predetermined number of aliquots collected during the reaction. Subsequently, each aliquot was centrifuged at 3000-3500 rpm/ 5 min to separate the catalyst. The supernatant was analyzed in a Gas Chromatograph equipped with a flame ionization detector (FID). The Shimadzu GC-2010 Plus model equipment is equipped with an AOC-20i auto-injector, flame ionization detector (FID) and Rtx®-Wax capillary column (30 m, x 0.25 mmID x 0.25 μm). Column conditions were: To = 353 K for 3 min, heating rate of 10 K / min to final temperature of 493 K, remaining for 3 min (total of 20 min); injector (523 K); detector (523 K); $H_2$ carrier gas at 1.2 $mLmin^{-1}$.

The conversion was calculated from the initial area of the substrate in each medium reaction, following the equation: $C = \left(\frac{(Ainitial - Afinal)}{Ainitial}\right) * 100$, where *Ainitial* and *Afinal* are the initial and final areas of the substrate. The selectivity values were calculated based on the areas of the chromatographic peaks of the products in relation to the areas of the chromatographic peaks of all quantified products, according to the equation: $S = \left(\frac{Aproduct}{\sum Aproduts}\right) * 100$, where *Aproduct* means the area value of a single product of interest and S is the selectivity value in %.

## 5. GENERAL REFERENCES

ALIZADEH, M. H.; TAYEBEE, R. Catalytic oxidation of aniline by aqueous hydrogen peroxide in the presence of some heteropolyoxometalates. **Journal of the Brazilian Chemical Society**, v. 16, n. 1, p. 108–111, fev. 2005.

AMINI, M.; HAGHDOOST, M. M.; BAGHERZADEH, M. Monomeric and dimeric oxido-peroxido tungsten(VI) complexes in catalytic and stoichiometric epoxidation. **Coordination Chemistry Reviews**, v. 268, p. 83–100, 2014.

BAHOU, K. et al. Relay Cross Metathesis for the Ascent of the Terpenoids. **ChemRxiv**, 2019.

BATALHA, D. C. et al. Cesium-Exchanged Lacunar Keggin Heteropolyacid Salts: Efficient Solid Catalysts for the Green Oxidation of Terpenic Alcohols with Hydrogen Peroxide. **ChemistrySelect**, v. 5, n. 6, p. 1976–1986, 14 fev. 2020a.

BATALHA, D. C. et al. Oxidation of terpenic alcohols with hydrogen peroxide promoted by Nb2O5 obtained by microwave-assisted hydrothermal method. **Molecular Catalysis**, v. 489, p. 110941, jun. 2020b.

BATALHA, D. C.; DA SILVA, M. J. Biodiesel Production over Niobium-Containing Catalysts: A Review. **Energies**, v. 14, n. 17, p. 5506, 3 set. 2021.

BECK, C.; MALLAT, T.; BAIKER, A. Epoxidation of allylic alcohols with TiO2-SiO2: Hydroxy-assisted mechanism and dynamic structural changes during reaction. **Catalysis Letters**, v. 88, n. 3–4, p. 203–209, 2003.

BERNAL, H. G. et al. NbP catalyst for furfural production: FT IR studies of surface properties. **Applied Catalysis A: General**, v. 502, p. 388–398, ago. 2015.

CARNITI, P. et al. Cooperative action of Brønsted and Lewis acid sites of niobium phosphate catalysts for cellobiose conversion in water. **Applied Catalysis B: Environmental**, v. 193, p. 93–102, set. 2016.

CATRINCK, M. N. et al. One-step process to produce furfural from sugarcane bagasse over niobium-based solid acid catalysts in a water medium. **Fuel Processing Technology**, v. 207, p. 106482, out. 2020.

CAVANI, F. Heteropolycompound-based catalysts: **Catalysis Today**, v. 41, n. 1–3, p. 73–86, maio 1998.

CHAGAS, P. et al. A novel hydrofobic niobium oxyhydroxide as catalyst: Selective cyclohexene oxidation to epoxide. **Applied Catalysis A: General**, v. 454, p. 88–92, mar. 2013.

CHAI, X. et al. Upconversion luminescence and temperature-sensing properties of Ho 3+ /Yb 3+ -codoped ZnWO 4 phosphors based on fluorescence intensity ratios. **RSC Advances**, v. 7, n. 64, p. 40046–40052, 2017.

CHOI, J. H. et al. Redox properties and oxidation catalysis of transition metal-substituted α-K5PW11O39(M·OH2) (M=MnII, CoII, NiII, and ZnII) Keggin heteropolyacid catalysts for liquid-phase oxidation of 2-propanol. **Journal of Molecular Catalysis A: Chemical**, v. 371, p. 111–117, maio 2013.

CLAYDEN, J.; GREEVES, N.; WARREN, S. Organic Chemistry Organic Chemistry. **Organic Chemistry Frontiers**, p. 1261, 2012.

CORMA, A.; GARCÍA, H. Lewis Acids: From Conventional Homogeneous to Green Homogeneous and Heterogeneous Catalysis. **Chemical Reviews**, v. 103, n. 11, p. 4307–4366, 1 nov. 2003.

CORONEL, N. C.; DA SILVA, M. J. Lacunar Keggin Heteropolyacid Salts: Soluble, Solid and Solid-Supported Catalysts. **Journal of Cluster Science**, v. 29, n. 2, p. 195–205, 22 mar. 2018.

DA SILVA, I. A.; MOTA, C. J. A. Conversion of CO2 to Light Olefins Over Iron-Based

Catalysts Supported on Niobium Oxide. **Frontiers in Energy Research**, v. 7, 28 maio 2019.

DA SILVA, M. J. et al. Monolacunary K8SiW11O39-Catalyzed Terpenic Alcohols Oxidation with Hydrogen Peroxide. **Catalysis Letters**, v. 148, n. 8, p. 2516–2527, 2 ago. 2018.

DA SILVA, M. J.; DE OLIVEIRA, C. M. Catalysis by Keggin Heteropolyacid Salts. **Current Catalysis**, v. 7, n. 1, p. 26–34, 7 mar. 2018.

DA SILVA, M. J.; LIBERTO, N. A. Soluble and Solid Supported Keggin Heteropolyacids as Catalysts in Reactions for Biodiesel Production: Challenges and Recent Advances. **Current Organic Chemistry**, v. 20, n. 12, p. 1263–1283, 3 mar. 2016.

DA SILVA, M. J.; TEIXEIRA, M. G. An unexpected behavior of H 3 PMo 12 O 40 heteropolyacid catalyst on the biphasic hydrolysis of vegetable oils. **RSC Advances**, v. 7, n. 14, p. 8192–8199, 2017.

DA SILVA, M. J.; TEIXEIRA, M. G. Assessment on the double role of the transition metal salts on the acetalization of furfural: Lewis and Brønsted acid catalysts. **Molecular Catalysis**, v. 461, p. 40–47, dez. 2018.

DA SILVA, M. J.; TEIXEIRA, M. G.; NATALINO, R. Highly selective synthesis under benign reaction conditions of furfural dialkyl acetal using SnCl 2 as a recyclable catalyst. **New Journal of Chemistry**, v. 43, n. 22, p. 8606–8612, 2019.

DE JONG, K. P. (ED.). **Synthesis of solid catalysts.** [s.l.] John Wiley & Sons, 2009.

DKHILALLI, F. et al. Structural, dielectric, and optical properties of the zinc tungstate ZnWO4 compound. **Journal of Materials Science: Materials in Electronics**, v. 29, n. 8, p. 6297–6307, 22 abr. 2018.

DNPM (DEPARTAMENTO NACIONAL DE PRODUÇÃO MINERAL). **Sumário Mineral 2017**. Disponível em: <https://www.gov.br/anm/pt-br/centrais-de-conteudo/publicacoes/serie-estatisticas-e-economia-mineral/sumario-mineral/sumariomineral_2017>. Acesso em: 20 abr. 2021.

DO PRADO, N. T.; OLIVEIRA, L. C. A. Nanostructured niobium oxide synthetized by a new route using hydrothermal treatment: High efficiency in oxidation reactions. **Applied Catalysis B: Environmental**, v. 205, p. 481–488, maio 2017.

DU, Y. et al. Kinetics and Mechanism of Acetalisation of Furfural to Furfural Diethyl Acetal with Ni–Al Layered Double Hydroxides Containing Lewis Acid Sites. **Progress in Reaction Kinetics and Mechanism**, v. 43, n. 1, p. 21–29, 1 mar. 2018.

ESTRADA, A. C. et al. Iron-substituted polyoxotungstates as catalysts in the oxidation of indane and tetralin with hydrogen peroxide. **Applied Catalysis A: General**, v. 366, n. 2, p. 275–281, set. 2009.

ESTRADA, A. C. et al. Catalytic activity of iron-substituted polyoxotungstates in the oxidation of aromatic compounds with hydrogen peroxide. **Monatshefte für Chemie - Chemical Monthly**, v. 141, n. 11, p. 1223–1235, 23 nov. 2010.

ESTRADA, A. C. et al. Silica supported transition metal substituted polyoxotungstates: Novel

heterogeneous catalysts in oxidative transformations with hydrogen peroxide. **Applied Catalysis A: General**, v. 392, n. 1–2, p. 28–35, jan. 2011a.

ESTRADA, A. C. et al. Oxidation of Polycyclic Aromatic Hydrocarbons with Hydrogen Peroxide in the Presence of Transition Metal Mono-Substituted Keggin-Type Polyoxometalates. **ChemCatChem**, v. 3, n. 4, p. 771–779, 11 abr. 2011b.

GAO, D.-M. et al. Synthesis of a hierarchically porous niobium phosphate monolith by a sol–gel method for fructose dehydration to 5-hydroxymethylfurfural. **Catalysis Science & Technology**, v. 8, n. 14, p. 3675–3685, 2018.

GAURAV, A.; NG, F. T. T.; REMPEL, G. L. A new green process for biodiesel production from waste oils via catalytic distillation using a solid acid catalyst – Modeling, economic and environmental analysis. **Green Energy & Environment**, v. 1, n. 1, p. 62–74, abr. 2016.

GONÇALVES, R. F. et al. Structural investigation and photoluminescent properties of ZnWO4:Dy3+ nanocrystals. **Journal of Materials Science: Materials in Electronics**, v. 28, n. 20, p. 15466–15479, 7 out. 2017.

GUO, Z. et al. Recent advances in heterogeneous selective oxidation catalysis for sustainable chemistry. **Chemical Society Reviews**, v. 43, n. 10, p. 3480, 2014.

HAJIASHRAFI, T.; SALEHI, S. Dysprosium-Organic Framework as a Heterogeneous Lewis acid Catalyst for the Sulfide Oxidation and as a precursor for the. v. 5, n. 1, p. 59–65, 2020.

HUANG, Y. et al. Hierarchical porous ZnWO4 microspheres synthesized by ultrasonic spray pyrolysis: Characterization, mechanistic and photocatalytic NO removal studies. **Applied Catalysis A: General**, v. 515, p. 170–178, abr. 2016.

INUMARU, K. et al. Porous Aggregates of Unidirectionally Oriented (NH 4 ) 3 PW 12 O 40 Microcrystallites: Epitaxial Self-Assembly. **Chemistry Letters**, v. 25, n. 7, p. 559–560, jul. 1996.

IWASE, Y. et al. Bimodal cesium hydrogen salts of 12-tungstosilicic acid, Cs H4−SiW12O40, as highly active solid acid catalysts for transesterification of glycerol tributyrate with methanol. **Journal of Catalysis**, v. 318, p. 34–42, out. 2014.

KAMIYA, Y. et al. Microporous Acidic Cesium Salt of 12-Tungstosilicic Acid Cs 3 HSiW 12 O 40 as a Size-selective Solid Acid Catalyst. **Chemistry Letters**, v. 39, n. 8, p. 881–883, 5 ago. 2010.

KARCZ, R. et al. Effect of cobalt location in Keggin-type heteropoly catalysts on aerobic oxidation of cyclooctane: Experimental and theoretical study. **Applied Catalysis A: General**, v. 542, p. 317–326, jul. 2017.

KITANO, T. et al. Brønsted Acid Property of Alumina-Supported Niobium Oxide Calcined at High Temperatures: Characterization by Acid-Catalyzed Reactions and Spectroscopic Methods. **The Journal of Physical Chemistry C**, v. 116, n. 21, p. 11615–11625, 31 maio 2012.

KOZHEVNIKOV, I. V. Sustainable heterogeneous acid catalysis by heteropoly acids. **Journal of Molecular Catalysis A: Chemical**, v. 262, n. 1–2, p. 86–92, 1 fev. 2007.

KOZHEVNIKOV, I. V. Catalysis by heteropoly acids and multicomponent polyoxometalates in liquid-phase reactions. **Chemical Reviews**, v. 98, n. 1, p. 171–198, 1998.

KUMAR, R. et al. Hydroxy-assisted chemo- and stereo-selective epoxidation catalysed by a titanium silicate molecular sieve (TS-1)/H2O2 system. **Journal of the Chemical Society, Chemical Communications**, n. 13, p. 1315–1316, 1995.

KUMARI, P. K. et al. Tungstophosphoric acid supported on mesoporouus niobiumoxophosphate: an efficient solid acid catalyst for etherification of 5-hydroxymethylfurfural to 5-ethoxymethylfurfural. **Catalysis Today**, v. 325, p. 53–60, mar. 2019.

LANGE, J.-P. et al. Furfural-A Promising Platform for Lignocellulosic Biofuels. **ChemSusChem**, v. 5, n. 1, p. 150–166, 9 jan. 2012.

LI, L. et al. Preparation of Keggin-type mono-lacunary phosphotungstic-ammonium salt and its catalytic performance in ammoximation of cyclohexanone. **Chemical Engineering Journal**, v. 280, p. 670–676, nov. 2015.

LI, W. B.; WANG, J. X.; GONG, H. Catalytic combustion of VOCs on non-noble metal catalysts. **Catalysis Today**, v. 148, n. 1–2, p. 81–87, 30 out. 2009.

LIOTTA, L. F. Catalytic oxidation of volatile organic compounds on supported noble metals. **Applied Catalysis B: Environmental**, v. 100, n. 3–4, p. 403–412, 20 out. 2010.

LIU, Z. et al. A facile microwave-hydrothermal method to fabricate B doped ZnWO 4 nanorods with high crystalline and highly efficient photocatalytic activity. **Materials Research Bulletin**, v. 94, p. 298–306, out. 2017.

LOPES, O. F. et al. Niobium oxides: an overview of the synthesis of Nb2O5 and its application in heterogeneous photocatalysis. **Química Nova**, 2014.

MARINS, N. H. et al. Radiopaque dental adhesive with addition of niobium pentoxide nanoparticles. **Polymer Bulletin**, v. 75, n. 6, p. 2301–2314, 17 jun. 2018.

MEJÍA, C. H.; VERBART, D. M. A.; DE JONG, K. P. Niobium-based solid acids in combination with a methanol synthesis catalyst for the direct production of dimethyl ether from synthesis gas. **Catalysis Today**, v. 369, p. 77–87, jun. 2021.

MIZUNO, N.; YAMAGUCHI, K.; KAMATA, K. Epoxidation of olefins with hydrogen peroxide catalyzed by polyoxometalates. **Coordination Chemistry Reviews**, v. 249, n. 17–18, p. 1944–1956, set. 2005.

MOLAEI, S.; GHADERMAZI, M. Selective and efficient oxidation of sulfides and thiols to their corresponding sulfoxides and disulfides catalyzed with praseodymium (III) and dysprosium (III) isonicotinamide (INA) complexes grafted onto modified mesoporous MCM-41. **Solid State Sciences**, v. 100, p. 106091, fev. 2020.

MONTEIRO, J. L. F.; VELOSO, C. O. Catalytic Conversion of Terpenes into Fine Chemicals. **Topics in Catalysis**, v. 27, n. 1–4, p. 169–180, fev. 2004.

MORENO, E. L.; RAJAGOPAL, K. Desafios da acidez na catálise em estado sólido. **Química**

**Nova**, v. 32, n. 2, p. 538–542, 2009.

NICO, C.; MONTEIRO, T.; GRAÇA, M. P. F. Niobium oxides and niobates physical properties: Review and prospects. **Progress in Materials Science**, v. 80, p. 1–37, jul. 2016.

NICOLAOU, K. C. et al. Activation of 6-endo over 5-exo hydroxy epoxide openings. Stereoselective and ring selective synthesis of tetrahydrofuran and tetrahydropyran systems. **Journal of the American Chemical Society**, v. 111, n. 14, p. 5330–5334, 1 jul. 1989.

OKUHARA, T.; NISHIMURA, T.; MISONO, M. Microporous Heteropoly Compound as a Shape Selective Catalyst : Cs 2.2 H 0.8 PW 12 O 40. **Chemistry Letters**, v. 24, n. 2, p. 155–156, fev. 1995.

PARK, H. W. et al. Decomposition of phenethyl phenyl ether to aromatics over CsxH3.0−xPW12O40 (X = 2.0–3.0) heteropolyacid catalysts. **Catalysis Communications**, v. 12, n. 1, p. 1–4, out. 2010.

PATEL, A. et al. Keggin-type lacunary and transition metal substituted polyoxometalates as heterogeneous catalysts: A recent progress. **Catalysis Reviews**, v. 58, n. 3, p. 337–370, 2 jul. 2016.

PATEL, K.; SHRINGARPURE, P.; PATEL, A. One-step synthesis of a Keggin-type manganese(II)-substituted phosphotungstate: structural and spectroscopic characterization and non-solvent liquid phase oxidation of styrene. **Transition Metal Chemistry**, v. 36, n. 2, p. 171–177, 24 mar. 2011.

RAHIMI-NASRABADI, M. et al. Facile Synthesis Optimization and Structure Characterization of Zinc Tungstate Nanoparticles. **Materials and Manufacturing Processes**, v. 30, n. 1, p. 34–40, 2 jan. 2015.

RASPOLLI GALLETTI, A. M. et al. Direct Alcoholysis of Carbohydrate Precursors and Real Cellulosic Biomasses to Alkyl Levulinates: A Critical Review. **Catalysts**, v. 10, n. 10, p. 1221, 21 out. 2020.

RATHNAYAKE, D. et al. Mesoporous Crystalline Niobium Oxide with a High Surface Area: A Solid Acid Catalyst for Alkyne Hydration. **ACS Applied Materials & Interfaces**, v. 12, n. 42, p. 47389–47396, 21 out. 2020.

RUBIO-CABALLERO, J. M. et al. Acetalization of furfural with zeolites under benign reaction conditions. **Catalysis Today**, v. 234, p. 233–236, out. 2014.

SANTOS, I. et al. A New Insight into the Oxidation of Cyclododecane with Hydrogen Peroxide in the Presence of Iron-Substituted Polyoxotungstates. **Synlett**, v. 2008, n. 11, p. 1623–1626, 11 jun. 2008.

SANTOS, J. S. et al. Mixed salts of cesium and ammonium derivatives of 12-tungstophosphoric acid: Synthesis and structural characterization. **Applied Catalysis A: General**, v. 394, n. 1–2, p. 138–148, fev. 2011.

SCHMAL, M. **Heterogeneous Catalysis and its Industrial Applications**. Cham: Springer International Publishing, 2016.

SCHWAB, W.; FUCHS, C.; HUANG, F.-C. Transformation of terpenes into fine chemicals. **European Journal of Lipid Science and Technology**, v. 115, n. 1, p. 3–8, jan. 2013.

SCIRÈ, S.; LIOTTA, L. F. Supported gold catalysts for the total oxidation of volatile organic compounds. **Applied Catalysis B: Environmental**, v. 125, p. 222–246, ago. 2012.

SERRA, S.; DE SIMEIS, D. Two Complementary Synthetic Approaches to the Enantiomeric Forms of the Chiral Building Block (2,6,6-Trimethyltetrahydro-2H-pyran-2-yl)methanol: Application to the Stereospecific Preparation of the Natural Flavor Linaloyl Oxide. **Catalysts**, v. 8, n. 9, p. 362, 28 ago. 2018.

SHIMA, H. et al. IR observation of selective oxidation of cyclohexene with H 2O2 over mesoporous Nb2O5. **Journal of Physical Chemistry C**, v. 113, n. 52, p. 21693–21699, 2009.

SHRINGARPURE, P. A.; PATEL, A. Supported undecatungstophosphate: An efficient recyclable bi-functional catalyst for esterification of alcohols as well as selective oxidation of styrene. **Chemical Engineering Journal**, v. 173, n. 2, p. 612–619, set. 2011.

SKRODCZKY, K. et al. Niobium pentoxide nanomaterials with distorted structures as efficient acid catalysts. **Communications Chemistry**, v. 2, n. 1, p. 129, 13 dez. 2019.

SOUZA, T. E. et al. Amphiphilic property of niobium oxyhydroxide for waste glycerol conversion to produce solketal. **Catalysis Today**, v. 254, p. 83–89, out. 2015.

SWIFT, K. A. D. Catalytic Transformations of the Major Terpene Feedstocks. **Topics in Catalysis**, v. 27, n. 1–4, p. 143–155, fev. 2004.

TANABE, K. Catalytic application of niobium compounds. **Catalysis Today**, v. 78, n. 1–4, p. 65–77, fev. 2003.

TEIXEIRA, M. G.; NATALINO, R.; DA SILVA, M. J. A kinetic study of heteropolyacid-catalyzed furfural acetalization with methanol at room temperature via ultraviolet spectroscopy. **Catalysis Today**, v. 344, p. 143–149, mar. 2020.

TUMMA, H.; NAGARAJU, N.; REDDY, K. V. Titanium (IV) oxide, an efficient and structure-sensitive heterogeneous catalyst for the preparation of azoxybenzenes in the presence of hydrogen peroxide. **Applied Catalysis A: General**, v. 353, n. 1, p. 54–60, jan. 2009.

VIEIRA, J. L. et al. Niobium phosphates as bifunctional catalysts for the conversion of biomass-derived monosaccharides. **Applied Catalysis A: General**, v. 617, p. 118099, maio 2021.

VILANCULO, C. B.; DA SILVA, M. J. Can Brønsted acids catalyze the epoxidation of allylic alcohols with H2O2? With a little help from the proton, the H3PMo12O40 acid did it and well. **Molecular Catalysis**, v. 512, n. April, 2021.

WEN, X.-J. et al. Fabrication of a zinc tungstate-based a p-n heterojunction photocatalysts towards refractory pollutants degradation under visible light irradiation. **Colloids and Surfaces A: Physicochemical and Engineering Aspects**, v. 573, p. 137–145, jul. 2019.

XIA, Q. et al. Energy-efficient production of 1-octanol from biomass-derived furfural-acetone in water. **Green Chemistry**, v. 17, n. 8, p. 4411–4417, 2015.

YAN, W. et al. Liquid-Phase Epoxidation of Light Olefins over W and Nb Nanocatalysts. **ACS Sustainable Chemistry and Engineering**, v. 6, n. 4, p. 4423–4452, 2018.

ZHENG, Y. et al. Transition metal-doped heteropoly catalysts for the selective oxidation of methacrolein to methacrylic acid. **Frontiers of Chemical Science and Engineering**, v. 10, n. 1, p. 139–146, 29 mar. 2016.

ZHOU, L. et al. Cesium salts supported heteropoly acid for oxidation of methacrolein to methacrylic acid. **Molecular Catalysis**, v. 433, p. 153–161, maio 2017.

ZHOU, Y. et al. Recent advances in polyoxometalate-based heterogeneous catalytic materials for liquid-phase organic transformations. **RSC Adv.**, v. 4, n. 79, p. 42092–42113, 12 ago. 2014.

ZIOLEK, M. et al. Search for reactive intermediates in catalytic oxidation with hydrogen peroxide over amorphous niobium(V) and tantalum(V) oxides. **Applied Catalysis B: Environmental**, v. 164, p. 288–296, mar. 2015.

## RESULTS: ARTICLES PUBLISHED/SUBMITTED IN SCIENTIFIC JOURNALS

The following four articles were published as results of the research studies developed and carried out in this PhD.

**PAPER 1: Cesium-Exchanged Lacunar Keggin Heteropolyacid Salts: Efficient Solid Catalysts for the Green Oxidation of Terpenic Alcohols with Hydrogen Peroxide**

*Paper published in Chemistry Select

ChemPubSoc Europe DOI: 10.1002/slct.201903437 Chemistry SELECT Full Papers Check for updates

Catalysis

# Cesium-Exchanged Lacunar Keggin Heteropolyacid Salts: Efficient Solid Catalysts for the Green Oxidation of Terpenic Alcohols with Hydrogen Peroxide

Daniel Carreira Batalha,[a] Sukarno Olavo Ferreira,[b] Rene Chagas da Silva,[b] and Márcio José da Silva*[a]

[a] *Dr. D. C. Batalha, Prof. M. J. da Silva*
Chemistry Department, Federal University of Viçosa, Viçosa, Zip Code 36570-000, Minas Gerais State, Brazil
phone: +55 31 3899–3071
E-mail: silvamj2003@ufv.br

[b] *Prof. S. O. Ferreira, Prof. R. C. da Silva*
Physics Department, Federal University of Viçosa, Viçosa, Zip Code 36570-000, Minas Gerais State, Brazil

Supporting information for this article is available on the WWW under https://doi.org/10.1002/slct.201903437

*ChemistrySelect* 2020, *5*, 1976 – 1986 **Wiley Online Library**

### Abstract

In this work, an innovative and green oxidative process to convert renewable and abundant raw material to more value-added fine chemicals was developed. Hydrogen peroxide, an environmentally benign oxidant, was used in Cs-exchanged lacunar Keggin heteropolyacid salts-catalyzed oxidation reactions of the terpenic alcohols (i.e., nerol was the model molecule). The activity of most outstanding catalyst ($Cs_8SiW_{11}O_{39}$) was compared with various catalysts. Epoxides and aldehydes, which are an attractive feedstock for fragrance and pharmaceutical industries were selectively obtained. Lacunar Keggin heteropolyacid salts containing Cesium as the counter ion (i.e., $Cs_7PW_{11}O_{39}$, $Cs_7PMo_{11}O_{39}$ and $Cs_8SiW_{11}O_{39}$) were easily synthesized and characterized by infrared spectroscopy, powdered X-rays diffraction, X-rays dispersive

spectroscopy, scanning electronic microscopy, thermal analysis, porosimetry analyses, diameter and pores distribution. The influences of the main reaction variables such as catalyst concentration, the stoichiometry of the reactants and reaction temperature were evaluated. The reaction scope was successfully extended to the other terpenic alcohols. The $Cs_8SiW_{11}O_{39}$ was the most active and selective lacunar salt. After five cycles of successive reuse, no loss of catalytic activity or selectivity was observed.

**Graphical Abstract**

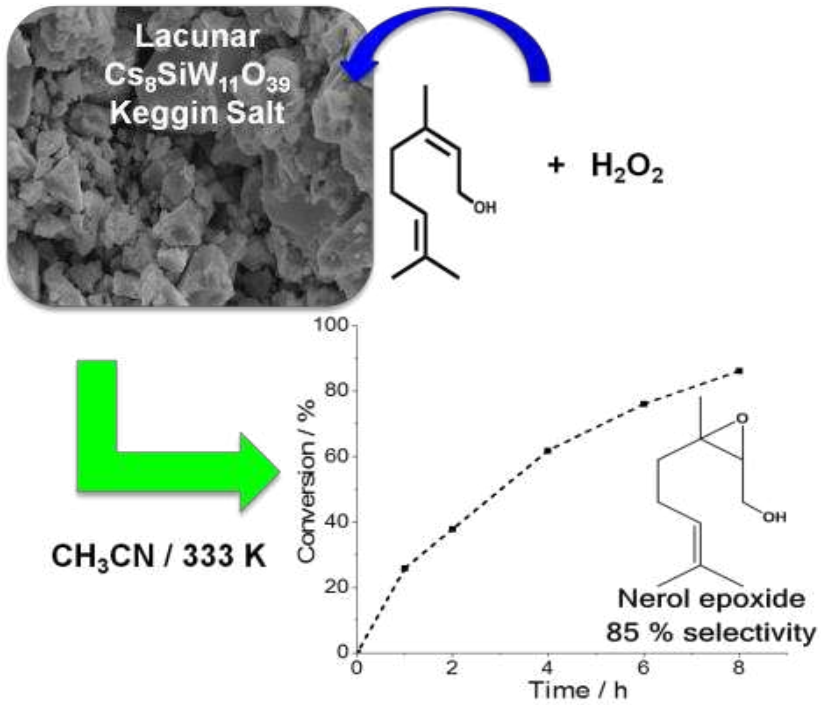


## 1. Introduction

Keggin heteropolyacids (HPAs) are a class of metal-Oxygen clusters with a high Brønsted acidity and are widely applied in a plethora of acid-catalyzed reactions.[1,2] These solid polyoxometalates presents a large variety of composition, structure and electronic properties, which makes them versatile catalysts in different reactions.[3] Therefore, in addition to be active in acid-catalyzed reactions, Keggin HPAs are also effective catalysts in oxidation reactions of different substrates. Several organic-heteropolyacid hybrids and heteropolyacid-based ionic hybrids were used as catalysts for oxidation of alcohols or epoxidation of olefins.[4–7]

Keggin HPAs have a low surface area and are soluble in polar solvents, hampering its use direct as solid catalysts. However, they have been used as solid-supported heterogeneous

catalysts after to be immobilized on matrixes such as silicas, activated Carbon, zeolites, alumina, and zirconia.[5,6] When they are supported on solids, the great challenge to be circumvented is to avoid the leaching problems triggered by the high polarity of the reaction medium and therefore, preserve its intrinsic activity.[7,8]

An efficient approach is converting the HPAs to insoluble salts, replacing their protons by cations of large radium.[9] This transformation results in efficient catalysts likewise Cesium phosphotungstate salts. The inclusion of Cesium as a counterion in the Keggin HPAs improves their thermal stability, increase their surface area as well as porosity properties.[10,11] In accordance with the literature, phosphotungstic acid is the most acidic and widely used Keggin HPA in acid-catalyzed reactions.[12] Several works have described the partial exchange of their protons by Cesium, resulting in solid catalysts with a higher activity than their soluble parent acids.[12–15]

The removal of one or more MO units (i. e., WO or MoO) of Keggin heteropolyanions gives to the HPAs a high activity and selectivity in oxidation reactions.[16] The lacunary structure of the heteropolyanion has a high nucleophilicity that favors the formation of the coordination compounds with metal cations, which are introduced in the lacunar octahedral.[17] Consequently, lacunar anions may be coordinated to the transition metal cations and are potentially active catalysts in redox transformations.[18,19] Recently, transition metal-substituted Keggin-type polyoxometalate salts were successfully used as catalysts in different oxidation reactions, such as desulfurization or oxidative amination, oxidations of alkanes, cycloalkanes, arenes, polyaromatics, and methacrolein, all of them with Hydrogen peroxide as the oxidant.[20–25]

Among the several organic substrates in oxidation reactions, terpenic alcohols are a renewable raw material that deserves to be highlighted, due to their two oxidizable sites; the hydroxyl group and the olefinic double bond.[26] The hydroxyl group can be oxidized to carbonyl, generating compounds that have attractive organoleptic properties for fragrancy industries.[27] Moreover, the olefinic double bonds can be epoxidized, generating chiral compounds which are important intermediates for the synthesis of drugs and agrochemicals.[28,29]

There is an aspect still less exploited in the literature; the vacancy created on the coordination sphere of the Tungsten or Molybdenum atoms present in the structure of heteropolyanion, generate potentially active catalysts, even without the introduction of transition metal cations.[30] Recently, Potassium-exchanged lacunar HPA salts demonstrated to be highly active in oxidation reactions of borneol, a secondary terpenic alcohol that has not

double bonds.[31] These oxidative processes become even more attractive when performed with an inexpensive and environmentally friendly oxidant (i.e., Hydrogen peroxide). This inexpensive, atom efficient and nonflammable oxidant, results only in water as by-product.[32] Therefore, the creation of a vacancy in the Keggin heteropolyanion, and the protons exchange by larger radium metal cations, led the lacunar Keggin HPA salts to be suitable catalysts for oxidation reactions with Hydrogen peroxide in heterogeneous catalysis conditions.[33]

In this work, we have investigated the catalytic activity of solid Keggin HPAs (i.e., Cesium-exchanged lacunar salts) in oxidation reactions of terpenic alcohols with Hydrogen peroxide. Three Cesium HPA salts were easily synthesized starting from their precursor salts. They were characterized by FT–IR, XRD, BET, TG–DSC, and EDS–SEM analyses, and had the strength and number of the acid sites determined by potentiometric titration with *n*-butylamine. Nerol was the model substrate used to assess the effects of the main reaction parameters (i.e., load of catalyst and oxidant, temperature and reaction time). The oxidation of other unsaturated terpenic alcohols (i.e., geraniol, linalool, β-citronellol and α-terpineol) was also studied. The most active lacunar salt catalyst (i.e., $Cs_8SiW_{11}O_{39}$) was successfully recovered and reused without loss selectivity or activity.

## 2. Results and Discussions

### *2.1. Characterization of the catalysts*

TG-DSC curves of Cesium-exchanged lacunar salts were obtained and displayed in Figure 1. Thermal analyses allowed to quantify the water present in the samples of different Cesium lacunar salt catalysts. Regardless of the Cesium salt, the main loss of water occurred at 333–463 K, corresponding the physisorbed water. A lower loss was noticed at 463-673 K, corresponding the water chemically bonded. The number of mols of $H_2O$/ mol of catalyst for $Cs_8SiW_{11}O_{39}$, $Cs_7PW_{11}O_{39}$, and $Cs_7PMo_{11}O_{39}$ lacunar salts was 6, 6 and 5, respectively.

At temperatures range between 298 to 673 K, only water molecules were lost, and the Keggin heteropolyanion was minimally disturbed. However, at temperatures higher than 673 K, the decomposition of the heteropolyanion begins to occur. An endothermic peak at 750 K was noticed in DSC curves of two Cesium salts containing phosphorous (i.e., $Cs_7PW_{11}O_{39}$; and $Cs_7PMo_{11}O_{39}$). These observations are in accordance with the literature.[34-36] Although the decomposition of $Cs_8SiW_{11}O_{39}$ salt has also occurred, the peak endothermic was not visible. At

850 K, the Keggin anions were totally decomposed to oxides (i.e., $WO_3$, $MO_3$, $P_2O_5$, $SiO_2$), and the Cesium oxidized to $Cs_2O$.[34]

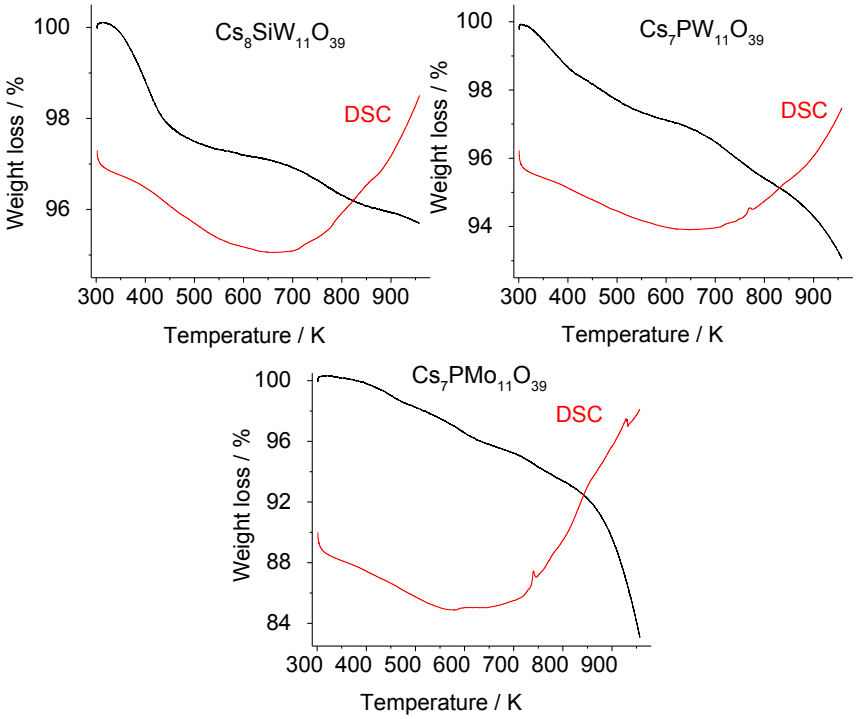


**Figure 1.** TG/DSC curves obtained from Cesium exchanged lacunar heteropoly salts

The surface area and porosity of the lacunar salts were analyzed (Table 1). The protons exchange by Cesium in lacunar salts resulted in an expressive increase of the surface area, since that Keggin HPAs have commonly a low surface area (*ca.* 3.0 $m^2\ g^{-1}$).[8]

**Table 1.** Characterization of the catalysts through the physical adsorption of Nitrogen

| Catalyst | $S_{BET}$ ($m^2\ g^{-1}$) | $V_{DFT}$ ($cm^3\ g^{-1}$) | D (Å) |
|---|---|---|---|
| $Cs_8SiW_{11}O_{39}$ | 11.7 | 0.010 | 31.7 |
| $Cs_7PW_{11}O_{39}$ | 9.8 | 0.010 | 31.7 |
| $Cs_7PMo_{11}O_{39}$ | 5.6 | 0.008 | 27.7 |

$S_{BET}$ = specific surface area; $V_{DFT}$ = pore volume e D = medium pore diameter

The Cesium silicotungstate lacunar salt (i.e., $Cs_8SiW_{11}O_{39}$) had a slightly larger surface area than that the phosphotungstate (i.e., $Cs_7PW_{11}O_{39}$). Conversely, the Cesium phosphomolybdate (i.e., $Cs_7PMo_{11}O_{39}$) presented the lowest surface area.

The literature has described different values for the surface area of saturated Cesium phosphotungstate or phosphomolybdate salts (i.e., $Cs_3PW_{12}O_{40}$, $Cs_3PMo_{12}O_{40}$), which may

vary of 40-190 $m^2$ $g^{-1}$.[14,37,38] Ever since a long time, the characterization of the Cesium partially exchanged salts (i.e., $Cs_{3-x}H_xPW_{12}O_{40}$) have been widely exploited.[37-39] Nonetheless, data about the surface area of the lacunar Cesium salts are scarce, hampering a comparison.

Differently from surface area measurements, diameter and pore volume of the Cesium lacunar salts had a minimum variation. Pore diameter range presented by the salts (ca. 27.7-31.7 Å) (Table 1) was enough to assure that they are mesoporous materials, which have size pores ranging of 20-500 Å.[40]

The $N_2$ adsorption–desorption isotherms and the pores size distribution are shown in Figure 2. According to the IUPAC recommendations, the isotherms of the salts were classified as type IV, which are characteristic of mesoporous materials. The presence of a slight hysteresis suggests that the isotherms are type H3, characteristics of plate-like particle aggregates originating pores in the form of slits.[41]

The profile of pore diameter distribution curves of the salts showed that almost all the pores have diameters between 20 and 150 Å, confirming that they are mesoporous material. The maximum diameter placed at 50-60 Å was likewise to the observed for saturated Keggin Cesium salts.[37]

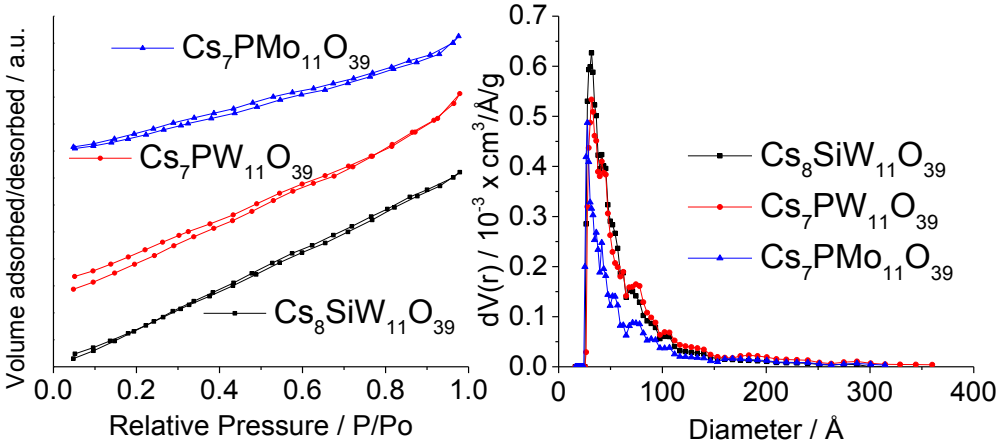


**Figure 2.** Isotherms of physical adsorption/ desorption of $N_2$ and pore diameter distribution for lacunar Cesium heteropoly salts

SEM images provides information about the morphology of the lacunar Cesium salts (Figure 3). It is possible to observe that the catalysts have different shapes and sizes, characterizing very heterogeneous grains, which were different from each other. It was also noted that they are composed of well compacted particle agglomerates, which may be the explanation for the low surface area.

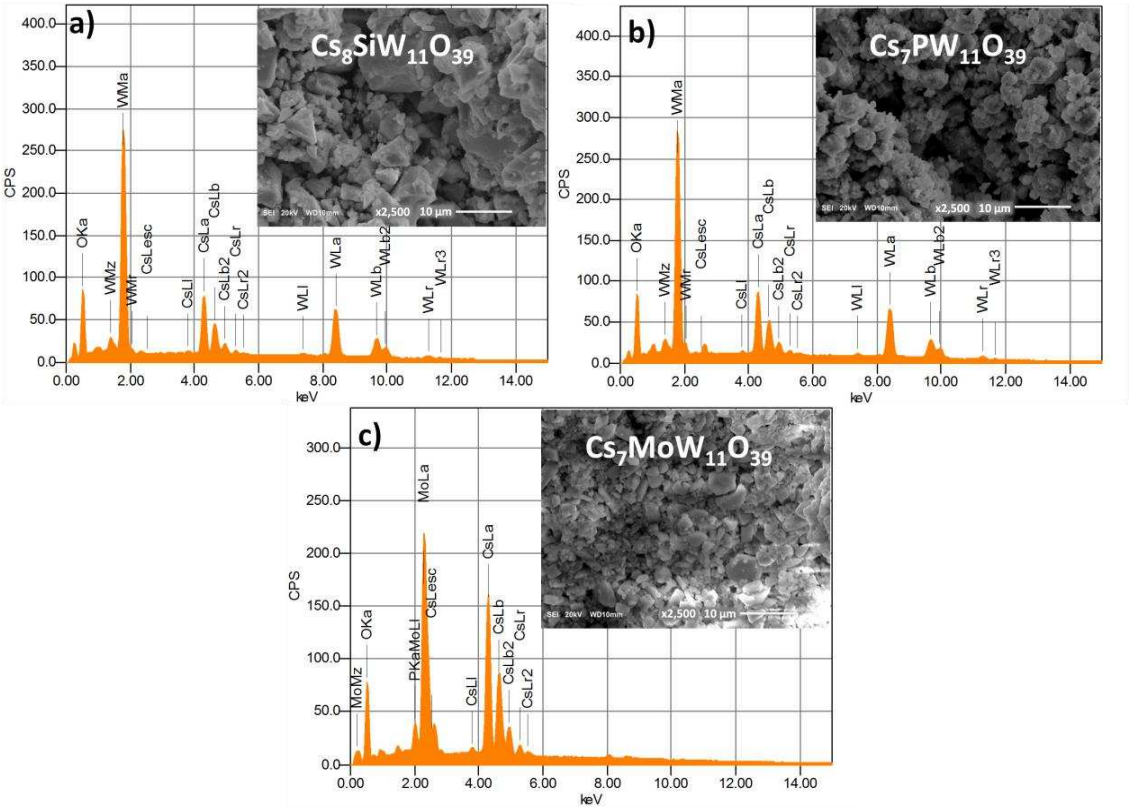


**Figure 3.** EDS spectrum representing composition (orange area) of the Cesium exchanged lacunar heteropoly salts

The constituent elements (i.e., Cs, P, Si, W, Mo, and O) of the samples of the Cesium exchanged lacunar salts were quantified by X-ray dispersive spectroscopy analysis (Table 1SM). The elemental compositions determined by EDS were close to the theoretical values, indicating a successful formation of the $Cs^+$ heteropoly salt catalysts.

Infrared spectroscopy is a useful tool to verify the presence of typical vibrations of the bonds present in the Keggin anion, that is the primary structure of these heteropoly compounds. The region of 1200 to 400 $cm^{-1}$ of FT-IR spectra shows the typical absorption bands (i.e., fingerprint region) of the bonds present in the lacunar Keggin anion.[43] Moreover, when Phosphorus is the central element, FT-IR spectrum allow to assure that saturated heteropolyanion (i.e., $PW_{12}O_{40}^{3-}$ or $PMo_{12}O_{40}^{3-}$) was converted to lacunar anion (i.e., $PW_{11}O_{40}^{7-}$ or $PMo_{11}O_{40}^{7-}$).[33,42]

Infrared spectra of phosphotungstate anion displayed absorption bands at following wavenumbers: 1081, 982, 920, 888 and 790 $cm^{-1}$. These data agree with literature and were assigned to the stretching of P-Oa, W-Od, W-Ob-W and W-Oc-W bonds, respectively.[43,44]

It can be easily done by verifying if there was a splitting of the absorption band corresponding to the vibration of P–O bond, which is commonly noticed at 1080 $cm^{-1}$ in FT-IR spectrum of saturated heteropolyanions. This splitting generates two new absorption bands at

neighboring of this region. Figures 4 and 5 clearly shows that this band in the spectra of both heteropolyacids, and their saturated Cesium salts remained intact.[42]

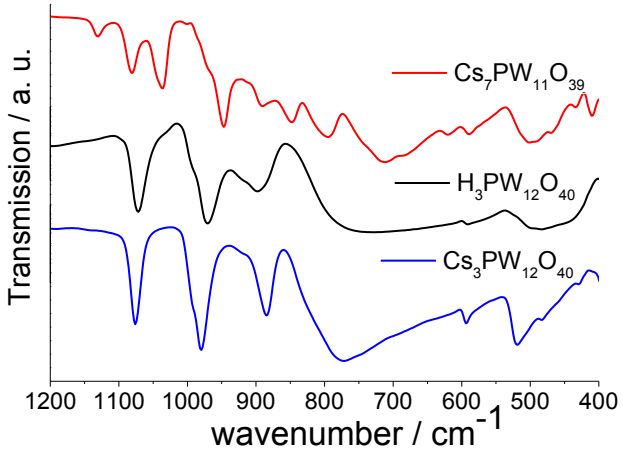


**Figure 4.** FT-IR spectra of lacunar Cesium phosphotungstate salt, phosphotungstic acid and saturated Cesium phosphotungstate salt

Another important aspect is that the absorption bands present in the infrared of heteropolyanion of saturated Cesium salt were very similar to the acid precursor. However, at low wavenumber (ca. 600-400 $cm^{-1}$), some absorption bands were also noticed and were assigned to the presence of Cesium cation. These bands were seen also in the spectra of lacunar Cesium phosphotungstate or phosphomolybdate (Figures 4 and 5).

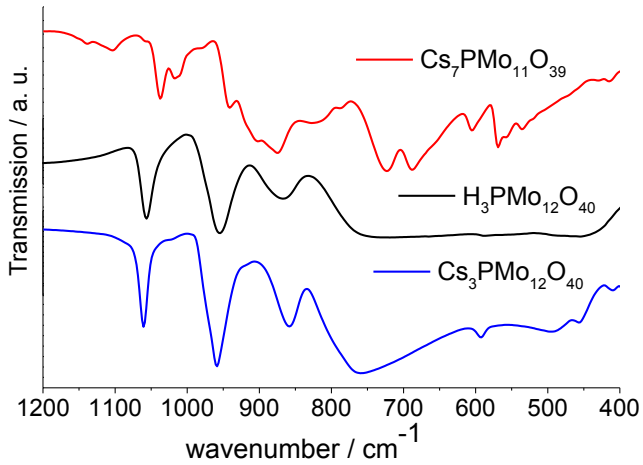


**Figure 5.** FT-IR spectra of lacunar Cesium phosphomolybdate salt, phosphomolybdic acid and saturated Cesium phosphomolybdate salt

If compared to the absorption bands of saturated heteropolyanions, the absorption bands of both Tungsten and Molybdenum salts were shifted to a lower wavenumber, which was attributed to the effect provoked by the higher radius of Cesium ion.[45]

FT-IR spectrum of the saturated anion (i.e., $PW_{12}O_{40}^{3-}$) displayed a typical absorption band at wavenumber 1080 $cm^{-1}$, which was assigned to the stretching of P–$O_a$ bond (Figure 4).

Unlikely, in the FT-IR spectrum of lacunar anion $PW_{11}O_{39}^{7-}$, this vibration resulted in two new bands observed at 1088 and 1037 $cm^{-1}$.

This splitting was the consequence of the vacancy resulting of the removal of one W–O unit, that leads to a decrease in the symmetry of the central unit $PO_4$. Therefore, this is evidence that the lacunar salt was formed.[19]

For the Keggin $PMo_{12}O_{40}^{3-}$ anion, characteristic bands are expected in the regions 1080-1060 $cm^{-1}$ ($\nu_{as}$ P-$O_a$), 990-960 $cm^{-1}$ ($\nu_{as}$ Mo = $O_d$), 900-870 $cm^{-1}$ ($\nu_{as}$ Mo-$O_b$-Mo) and 810-760 $cm^{-1}$ ($\nu_{as}$ Mo-$O_c$-Mo) (Figure 5).[46] Although not very significant, it can be noted that they were slightly shifted toward a lower wavenumber in FT-IR spectrum of $Cs_7PMo_{11}O_{39}$ salt.

As cited for Tungsten salt, the generation of two bands at 1038 and 1016 $cm^{-1}$, assigned to the vibration of P–$O_a$ bond, was attributed to the formation of a characteristic vacancy of the lacunar salts.[46-49]

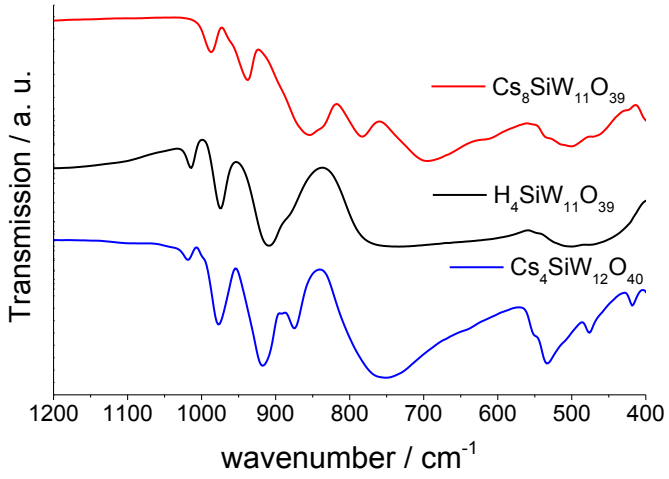


**Figure 6.** FT-IR spectra of lacunar Cesium silicotungstate salt, silicotungstic acid and saturated Cesium silicotungstate salt

FT-IR spectra of silicotungstic catalysts were also obtained and compared (Figure 6). It is known that the absorption bands of $SiW_{11}O_{39}^{8-}$ anion may be present at 952 $cm^{-1}$, 885 $cm^{-1}$, 870 $cm^{-1}$, 797 and 725 $cm^{-1}$ wavelength numbers, which were observed in the spectrum of the $Cs_8SiW_{11}O_{39}$ salt with values 987 $cm^{-1}$ ($\nu_{as}$ W = $O_d$), 939 $cm^{-1}$ ($\nu_{as}$ Si-$O_a$), 856 $cm^{-1}$ ($\nu_{as}$ W-$O_b$-W), 783-696 $cm^{-1}$ ($\nu_{as}$ W-$O_c$-W).[18,42,46]

Nonetheless, unlike of the absorption band attributed to P-O bond, the stretching band of Si-O bond observed in the spectrum of lacunar salt did not undergo a split. Conversely, similarly to the observed in the infrared spectra of lacunar phosphotungstate or phosphomolybdate, at low wavenumber the absorption bands assigned to the Cesium presence were noticed. It can be clearly seen in the FT-IR spectra of three different lacunar Cesium salts (Figure 1SM).

When we compared the spectra of three lacunar Cesium salts with those obtained for the saturated salts, we have found there is a higher number of bands in the region between 950 and 700 $cm^{-1}$, an effect that is consequence of the loss of symmetry generated by removal of one MO unit (M = W, Mo).[50]

The diffractograms of lacunar salts were recorded and correlated with the parent HPAs (Figure 7), and were also compared with the literature.[51] The powder XRD patterns of samples confirms the presence of the secondary structure in HPAs and their lacunar salts.[52] The diffraction lines of the salts presented a similar shape; some were shifted to the lower angles, with a small change of relative intensity, suggesting that although comparable, the structure of anions is slightly different, due to the removal of addenda atom (i.e., W or Mo). This effect was previously reported by Patel et. al, when synthesized Cesium phosphotungstate salts.[53]

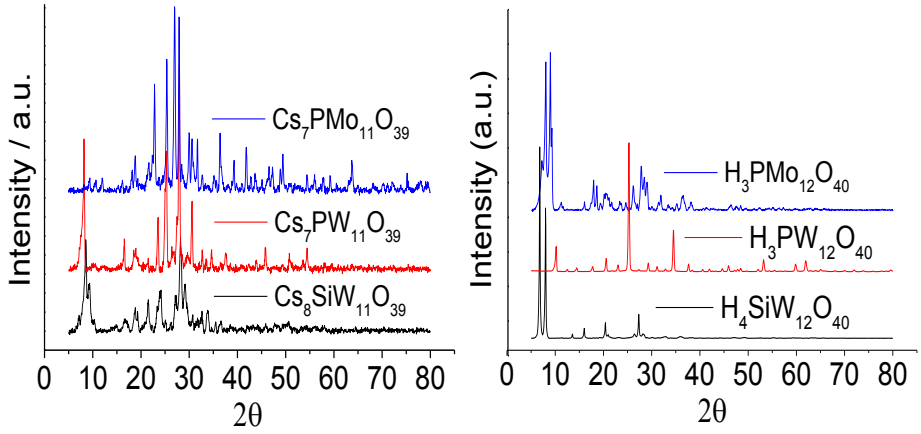


**Figure 7.** Powder XRD patterns of Cesium exchanged silicotungstate, phosphotungstate, and phosphomolybdate lacunar salts and their parent HPAs

Comparing XRD patterns of lacunar Cesium salts with parent acids, it is possible to note that they had unlike degrees of crystallinity, leading to the conclusion that the presence of the larger radium cation (i.e., $Cs^{+}$ ion) contributed to change the crystalline structure of the materials, thus forming a new crystalline phase with different network parameters.

Although we have not found XRD card to a direct contrast, a comparison with literature suggest that $Cs_7PMo_{11}O_{39}$ has a *P42/ncm* space group [54]. In the supplemental material, we have included the XRD patterns of heteropolyacid, saturated Cesium salt and lacunar Cesium salt for each one of heteropoly catalysts synthesized (Figures 2SM-4SM). The comparison of these X-ray diffractograms allows conclude that the either the inclusion of a Cesium cation as well as the removal of one MO unit noticeably increases the number and the intensity of the diffraction lines of Keggin anion.

A comparison of XRD patterns of $Cs_4SiW_{12}O_{40}$ and literature assure that the saturated Cesium salt diffractogram presented high intensity peaks (i.e., labelled with Miller indices, Figure 4SM), that were assigned to the cubic Pn3-m space group (# 224) [55].

The diffractogram of lacunar salt $Cs_8SiW_{11}O_{39}$ displayed a lower crystallinity, with peaks of lower intensity and greater enlargement. The profile of this diffractogram showed characteristic peaks at angles near to 10 and 28° range 2θ, confirming the formation of a typical crystalline phase.[53] The same was observed for the $Cs_7PW_{11}O_{39}$ and $Cs_7PMo_{11}O_{39}$ salts, whose XRD profiles have peaks similar those reported in the literature.[56,57]

From the XRD spectra, it was possible to calculate the crystallite size of three different Cesium salts using the Scherrer equation (Equation 1). In this equation, "K" is a constant that depends on the shape of the particles, which generally goes from 0.9–1.0; "λ" is the wavelength of the electromagnetic radiation, "β" is the width at half the height of the most intense diffraction peak in radians, and "cos θ" referring to the angle of the peak in question also in radians.

$$\text{Crystallite size} = (K \times \lambda) / (\beta \times \cos \theta)$$

(Equation 1)

Were obtained the values 28, 47 and 70 nm for crystallite size of the lacunar salts (i.e., $Cs_8SiW_{11}O_{39}$, $Cs_7PW_{11}O_{39}$ and $Cs_7PMo_{11}O_{39}$, respectively), thus confirming the lower crystallinity for the $Cs_8SiW_{11}O_{39}$ salt, followed by $Cs_7PW_{11}O_{39}$ and $Cs_7PMo_{11}O_{39}$.

The total acidity of the Cesium lacunar salts and their parent HPAs was determined by potentiometric titration using *n*-butylamine (Figure 8). The initial electrode potential ($E_i$) allows classify the strength of the acid sites; very strong ($E_i > 100$ mV), strong ($0 < E_i < 100$ mV), weak $E_i < 0$ mV) and very weak ($E_i < -100$ mV).[58]

The values of E*i* exhibited by the acid sites of lacunar catalysts are classified as "very weak", assuring that almost all the protons were exchanged by Cesium cations (Figure 8). These results agree with the literature.[59]

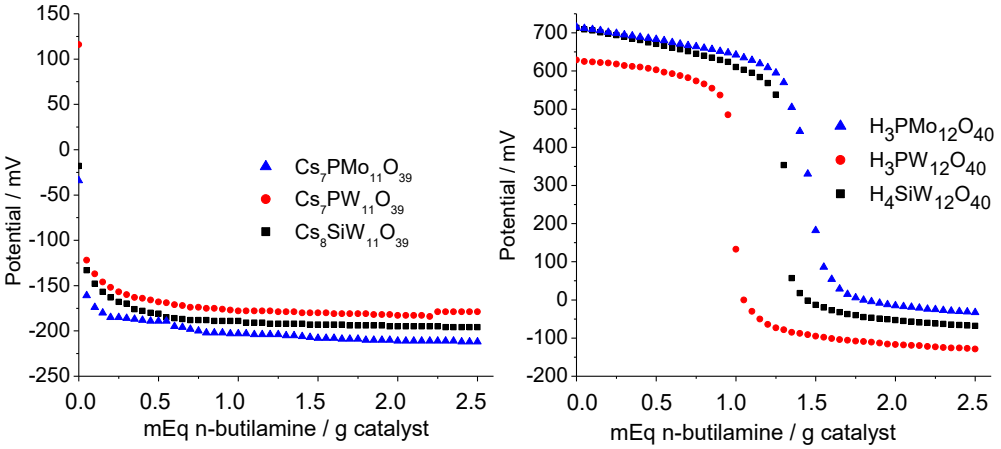


**Figure 8.** Potentiometric titration curves with n-butylamine of the synthesized salts and respective HPAs

*2.2. Catalytic tests*

Initially, we investigated the catalytic activity of metal unexchanged-Keggin HPAs. In this case, the Keggin anions were intact; it means that no structural vacancy was created in the HPA and that their high Brønsted acidity was untouched. Figure 9 displays main results of conversion and reaction selectivity.

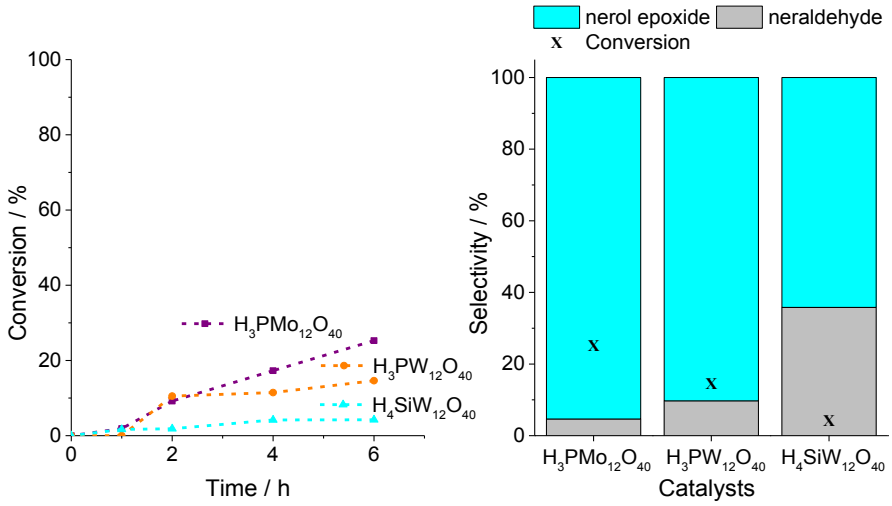


**Figure 9.** Conversion and selectivity of nerol oxidation reactions with $H_2O_2$ in the presence of Keggin heteropolyacid catalysts[a]
[a]Reaction conditions: nerol (1.38 mmol), $H_2O_2$ (2.75 mmol), temperature (333 K), catalyst (4 mol%), $CH_3CN$ (10 mL)

Regardless the high selectivity for oxidation products (i.e., nerol epoxide and neraldehyde), a poor conversion was achieved in HPA-catalyzed reactions. This suggests that in the presence of saturated anions, the efficiency of oxidation reactions is compromised, regardless of the total solubility of catalysts.

The activity of lacunar Cesium salts was evaluated, and the results are presented in Figure 8. Unlike the parent HPAs, the totally exchanged Cesium salts were almost insoluble. This modification reduced the activity of HPAs salts, except for the silicotungstate catalyst. Noticeably, this catalyst was highly active achieving a conversion close to 90% after 8 h of reaction (Figure 9). Contrariwise, the reactions in the presence of Cesium phosphotungstate or phosphomolybdate salts had a low conversion (ca. 5%, Figure 10).

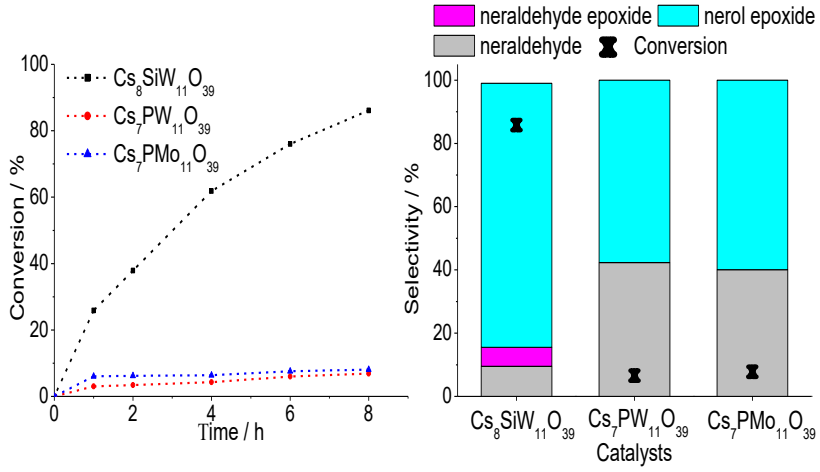


**Figure 10.** Conversion and selectivity of nerol oxidation reactions with $H_2O_2$ in the presence of Cesium exchanged lacunar HPA salts[a]
[a]Reaction conditions: nerol (1.38 mmol), $H_2O_2$ (2.75 mmol), temperature (333 K), catalyst (4 mol%), $CH_3CN$ (10 mL)

Silicotungstate lacunar salt previously demonstrated to be an active catalyst in oxidation reactions; $K_8SiW_{11}O_{39}$ efficiently catalyzed the borneol oxidation with $H_2O_2$ to camphor.[31] Although a different substrate (i.e., secondary, saturated and cyclic alcohol), and a different solvent (dimethylacetamide) have been used in that work, $K_8SiW_{11}O_{39}$ was an effective catalyst, and the oxidations reactions achieved a high TON.[31]

Notwithstanding heteropolyanion present in the Cesium salt catalysts, neraldehyde and mainly nerol epoxide were always the major products (Scheme 1). These main reaction products were identified by GC-MS analyses (supplemental material). However, only in the presence of $Cs_8SiW_{11}O_{39}$, neraldehyde epoxide was detected.

The high epoxide selectivity is a positive aspect of this catalyst; in general, epoxidation processes have been carried out with corrosive stoichiometric organic oxidants (i.e., *meta*-chloroperbenzoic acid), which are difficult to handling and unfriendly to the environment.[60]

The highest activity of the $Cs_8SiW_{11}O_{39}$ salt may be related to their physical properties. Among the three Cesium salts, it presented the highest surface area (Table 1). Moreover, according to the X-rays diffractogram shown in Figure 7, it exhibited a lower crystallinity than

others, with larger diffraction peaks. This feature may have favored the interaction between the hydroxyl groups of peroxide and the surface of $Cs_8SiW_{11}O_{39}$ catalyst, which may have allowed a higher number of interactions with oxidant molecules. Therefore, a greater number of reactive Oxygen species may be formed, due to the cleavage of O–O bonds of $H_2O_2$, improving the epoxidation.[58,61]

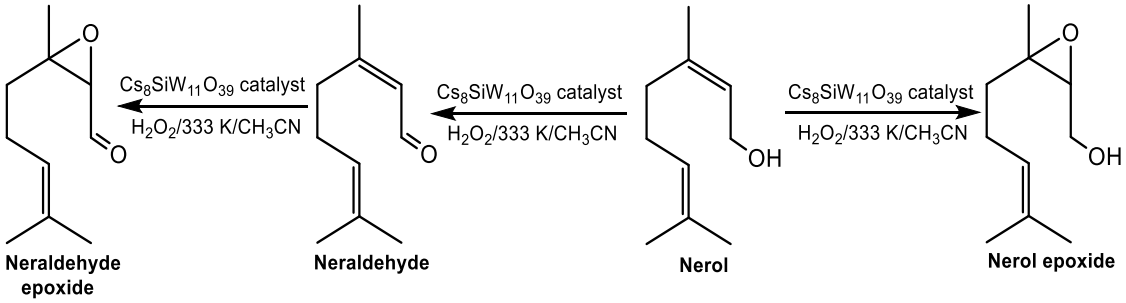


**Scheme 1.** Main products of nerol oxidation with Hydrogen peroxide obtained in reactions in the presence of Cesium exchanged lacunar salts

Once the $Cs_8SiW_{11}O_{39}$ was the most active catalyst, it was selected to study the impact of main reaction parameters. Figure 11 displays the effects of oxidant load on the conversion and reaction selectivity. A higher oxidant load enhanced the reaction conversion; conversely, the selectivity was minimally affected and nerol epoxide was always the major product.

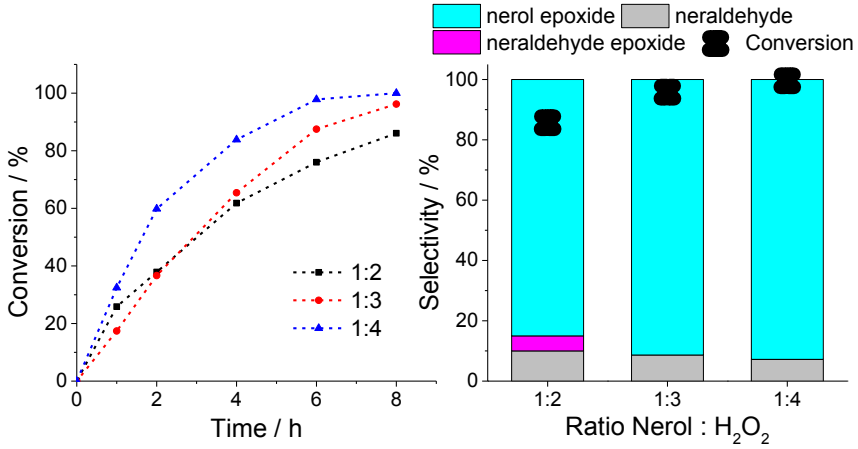


**Figure 11.** Effect of nerol:$H_2O_2$ molar ratio on the conversion and selectivity of the $Cs_8SiW_{11}O_{39}$-catalyzed oxidation reactions[a]
[a]Reaction conditions: nerol (1.38 mmol), temperature (333 K), catalyst (4 mol%), $CH_3CN$ (10 mL), time (8 h)

Although an increase of oxidant load has resulted in a slight improvement on conversion and selectivity, we decided to keep the proportion between oxidant and nerol equal to 2:1 on the next catalytic runs, aiming to make the effects more visible.

The catalyst concentration should not affect the conversion of the reactions that had achieved the equilibrium. However, the kinetic curves shown in Figure 12 demonstrated that

within the period investigated, none of them reached a stationary conversion, indicating that they are out of the equilibrium. The reactions carried out with a catalyst load lower than 2 mol%, accomplished different conversions, nonetheless, with concentrations varying of 3 to 5 mol%, comparable results were attained.

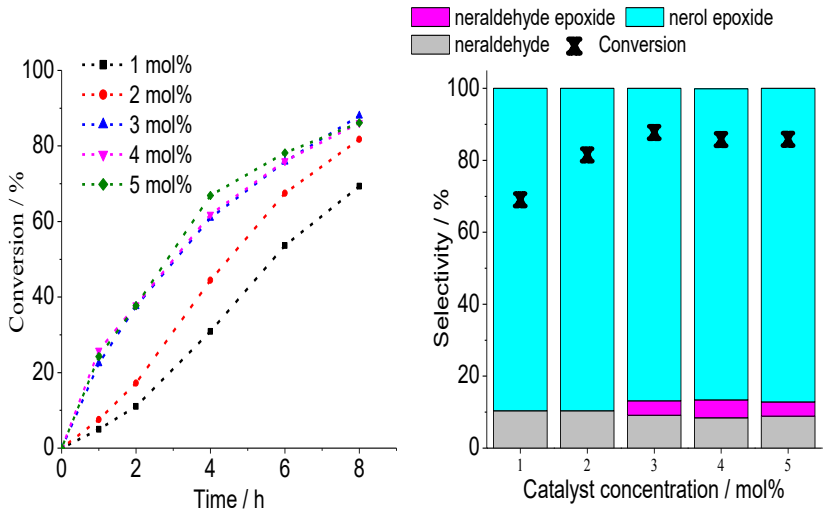


**Figure 12.** Effect of catalyst concentration on the conversion and selectivity of the $Cs_8SiW_{11}O_{39}$-catalyzed nerol oxidation reactions with $H_2O_2$[a]
[a]Reaction conditions: nerol (1.4 mmol), $H_2O_2$ (2.8 mmol), temperature (333 K), $CH_3CN$ (10 mL)

Since that the reactions with a catalyst concentration higher than 4 mol% have not presented any beneficial effect, this was the load used in the next experiments, for instance, when the temperature effects were assessed. The kinetic curves of reactions and the conversion and selectivity accomplished are shown in Figure 13.

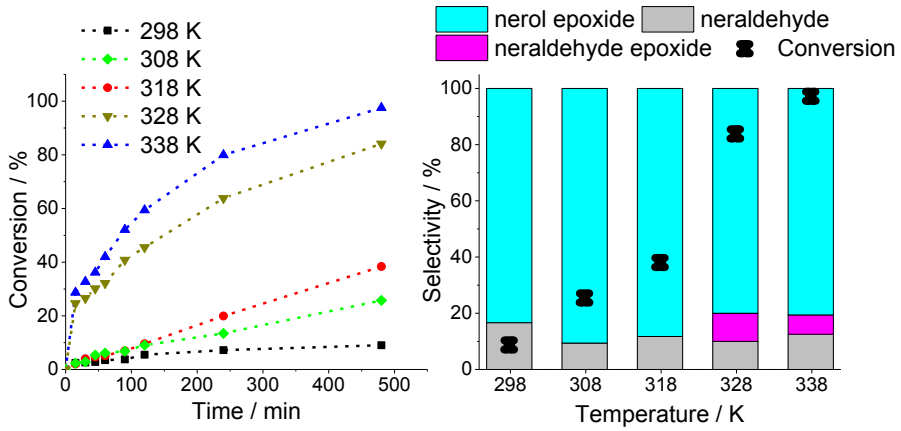


**Figure 13.** Effects of temperature on the conversion and selectivity of the $Cs_8SiW_{11}O_{39}$-catalyzed nerol oxidation reactions with $H_2O_2$[a]
[a]Reaction conditions: nerol (1.4 mmol), $H_2O_2$ (2.75 mmol), catalyst (4 mol %), $CH_3CN$ (10 mL)

The high conversions achieved at high temperatures are evidence of the endothermic character of the reaction. The reaction selectivity was also impacted; while nerol epoxide and

neraldehyde were formed in all the reactions, only at temperatures higher than 318 K neraldehyde epoxide was obtained.

The catalytic activity of $Cs_8SiW_{11}O_{39}$ was compared to their precursor salts (Figure 14). This assessment may be very useful to understand which are the real active sites of the $Cs_8SiW_{11}O_{39}$ catalyst, and what their importance in the oxidation reactions.

The results shown in Figure 14 suggests that there is some synergy between Silicon and Tungsten atoms present in the structure of lacunar silicotungstate heteropolyanion; although nerol epoxide was the main product in all the reactions, only in the presence of $Cs_8SiW_{11}O_{39}$ catalyst the nerol oxidation reaction attained a high conversion (*ca*. 90%).

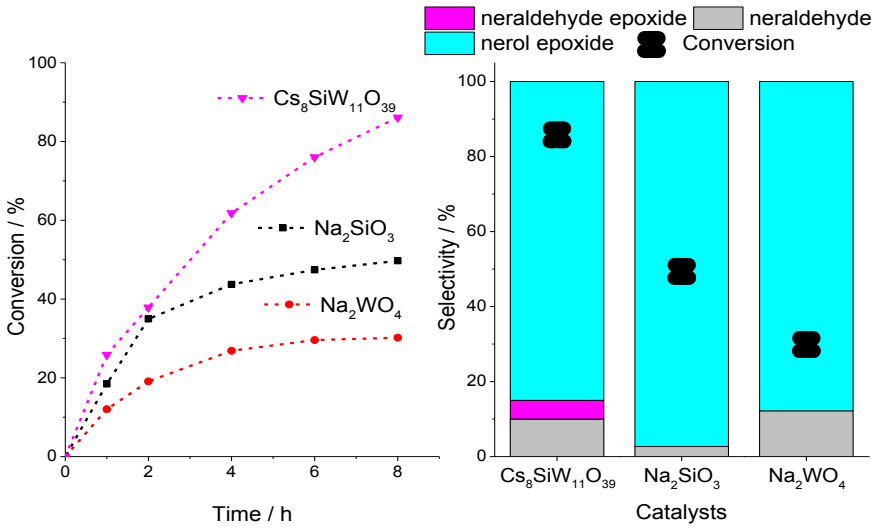


**Figure 14.** Comparison of the catalytic activity of the precursor salts and $Cs_8SiW_{11}O_{39}$ on the nerol oxidation reactions with $H_2O_2$[a]
[a]Reaction conditions: nerol (1.38 mmol), $H_2O_2$ (2.75 mmol), temperature (333 K), catalyst (4 mol%), $CH_3CN$ (10 mL)

The effects of proton exchanges by different alkaline metal cations were also assessed (Figure 15). It was verified that the size of cation radium affected the solubility of lacunar silicotungstate salts; in according with sequence $Cs^+ > K^+ > Na^+$, the salts of Cesium, Potassium, and Sodium were insoluble, partially or completely soluble, respectively.

The reactions in the presence of Cesium or Sodium silicotungstate salts (i.e., lacunar salts) have achieved highest conversion. However, Sodium silicotungstate-catalyzed reactions achieved the maximum conversion faster than that in the presence of the Cesium salt. There is a key aspect unequivocally demonstrated in Figure 15; the vacancy on Cesium heteropolyanion salt also played a vital role. While saturated Cesium silicotungstate salt (i.e., $Cs_4SiW_{12}O_{40}$) was almost inactive, the lacunar salt was the most effective (i.e., $Cs_8SiW_{11}O_{39}$). Moreover, we also

demonstrated the Cesium cation had also an important effect; the reactions in the presence of lacunar Potassium silicotungstate salt achieved only a poor conversion (ca. 20%).

When we compared the performance of silicotungstate catalysts, we realized that the activity obeyed the trends: $H_4SiW_{12}O_{40(soluble)} \approx Cs_4SiW_{12}O_{40(insoluble)} < K_8SiW_{11}O_{39(partially\ soluble)} < Cs_8SiW_{11}O_{39(insoluble)} \leq Na_8SiW_{11}O_{39(soluble)}$ (Figures 9 and 15). Therefore, we concluded that two aspects played a pivotal aspect on these reactions: the vacancy on the heteropolyanion and the solubility of the catalyst. Nevertheless, it is not the only important characteristic to be considered; although being equally insoluble, the $Cs_7PW_{11}O_{39}$ and $Cs_7PMo_{11}O_{39}$ catalysts had a low activity (Figure 10). Thus, the composition of heteropolyanion has also an essential role on catalytic activity.

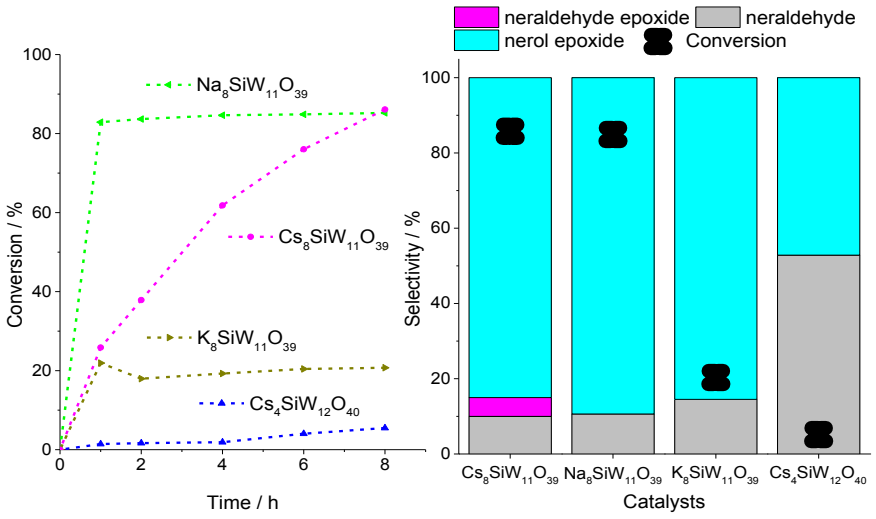


**Figure 15.** Conversion and selectivity of the nerol oxidation by $H_2O_2$ catalyzed by different metal exchanged-silicotungstate salts[a]
[a]Reaction conditions: nerol (1.38 mmol), $H_2O_2$ (2.75 mmol), temperature (333 K), catalyst (4 mol%), $CH_3CN$ (10 mL)

The efficiency of $Cs_8SiW_{11}O_{39}$ catalyst was also evaluated on the oxidation reactions of other terpenic alcohols (Figure 16). Our main objective was to verify how the electronic and steric effects may affect the oxidation or epoxidation of different olefinic double bonds. All the alcohols have olefinic double bonds, which may be potentially epoxidized (Figure 17). However, all the trisubstituted double bonds without an allylic hydroxyl group were not epoxidized.

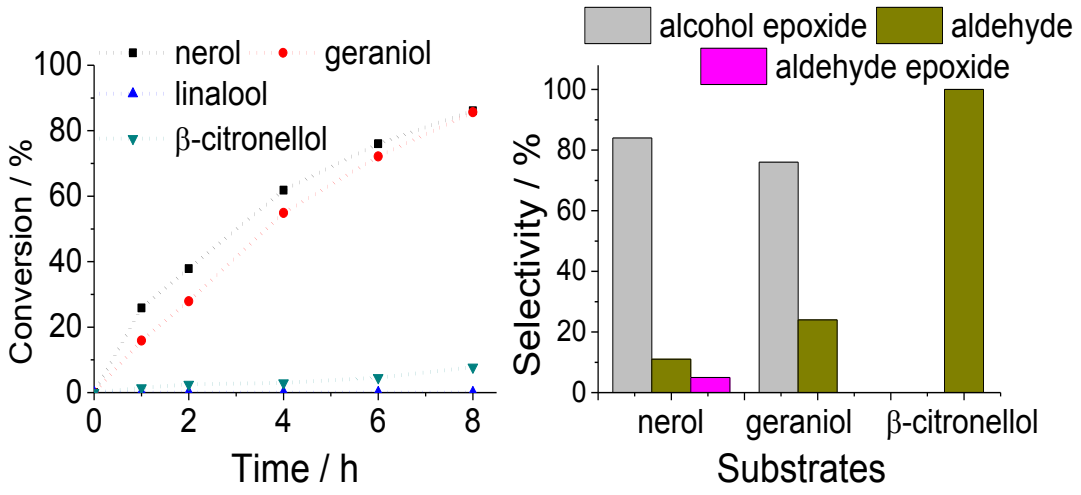


**Figure 16.** Conversion and selectivity of $Cs_8SiW_{11}O_{39}$-catalyzed terpenic alcohols oxidation by $H_2O_2$[a] [a]Reaction conditions: terpenic alcohol (1.38 mmol), $H_2O_2$ (2.75 mmol), temperature (333 K), catalyst (4 mol%), $CH_3CN$ (10 mL)

The presence of two donating methyl groups hampered the epoxidation of this double bond. Conversely, the allylic hydroxyl groups may activate the double bonds by the electron withdrawing effect, explaining the formation of the nerol and geraniol epoxides. A similar successful reaction was achieved by Balula et al., when used homogeneous lacunar catalyst (i.e., $PW_{11}$) to oxidize geraniol with $H_2O_2$ in $CH_3CN$ solutions.[62] Surprisingly, the terminal double bond of linalool was unreactive. Nonetheless, molecular models clearly showed that it is a consequence of high steric hindrance caused by the two allylic methyl groups of linalool (Figure 17).

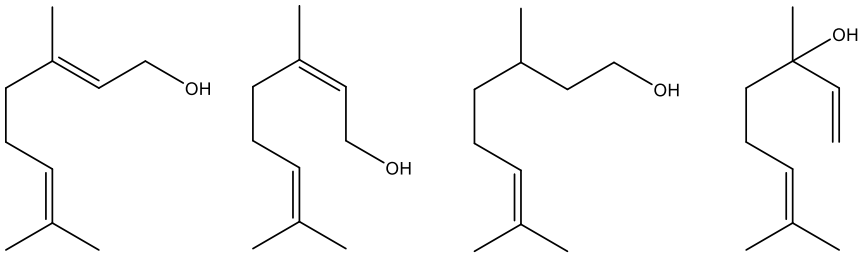


**Figure 17.** Structure of terpenic alcohols

The reactivity of hydroxyl groups in relation to the oxidation was also different. However, even though nerol, geraniol, and β-citronellol having terminal hydroxyl groups, only the reactions with allylic alcohols achieved high conversions (ca. 90%; Figure 16).

The reusability of the most active silicotungstate catalyst (i.e., $Cs_8SiW_{11}O_{39}$) was evaluated (Figure 18). We have observed that even after the fifth consecutive reaction, the catalyst showed only a little decrease of efficiency; high conversion (90%) and selectivity (85%

for epoxide nerol) were reached. In addition, high recovery rates of catalyst were obtained in all the reuses.

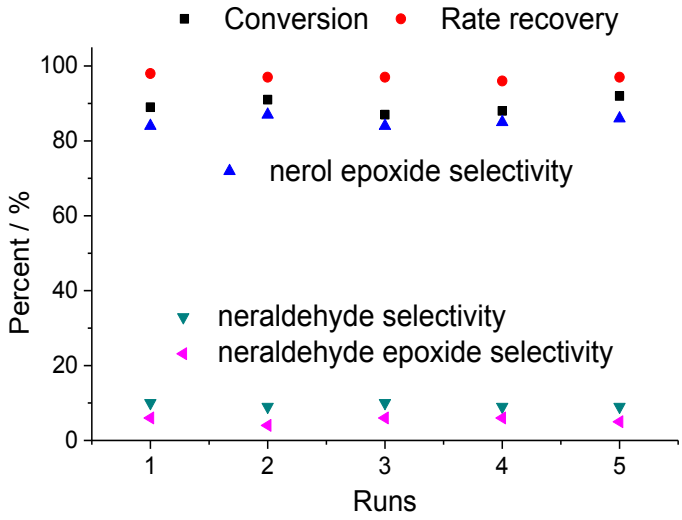


**Figure 18.** Recovery/ reuse of $Cs_8SiW_{11}O_{39}$ catalyst on nerol oxidation with Hydrogen peroxide[a]
[a]Reaction conditions: nerol (1.375 mmol), $H_2O_2$ (2.750 mmol), temperature (333 K), time (8 h), catalyst (4 mol%), $CH_3CN$ (10 mL)

The integrity of catalyst after fifth reuse cycle was checked trough analysis of XRD, FT-IR, porosity, and titration of acid sites with n-butylamine (Table 2SM, Figures 5SM–7SM, Supplemental material). A comparison of XRD diffractograms of the fresh catalyst and after it has been reused five times showed that there was a loss of crystallinity, with enlargement of diffraction peaks (Figure 5SM). However, the surface area and porosity of the catalyst remained almost the same (Table 2SM). The main absorption bands of reused catalyst were very similar to the fresh catalyst, indicating that Keggin anion remained intact. Therefore, we can conclude that despite the changes on crystallinity level, the catalyst was stable and active after has been fifth times reused.

## 3. Conclusions

The efficiency of various Keggin heteropolyacid salts was evaluated in oxidation reactions of the nerol with Hydrogen peroxide. Highlighted, lacunar Cesium silicotungstate salt was the most active and selective catalyst. The activity of most outstanding catalyst (i.e., $Cs_8SiW_{11}O_{39}$) was compared with various catalysts; their precursor salts (i.e., $Na_2SiO_3$ and $Na_2WO_4$), other lacunar Cesium HPA salts (i.e., $Cs_7PW_{11}O_{39}$, $Cs_7PMo_{11}O_{39}$), other lacunar silicotungstates (i.e., $Na_8SiW_{11}O_{39}$ and $K_8SiW_{11}O_{39}$), and their parent Keggin HPAs. It was demonstrated that the presence of Silicon in the Keggin anion, as well as the presence of a vacancy in the heteropolyanion (i.e., $Cs_4SiW_{12}O_{40}$ was almost inactive), were the key aspects for these

reactions. Once having been established that catalysts with lacunar silicotungstate anions were the most active, we have assessed the effect of countercation. Lacunar Sodium undecasilicotungstate (i.e., $Na_8SiW_{11}O_{39}$), a soluble catalyst was also highly active. Conversely, lacunar Potassium undecasilicotungstate (i.e., $K_8SiW_{11}O_{39}$), that is an insoluble solid catalyst likewise the Cesium salt, presented a lower efficiency. It can be assigned to its lower surface area if compared to the Cesium salt. Effects of the main reaction parameters were investigated, being the 1:4 molar ratio of substrate to oxidant, 3 mol% of catalyst load, and 333 K the best reaction conditions. The alcohol structure showed to be a pivotal aspect on this reaction; while geraniol and nerol (i.e., allylic alcohols) were virtually converted to epoxides, with a minor formation of aldehyde, β-citronellol provided mainly β-citronellal with a low conversion. Linalool, tertiary alcohol, was not epoxidized under our reaction conditions. The reusability of $Cs_8SiW_{11}O_{39}$ catalyst was another aspect successfully investigated; it was recovered and reused without loss in activity or selectivity during five reuse cycles.

**Supporting Information Summary**

The details of the synthesis and catalysts characterization are in supporting information as well as the general procedure used on catalytic runs. The scanning electron microscopy (SEM) images obtained with 2,500x magnification of metal-substituted phosphotungstic acid Potassium salts and their EDS spectra were also presented on this section.

**Acknowledgements**

The authors thank the Federal University of Viçosa, the PPGMQ-MG, and the development agencies CNPq and FAPEMIG. This study was financed in part by the Coordenação de Aperfeiçoamento de Pessoal de Nível Superior – Brasil (CAPES) – Finance Code 001.

**Conflict of Interest**

The authors declare no conflict of interest.

**Keywords:** green oxidation • heterogeneous catalysis • lacunar Cesium heteropolyacid salt • renewable feedstock

**References**

[1] Y. Zheng, H. Zhang, L. Wang, S. Zhang, S. Wang, *Front. Chem. Sci. Eng.* **2016**, *10*, 139-146.
[2] M. J. da Silva, M. G. Teixeira, *RSC Adv.* **2017**, *7*, 8192-8199.

[3] A. Gaurav, F. T. T. Ng, G. L. Rempel, *Green Energy Environ.* **2016**, *1*, 62.

[4] M. Aminia, M. M. Haghdoostb, M. Bagherzadeh, *Coordin. Chem. Rev.* **2014**, *268*, 83–100.

[5] S. S. Wang, G.-Y. Yang, *Chem. Rev.* **2015**, *115*, 4893−4962.

[6] A. C. Estrada, I. C. M. S. Santos, M. M. Q. Simoes, M. P. M. S. Neves, J. A. S. Cavaleiro, A. M. V. Cavaleiro, *Appl. Catal., A* **2011**, *392*, 28-35.

[7] Y. Zhou, G. Chen, Z. Long, J. Wang, *RSC Adv.* **2014**, *4*, 42092-42113.

[8] M. J. da Silva, N. A. Liberto, *Curr. Org. Chem.* **2016**, *20*, 1263-1283.

[9] M. J. da Silva, C. M. de Oliveira, *Curr. Catal.* **2018**, *7*, 26-34.

[10] T. Okuhara, T. Nishimura, M. Misono, *Chem. Lett.* **1995**, *24*, 155-156.

[11] K. Inumaru, H. Nakajima, T. Ito, M. Misono, *Chem. Lett.* **1996**, *25*, 559-561.

[12] I. V. Kozhevnikov, *Chem. Rev.* **1998**, *98*, 171-198.

[13] Y. Kamiya, S. Sano, Y. Miura, Y. Uchida, Y. Ogawa, Y. Iwase, T. Okuhara, *Chem. Lett.* **2010**, *39*, 881-883.

[14] Y. Iwase, S. Sano, L. Mahardiani, R. Abe, Y. Kamiya, *J. Catal.* **2014**, *318*, 34-42.

[15] H. W. Park, S. Park, D. R. Park, J. H. Choi, I. K. Song, *Catal. Commun.* **2010**, *12*, 1-4.

[16] S. Rana, S. Mallick, L. Mohapatra, G. B. B. Varadwaj, K. M. Parida, *Catal. Today* **2012**, *198*, 52-58.

[17] N. Mizuno, K. Yamaguchi, K. Kamata, *Coord. Chem. Rev.* **2005**, *249*, 1944-1956.

[18] J. H. Choi, J K. Kim, D. R. Park, T. H. Kang, J. H. Song, I. K. Song, *J. Mol. Catal. A: Chem.* **2013**, *371*, 111-117.

[19] R. Karcz, P. Niemiec, K. Pamin, J. Połtowicz, J. Kryściak-Czerwenka, B. D. Napruszewska, A. Michalik-Zym, M. Witko, R. Tokarz-Sobieraj, E. M. Serwicka, *Appl. Catal., A* **2017**, *542*, 317-326.

[20] L. Zhou, L. Wang, Y. Diao, R. Yan, S. Zhang, *Mol. Catal.* **2017**, *433*, 153-161.

[21] A. C. Estrada, M. M. Q. Simoes, I. C. M. S. Santos, M. G. P. M. S. Neves, J. A. S. Cavaleiro, A. M. V. Cavaleiro, *ChemCatChem* **2011**, *3*, 771-779.

[22] K. Patel, P. Shringarpure, A. Patel, *Transition Met. Chem.* **2011**, *36*, 171-177.

[23] I. C. M. S. Santos, M. M. Q. Simoes, M. S. S. Balula, M. G. P. M. S. Neves, J. A. S. Cavaleiro, A. M. V. Cavaleiro, *Synlett* **2008**, *2008*, 1623-1626.

[24] A. C. Estrada, M. M. Q. Simoes, I. C. M. S. Santos, M. G. P. M. S. Neves, A. M. S. Silva, J. A. S. Cavaleiro, A. M. V. Cavaleiro, *Appl. Catal., A* **2009**, *366*, 275-281.

[25] A. C. Estrada, M. M. Q. Simoes, I. C. M. S. Santos, M. G. P. M. S. Neves, J. A. S. Cavaleiro, A. M. V. Cavaleiro, *Monatsh. Chem.* **2010**, *141*, 1223-1235.

[26] L. A. S. Viana, G. R. N. da Silva, M. J. da Silva, *Catal. Lett.* 2018, *148*, 374-382.

[27] Z. Guo, B. Liu, Q. Zhang, W. Deng, Y. Yang, *Chem. Soc. Rev.* **2014**, *43*, 3480-3524.

[28] S. Serra, D. De Simeis, *Catalysts* **2018**, *8*, 362.

[29] K. C. Nicolaou, C. V. C. Prasad, P. K. Somers, C. K. Hwang, *J. Am. Chem. Soc.* **1989**, *111*, 5330-5334.

[30] L. Li, B. Liu, Z. Wu, X. Yuan, H. Luo, *Chem. Eng. J.* **2015**, *280*, 670-676.

[31] M. J. da Silva, P. H. S. Andrade, S. O. Ferreira, C. B. Vilanculo, C. M. Oliveira, *Catal. Lett.* **2018**, *148*, 2516.

[32] P. T. Anastas, M. M. Kirchhoff, *Acc. Chem. Res.* **2002**, *35*, 686-694.

[33] N. C. Coronel, M. J. da Silva, *J. Cluster Sci.* **2018**, *29*, 195-205.

[34] J. S. Santos, J. A. Dias, S. C. L. Dias, F. A. C. Garcia, J. L. Macedo, F. S. G. Sousa, L. S. Almeida, *Appl. Catal., A* **2011**, *394*, 138-148.

[35] A. Vakulenko, Y. Dobrovolsky, L. Leonova, A. Karelin, A. Kolesnikova, N. Bukun, *Solid State Ionics* **2000**, *136*, 285-290.

[36] L. R. Pizzio, M. N. Blanco, *Microporous Mesoporous Mater.* **2007**, *103*, 40-47.

[37] Y. Miura, H. Imai, T. Yokoi, T. Tatsumi, Y. Kamiya, *Microporous Mesoporous Mater.* **2013**, *174*, 34-43.

[38] M. Sun, J. Zhang, C. Cao, Q. Zhang, Y. Wang, H. Wan, *Appl. Catal., A* **2008**, *349*, 212-221.

[39] T. Okuhara, H. Watanabe, T. Nishimura, K. Inumaru, M. Misono, *Chem. Mater.* **2000**, *12*, 2230-2238.

[40] M. Thommes, K. Kaneko, A. V. Neimark, J. P. Olivier, F. Rodriguez-Reinoso, J. Rouquerol, K. S. Sing, *Pure Appl. Chem.* **2015**, *87*, 1051-1069.

[41] K. S. W. Sing, *Pure Appl. Chem.* **1985**, *57*, 603-619.

[42] Ch. R. Kumar, S. Gatla, O. Mathon, S. Pascarelli, N. Lingaiah, *Appl. Catal., A* **2015**, *502*, 297-304.

[43] Ch. R. Kumar, K. T. V. Rao, P. S. S. Prassad, N. Lingaiah, *J. Mol. Catal. A: Chem.* **2011**, *337*, 17-24.

[44] C. Rocchiccioli-Deltcheff, M. Fournier, R. Franck, R. Thouvenot, *Inorg. Chem.* **1983**, *22*, 207-216.

[45] O. A. Kholdeeva, M. P. Vanina, M. N. Timofeeva, R. I. Maksimovskaya, T. A., Trubitsina, M. S. Melgunov, E. B. Burgina, J. Mrowiec-Bialon, A. B. Jarzebski, C. L. Hill, *J. Catal.* **2004**, *226*, 363–371.

[46] D. Bajuk-Bogdanović, I. Holclajtner-Antunovi, M. Todorovi, U. B. Mio, J. Zakrzewska, *J. Serb. Chem. Soc.* **2008**, *73*, 197-209.

[47] A. Popa, V. Sasca, D. Bajuk–Bogdanovi, I. Holclajtner–Antunovic, *J. Therm. Anal. Calorim.* **2016**, *126*, 1567-1577.

[48] C. Rocchiccioli-Deltcheff, M. Fournier, *J. Chem. Soc., Faraday Trans.* **1991**, *87*, 3913-3920.

[49] N. Mizuno, M. Misono, *Chem. Rev.* **1998**, *98*, 199-218.

[50] C. Paze, S. Bordiga, A. Zecchina, *Langmuir* **2000**, *16*, 8139-8144.

[51] F. J. Berry, G. R. Derrick, M. Mortimer, *Polyhedron* **2014**, *68*, 17-22.

[52] J. A. F. Gamelas, M. R. Soares, A. Ferreira, A. M. V. Cavaleiro, *Inorg. Chim. Acta* **2003**, *342*, 16-22.

[53] L. Méndez, R. Torviso, L. Pizzio, M. Blanco, *Catal. Today* **2011**, *173*, 32-37.

[54] P. Shringarpure, B. Tripuramallu, K. Patel, A. Patel, *J. Coordin. Chem.* **2011**, *64,* 4016–4028.

[55] A. Patel, S. Pathan, *J. Coordin. Chem.* **2012**, *65,* 3122–3132.

[56] Y. Ogasawara, S. Uchida, T. Maruichi, R. Ishikawa, N. Shibata, Y. Ikuhara, N. Mizuno, *Chem. Mater.* **2013**, *25*, 905−911.

[57] M. Sun, J. Zhang, C. Cao, Q. Zhang, Y. Wang, H. Wan, *Appl. Catal., A* **2008**, *349*, 212-221.

[58] R. A. Frenzel, G. P. Romanelli, L. R. Pizzio, *Mol. Catal.* **2018**, *457*, 8-16.

[59] N. Essayem, G. Coudurier, M. Fournier, J. Vedrine, *Catal. Lett.* **1995**, *34*, 223-235.

[60] H. Hussain, A. Al-Harrasi, I. R. Green, I. Ahmed, G. Abbas, N. Ur Rehman, *RSC Adv.* **2014**, *4*, 12882-12917.

[61] M. Ziolek, I. Sobczak, P. Decyk, L. Wolski, *Catal. Commun.* **2013**, *37*, 85-91.

[62] S. S. Balula, I. C. M. S. Santos, L. Cunha-Silva, A. P. Carvalho, J. Pires, J. C. Freire, J. A. S. Cavaleiro, B. de Castro, A. M. V. Cavaleiro, *Catal. Today* **2013**, *203*, 95–102.

**Supporting Information**

# Cesium-Exchanged Lacunar Keggin Heteropolyacid Salts: Efficient Solid Catalysts for the Green Oxidation of Terpenic Alcohols with Hydrogen Peroxide

Daniel Carreira Batalha, Sukarno Olavo Ferreira, Rene Chagas da Silva, and Márcio José da Silva*

## Experimental Section

### Catalyst preparation

Cesium salts $Cs_yXM_{11}O_{39}$ (X = Si or P; M = W or Mo; y = 8 or 7) were synthesized by precipitation according to the methodology adapted from the literature.[31] Unlike most processes in the literature,[1,2] which using the HPAs as starting reactants to synthesize the salts, herein were used solely salts as precursor: $Na_2SiO_3$ (2.5 mmol) and $Na_2WO_4.2H_2O$ (0.028 mol) for the $Cs_8SiW_{11}O_{39}$ lacunar salt; $Na_2WO_4.2H_2O$ (0.028 mol) and $Na_2HPO_4.7H_2O$ (2.5 mmol) for the $Cs_7PW_{11}O_{39}$ salt; $Na_2MoO_4$ (0.028 mol) and $Na_2HPO_4.7H_2O$ (2.5 mmol) for the $Cs_7PMo_{11}O_{39}$ lacunar salt.

Typically, an acidic aqueous solution containing the Tungsten or Molybdenum precursor (i.e., $Na_2WO_4$ or $Na_2MoO_4$), were added to the other solution containing the Silicon or phosphorus precursor salt (i.e., $Na_2SiO_3$ or $Na_2HPO_4$), depending on the goal heteropolyanion (i.e., $SiW_{12}O_{40}^{4-}$, $PW_{12}O_{40}^{3-}$ or $PW_{12}O_{40}^{3-}$). These solutions were stirred for 30 minutes at room temperature, resulting in the saturated Sodium HPA salts (i.e., $Na_3PW_{12}O_{40}$, $Na_3PMo_{12}O_{40}$ and $Na_4SiW_{12}O_{40}$). An addition of HCl (*ca*. 0.10 mol L-) adjusted the pH to the adequate range (pH = 5.4, $SiW_{11}O_{39}^{8-}$ and $PW_{11}O_{39}^{7-}$; pH = 4.5, $PMo_{11}O_{39}^{7-}$), converting the saturated anions to lacunar anions. The solutions were stirred and heated at 353 K / 60 min. Then, after cooling the solution to room temperature, 0.1 mol of $CsCl_{(s)}$ was added to precipitate the Cesium HPA salt. The solid salt obtained was washed twice (50 mL, 1.0 $molL^{-1}$ $CsCl_{(aq)}$), and once with 50 mL of cold distilled water, being then dried to the air. After this step, Cesium salts were dried in an oven at 423 K / 5 h.

### Catalyst characterization

Surface areas were determined by the Brunauer-Emmett-Teller (BET) method, and the diameter and pores volume distribution were calculated according to the Functional Density Theory (DFT), performed on NOVA 1200 Quantachrome, through the isotherms of physical adsorption/desorption of $N_2$, at 77 K.

FT-IR spectra of the synthesized catalysts were recorded in Varian 660-IR equipment with attenuated total reflectance accessory (FT-IR/ATR), in a spectral range of 400 to 4000 $cm^{-1}$. The powder diffraction patterns of the Cesium salts were obtained by X-ray diffraction (XRD) in a Bruker D8 Discovery diffractometer, operating at 40 kV acceleration voltage, 40 mA current, in the copper emission line (Cu-Kα, λ = 1.5418 Å), with a scanning rate of 0.3°/ min for a 2θ angle of 5-80°.

Thermogravimetric analysis (TG-DSC) were performed in a Perkin Elmer simultaneous thermal analyzer (STA) 6000. Approximately 10 mg of sample was loaded into standard alumina crucible, which was heated from 298 to 973 K at rate 10 $Kmin^{-1}$ under Nitrogen flow. SEM images were obtained in a JEOL JSM-6010/LA microscope equipped with an energy-dispersive spectrometry system (EDS). All the SEM images and the EDS spectra were recorded using 20 kV acceleration potential and 10 mm working distance.

The number and strength of the acid sites of the $Cs^+$ exchanged lacunar HPA salts were determined by *n*-butylamine potentiometric titration using a BEL potentiometer, model W3B, with glass electrode. Typically, a solid sample (*ca.* 50 mg) was suspended in $CH_3CN$ (*ca*. 30 mL) and magnetically stirred by 3 h. Posteriorly, the suspension was slowly titrated with *n*-butylamine solution (portions of *ca.* 100 μL, 0.025 $molL^{-1}$), until the electrode potential to keep stable after the addition of the titrant.

**Catalytic tests**

The catalytic activity of the lacunar salts was evaluated in nerol oxidation reactions with $H_2O_2$. The reactions were carried out in liquid phase with magnetic stirring, in a glass reactor coupled with a reflux condenser, heated in glycerin batch at atmospheric pressure. Typically, $H_2O_{2(aq)}$ (*ca*. 35 wt.%) and nerol (*ca.* 1.385 mmol) were solved in $CH_3CN$ (*ca*. 10 mL) and heated to 333 K. After to add the solid catalyst (lacunar Cs HPA salt, 4 mol%), the reaction was started.

The reaction progress was followed by 8 h, collecting aliquots at regular time intervals. Toluene was an internal standard. Before the analysis, the suspensions were centrifuged, and the supernatant was analyzed on a GC-2010 Plus Shimadzu Gas Chromatograph, fitted with capillary column and flame ionization detector (FID).

The catalyst was recovered and reused as follows. After the end of the reaction, the solution was centrifuged, and the supernatant discarded; the solid was washed twice with $CH_3CN$, and after the removal of the catalyst it was dried in an oven at 353 K/ 4 h, being then weighted and reused.

**GC-MS data of main products**

**Nerol epoxide (3,7-Dimethyl-2,3-epoxy-6-octenol)**

EI-MS 70 eV, *m/z* (rel. int.%): 152 $[M–H_2O]^+$ (1), 137 (1), 109 (67), 95 (27), 82 (40), 69 (65), 67 (68), 55 (35), 43 (89), 41 (100).

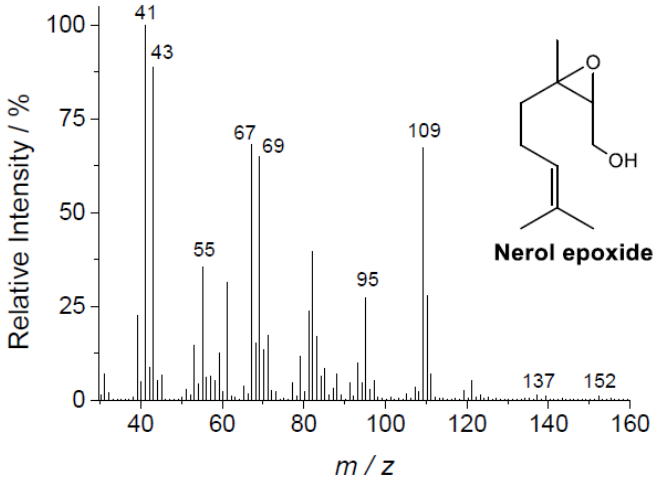


**Neraldehyde**

EI-MS 70 eV, *m/z* (rel. int.%): 152 $[M]^+$ (1), 94 (27), 84 (24), 69 (80), 53 (14), 41 (100), 39 (23).

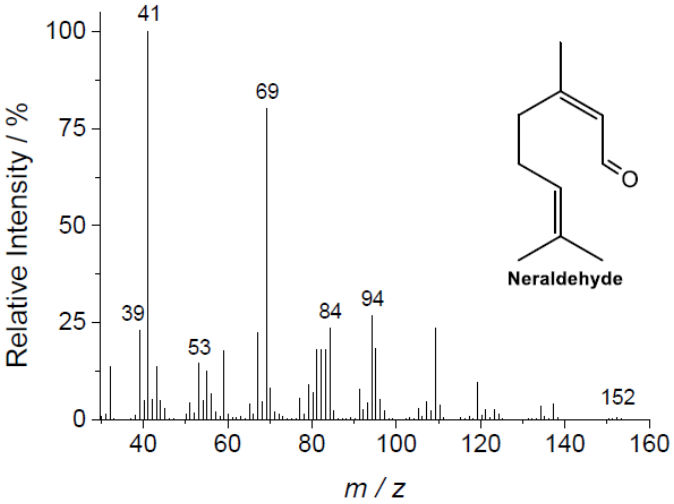

**References:**

[1] Y. Watanabe, S. Laschat, M. Budde, O. Affolter, Y. Shimada, V. B. Urlacher, *Tetrahedron*, **2007**, *63*, 9413-9422.

[2] A. Delazar, R. G. Reid, S. D. Sarker, *Chem. Nat. Compd.*, **2004**, *40*, 24-27.

**List of Figures:**



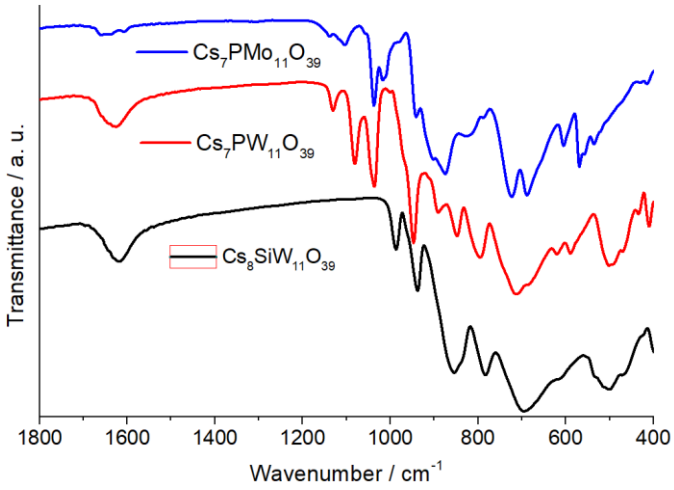


**Figure 1SM.** FT-IR spectra of Cesium exchanged lacunar heteropoly salts

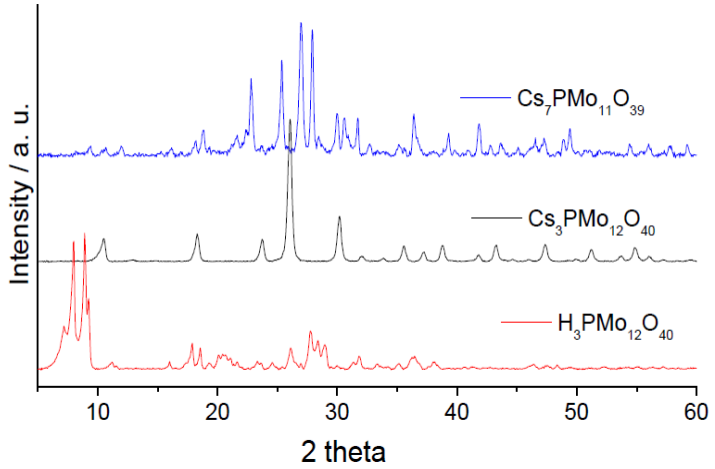


**Figure 2SM.** XRD patterns of lacunar Cesium phosphomolybdate salt, phosphomolybdic acid and saturated Cesium phosphomolybdate salt

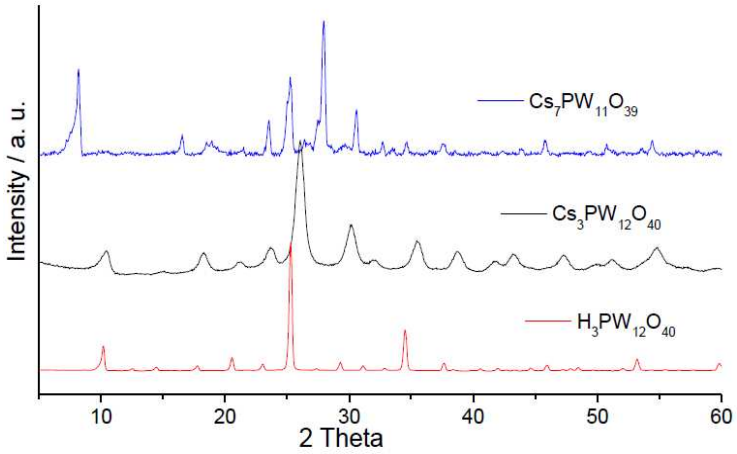


**Figure 3SM.** XRD patterns of lacunar Cesium phosphotungstate salt, phosphotungstic acid and saturated Cesium phosphotungstate salt

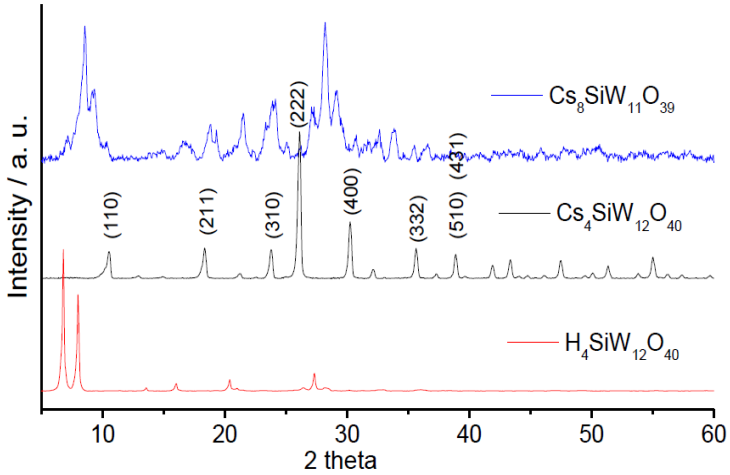


**Figure 4SM.** XRD patterns of lacunar Cesium silicotungstate salt, saturated Cesium silicotungstate salt and silicotungstic acid

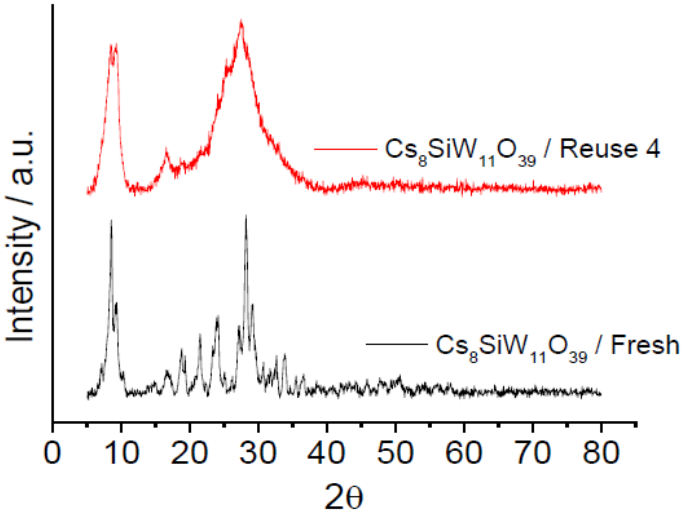


**Figure 5SM.** X-ray diffractograms of fresh lacunar Cesium silicotungstate and after the fourth reuse

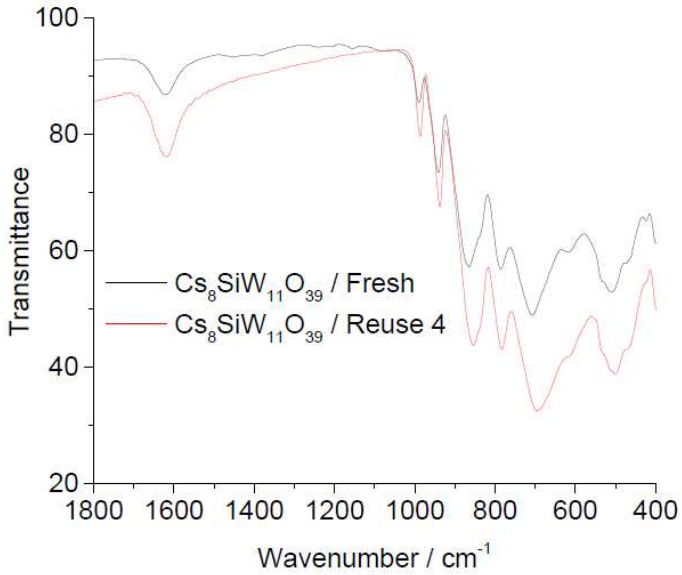


**Figure 6SM.** FT-IR spectra of fresh lacunar Cesium silicotungstate and after the fourth Reuse

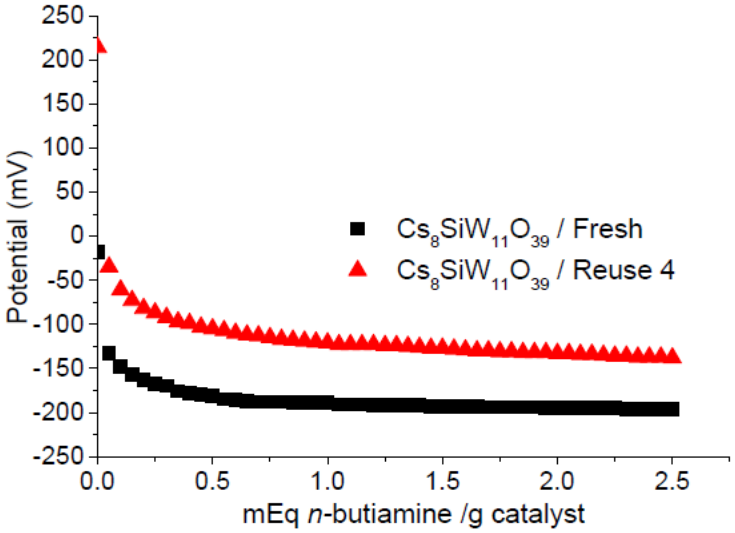


**Figure 7SM.** Potentiometric titration of the fresh lacunar Cesium silicotungstate and after the fourth reuse

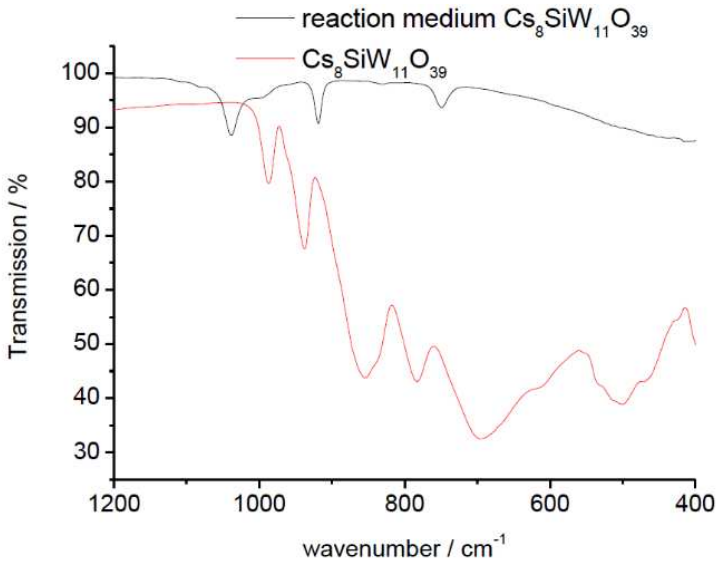


**Figure 8SM.** FT-IR spectrum of fresh $Cs_8SiW_{11}O_{39}$ and spectrum of liquid solution after the reaction[a]

[a]Samples for analysis in reaction medium were prepared as well as in the nerol oxidation reaction: Nerol (1.38 mmol), $H_2O_2$ (2.8 mmol), temperature (333 K), catalyst (4 mol%), $CH_3CN$ (10 mL)

**Table 1SM.** X-rays dispersive spectroscopy analysis of the Cesium exchanged lacunar salts

| Catalyst | % Theoretical | | | | | | % Real | | | | | |
|---|---|---|---|---|---|---|---|---|---|---|---|---|
| Elements | Cs | Si | P | W | Mo | O | Cs | Si | P | W | Mo | O |
| $Cs_8SiW_{11}O_{39}$ | 13.6 | 1.7 | - | 18.6 | - | 66.1 | 14.7 | - | - | 22.8 | - | 62.5 |
| $Cs_7PW_{11}O_{39}$ | 12.1 | - | 1.7 | 19.0 | - | 67.2 | 16.4 | - | - | 23.2 | - | 60.4 |
| $Cs_7PMo_{11}O_{39}$ | 12.1 | - | 1.7 | - | 19,0 | 67.2 | 22.0 | - | 2.8 | - | 22.9 | 52.3 |

**Table 2SM.** Characterization of the catalysts (fresh and reuse 4) through the physical adsorption of Nitrogen

| Catalysts | $S_{BET}$ ($m^2g^{-1}$) | $V_{DFT}$ ($cm^3g^{-1}$) | D (Å) |
|---|---|---|---|
| $Cs_8SiW_{11}O_{39}$ / Fresh | 11.3 | 0.010 | 31.7 |
| $Cs_8SiW_{11}O_{39}$ / Reuse 4 | 12.3 | 0.012 | 23.2 |

$S_{BET}$ = specific surface area; $V_{DFT}$ = pore volume e D = mean pore diameter

**PAPER 2: Oxidation of terpenic alcohols with Hydrogen peroxide promoted by $Nb_2O_5$ obtained by microwave-assisted hydrothermal method**

*Published in Molecular Catalysis

Molecular Catalysis 489 (2020) 110941

Contents lists available at ScienceDirect

Molecular Catalysis

journal homepage: www.elsevier.com/locate/mcat

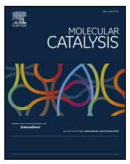

# Oxidation of terpenic alcohols with hydrogen peroxide promoted by $Nb_2O_5$ obtained by microwave-assisted hydrothermal method

Daniel Carreira Batalha[a], Natália Hadler Marins[b], Ricardo Marques e Silva[b], Neftalí Lenin Villarreal Carreño[b], Humberto Vieira Fajardo[c], Márcio José da Silva[a,*]

[a] Chemistry Department, Federal University of Viçosa, Viçosa, Minas Gerais, 36570-900, Brazil
[b] Graduate Program in Materials Science and Engineering, Technology Development Center, Federal University of Pelotas, Pelotas, Rio Grande Do Sul, 96010-610, Brazil
[c] Chemistry Department, Institute of Exact and Biological Sciences, Federal University of Ouro Preto, Ouro Preto, Minas Gerais, 35400-000, Brazil

## Abstract

The present work describes the synthesis of Niobium oxides by microwave-assisted hydrothermal method and their evaluation as a solid catalyst in oxidation reactions of terpenic alcohols with Hydrogen peroxide. Effects of main parameters of synthesis were assessed and all the prepared catalysts were characterized by physical adsorption/ desorption analyses of Nitrogen, infrared and Raman spectroscopies, scanning electron microscopy and powder X-rays diffraction analyses. The strength and number of acidic sites of the catalysts were determined by potentiometric titration. Morphological and structural characterization corroborate with the activity and selectivity achieved by the Niobium oxides. The reusability of the catalyst was evaluated. The impacts of main reaction variables such as temperature, catalyst, and oxidant load were assessed. Niobium oxide demonstrated to be an effective catalyst, selectively converting the nerol (model molecule) to epoxide and aldehyde. Oxidation of various terpenic alcohols was investigated. Only geraniol and nerol were selectively epoxidized, suggesting a hydroxyl group assisted reaction. Although being also allylic alcohol, linalool was unreactive toward epoxidation due to the presence of a methyl group at the same Carbon atom than the hydroxy group. The use of an environmentally cheap friendly oxidant ($H_2O_2$) and efficient solid catalyst ($Nb_2O_5$) are positive aspects of this process.

## Graphical Abstract

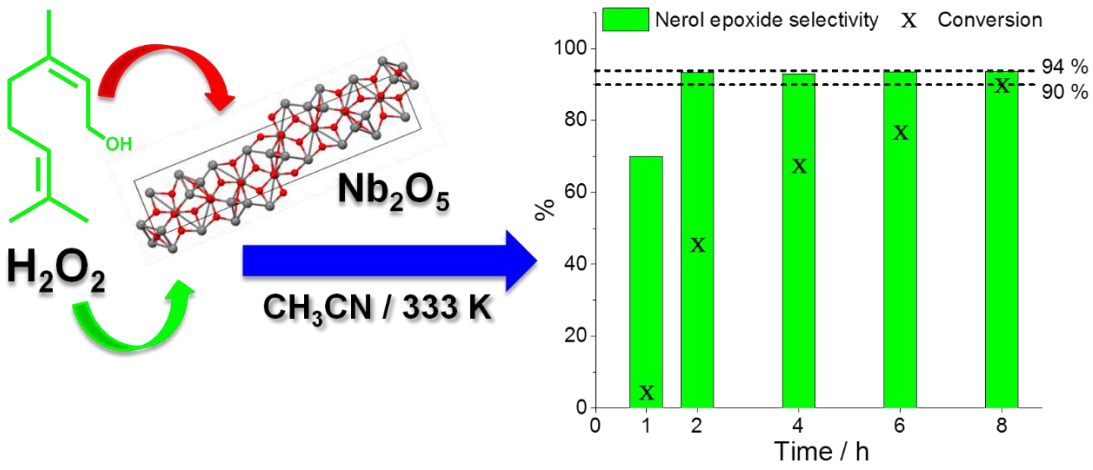


**Keywords**

Niobium oxide; Heterogeneous catalysis; Hydrogen peroxide; Nerol

## Introduction

The conversion of abundant and renewable raw materials to high value-added chemicals assumed great importance due to economic and environmental reasons [1–3]. Fine chemicals, pharmaceutical, and fragrance industries are each time more dependent on sustainable processes that use friendly reactants, recyclable catalysts, and inexpensive feedstocks [4,5].

Among the natural origin feedstock, monoterpenes deserve to be highlighted due to wide application as an ingredient of perfumes, flavors, and food, all motivated by their attractive organoleptic properties [6–8]. Terpenic alcohol derivatives as epoxides are building block in synthesis of chiral compounds, while carbonyl products as aldehydes and ketones are valuable ingredients of perfume, whose obtention per pass through oxidative processes where clean oxidant and solid catalysts are highly desirable [9–12]. However, the presence of two oxidizable sites in terpenic alcohols (i.e., the double bond and a hydroxyl group) may hamper the control of the reaction selectivity [13].

Green oxidants as Hydrogen peroxide are very appealing; similarly, to the molecular Oxygen, it generates water as an only by-product. However, unlikely molecular Oxygen, it has the advantage to be liquid, and not flammable at room conditions. Moreover, it is soluble in water and polar solvents, safe handling, and it is a cost-effective and atom-efficient oxidant [14,15]. When used in the presence of solid catalysts, Hydrogen peroxide can interact with the

catalyst surface and induce homo- or heterolytic cleavage of O–O bond in $H_2O_2$, which may generate different oxidative species [16,17]. The direct oxidation of olefin or alcohol by Hydrogen peroxide is always kinetically unfavored and impeded by the high energy barrier of the Oxygen transfer reaction from oxidant to the substrate [18,19]. Thus, several catalysts that facilitate the oxidation providing a low energy pathway, have been proposed. In special, various metal oxides or salt-based catalysts have demonstrated to be active in either oxidation or epoxidation reactions [20–22].

The use of a heterogeneous catalyst leads to a cleaner process, since it reduces the waste generation, allows the recovery and the reuse of the catalyst, and diminish the cost of the processes. Different strategies have been proposed to obtain efficient heterogeneous catalysts in epoxidation or oxidation reactions of functionalized olefins with Hydrogen peroxide. For a long time, $Ti/SiO_2$ catalysts have been preferred in the epoxidation of terpenic alcohols [23]. Mixed oxides, solid-supported metals, framework-substituted molecular sieves, and modified mesoporous silica are also examples of active catalysts on these reactions [24–26].

Nevertheless, in reactions that use heterogenized homogeneous catalysts, the leaching provoked by the high polarity of the reactants (i.e., aqueous Hydrogen peroxide) is always an obstacle that may compromise the reuse of the catalyst. Therefore, the development of a stable, recyclable, and truly heterogeneous catalyst, which achieves epoxidation rates and selectivity likewise the homogeneous counterparts is still a challenge to be overcome. Recently, to circumvent the leaching of the active phase in solid catalysts, we have synthesized insoluble Keggin heteropolyacid salts, which were successfully tested as catalysts in terpenic alcohol oxidation reactions with Hydrogen peroxide [27].

The use of solid metal oxide as the catalyst excludes the possibility of leaching. Niobium oxide has desirable properties to be used as a heterogeneous catalyst. It has a high surface area and good thermal stability. Moreover, $Nb_2O_5$ has Brønsted and Lewis acidic sites in their structure, being potentially a bifunctional catalyst [28]. Niobium-containing catalysts can be prepared in several routes such as sol-gel, grafting, hydrothermal, coprecipitation, or polymeric precursor methods [29–32]. The treatment of Niobium catalysts with Hydrogen peroxide is a strategy that improves their activity in oxidation reactions [33].

Due to these features, Niobium oxide has been an efficient catalyst in different oxidation reactions. Nanoparticles of Niobium oxide were synthesized through microwave-assisted method and used as catalysts in aniline oxidation reactions with Hydrogen peroxide in liquid phase [34]. The same reaction was also efficiently performed when $Al_2O_3$/ $AlNbO_4$ were applied as the catalyst [35]. Cerium-Chromium-Niobium oxides were successfully evaluated in

processes to deep oxidation of dichloroethane, demonstrating have potential industrial application [36]. Conversely, the high acidity of Niobium oxides makes them efficient and reusable acid catalysts in xylose dehydration processes to furfural production [37].

In this work, Niobium oxides were prepared by microwave-assisted hydrothermal method and evaluated in oxidation reactions of terpenic alcohols with Hydrogen peroxide. The impacts of the temperature of synthesis on the physical and structural properties of Niobium oxides were assessed. The solid catalysts were characterized by FT-IR and Raman spectroscopy analyses, physical adsorption/ desorption of Nitrogen, thermogravimetry and powder XRD analyses. Acidity properties were determined by *n*-butylamine potentiometric titration. The nerol oxidation was studied in detail. The effects of main reaction parameters such as temperature, oxidant, and catalyst loads were also investigated. Special attention was paid to describe the reaction mechanism. The reaction scope was also extended to other terpenic alcohols.

## Experimental

### *Catalyst preparation*

$Nb_2O_5$ was synthesized by microwave-assisted hydrothermal method as previously described [38,39]. Ammonium Niobium oxalate was dispersed in distilled water under stirring for 30 min. Following, Hydrogen peroxide was dropped in the solution and stirred for 30 min. The final solution was poured into a Teflon autoclave and placed in a microwave oven (Electrolux, MEF41, Brazil). The catalysts were synthesized at 433 K for different times (2, 4, and 8 h) under the constant pressure of 85 psi. After cooling, the precipitate was washed with absolute ethanol (LabSynth, Brazil), and dried in an oven (DeLeo, A5SE, Brazil) at 323 K for 24 h under air atmosphere. The Scheme 1 below briefly shows the Niobium oxides synthesis used as catalysts.

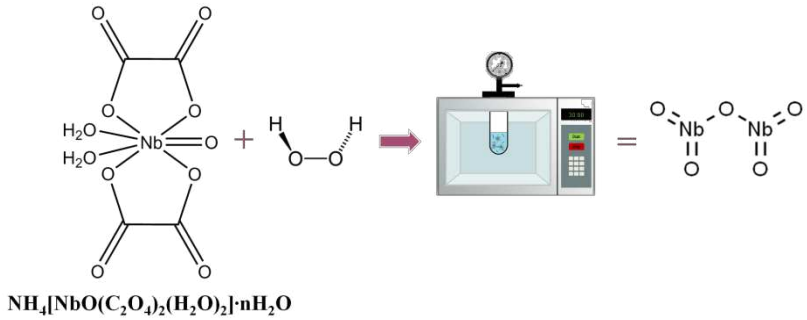


**Scheme 1.** $Nb_2O_5$ synthesis by microwave-assisted hydrothermal method

*Catalyst characterization*

Textural properties of Niobium oxides were obtained at 77 K in a NOVA 1200 Quantachrome equipment. The Brunauer-Emmett-Teller equation was applied to the isotherms of adsorption/ desorption of $N_2$, which provided the surface area of the solids. Diameter and pore volume distribution was calculated according to the DFT method. The morphologies of the catalysts were investigated by scanning electron microscopy (SEM) using a microscope SSX-550, SHIMADZU, Japan.

Infrared spectroscopy analyses were performed in KBr pellets using an ABB Bomen MB 3000 FTIR spectrometer (Quebec, Canada) equipped with ZnSe optics and a deuterated triglycine sulfate (DTGS) detector set at a 4 $cm^{-1}$ resolution and wavenumber range of 400−4000 $cm^{-1}$.

XRD pattern of the $Nb_2O_5$ powders was analyzed by X-ray diffraction (Shimadzu, XRD 6000, Japan), using a diffractometer with $CuK_\alpha$ radiation ($\lambda$ = 1.5418 Å), and a scan range of 20-70°. Crystallite sizes were calculated using the Scherrer equation:

$$L = \frac{K.\lambda}{\beta.cos\theta} \quad (1)$$

Where $\lambda$ is the X-ray wavelength in nanometer (nm), $\beta$ is the peak width of the diffraction at half maximum height resulting from small crystallite size in radians, and $K$ is a constant related to crystallite shape, normally taken as 0.89.

Raman spectra were recorded in a Horiba/Jobin-Yvon Labram-HR spectrometer equipped with He-Ne laser (laser excitation lines of 632.8 nm and 18 mW of power) and an Olympus microscope. The analyses were carried out with an acquisition time of 5 s with 10 accumulations in the region of 60 to 1200 $cm^{-1}$ and a 100x microscope objective.

The amount and strength of the acidic sites of Niobium oxides were determined by *n*-butylamine potentiometric titration using a BEL potentiometer (model W3B) with a glass electrode. Typically, 50 mg of $Nb_2O_5$ was suspended in $CH_3CN$ (*ca*. 30 mL) and magnetically stirred for 3 h. Posteriorly, the suspension was titrated with slow addition of portions of *n*-butylamine (*ca.* 0.025 $molL^{-1}$) until that the electrode potential remained stable after the addition of the titrant again.

*Catalytic tests*

Oxidation reactions were carried out in liquid phase using a glass reactor fitted (ca. 50 mL) with a reflux condenser and sampling septum, in a glycerin batch under magnetic stir and heating. Typically, $H_2O_{2(aq)}$ (ca. 35 wt. %) and nerol (1.375 mmol) were dissolved in $CH_3CN$ (ca. 10 mL) and heated to 333 K. The addition of Niobium started the reaction, which proceeded for 8 h.

Aliquots were collected at regular time intervals. Before the analysis, the aliquots were centrifuged, and the supernatant was analyzed on a GC-2010 Plus Shimadzu Gas Chromatograph with a flame ionization detector (FID), equipped with an auto-injector AOC-20i, and fitted with a capillary column Rtx®-Wax (30 m x 0.25 mmID x0.25 μm). The chromatographic conditions were initial temperature (353 K/ 3 min), heating rate (10 K / min until 493 K), which was kept constant 3 min. Injector and detector temperatures were 523 K and 523 K, respectively. Hydrogen was the carrier gas (1.2 $mLmin^{-1}$).

## Results and discussion

### *Catalysts characterization*

Table 1 shows the surface area, volume, and pore diameter values quantified by the BET and DFT methods of $Nb_2O_5$ catalysts.

**Table 1.** Characterization of the catalysts through the physical adsorption of Nitrogen[a]

| Catalyst | $S_{BET}$ ($m^2/g$) | $V_{DFT}$ ($cm^3/g$) | D (Å) |
|---|---|---|---|
| $Nb_2O_5$ - 2 h | 17.4 | 0.035 | 31.7 |
| $Nb_2O_5$ - 4 h | 107.4 | 0.095 | 16.9 |
| $Nb_2O_5$ - 8 h | 215.9 | 0.340 | 16.9 |

[a]$S_{BET}$ = surface area; $V_{DFT}$ = cumulative pore volume; D = pore diameter

An increase in the time of synthesis resulted in an improvement of surface area and a higher volume of pores. Conversely, pores diameters were lower when longer times were used. This effect was also verified by us in a previous work [39]. We can consider that each rod that compose this material is composed of several rods with smaller diameters. The synthesis time influences the rods growth; if a greater time of synthesis is used, larger will be the size of the stem. As a result, may occurs an increase in surface area and pore volume [39].

The catalyst $Nb_2O_5$ - 2 h presented the lowest values of surface area and pore volume but showed a larger value in its diameter, above 30 Å, characteristic of a mesoporous material.

In contrast, the two other oxides showed an increasing on the surface area and pore volume when the synthesis time was increased. Since pore diameter was reduced to values lower than 20 Å, we can conclude that micropores were formed in the materials [38,39].

Fig. 1 shows the physical adsorption/desorption isotherms of $N_2$ and pore diameter distributions. According to IUPAC recommendations, the isotherms of the synthesized salts can be classified as type V, characteristic of microporous and mesoporous materials.

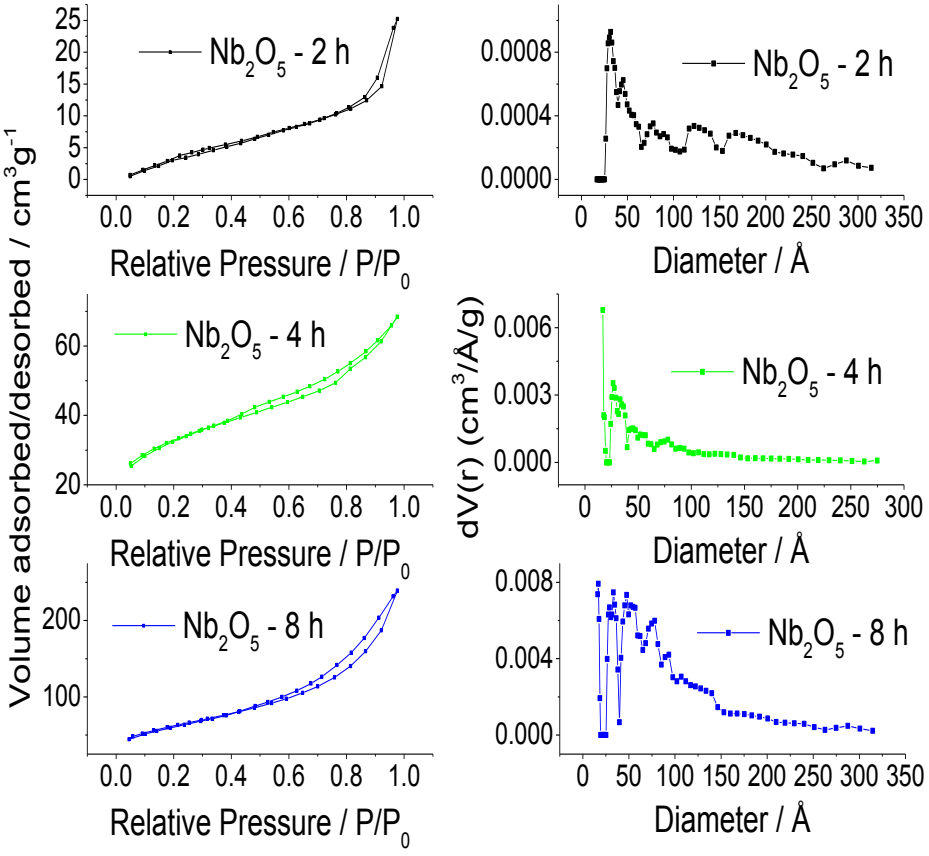


**Fig. 1.** Isotherms of physical adsorption/desorption of $N_2$ and pore diameter distribution for Niobium oxides

The hysteresis observed in the isotherm curves can be classified as H3 type, which is typical of plate-shaped particle aggregates giving rise to slit pores [40]. According to the pore diameter distribution curve profiles, the Niobium oxides synthesized presented diameters in the range of micro and mesoporous.

FT-IR spectra presented bands at approximately 1100 $cm^{-1}$ that were assigned to the asymmetric stretching of Nb–O–Nb bonds (Fig. 2) [41,42]. The broad band at 3600−3200 $cm^{-1}$ region refers to the vibration modes of Hydrogen-bonded hydroxyl groups. The presence of bands at 1700 $cm^{-1}$ reinforces the Nb-linked $OH^-$ groups.

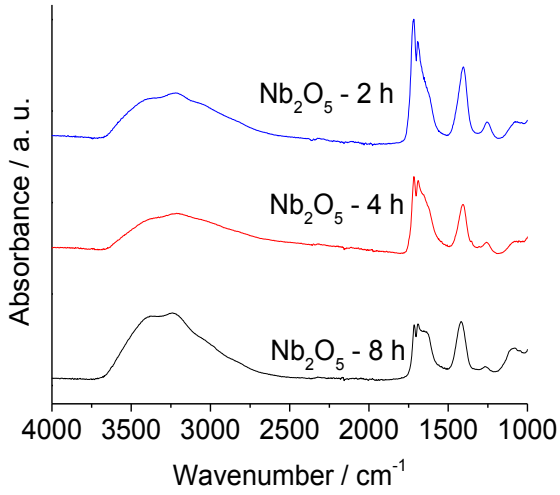


**Fig. 2.** FT-IR spectra obtained from $Nb_2O_5$ catalysts

It is noteworthy that the intensities of the bands in this last region varied according to the synthesis time, suggesting that shorter synthesis times favored a higher presence of the hydroxyl groups. The ability of these groups to bind to $H_2O_2$ molecules generating different reactive Oxygen species may improve the activity of these Niobium oxides in oxidation reactions [41,43].

Fig. 3 represents the X-rays diffractograms of the three synthesized catalysts. The literature describes the existence of four different phases for $Nb_2O_5$: $Nb_2O_5.nH_2O$ (amorphous), TT-$Nb_2O_5$ (hexagonal), T-$Nb_2O_5$ (orthorhombic) and H-$Nb_2O_5$ (monoclinic) [44]. The diffractograms revealed by XRD analyses indicate the peaks are related to the hexagonal phase (JCPDS No. 28-0317) [39]. The broad peak noticed at 26° is assigned to the amorphous phase due to the use of hydrated starting materials and water. The presence of weak peaks is due to the low temperature used in the synthesis, which influenced their crystallinity [45,46]. The $Nb_2O_5$ samples of 2 h, 4 h, and 8 h exhibited crystallite sizes of 12.7 nm, 14.8 nm, and 15.1 nm, respectively.

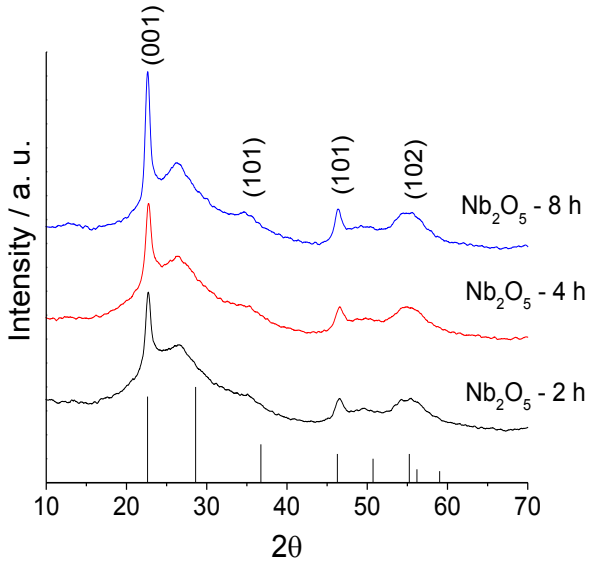


**Fig. 3.** Powder XRD patterns of $Nb_2O_5$ synthesized at different times

Fig. 4 presents the Raman spectra of the three $Nb_2O_5$ samples. It was found that they had distinct profiles, indicating the presence of more than one phase in each material. Bands in the region of 200−300 $cm^{-1}$ were assigned to the stretching of Nb–O–Nb bonds [46].

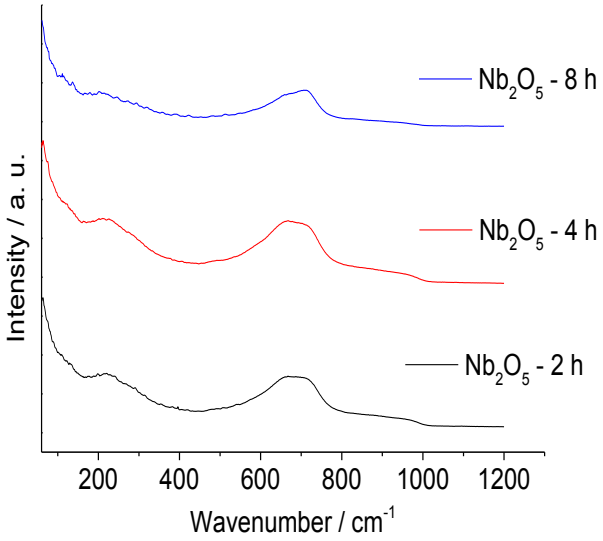


**Fig. 4.** Raman spectra of the three different synthesized Niobium

The absorption bands in the 570−770 $cm^{-1}$ region refer to the symmetrical stretching modes of the Nb–O bonds ($NbO_6$, $NbO_7$, and $NbO_8$) [46,47]. For the two samples synthesized in shorter time, 2 and 4 h, the single band in this region may indicate the greater presence of the amorphous phase. For the catalyst synthesized for 8 h, this band has a small shoulder closer to 700 $cm^{-1}$, which may indicate the greater formation of the orthorhombic phase due to longer synthesis time [48]. This indicates that the time of synthesis affected the proportion between these two phases.

The broad band more pronounced in the spectra of catalysts synthesized at 2 and 4 h, present in the 900-1000 $cm^{-1}$ region, were assigned to the symmetrical and asymmetrical stretching of terminal bonds Nb = O, which is associated with Lewis acid sites [47]. This stretching band is related to the crystallinity degree of the sample; the more intense is the band, the lower is the crystallinity and more acid is the material [47–49]. This same phenomenon is little noticed for the sample synthesized for 8 h, confirming the higher crystallinity and may indicate a lower number of Lewis acid sites for this material.

The lower crystallinity degree of the $Nb_2O_5$ - 2 h catalyst can be verified by the XRD graph. Comparing the results shown by XRD and IR, it should be noted the shorter is the catalyst synthesis times, the lower is the crystallinity and more intense is the $OH^-$ grouping bands in IR spectra. According to Ziolek et al, the activity for Niobium oxides varies according to its crystallinity, being a parameter proportional to the number of hydroxyl groups present on the catalyst surface [17,43].

Fig. 5 shows the potentiometric titration curves of three synthesized Niobium oxides. The initial electrode potential (E*i*) indicates the maximum acidity strength and the total number of acidic sites being provided by the inflection value of titration curve (ca. mEq *n*-butylamine / g catalyst), which was obtained from the minimum of the first derivative of each titration curve. The strength of the sites can be classified according to the scale: E*i* > 100 mV (very strong), 0 < E*i* < 100 mV (strong), -100 < E*i* < 0 mV (weak) e E*i* < -100 mV (very weak) [50].

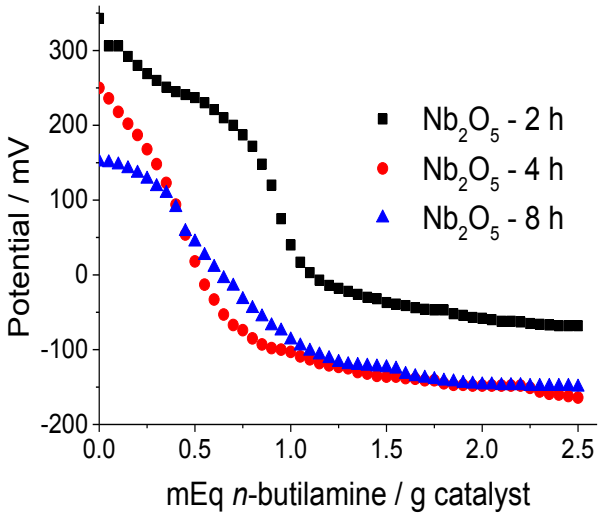


**Fig. 5.** Potentiometric titration curves with *n*-butylamine of the Niobium oxides

All the Niobium catalysts presented very strong acidic sites as demonstrated by the high E*i* values showed in Fig. 5, which was higher than 100 mV. Moreover, as higher the synthesis time, lower was the acidity strength. The number of total acidic sites (ca. mEq of *n*-

butylamine/ g of catalyst) followed the order 0.95, 0.45, and 0.40 for $Nb_2O_5$ - 2 h, $Nb_2O_5$ - 4 h and $Nb_2O_5$ - 8 h oxides, respectively. Therefore, the solid $Nb_2O_5$ - 2 h showed both the strongest acid sites and the greatest number of total acidic sites.

It is important to highlight that the results of potentiometric titration reinforce those provided by IR spectra, which evidenced that the $Nb_2O_5$ - 2 h material has the highest number of Brønsted acidic sites. According to the IR spectra of Niobium oxide catalysts, the stretching bands at 1700 $cm^{-1}$ wavenumber indicates the presence of the Brønsted acid sites. These vibration bands are correlated with the bonds between Nb and $OH^-$ groups [39]. The intensity of this band is linked to the number of Brønsted acid sites present in the catalyst surface. As can be seen, the $Nb_2O_5$ - 2 h catalyst presented the highest number of acid sites (ca. 0.95) and the more intense vibration band at 1700 $cm^{-1}$ wavenumber (see Fig. 2).

Fig. 6 shows SEM micrographs of synthesized Niobium oxides. The $Nb_2O_5$ particles were moderately aggregated and exhibited an approximately spherical shape, regardless of the synthesis times. Although this aspect it is not totally clear on the SEM images, previous works showed that this material presented a spherical shape [39].

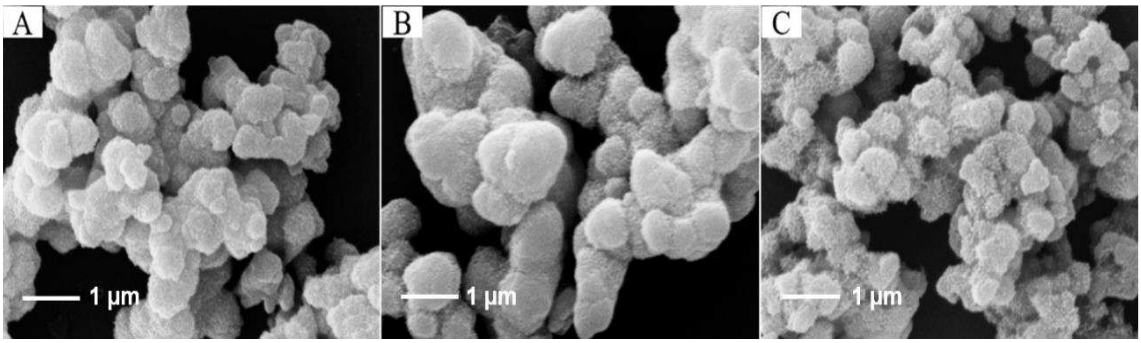


**Fig. 6.** SEM micrographs at x15000 magnification of $Nb_2O_5$ - 2h (A), $Nb_2O_5$ - 4 h (B), and $Nb_2O_5$ - 8 h (C) catalysts

The morphologies varied with an increase of hydrothermal treatment. At longer synthesis times, materials roughness increases. Although the SEM images are unable to provide information about the pores size, we have found that the formation of particles with larger surface area and high pore volume was obtained when a longer synthesis time was used [39,51]. The BET analyses and porosimetry support this conclusion (Table 1).

*Catalytic tests*

The catalytic performance of synthesized Niobium oxides was assessed in the nerol oxidation reaction with $H_2O_2$. Fig. 7 displays the kinetic curves and selectivity achieved after 8 h of reaction, following conditions selected from the literature [32].

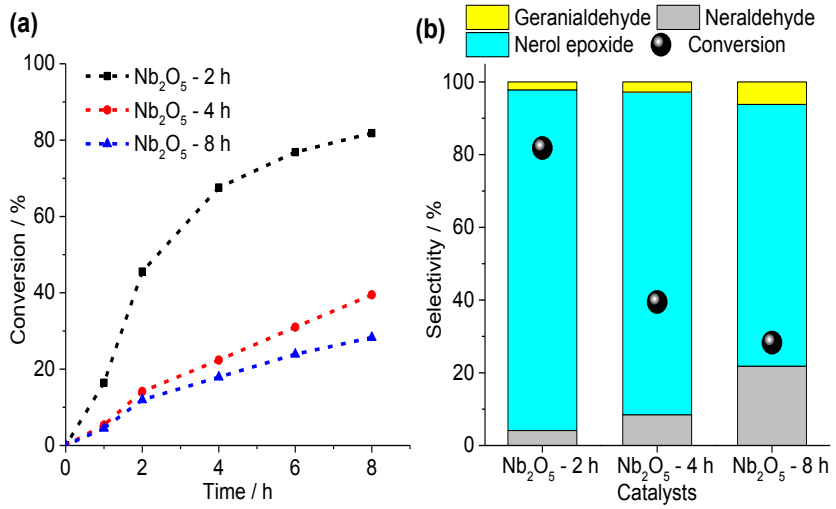


**Fig. 7.** Effect of $Nb_2O_5$ catalyst treatment time on the kinetic curves (a), conversion and products selectivity (b) of nerol oxidation with $H_2O_2$[a]
[a]Reaction conditions: nerol (1.375 mmol), $H_2O_2$ (2.750 mmol), temperature (333 K), catalyst (4 mol%), $CH_3CN$ (10 mL)

Although an excess of Hydrogen peroxide has been used (ca. 2:1 in relation to nerol), only a poor conversion (ca. 5 %) was obtained in the absence of a catalyst (omitted by simplification). Conversely, in the Niobium oxide-catalyzed reactions the nerol was selectively converted to oxidation products (Scheme 2).

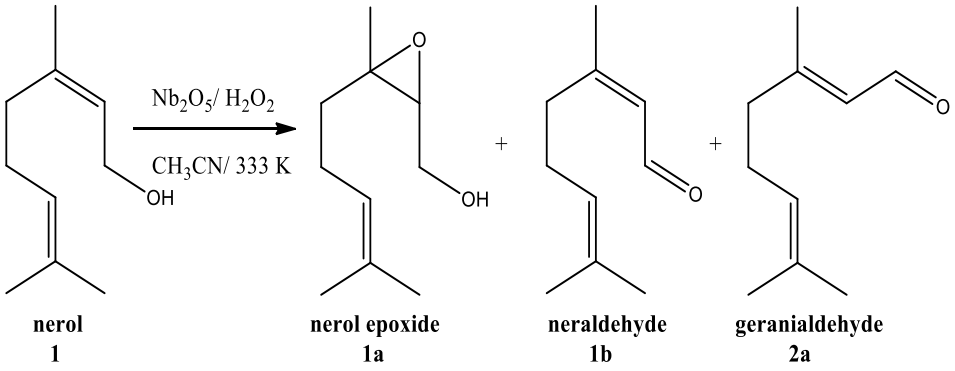


**Scheme 2.** Oxidation products of nerol obtained in $Nb_2O_5$-catalyzed reactions

The $Nb_2O_5$ - 2 h catalyst was much more efficient than other synthesized oxides. The highest conversion (ca. 82 %) and selectivity toward nerol epoxide (ca. 94 %) was achieved after 8 h of reaction. Notably, these results were superior that achieved by Niobium oxides prepared by the peroxidation method [52]. Even though nerol epoxide has been the major

product in all the reactions, the selectivity toward carbonyl products (i.e., 1b and 2a) was gradually improved when Niobium catalysts were synthesized at longer times. Conversely, the terminal double bond of the nerol remained untouchable along with the reaction, probably due to the steric hindrance triggered by two methyl groups.

A comparison of the characterization data of Niobium oxides and their catalytic activity leads to a conclusion that the surface properties and acidity of Niobium oxides played an essential role in this reaction. The most acidic catalyst ($Nb_2O_5$ - 2 h; Fig. 5) with the lowest surface area (Table 1) was the most efficient, achieving the highest conversion.

On the other hand, catalysts synthesized at longer periods showed a different selectivity; while the selectivity of aldehydes increased, the selectivity of epoxide products was reduced, which may be assigned to a modification on the catalyst surface.

Balker et al reported that the alcohols are preferentially oxidized by Hydrogen peroxide to carbonyl products when Ti silicate (i.e., TS-1) is the catalyst [26]. However, Tatsumi et al. described that this reaction is suppressed if allylic hydroxyl groups are present and, consequently, epoxide becomes the major product [53]. Investigating the geraniol epoxidation with $H_2O_2$ over TS-1 catalysts, those authors demonstrated that the epoxidation of allylic alcohols is a hydroxy-assisted reaction. Therefore, based on the literature and experimental data obtained we propose that on Niobium-catalyzed oxidation of nerol involves an intermediate as depicted in Scheme 3.

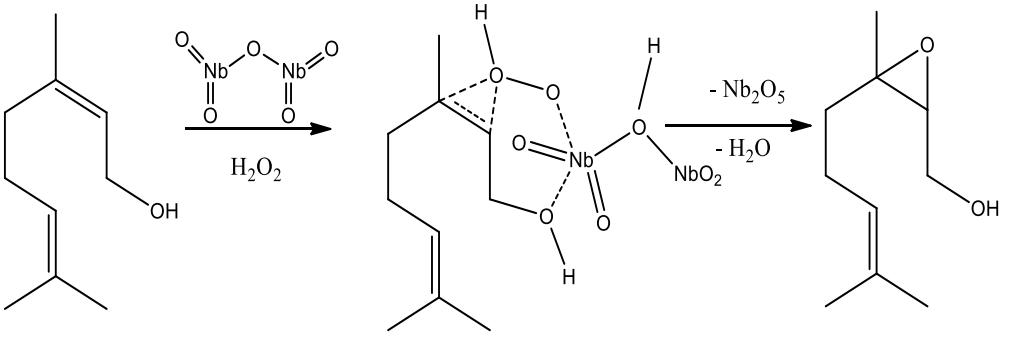


**Scheme 3.** $Nb_2O_5$-catalyzed hydroxy-assisted epoxidation of nerol with $H_2O_2$ adapted from [26]

The literature describes the oxidation of geraniol by Hydrogen peroxide in Tungsten, Titanium, or Vanadium-catalyzed reactions; on these processes, steps such as the coordination of metal oxide catalyst to the olefin double bond, as well as the peroxidation of the metal are always involved [54]. In general, after the peroxidation step, a three-centered ring intermediate involving the metal oxide and an Oxygen atom of peroxide is formed; however, it was omitted in Scheme 3 aiming to do cleaner the reaction. Only the peroxide group (i.e., OOH) bonded to the metal center was depicted herein.

The change in chemoselectivity can be attributed to the coordination of the nerol on the surface of $Nb_2O_5$. It is very important to highlight that analogously to the described by Adams et al and Kumar et al., we are supposing that the transition state of the epoxidation of nerol involves the coordination of the allylic hydroxyl group to the Nb active site; it means that the double bond interacts with one peroxidic Oxygen atom, not the Niobium oxide-Oxygen atom [23,55].

The peroxidation step of the Niobium catalyst and the interaction with the organic substrate is attributed to the different species of active sites present in the Niobium catalyst. Lewis acidic sites and Brønsted acidic sites allow the simultaneous adsorption of the oxidant and the organic substrate even in the presence of water [56].

We can conclude that once the $Nb_2O_5$ - 2 h presented a higher Brønsted acidity (see IR spectra and acidity measurements, Fig. 2, Fig. 5), the interaction of nerol hydroxyl group with the peroxidized catalyst is more favorable, therefore, epoxide was the major product (Fig. 7). Conversely, when the catalysts have lower Brønsted acid sites number (i.e., because they were synthesized in 4 or 8 h), the epoxide selectivity is lowered, favoring the formation of the neraldehyde ($Nb_2O_5$ - 4 and 8 h, Fig. 7).

XRD also demonstrated that the $Nb_2O_5$ - 2 h catalyst presented the lowest crystallinity among the three materials. These characteristics positively contributed to improving the interaction of the $H_2O_2$ and nerol with the catalyst surface [17,57]. The $Nb_2O_5$ - 2 h catalyst was selected to study the effect of main reaction parameters due to its better performance.

*Effects of catalyst load*

The impacts of catalyst load were evaluated keeping constant the other variables in the reaction. Fig. 8 shows the kinetic curves, conversion, and selectivity achieved in reactions with a load of catalyst ranging from 0.5 to 4 mol%.

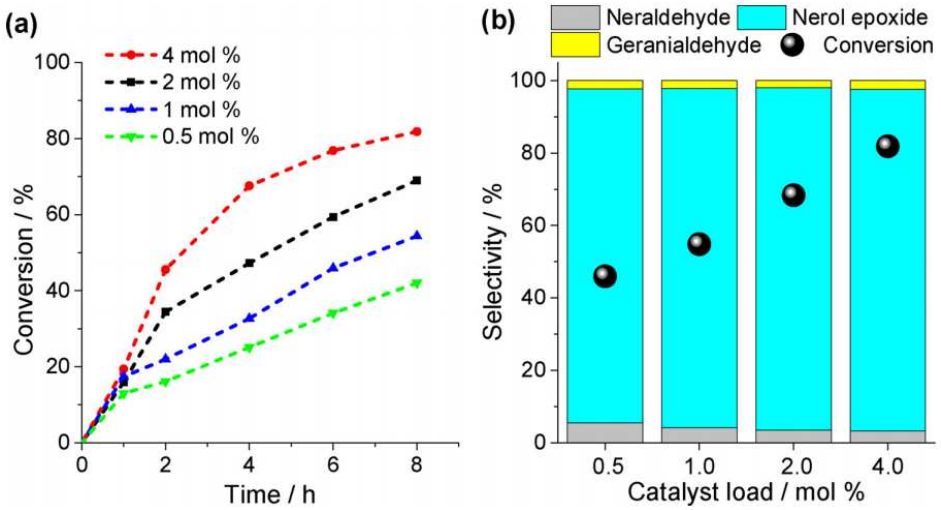


**Fig. 8.** Effect of catalyst load on the kinetic curves (a), conversion and products selectivity (b) of the nerol oxidation with $H_2O_2$ over $Nb_2O_5$ - 2 h[a]
[a]Reaction conditions: nerol (1.375 mmol), $H_2O_2$ (2.750 mmol), temperature (333 K), $CH_3CN$ (10 mL)

Although no shown in Fig. 8, a control experiment was carried out without the presence of the catalyst. When nerol and Hydrogen peroxide were heated and stirred during 8 h of reaction, no oxidation product or epoxide was detected. It is a guarantee that the formation of these compounds depends on the presence of the $Nb_2O_5$-2 h catalyst.

Conversely, while the reactions were performed in the presence of the Niobium oxide catalyst, nerol epoxide and the carbonylic products were obtained, with the highest selectivity toward epoxide.

With 4 mol% of catalyst load, the reaction achieved 82% of conversion. When we performed reactions with higher loads of catalyst, no significant difference was observed in the conversions, which varied from 82 to 87%. This enhancement of conversion is a consequence of a higher acidic sites number, feasible when a higher concentration is used. Therefore, lower catalysts loadings were used (ca. 2.0-0.5 mol%). At this range of catalyst load, the reaction conversions were gradually diminished. Notwithstanding, the reaction selectivity remained basically unaltered; nerol epoxide was always the main product (ca. 94%), and aldehydes of nerol and geraniol were the secondary products. It is evidence that selectivity depends on the nature of the catalyst.

*Effects of oxidant: substrate ratio*

The results for $Nb_2O_5$ - 2 h catalyst in reaction with different amounts of oxidant are presented in Fig. 9. An improvement in the conversion was obtained using a higher oxidant load.

However, this effect was only noticed when the reactions were performed with 2 mol% of catalyst.

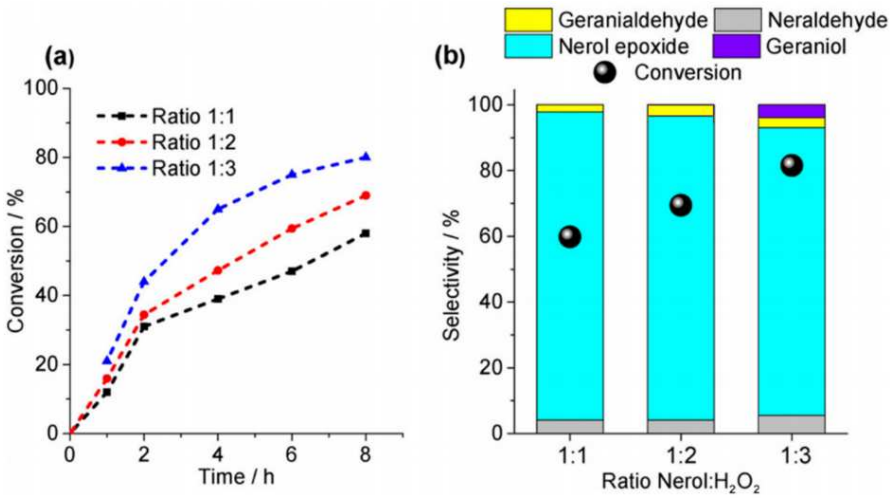


**Fig. 9.** Effect of substrate: oxidant ratio on the kinetic curves (a), conversion and products selectivity (b) of the nerol oxidation by $H_2O_2$ in the presence of $Nb_2O_5$ - 2 h catalyst[a]
[a]Reaction conditions: Nerol (1.375 mmol), temperature (333 K), catalyst (2 mol%), $CH_3CN$ (10 mL)

The presence of a higher load of oxidant also resulted in an increase in the amount of water in the solution. This aspect changed the chemoselectivity of the reaction, although nerol epoxide has continued to be the main product. The water benefited the isomerization of nerol to geraniol, which was formed when the proportion of $H_2O_2$: nerol was 1:3. There was an increase in the selectivity for geranialdehyde. However, the nerol epoxide selectivity was close to 90%. No significant amount of geraniol epoxide was detected along with the reactions.

*Effects of reaction temperature*

The impacts of temperature on the kinetic curves, conversion, and selectivity of nerol oxidation were assessed using the optimized conditions (ca. 2:1 oxidant: substrate ratio, 4 mol% of catalyst) (Fig. 10).

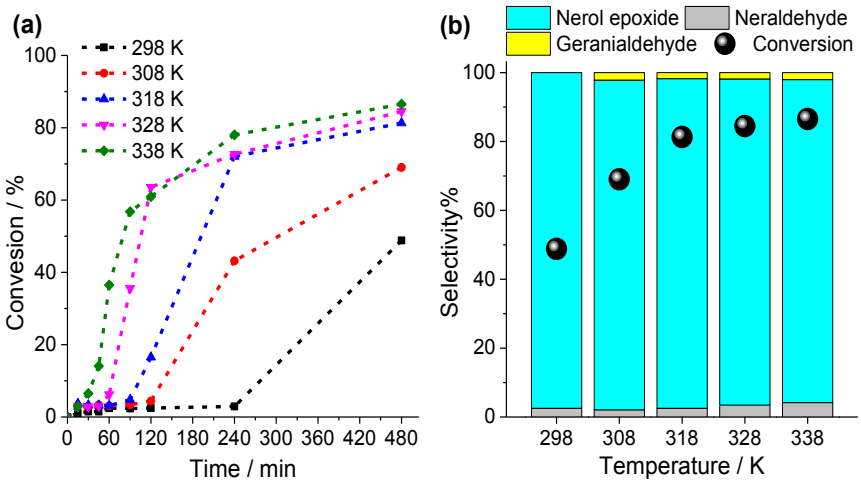


**Fig. 10.** Effects of temperature on the kinetic curves (a), conversion and products selectivity (b) of the nerol oxidation with $H_2O_2$ over $Nb_2O_5$ - 2 h catalyst[a]
[a]Reaction conditions: nerol (1.375 mmol), $H_2O_2$ (2.750 mmol), catalyst (4 mol%), $CH_3CN$ (10 mL)

When the reactions were carried out at different temperatures, an induction period at the process beginning was noticed, mainly at the lowest temperatures. We suppose that at low temperatures, the catalyst peroxidation step is less favored. Consequently, a minimum amount of substrate is consumed within the initial period of reaction. This effect was being suppressed when higher temperatures were used. On the other hand, the reaction selectivity remained almost the same; at the end of the reactions, nerol epoxide was obtained always with a selectivity close to 94%.

*Effects of terpenic alcohol structure*

The catalytic activity of $Nb_2O_5$ - 2 h was also tested on the oxidation of different terpenic alcohols. Fig. 11 displays all the terpenic alcohols investigated; allylic acyclic primary alcohols (nerol and geraniol), allylic acyclic tertiary alcohol (linalool) or cyclic (α-terpineol) were selected. It is important to note that although the hydroxyl group of tertiary alcohols is not oxidizable (i.e., linalool and α-terpineol), these substrates have double bonds which may be epoxidized.

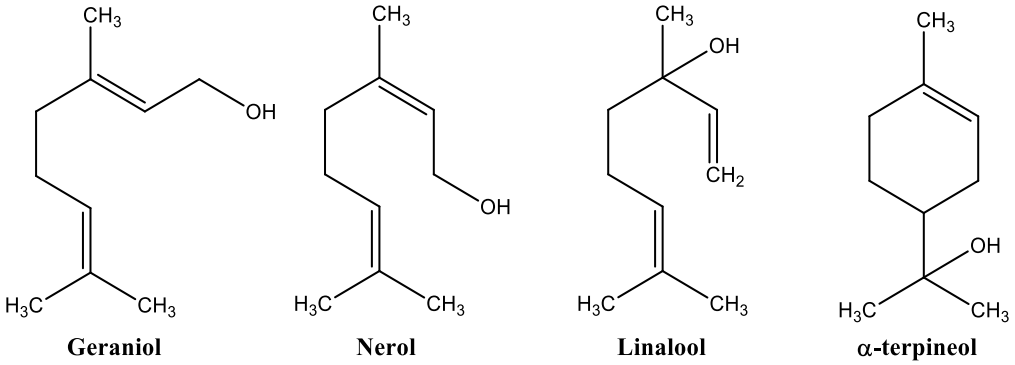


**Fig. 11.** Structure of terpenic alcohols

Among the evaluated alcohols, only nerol and their geometric isomer geraniol were selectively oxidized, providing their epoxides as main products. Therefore, only the selectivity of these two alcohols is displayed in Fig. 12. The double bond of α-terpineol remained untouchable and no epoxide was detected. This result is reinforcing that the epoxidation is a hydroxy-assisted reaction.

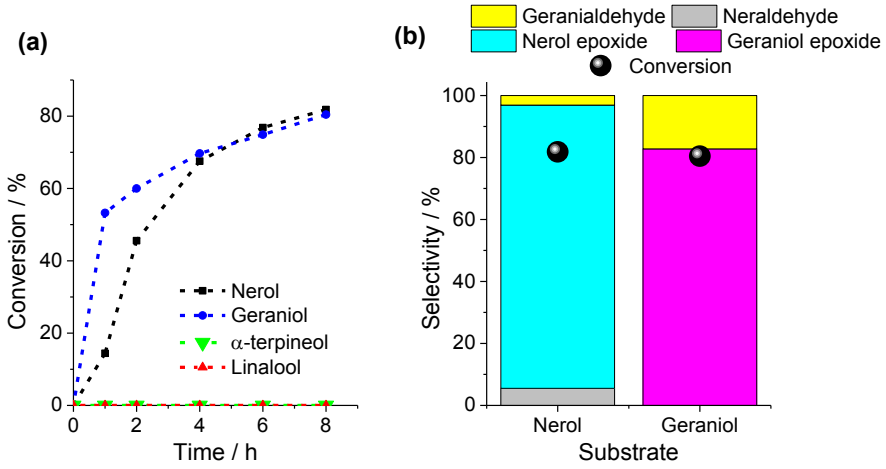


**Fig. 12.** Kinetic curves (a), conversion and products selectivity (b) of $Nb_2O_5$ - 2 h-catalyzed terpenic alcohols oxidation by $H_2O_2$[a]
[a]Reaction conditions: terpenic alcohol (1.375 mmol), $H_2O_2$ (2.750 mmol), temperature (333 K), catalyst (4 mol%), $CH_3CN$ (10 mL)

Although linalool has an allylic hydroxyl group likewise geraniol and nerol, it was not epoxidized. It can be attributed to the hysteric hindrance provoked by the methyl group, which is bonded to the same Carbon atom that the hydroxyl group. On the other hand, these three allylic alcohols have another double bond disubstituted that due to the absence of an allylic hydroxy group and a high steric hindrance remained intact.

The reaction selectivity showed that the oxidation of the hydroxy group of geraniol to aldehyde was easier than nerol. This higher selectivity for aldehyde was a consequence of a lower formation of epoxide; possibly, the formation of the transition state that led to the epoxide more favourably for nerol than geraniol. It is well established that geraniol has a *trans*-ol and

nerol a *cis*-ol configuration around the trisubstituted Carbon-Carbon double bond. Consequently, the interaction of Niobium with the hydroxyl group of nerol is more effective.

Although the selectivity obtained herein have been comparable to those achieved in oxidation reactions carried out over $WO_3$-$SiO_2$ mesoporous catalysts, the conversions were higher even at a lower temperature [25].

*Recovery and reuse of $Nb_2O_5$ - 2 h catalyst*

The catalyst was easily recovered from the reaction medium by centrifugation. High recovery rates were achieved (ca. 95%). Although the conversion did not reach 40%, the reaction maintained the high selectivity for nerol epoxide (Fig. 13).

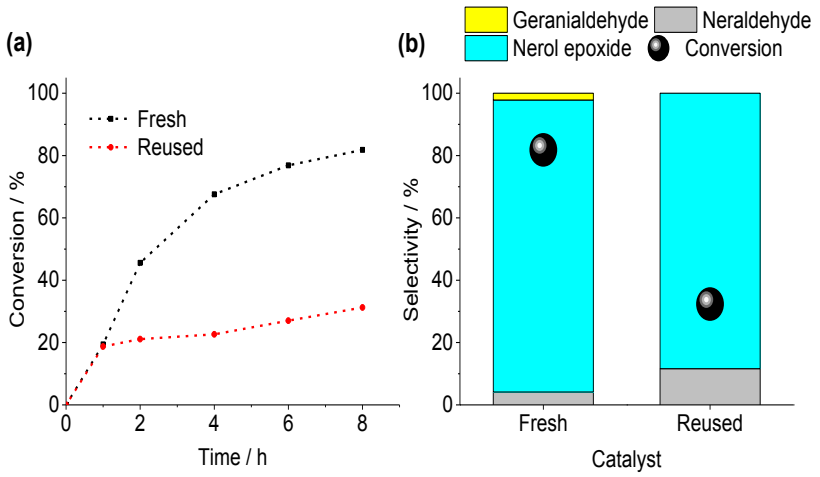


**Fig. 13.** Conversion (a) and selectivity (b) of nerol oxidation reactions with $H_2O_2$ in the presence of $Nb_2O_5$ - 2 h (fresh and reused). The black ball on b graphic represents the conversion at 8 h of reaction[a]
[a]Reaction conditions: Nerol (1.375 mmol), $H_2O_2$ (2.750 mmol), temperature (333 K), catalyst (4 mol%), $CH_3CN$ (10 mL)

To try understanding the reason for the drop in the activity of $Nb_2O_5$ - 2 h catalyst after it has been reused, we carried out analyses of FT-IR spectroscopy and XRD patterns and compared them with the data obtained from the fresh catalyst.

The IR spectra (Fig. 14) showed a decrease in the intensity of the band regarding the binding of Nb to the $OH^-$ groups, at wavenumbers 1700 $cm^{-1}$, after the catalyst has been reused. On the basis of the literature, it is correct to state that it is suggestive that there are less $OH^-$ groups on the catalyst surface [41].

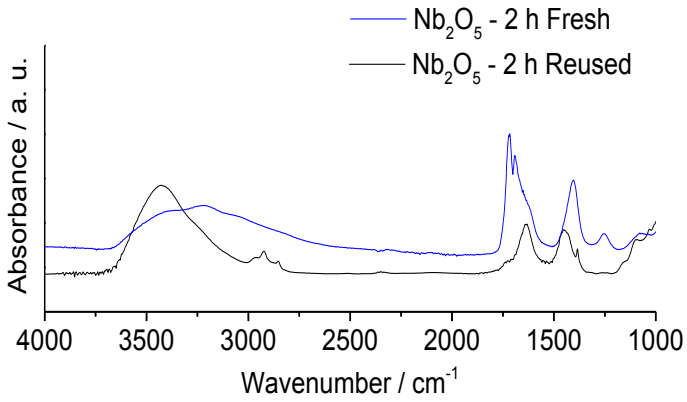


**Fig. 14.** FT-IR spectra obtained from $Nb_2O_5$ - 2 h fresh and reused catalysts

On the other hand, the analysis of the XRD patterns revealed an increase in crystallinity for the reused catalyst (Fig. 15). According to Ziolek et al, an increase of this parameter is directly related to the loss of availability of $OH^-$ groups on the catalyst surface [17]. The catalytic activity of the Niobium oxides varies according to the number of hydroxyl groups present on the catalyst surface; with less hydroxyl groups, the catalyst has lower activity [17,41].

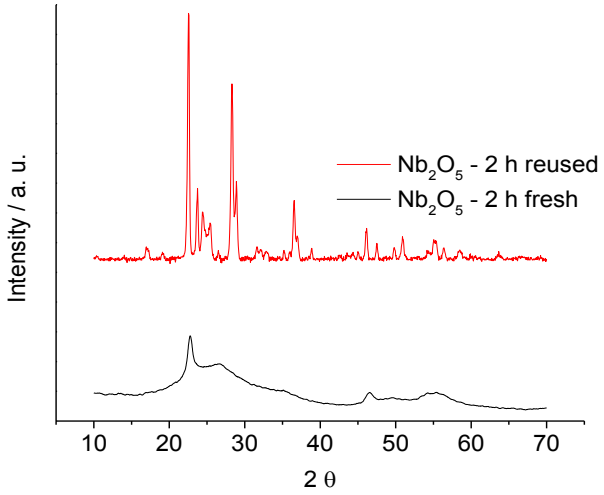


**Fig. 15.** XRD patterns obtained from the $Nb_2O_5$ - 2 h fresh and reused catalysts

Therefore, we can conclude that the main change that occurred on the $Nb_2O_5$ - 2 h catalyst after it has been recovered and reused was the lower availability of hydroxyl groups on their surface. The loss of surface hydroxyl groups suggests that the catalyst also had their strength acidity reduced. Moreover, the interaction with the Hydrogen peroxide oxidant may be also compromised, triggering a significant decrease in the activity of the reused catalyst in subsequent nerol oxidation reactions. Literature has described that the hydroxyl groups may

have the ability to bind to $H_2O_2$ molecules generating different reactive Oxygen species, which may favor the activity of these Niobium oxides in oxidation reactions [40,42].

Finally, an additional test was carried to verify if a possible leaching of catalyst could have contributed to their deactivation. The Niobium oxide was stirred and heated in the absence of the oxidant in solution without the presence of the nerol. After the removal of solid catalyst through centrifugation, nerol and oxidant were added to the supernatant and the reaction monitored during 8 h. No conversion was noticed as well as no oxidation product was detected. It is a guarantee that the $Nb_2O_5$-catalyzed reaction was truly heterogeneous. Besides the high recovery rate of catalyst achieved in the reuse, this evidence assures that the catalyst is almost insoluble in the reaction.

## Conclusions

The microwave-assisted hydrothermal method was efficient to produce Niobium oxides with controlled morphological properties, which demonstrated to be effective catalysts for the selective epoxidation of allylic terpenic alcohols with Hydrogen peroxide. Reactions were conveniently carried out in the presence of a solid catalyst (i.e., $Nb_2O_5$ - 2 h), and Hydrogen peroxide, an inexpensive and green oxidant.

Notwithstanding its lowest surface area, the most active catalyst was $Nb_2O_5$ - 2 h, a consequence of the highest amount of strongest acidic sites, which favored the interaction of the catalyst surface with terpenic alcohol. XRD patterns, IR and Raman spectra obtained from Niobium oxides assisted in the interpretation of catalytic test results through the acidity presented by the materials.

Likewise described for Tungsten or Titanium catalyzed reactions, the epoxidation of allylic terpenic alcohols with $H_2O_2$ is a hydroxy-assisted reaction. Therefore, the $Nb_2O_5$ - 2 h catalyst that had a higher number of Brønsted acidic site was the most active. The reactivity of other terpenic alcohols was also evaluated. Linalool, another allylic alcohol was unreactive, the consequence of high steric hindrance of the tertiary hydroxy group. The double bond of α-terpineol was not epoxidized, possibly due to the absence of an allylic hydroxy group. The stereochemistry of nerol makes it more reactive than geraniol, consequently, higher conversion and selectivity toward epoxide was achieved. The reusability of catalysts was investigated. High recovery rates (ca. 95%) were obtained. After recovery, the solid catalyst was reused without loss of selectivity, however, there was a significant decrease of conversion. Infrared

spectroscopy analysis and XRD patterns of the reused catalyst showed that there was a loss of hydroxyl groups on the catalyst surface, which compromised their activity.

## Credit author statement

I, Marcio Jose da Silva, corresponding author of this paper, state that:
The corresponding author is responsible for ensuring that the descriptions are accurate and agreed by all authors.
Authors equally contributed to the paper.

## Declaration of Competing Interest

The authors declare that they have no known competing financial interests or personal relationships that could have appeared to influence the work reported in this paper.

## Acknowledgements

The authors thank the Federal University of Viçosa, the PPGMQ-MG, and the development agencies CNPq and FAPEMIG. This study was financed in part by the Coordenação de Aperfeiçoamento de Pessoal de Nível Superior – Brasil (CAPES) – Finance Code 001.

## References

[1] F. Cavani, N. Ballarini, S. Luciani, Catalysis for society: towards improved process efficiency in catalytic selective oxidations, Top. Catal. 52 (2009) 935–947. https://doi.org/10.1007/s11244-009-9244-y.

[2] W. Schwab, C. Fuchs, F. Huang, Transformation of terpenes into fine chemicals, Eur. J. Lipid Sci. Technol. 115 (2013) 3–8. https://doi.org/10.1002/ejlt.201200157.

[3] P. Gallezot, Catalytic routes from renewables to fine chemicals, Catal. Today 121 (2007) 76–91. https://doi.org/10.1016/j.cattod.2006.11.019.

[4] M. Besson, P. Gallezot, C. Pinel, Conversion of biomass into chemicals over metal catalysts, Chem. Rev. 114 (2013) 1827–1870. https://doi.org/10.1021/cr4002269.

[5] P. T. Anastas, M. M. Kirchhoff, Origins, current status, and future challenges of green chemistry, Acc. Chem. Res. 35 (2002) 686–694. https://doi.org/10.1021/ar010065m.

[6] L. A. S. Viana, G. R. N. Da Silva, M. J. Da Silva, A Highly Selective $Na_2WO_4$-Catalyzed Oxidation of Terpenic Alcohols by Hydrogen Peroxide, Catal. Lett. 148 (2018) 374–382. https://doi.org/10.1007/s10562-017-2246-7.

[7] K. A. D. Swift, Catalytic transformations of the major terpene feedstocks, Top. Catal. 27 (2004) 143–155. https://doi.org/10.1023/B:TOCA.0000013549.60930.da.

[8] E. J. Lenardao, G. V. Botteselle, F. De Azambuja, G. Perin, R. G. Jacob, Citronellal as key compound in organic synthesis, Tetrahedron, 63 (2007) 6671–6712. DOI: 10.1016/j.tet.2007.03.159.

[9] S. Serra, D. De Simeis, Two Complementary Synthetic Approaches to the Enantiomeric Forms of the Chiral Building Block (2, 6, 6-Trimethyltetrahydro-2H-pyran-2-yl) methanol: Application to the Stereospecific Preparation of the Natural Flavor Linaloyl Oxide, Catalysts, 8 (2018) 362. https://doi.org/10.3390/catal8090362.

[10] J. L. F. Monteiro, C. O. Veloso, Catalytic conversion of terpenes into fine chemicals, Top. Catal. 27 (2004) 169–180. https://doi.org/10.1023/B:TOCA.0000013551.99872.8d.

[11] M. J. Da Silva, D. A. M. Ayala, Unravelling transition metal-catalyzed terpenic alcohol esterification: a straightforward process for the synthesis of fragrances, Catal. Sci. Technol. 6 (2016) 3197–3207. https://doi.org/10.1039/C5CY01538C.

[12] Z. Guo, B. Liu, Q. Zhang, W. Deng, Y. Wang, Y. Yang, Recent advances in heterogeneous selective oxidation catalysis for sustainable chemistry, Chem. Soc. Rev, 43 (2014) 3480–3524. https://doi.org/10.1039/C3CS60282F.

[13] L. A. F. Azevedo, L. Menini, E. V. Gusevskaya, Functionalization of the naturally occurring linalool and nerol by the palladium catalyzed oxidation of their trisubstituted olefinic bonds, J. Mol. Catal. A: Chem. 426 (2017) 429–434. https://doi.org/10.1016/j.molcata.2016.07.033.

[14] S. Sakaguchi, Y. Nishiyama, Y. Ishii, Selective oxidation of monoterpenes with hydrogen peroxide catalyzed by peroxotungstophosphate (PCWP), J. Org. Chem. 61 (1996) 5307–5311. https://doi.org/10.1021/jo960275q.

[15] J. Piera, J. Baeckvall, Catalytic oxidation of organic substrates by molecular oxygen and hydrogen peroxide by multistep electron transfer—a biomimetic approach, Angew. Chem., Int. Ed. 47 (2008) 3506–3523. https://doi.org/10.1002/anie.200700604.

[16] V. M. Vaschetti, A. L. Cánepa, D. Barrera, K. Sapag, G. A. Eimer, S. G. Casuscelli, Limonene oxyfunctionalization over Cu-modified silicates employing hydrogen peroxide and t-Butyl hydroperoxide: Reaction pathway analysis, Mol. Catal. 481 (2018) 110234. https://doi.org/10.1016/j.mcat.2018.11.005.

[17] M. Ziolek, I. Sobczak, P. Decyk, K. Sobanska, P. Pietrzyk, Z. Sojka, Search for reactive intermediates in catalytic oxidation with hydrogen peroxide over amorphous niobium(V) and tantalum(V) oxides, Appl. Catal., B 164 (2015) 288–296. https://doi.org/10.1016/j.apcatb.2014.09.024.

[18] R. Noyori, M. Aoki, K. Sato, Green oxidation with aqueous hydrogen peroxide, Chem. Commun. 16 (2003) 1977–1986. https://doi.org/10.1039/B303160H.

[19] W. Zhao, Y. Zhang, B. Ma, Y. Ding, W. Qiu, Oxidation of alcohols with hydrogen peroxide in water catalyzed by recyclable Keggin-type tungstoborate catalyst, Catal. Commun. 11 (2010) 527–531. https://doi.org/10.1016/j.catcom.2009.12.010.

[20] C. B. Vilanculo, M. J. da Silva, S. O. Ferreira, M. G. Teixeira, A rare oxidation of camphene to acid and aldehyde in the presence of Lacunar Keggin heteropoly salts, Mol. Catal. 478 (2019) 110589. https://doi.org/10.1016/j.mcat.2019.110589.

[21] D. E. De Vos, B. F. Sels, P. A. Jacobs, Practical heterogeneous catalysts for epoxide production, Adv. Synth. Catal. 345 (2003) 457–473. https://doi.org/10.1002/adsc.200390051.

[22] C. Wang, H. Yamamoto, Tungsten-catalyzed asymmetric epoxidation of allylic and homoallylic alcohols with hydrogen peroxide, J. Am. Chem. Soc. 136 (2014) 1222–1225. https://doi.org/10.1021/ja411379e.

[23] R. Kumar, G. C. G. Pais, B. Pandey, and P. Kumar, Hydroxy-assisted chemo- and stereo-selective epoxidation catalysed by a titanium silicate molecular sieve (TS-1)/$H_2O_2$ system, J. Chem. Soc., Chem. Commun. 13 (1995) 1315–1316. https://doi.org/10.1039/C39950001315.

[24] N. Marin-Astorga, J. J. Martinez, G. Borda, J. Cubillos, D. N. Suarez, H. Rojas, Control of the chemoselectivity in the oxidation of geraniol over lanthanum, titanium and niobium catalysts supported on mesoporous silica MCM-41, Top. Catal. 55 (2012) 620–624. https://doi.org/10.1007/s11244-012-9840-0.

[25] F. Somma, G. Strukul, Oxidation of geraniol and other substituted olefins with hydrogen peroxide using mesoporous, sol–gel-made tungsten oxide–silica mixed oxide catalysts, J. Catal. 227 (2004) 344–351. https://doi.org/10.1016/j.jcat.2004.07.006.

[26] M. Dusi, T. Mallat, A. Baiker, Epoxidation of functionalized olefins over solid catalysts, Catal. Rev. 42 (2000) 213–278. https://doi.org/10.1081/CR-100100262.

[27] M. J. Da Silva, P. H. S. Andrade, S. O. Ferreira, C. B. Vilanculo, C. M. Oliveira, Monolacunary $K_8SiW_{11}O_{39}$-Catalyzed Terpenic Alcohols Oxidation with Hydrogen Peroxide, Catal. Lett. 148 (2018) 2516–2527. https://doi.org/10.1007/s10562-018-2434-0.

[28] E. L. Moreno, K. Rajagopal, Challenges of catalysis acidity in solids, Quím. Nova 32 (2009) 538–542. http://dx.doi.org/10.1590/S0100-40422009000200044.

[29] A. Esteves, L. C. A. Oliveira, T. C. Ramalho, M. Goncalves, A. S. Anastacio, H. W. P. Carvalho, New materials based on modified synthetic $Nb_2O_5$ as photocatalyst for oxidation of organic contaminants, Catal. Commun. 10 (2008) 330–332. https://doi.org/10.1016/j.catcom.2008.09.012.

[30] A. C. Silva, D. Q. L. Oliveira, L. C. A. Oliveira, A. S. Anastácio, T. C. Ramalho, J. H. Lopes, H. W. P. Carvalho, C. E. R. Torres, Nb-containing hematites $Fe_{2-x}Nb_xO_3$: The role of $Nb^{5+}$ on the reactivity in presence of the $H_2O_2$ or ultraviolet light, Appl. Catal., A 357 (2009) 79–84. https://doi.org/10.1016/j.apcata.2009.01.014.

[31] C. Tiozzo, C. Bisio, F. Carniato, M. Guidotti, Grafted non-ordered niobium-silica materials: Versatile catalysts for the selective epoxidation of various unsaturated fine chemicals, Catal. Today 235 (2014) 49–57. https://doi.org/10.1016/j.cattod.2014.02.027.

[32] C. Tiozzo, C. Palumbo, R. Psaro , C. Bisio , F. Carniato, A. Gervasini, P. Carniti, M. Guidotti, The stability of niobium-silica catalysts in repeated liquid-phase, epoxidation tests: A comparative evaluation of in-framework and grafted mixed oxides, Inorg. Chim. Acta 431 (2015) 190–196. https://doi.org/10.1016/j.ica.2015.01.048.

[33] J. V. Coelho, L. C. A. Oliveira, F. C. C. Moura, P. P. De Souza, C. A. Silva, K. B. Batista, M. J. Da Silva, β-pinene oxidation by hydrogen peroxide catalyzed by modified niobium-MCM, Appl. Catal., A 419 (2012) 215–220. https://doi.org/10.1016/j.apcata.2012.01.032.

[34] W. M. Ventura, D. C. Batalha, H. V. Fajardo, J. G. Taylor, N. H. Marins, B. S. Noremberg, T. Tańskic, N. L. V. Carreño, Low temperature liquid phase catalytic oxidation of aniline promoted by niobium pentoxide micro and nanoparticles, Catal. Commun. 99 (2017) 135–140. http://dx.doi.org/10.1016/j.catcom.2017.06.004.

[35] D. C. Batalha, S. C. Luz, J. G. Taylor, H. V. Fajardo, B. S. Noremberg, I. J. S. Cherubin, R. M. Silva, M. R. F. Gonçalves, C. P. Bergmann, A. Valentini, N. L. V. Carreño, Application of $Al_2O_3/AlNbO_4$ in the oxidation of aniline to azoxybenzene, Chem. Pap. 74 (2020) 543–553. https://doi.org/10.1007/s11696-019-00897-5.

[36] J. Wan, P. Yang, G. Xiaolin, R. Zhou, Investigation on the structure-activity relationship of $Nb_2O_5$ promoting $CeO_2$-$CrO_x$-$Nb_2O_5$ catalysts for 1,2-dichloroethane elimination, Mol. Catal. 470 (2019) 75–81. https://doi.org/10.1016/j.mcat.2019.03.010.

[37] N. K. Gupta, A. Fukuoka, K. Nakajima, Amorphous $Nb_2O_5$ as a selective and reusable catalyst for furfural production from xylose in biphasic water and toluene. ACS Catal. 7 (2017) 2430–2436. https://doi.org/10.1021/acscatal.6b03682.

[38] N. H. Marins, C. T. Meereis, R. M. Silva, C. P. Ruas, A. S. Takimi, N. L. Carreño, F. A. Ogliari, Radiopaque dental adhesive with addition of niobium pentoxide nanoparticles, Polym. Bull. 75 (2018) 2301–2314. https://doi.org/10.1007/s00289-017-2150-8.

[39] M. Thommes, K. Kaneko, A. V. Neimark, J. P. Olivier, F. R. Reinoso, J. Rouquerol, K. S. Sing, Physisorption of gases, with special reference to the evaluation of surface area and pore size distribution (IUPAC Technical Report). Pure Appl. Chem. 87 (2015) 1051–1069. https://doi.org/10.1515/pac-2014-1117.

[40] T. Athar, A. Hashmi, A. Al-Hajry, Z. A. Ansari, S. G. Ansari, One-Pot Synthesis and Characterization of $Nb_2O_5$ Nanopowder, J. Nanosci. Nanotechnol. 12 (2012) 7922–7926. https://doi.org/10.1166/jnn.2012.6645.

[41] D. C. Castro, R. P. Cavalcante, J. Jorge, M. A. Martines, L. Oliveira, G. A. Casagrande, A. Machulek Jr, Synthesis and characterization of mesoporous $Nb_2O_5$ and its application for photocatalytic degradation of the herbicide methylviologen, J. Braz. Chem. Soc. 27 (2016) 303–313. http://dx.doi.org/10.5935/0103-5053.20150244.

[42] M. Ziolek, I. Sobczak, P. Decyk, L. Wolski, The ability of $Nb_2O_5$ and $Ta_2O_5$ to generate active oxygen in contact with hydrogen peroxide. Catal. Commun. 37 (2013) 85–91. https://doi.org/10.1016/j.catcom.2013.03.032.

[43] R. Brayner, F. Bozon-Verduraz, Niobium pentoxide prepared by soft chemical routes: morphology, structure, defects and quantum size effect, Phys. Chem. Chem. Phys. 5 (2003) 1457–1466. https://doi.org/10.1039/B210055J.

[44] W. M. Ventura, D. C. Batalha, H. V. Fajardo, J. G. Taylor, N. H. Marins, B. S. Noremberg, T. Tańskic, N. L. V. Carreño, Low temperature liquid phase catalytic oxidation of aniline promoted by niobium pentoxide micro and nanoparticles, Catal. Commun. 99 (2017) 135–140. https://doi.org/10.1016/j.catcom.2017.06.004.

[45] R. Turco, A. Aronnec, P. Carniti, A. Gervasini, L. Minieric, P. Pernicec, R. Tessera, R. Vitiello, M. Di Serio, Influence of preparation methods and structure of niobium oxide-based catalysts in the epoxidation reaction, Catal. Today 254 (2015) 99–103. https://doi.org/10.1016/j.cattod.2014.11.033.

[46] I. Nowak, M. Ziolek, Niobium Compounds: Preparation, Characterization, and Application in Heterogeneous Catalysis, Chem. Rev. 99 (1999) 3603–3624. https://doi.org/10.1021/cr9800208.

[47] O. F. Lopes, E. C. Paris, C. Ribeiro, Synthesis of $Nb_2O_5$ nanoparticles through the oxidant peroxide method applied to organic pollutant photodegradation: A mechanistic study. Appl. Catal., B 144 (2014) 800–808. https://doi.org/10.1016/j.apcatb.2013.08.031.

[48] S. M. Maurer, E. I. Ko, Structural and acidic characterization of niobia aerogels. J. Catal. 135 (1992) 125–134. https://doi.org/10.1016/0021-9517(92)90274-L.

[49] S. K. N. Ayudhya, A. Soottitantawat, P. Praserthdam, C. Satayaprasert, Effect of aging on the properties of mesoporous niobium oxide. Mater. Chem. Phys. 110 (2008) 387–392. https://doi.org/10.1016/j.matchemphys.2008.02.027.

[50] L. R. Pizzio, M. N. Blanco, A contribution to the physicochemical characterization of nonstoichiometric salts of tungstosilicic acid, Microporous Mesoporous Mater. 103 (2007) 40–47. https://doi.org/10.1016/j.micromeso.2007.01.036.

[51] N. H. Marins, B. E. J. Lee, R. M. Silva, A. Raghavan, N. L. V. Carreno, K. Grandfield, Niobium pentoxide and hydroxyapatite particle loaded electrospun polycaprolactone/gelatin membranes for bone tissue engineering, Colloids Surf., B 182 (2019) 110386. https://doi.org/10.1016/j.colsurfb.2019.110386.

[52] J. Cubillos, J. Martínez, H. Rojas, N. Marín-Astorga, Oxidation of geraniol using niobia modified with hydrogen peroxide, Rev. Fac. Ing., Univ. Antioquia 91 (2019) 106–112. https://doi.org/10.17533/udea.redin.n91a10.

[53] T. Tatsumi, M. Yako, M. Nakamura, Y. Yuhara, and H. Tominaga, Effect of alkene structure on selectivity in the oxidation of unsaturated alcohols with titanium silicalite-1 catalyst, J. Mol. Catal. A 78 (1993) L41–L45.

[54] M. Aminia, M. M. Haghdoostb, M. Bagherzadeh, Monomeric and dimeric oxido–peroxido tungsten(VI) complexes in catalytic and stoichiometric epoxidation, Coord. Chem. Rev. 268 (2014) 83–100. https://doi.org/10.1016/j.ccr.2014.01.035.

[55] W. Adam, A. Corma, T. I. Reddy, M. Renz, Diastereoselective catalytic epoxidation of chiral allylic alcohols by the TS-1 and Ti-β zeolites: evidence for a hydrogen-bonded, peroxy-type loaded complex as oxidizing species. J. Org. Chem. 62 (1997) 3631–3637. https://doi.org/10.1021/jo970364i.

[56] I. W. C. E. Arends, R.A. Sheldon, Activities and stabilities of heterogeneous catalysts in selective liquid phase oxidations: recent developments, Appl. Catal., A 212 (2001) 175–187. https://doi.org/10.1016/S0926-860X(00)00855-3.

[57] L. C. A. Oliveira, N. T. Costa, J. R. Pliego Jr., A. C. Silva, P. P. Souza, P. S. O. Patrício, Amphiphilic niobium oxyhydroxide as a hybrid catalyst for sulfur removal from fuel in a biphasic system. Appl. Catal., B 147 (2014) 43–48. https://doi.org/10.1016/j.apcatb.2013.08.003.

**PAPER 3: Dysprosium-doped Zinc tungstate nanospheres as highly efficient heterogeneous catalysts in green oxidation of terpenic alcohols with Hydrogen peroxide**

*Published in New Journal of Chemistry

NJC

ROYAL SOCIETY OF CHEMISTRY

PAPER

View Article Online
View Journal | View Issue

Check for updates

Cite this: *New J. Chem.*, 2021, 45, 6661

# Dysprosium-doped zinc tungstate nanospheres as highly efficient heterogeneous catalysts in green oxidation of terpenic alcohols with hydrogen peroxide†

Daniel Carreira Batalha,[a] Kellen Cristina Mesquita Borges,[b] Rosana de Fátima Gonçalves,[b] Murillo Henrique de Matos Rodrigues,[b] Mário Júnior Godinho,[b] Humberto Vieira Fajardo,[c] Carlos Giovani de Oliveira Bruziquesi[d] and Márcio José da Silva *[a]

[a] *Chemistry Department, Federal University of Viçosa, Campus Universitário, Avenue P. H. Rolfs, s/n, Viçosa, Minas Gerais, CEP 36570-900, Brazil. E-mail: silvamj2003@ufv.br; Tel: +55 31 3899-3071*

[b] *Chemistry Institute, Federal University of Catalão, Catalão, Goiás CEP 75.704-020, Brazil*

[c] *Chemistry Department, Federal University of Ouro Preto, Ouro Preto CEP 35400-000, Minas Gerais, Brazil*

[d] *Chemistry Department, Federal University of Minas Gerais, Belo Horizonte, Minas Gerais, Zip code 31279-201, Brazil*

Received 17th November 2020, Accepted 4th March 2021

DOI: 10.1039/d0nj05623e

† Electronic supplementary information (ESI) available. See DOI: 10.1039/d0nj05623e

## Abstract

A green route to oxidize terpenic alcohols (nerol and geraniol) with $H_2O_2$ over a solid catalyst was developed. The Dy-doped $ZnWO_4$ catalyst was synthesized by coprecipitation and microwave-assisted hydrothermal heating, containing different Dysprosium loads. All the catalysts were characterized through infrared spectroscopy, powder X-ray diffraction, surface area and porosimetry, transmission electronic microscopy image, and *n*-butylamine potentiometric titration analyses. The influence of main reaction parameters such as temperature, the stoichiometry of reactants, loads, and catalyst nature was assessed. $ZnWO_4$ 2.0 mol% Dy was the most active catalyst achieving the highest conversion (98%) and epoxide selectivity (78%) in nerol oxidation. The reaction scope was extended to other terpenic alcohols (*i.e.*, geraniol, borneol, and α-terpineol). The highest activity of $ZnWO_4$ 2.0 mol% Dy was

assigned to the lower crystallite size, higher surface area and pore volume, higher acidity strength and the greatest Dysprosium load.

**Graphical abstract**

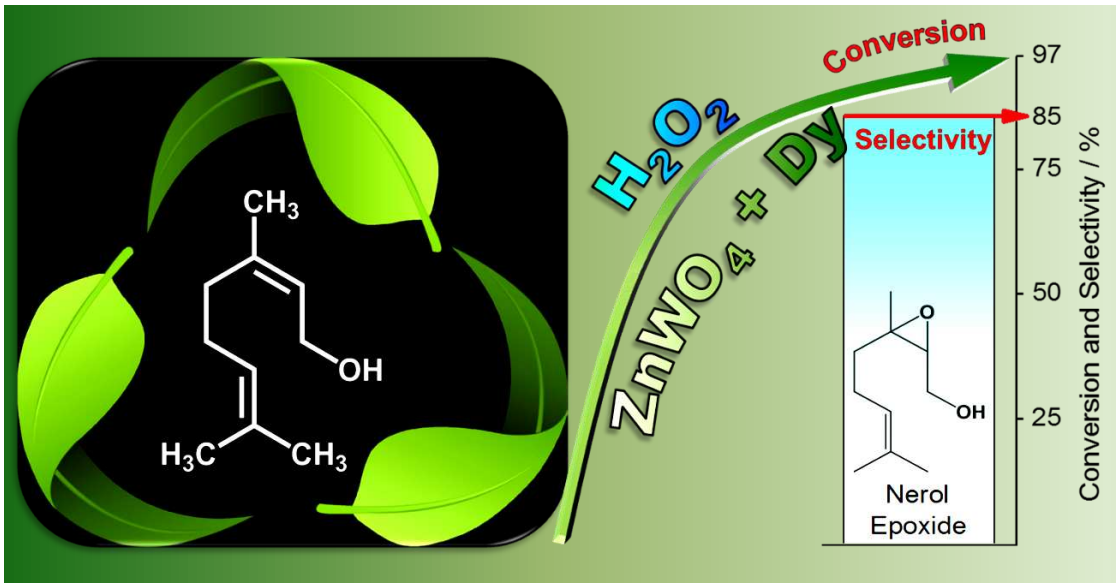


**Introduction**

Terpenic alcohols are abundant and renewable feedstock that has risen great interest for application in fine chemistry.[1–3] In particular, their oxidation and epoxidation reactions led to attractive products for perfume, fragrance, and pharmaceutical industries.[4–7] The presence of two oxidizable sites (*i.e.*, the hydroxyl group and the double bond) make these substrates sources of carbonylic products, and chiral compounds, which are both potential drug intermediates, thereby being valuable compounds to the fine chemical industry.[8–10]

Besides the use of a renewable raw material, the application of an environmentally benign oxidant makes the oxidative processes even more desirable and tuned with the principles of green chemistry.[11] In this sense, Hydrogen peroxide has great advantages such as the generation of water as the only by-product, low cost, non-flammability, and easy handling. Its efficiency as an oxidant is even more prominent due to its ability to bond to the surface of a solid catalyst giving reactive Oxygen species that will directly participate in oxidation reactions.[12,13]

Among the various catalysts used in oxidations of terpenic alcohols with Hydrogen peroxide, Keggin polyoxometalates should be highlighted due to their high structural versatility that allows their use as homogeneous and heterogeneous catalysts.[14–16] Various metal-

exchanged lacunar heteropolyacid salts (*i.e.*, Cesium, Potassium, or Sodium) have been demonstrated to be highly efficient in the oxidation of terpenic alcohols such as geraniol, nerol, borneol, and linalool.[17–19]

In this sense, solid catalysts play an essential role in making the oxidation processes greener by generating fewer effluents and residues than homogeneous counterparts, reducing their environmental impact. In addition, solid catalysts can be easily recovered and reused. The doping of solid catalysts with different elements can trigger a synergism that significantly improves their efficiency in oxidation processes. For instance, Zinc tungstate ($ZnWO_4$) has been used in photocatalysis, due to its electronic properties, good stability, and low cost.[20–22] Nonetheless, their doping with rare earth elements can bring not only structural benefits, in terms of particle size and surface area, but also electronic properties, consequently increasing their catalytic activity.[23] Some of these properties can be interesting in oxidation reactions, such as the presence of Lewis acid sites, and high stability.[24–26] The use of Dysprosium as a dopant has been demonstrated to be an efficient option in various oxidative processes.[27]

In this work, we describe the synthesis of efficient Zinc tungstate catalysts doped with Dysprosium by a simple coprecipitation methodology, followed by microwave-assisted hydrothermal synthesis. The catalysts were properly characterized by different methodologies and evaluated in oxidation reactions with Hydrogen peroxide of various terpenic alcohols, which are renewable origin feedstock of interest for the synthesis of fragrances, fine chemicals, and drug intermediates. Nerol was the model molecule. The influence of the main reaction parameters and the reuse of the solid catalyst were assessed.

## Experimental

### Synthesis

The catalysts were synthesized through the coprecipitation method at room temperature followed by the microwave hydrothermal method (MWH – in a microwave system of 2.45 GHz, with a maximum power of 800 W). Four catalysts with different Dy loads: $ZnWO_4$ – pure; $ZnWO_4$ – 0.5% Dy; $ZnWO_4$ – 1.0% Dy and $ZnWO_4$ – 2.0% Dy, were synthesized. Sodium tungstate (VI) dihydrate ($Na_2WO_4 \cdot 2H_2O$; 99% purity, Sigma-Aldrich), Zinc nitrate hexahydrate ($Zn(NO_3)_2 \cdot 6H_2O$, 99.5% purity, Aldrich), and Dysprosium(III) nitrate hexahydrate ($Dy(NO_3)_3 \cdot 6H_2O$; 99.999% purity, Aldrich) were used as synthesis precursors. Firstly, $Na_2WO_4 \cdot 2H_2O$ (*ca.* $5 \times 10^{-3}$ mol) was dissolved in deionized water (50 mL) with constant

stirring. Separately, $Zn(NO_3)_2 \cdot 6H_2O$ (*ca.* $5 \times 10^{-3}$ mol) was dissolved in deionized water (50 mL) at pH = 6. Afterward, the $Dy(NO_3)_3 \cdot 6H_2O$ dopant (*ca.* 0.5, 1.0, 2.0 mol%) was added to the aqueous solutions containing $Zn^{2+}$ ions, and subsequently, this solution was added to the $WO_4^{2-}$ solution, heated at 363 K, and stirred for 30 min. Immediately, a white suspension was formed and placed in a Teflon autoclave. Finally, the Teflon autoclave containing the solution was heated in a microwave system at 413 K for 1 h. The heating rate in this system was fixed at 25 $Kmin^{-1}$, and the pressure inside the autoclave was stabilized at 245 kPa. The formed suspension was washed with deionized water to neutralize the solution. White precipitates were collected and dried at 333 K.

**Characterization**

To assist the interpretation of the results of the catalytic tests and to verify the effects of structural properties, the catalysts were analyzed by several techniques of physical–chemical characterization.

Brunauer–Emmett–Teller (BET) and Density Functional Theory (DFT) methods were used to determine the surface area, distribution of average diameter, and pore volume of the catalysts, respectively. The porosimetry analyses were performed on the NOVA 1200 Quantachrome equipment, using the isotherms of physical adsorption/desorption of $N_2$, at 77 K. All catalytic materials were characterized by X-ray diffraction (XRD) using a D/Max-2500PC diffractometer (Rigaku, Japan), (Cu-Kα radiation $\lambda$ = 1.5418 Å) in the $2\theta$ range from 10° to 70° at a scanning rate of 0.02° $min^{-1}$. Crystallite sizes were calculated using the Scherrer equation:

$$L = \frac{K.\lambda}{\beta.cos\theta} \quad (1)$$

where $\lambda$ is the X-ray wavelength (nm), $\beta$ is the peak width of the diffraction peak profile at half maximum height resulting from small crystallite size in radians, and $K$ is a constant related to the crystallite shape, normally taken as 0.89.

Fourier transform infrared spectroscopy (FT-IR) spectra were recorded on a PerkinElmer Spectrometer, model Frontier. The shape, size, and form of the nanocrystals were analyzed by high-resolution transmission electron microscopy (HR-TEM) with a Tecnai G2-F20 microscope (200 kV). The strength of the acidic sites of Dy-doped tungstate catalysts was determined by ammonia temperature-programmed desorption ($NH_3$-TPD) performed on a CHEMBET-3000 TPR/TPD chemisorption analyzer (Quantachrome instrument). As such, 0.2

g was inserted in a U-shaped quartz tube and degassed for 1 hour under a He gas flux of 80 mL $min^{-1}$ (99.99%) at 393 K. After pre-treatment, the sample was cooled to 303 K, and it was kept in contact with the $NH_3$ gas flux of 40 mL $min^{-1}$ (99.9%) for 10 minutes, to saturate the acidic sites through the chemical adsorption of the probe molecule. Then, a He flux of 40 L $min^{-1}$ was set up for 10 minutes without heating, to remove an eventual physisorbed ammonia quantity, and immediately after, the material was heated up at a rate of 283 K $min^{-1}$ to 1173 K. Additionally, the strength of the acidic sites of Dy-doped tungstate catalysts also was determined by potentiometric titration with *n*-butylamine solution, using a BEL potentiometer (model W3B) with a glass electrode. To do this, each catalyst was suspended in acetonitrile and magnetically stirred for 3 h. In the next step, the suspension was titrated with *n*-butylamine (0.025 $molL^{-1}$) solution in acetonitrile.

**Catalytic tests**

The catalytic runs were carried out in the liquid phase with magnetic stirring, in a glass reactor coupled to the reflux condenser, heated in a water batch at atmospheric pressure. Typically, $H_2O_{2(aq)}$ (*ca.* 34 wt%) and nerol (*ca.* 1.375 mmol) were dissolved in $CH_3CN$ (*ca.* 10 mL) and heated to 333 K. After adding the solid catalyst, the reaction was started. The reaction progress was followed for 8 h, periodically collecting aliquots that were analyzed in a Shimadzu GC-2010 Plus equipped with an AOC-20i auto-injector and a flame ionization detector (FID). All the products were duly identified, and it was confirmed that spectrometry mass analysis was performed in Shimadzu GCMS-QP2010 Ultra equipment.

**Results and discussion**

**Characterization of the catalysts**

The main structural properties of the catalysts were determined aiming to support the results of the catalytic activity of the synthesized samples. Table 1 shows the results of porosimetry analysis obtained from the adsorption/desorption of $N_2$.

**Table 1.** Characterization of the catalysts through the physical adsorption of Nitrogen

| Catalysts | $S_{BET}$ ($m^2.g^{-1}$) | $V_{DFT}$ ($cm^3.g^{-1}$) | $D_{DFT}$ (Å) |
|---|---|---|---|
| $ZnWO_4$ | 59.8 | 0.212 | 122.3 |
| $ZnWO_4$ 0.5 mol% Dy | 59.1 | 0.161 | 93.3 |
| $ZnWO_4$ 1.0 mol% Dy | 60.6 | 0.171 | 93.3 |
| $ZnWO_4$ 2.0 mol% Dy | 85.2 | 0.187 | 78.0 |

$S_{BET}$ = surface area; $V_{DFT}$ = cumulative pore volume; $D_{DFT}$ = pore diameter

The doping level of Dy on the Zinc tungstate salts increased the surface area of these materials. The higher the Dy load, the greater the observed increase (Table 1). This effect was more noticeable when 2.0 mol% of Dy was loaded into Zinc tungstate. Conversely, an increase in the Dy load led to lowering of both the volume and pore size. These two opposite effects may be closely related to the pore shape of each solid.

A plausible explanation for this increase in the surface area is that the $Dy^{3+}$ ions may be punctually replacing $Zn^{2+}$ ions in the crystalline structure of Zinc tungstate, altering their properties. It is ascribed to the greater ionic radium of $Dy^{3+}$ when compared to $Zn^{2+}$ (*ca.* 102 pm and 74 pm, respectively).[21] The effect will be confirmed by the XRD and FT-IR analysis (Fig. 2).

The isotherms presented in Fig. 1a help to understand this phenomenon. All isotherms have a type V profile with H2 type hysteresis, which best matches weak interactions between adsorbents and adsorbates typical of micro and mesoporous materials.

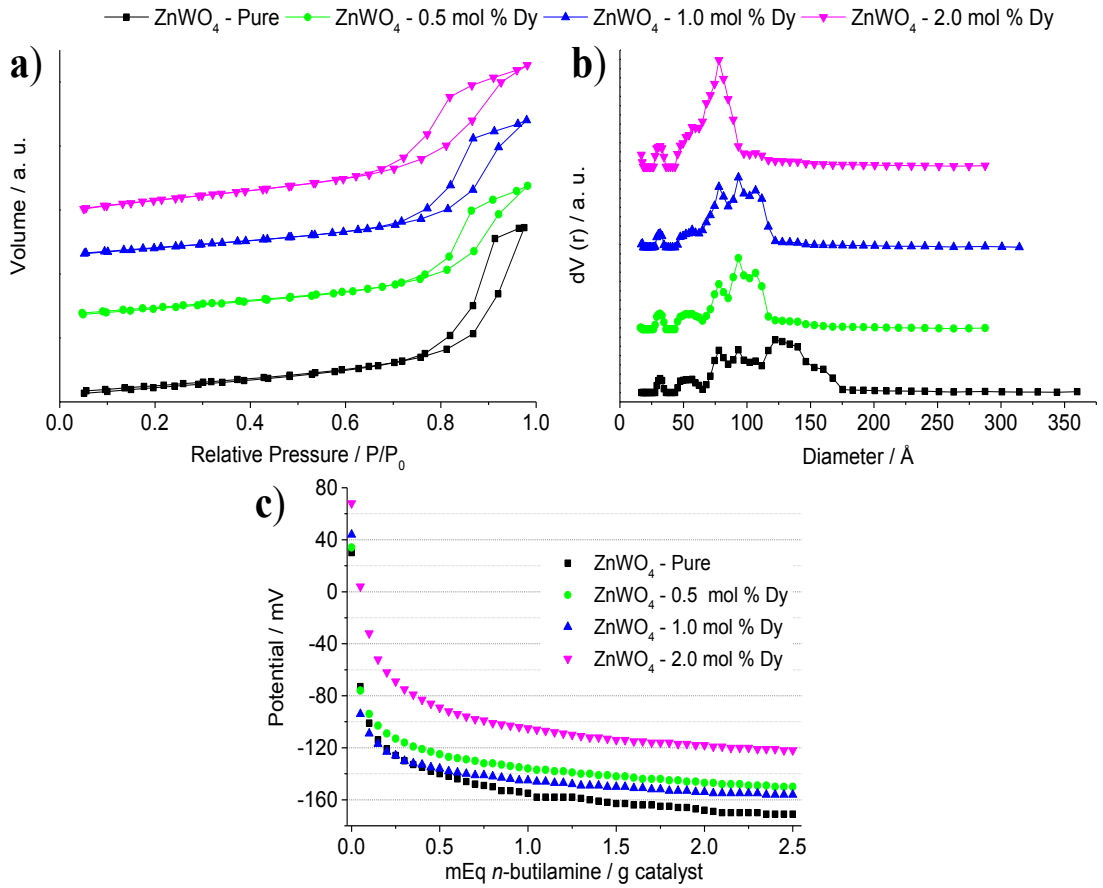


**Fig. 1** (a) Isotherms of adsorption/desorption of $N_2$, (b) pore diameter distribution b) and (c) potentiometric titration curves with *n*-butylamine of the synthesized catalysts

Through the data in Table 1 and the pore distribution in Fig. 1b, it is possible to conclude that all the catalysts predominantly have mesopores. The key to the reported differences in surface areas may be related to the slope of the desorption curves. The $ZnWO_4$ – pure, $ZnWO_4$ – 0.5 mol% Dy and $ZnWO_4$ – 1.0 mol% Dy catalysts have the same and steeper desorption branch compared to the $ZnWO_4$ – 2.0 mol% Dy desorption branch. It may be related to a more homogeneous distribution of the accessible pores, as illustrated in Fig. 1b. This characteristic can be directly linked to the Dy load present in the catalyst.[27,28]

We have found that the greater the amount of Dy, the higher the heterogeneity in the distribution of pores, that is, the number of pores within a narrow range of diameters is also higher. The decrease in Dy load results in a more homogeneous distribution of the number of pores of different pore diameter ranges. However, these structural changes do not change the fact that the material is mesoporous, since most of the quantified pores belong to the region of 20 to 500 Å in diameter, characteristic of mesopores.

As can be seen in the next sections, the differences evidenced by the results of Nitrogen adsorption/desorption isotherms can be important to justify the different results achieved in nerol oxidation reactions by these catalysts.

Fig. 1c shows the potentiometric titration curves of the four synthesized catalysts. According to Pizzio and Blanco (2007),[29] all the catalytic materials whose solutions have an initial electrode potential between 0 and 100 mV are characterized as catalysts with strong acidic sites. Fig. 1c shows that when Zinc tungstate catalysts were doped with Dy, the strength of acid sites increased. Moreover, a higher Dy load gives stronger acidity strength to the solid Zinc tungstate. These results agree with the literature.[30–32]

Fig. 2a shows the XRD diffraction patterns of the synthesized catalysts, together with the main Miller indices, which were properly indexed to the monoclinic wolframite Zinc tungstate structure according to the ICDD Card number 00-015-0774. Through this analysis, it is possible to notice the differences between the XRD diffraction profiles of different Dy-doped $ZnWO_4$ catalysts. As the amount of Dy increases in the catalyst structure, a loss of crystallinity is noticed. This factor was confirmed by calculating the crystallite size using the Scherrer equation.

The values of crystallite sizes obtained for the catalytic materials were the following: pure (24 nm), 0.5 mol% Dy (13 nm), 1.0 mol% Dy (9 nm), and 2.0 mol% Dy (7 nm). Therefore, an increase in the doping of Dy led to lower size of the crystallite.

Although an enlargement of typical diffraction peaks of $ZnWO_4$ and a diminishment in their intensities have occurred most of them remained in the diffractograms even when the highest load of $Dy^{3+}$ (*ca.* 2.0 mol%) was present. This behavior may be related to the size of the ionic radius of $Dy^{3+}$, which is larger than the radius of $Zn^{2+}$ ions, triggering an expansion of the crystalline network of the material, mainly while a greater amount of Dysprosium is doped on the $ZnWO_4$ sites.[32] This different crystallinity may help to explain the different catalytic activity of these materials.

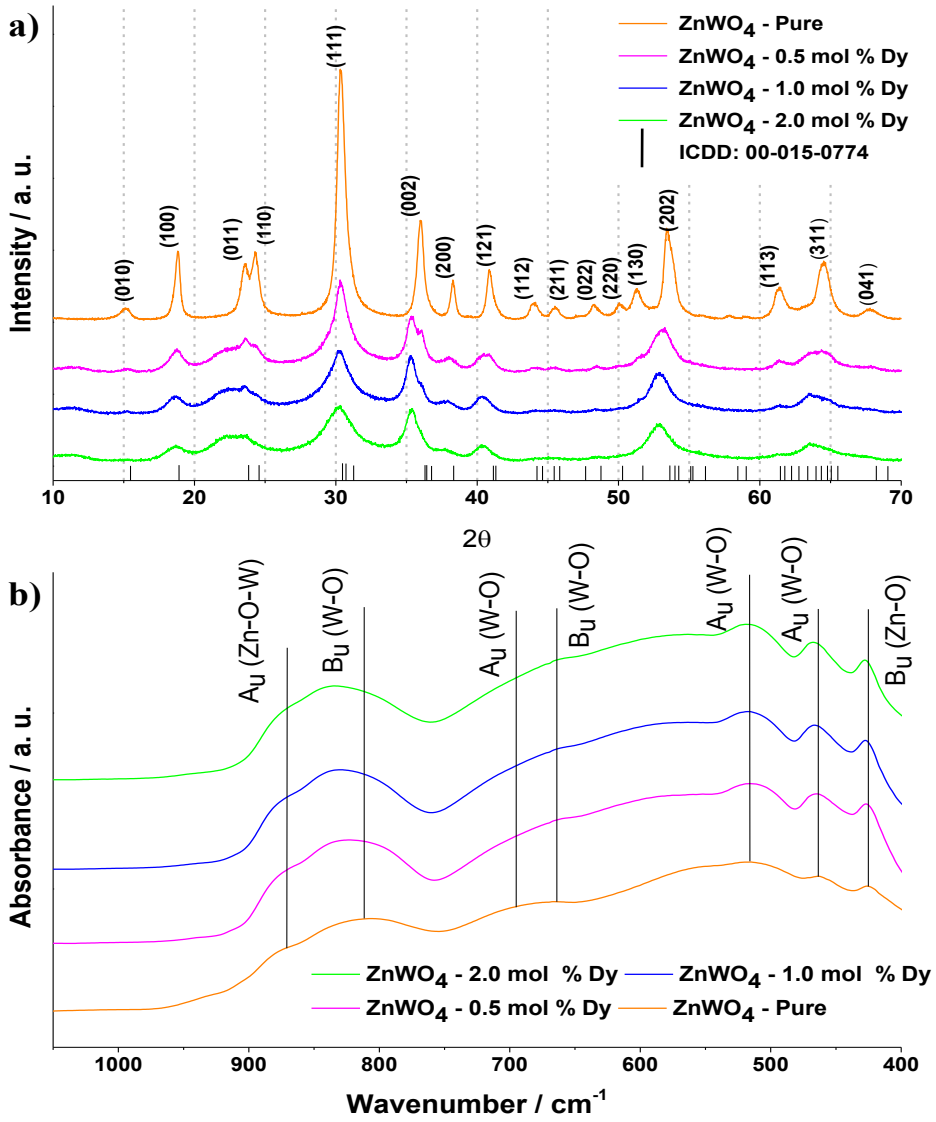


**Fig. 2** Powder XRD patterns (a) and FT-IR spectra of the catalysts (b)

Fig. 2b displays the infrared spectra of the synthesized catalysts. Absorption bands placed in the region between 400 and 1050 $cm^{-1}$ can be visualized. At 870 $cm^{-1}$ close wavenumbers, a band attributed to the Zn–O–W bond vibration is noted, which is a consequence of bending and stretching deformations. The stretching vibrations of the W–O bond give absorption bands in the regions between 811 and 694 $cm^{-1}$. It is possible to observe that, as the concentration of Dy increases, there is a displacement of the band close to 811 $cm^{-1}$ toward a higher wavenumber. This may be related to an increase in vibration energy due to the presence of $Dy^{3+}$ ions, which consequently led to a deformation in the material's structure, reinforcing that previously said for the XRD results.[21,33] Still on the FTIR spectra, the bands referring to the bending vibrations of the W–O bonds are noticed at 463 and 664 $cm^{-1}$ wavenumbers. Finally, the absorption bands present at 516 and 425 $cm^{-1}$ wavenumbers can be

assigned to the symmetric and asymmetric stretching modes of the W–O and Zn–O bonds, respectively, for the $WO_6$ and $ZnO_6$ octahedral units.[21]

Fig. 3a–d shows the high-resolution transmission electron microscopy images of the catalytic materials. From them, it is possible to verify the contrasting differences in the shapes and particle sizes for the different solids. The profile of the pure catalyst (Fig. 3a) shows basically the nanorod structure with sizes varying between 11 and 59 nm. In contrast, as the concentration of Dy increases in each material (Fig. 3b–d), noticeable changes occur, such as an increase in the presence of nanospheres, besides the increase in particle uniformity, together with a decrease in size (0.5 mol% Dy: 2–37 nm; 1.0 mol% Dy: 3–19 nm and 2.0 mol% Dy: 3–7 nm).

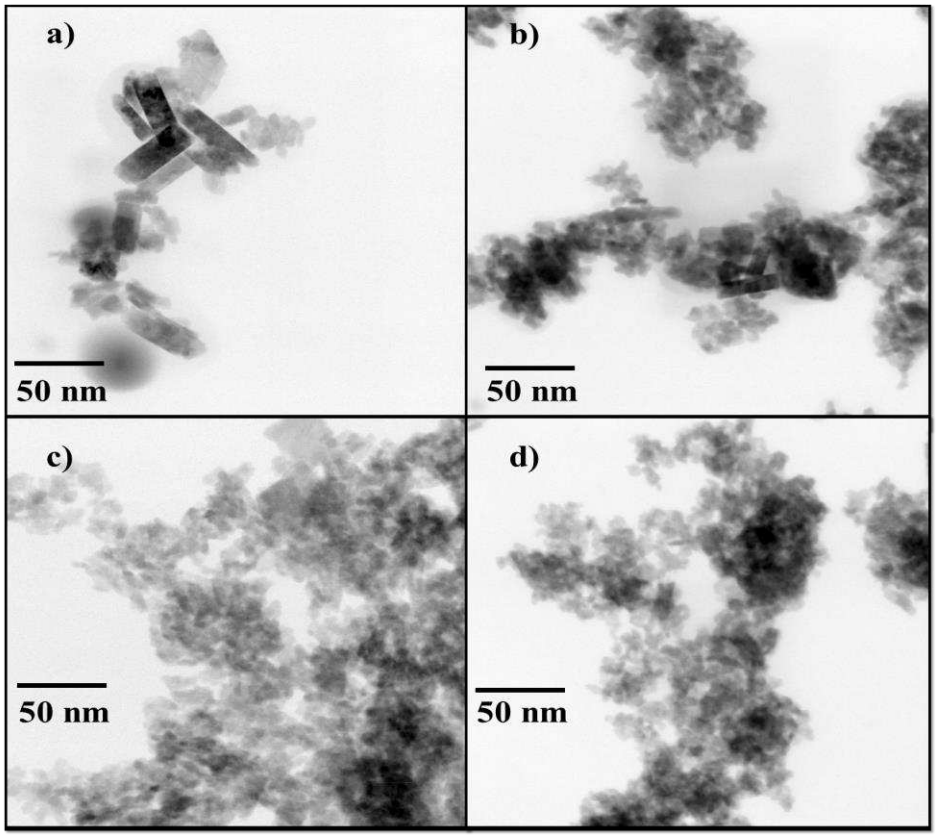


**Fig. 3** TEM image of the nanocrystals: a) $ZnWO_4$ - Pure; b) $ZnWO_4$ - 0.5 mol % Dy; c) $ZnWO_4$ - 1.0 mol % Dy and d) $ZnWO_4$ - 2.0 mol % Dy

It should be highlighted that when the catalysts are doped with 1.0 and 2.0 mol% Dy, they basically have nanospheres, indicating the influence of the presence of rare earth elements in the shape of the catalysts. It is important to emphasize that it was possible to obtain nanostructured materials by simple methodologies of synthesis and with high potential in oxidation reactions.

Fig. 4 shows high-resolution TEM images (HRTEM) obtained for the tungstate catalysts. It was demonstrated that the pure $ZnWO_4$, and $ZnWO_4$ doped with 0.5%, and 2% of Dy grew along the (002) direction with an interplanar distance of 0.250 nm, 0.256 nm, and 0.260 nm, respectively. For 1% Dy-doped $ZnWO_4$ an interplanar distance of 0.363 nm was measured relative to the crystallographic plane (110).

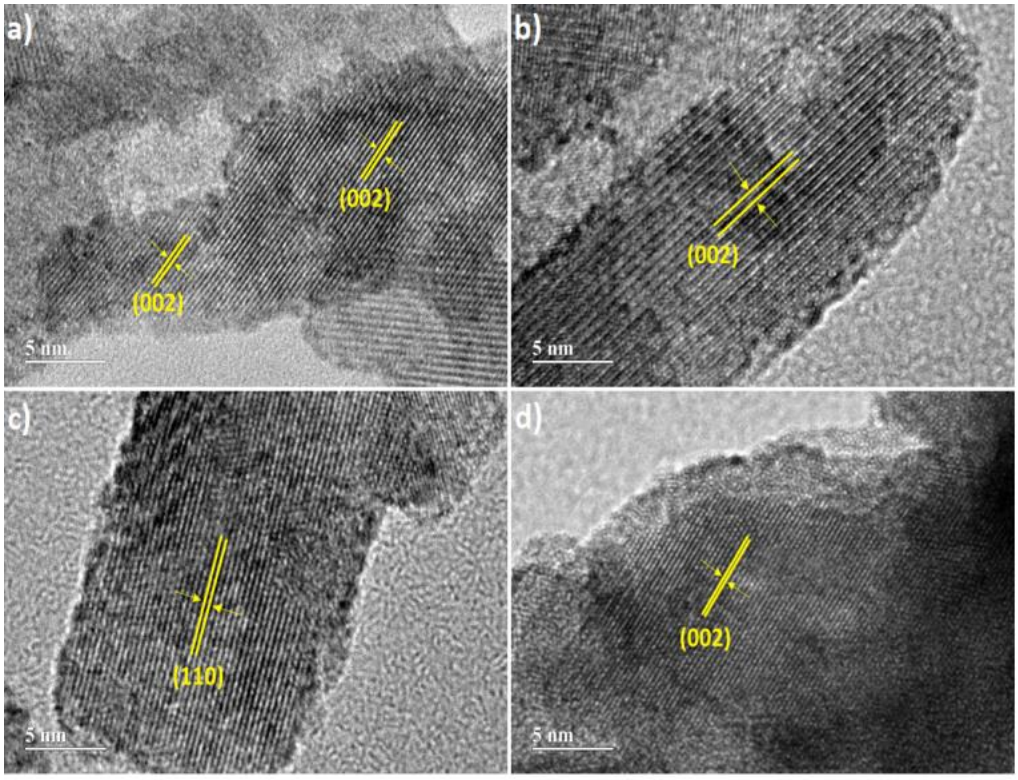


**Fig. 4** HRTEM image of: a) $ZnWO_4$ – pure; b) $ZnWO_4$ - 0.5 mol % Dy; c) $ZnWO_4$ - 1.0 mol % Dy and d) $ZnWO_4$ - 2.0 mol % Dy

Fig. 5 displays the TPD-$NH_3$ curves. Normally, it has been shown that the desorbed ammonia in the temperature ranges of 423–573 K, 573–773 K, and above 773 K was previously adsorbed on the weak, medium, and strong acid sites, respectively.[33–35] The TCD signals for $ZnWO_4$, $ZnWO_4$ 0.5% Dy, $ZnWO_4$ 1.0% Dy, and $ZnWO_4$ 2.0% Dy were integrated to assess the characteristic acidity strength of each catalyst, and the data are summarized in Table 2.

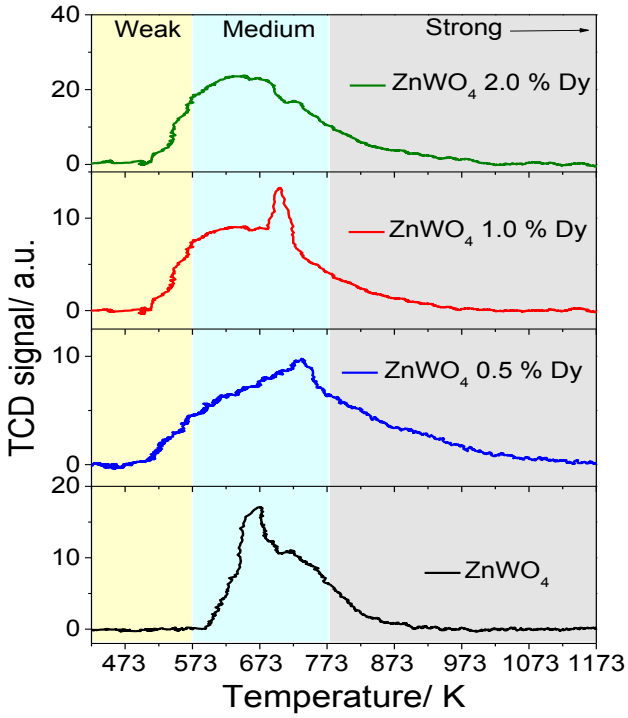


**Fig. 5** $NH_3$-TPD curves of $ZnWO_4$, $ZnWO_4$ 0.5 % Dy, $ZnWO_4$ 1.0 % Dy and $ZnWO_4$ 2.0 % Dy

**Table 2** Total integrated area of the TCD signal of $NH_3$-TPD profile and percentage of weak, medium and strong acidity (by integrating the respectively temperature ranges) of the $ZnWO_4$, $ZnWO_4$ 0.5 % Dy, $ZnWO_4$ 1.0 % Dy and $ZnWO_4$ 2.0 % Dy catalysts

| Catalysts | Total Area / a.u. | Weak / % | Medium / % | Strong / % |
|---|---|---|---|---|
| $ZnWO_4$ | 2042 | 0 | 84 | 16 |
| $ZnWO_4$ 0.5 % Dy | 2206 | 8 | 57 | 35 |
| $ZnWO_4$ 1.0 % Dy | 2548 | 10 | 75 | 15 |
| $ZnWO_4$ 2.0 % Dy | 5430 | 11 | 73 | 16 |

The integrated area values indicated that an increase in the Dy load increased the acidity strength. The $ZnWO_4$ 2.0% Dy catalyst displayed the highest content of medium acidity strength sites (highest area value, see Table 2). Nevertheless, the percentages of each type of acidity strength were different for each material. The $ZnWO_4$ catalyst had the highest content of medium acidic sites (84%), while the $ZnWO_4$ 0.5% Dy had the highest percentage of acidic sites of strong nature (35%).

Overall, the increase in Dy content suggests an increase in the proportion of weak acidic sites, with percentage values of 0, 8, 10, and 11% for the $ZnWO_4$, $ZnWO_4$ 0.5% Dy, $ZnWO_4$ 1.0% Dy and $ZnWO_4$ 2.0% Dy catalysts, respectively.

**Catalytic tests**

Initially, screening to select the most active catalyst was performed. Fig. 6 shows the kinetic curves with Zinc tungstate catalysts doped with different loads of Dysprosium, besides the pure Zinc tungstate.

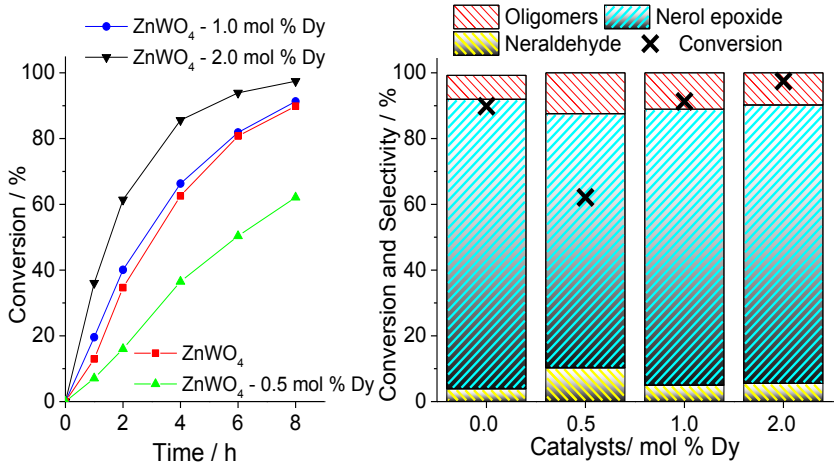


**Fig. 6** Conversion and selectivity of nerol oxidation reactions with $H_2O_2$ in the presence of Zinc tungstate catalysts. Reaction conditions: nerol (1.375 mmol), $H_2O_2$ (2.750 mmol), temperature (333 K), catalyst (15 mg), $CH_3CN$ (10 mL)

Clearly, an increase in Dy load had a beneficial effect on the catalytic activity. Nonetheless, the catalyst 0.5 mol% Dy/$ZnWO_4$ had the worst performance compared to pure $ZnWO_4$. It can be assigned to the differences of porosity between the Zinc tungstate and the Dy-doped catalysts (Table 1), to the crystallinity and Dy load.

The pure catalyst ($ZnWO_4$) presented the highest values of diameter and pore volume. On the other hand, an increase in Dy load had opposite effects in the porosity of doped catalysts; while the volume of pores was gradually increased with a higher load, the diameter of the pores was being decreased, mainly for the highest load of Dy (Table 1). Therefore, when we correlate only the activity of Dy-doped $ZnWO_4$ catalysts, we concluded that the catalyst with the largest volume of pores (*ca.* 0.187 $cm^3\ g^{-1}$) was the most active. When we verified the volume of the pores of the undoped catalyst we realize that its pores are still bigger (*ca.* 0.210 $cm^3\ g^{-1}$) than the most active catalyst. It may explain the high activity of pure $ZnWO_4$. Another key aspect is that the tungstate catalyst can itself catalyze oxidations with Hydrogen peroxide.[20] Conversely, the catalyst with the lowest Dy load was less active due to its pores with the lowest volume.

However, the Dy load plays an essential role too. When the catalysts are doped with a load higher than 0.5 mol% Dy, this additional active site is present in enough amounts to compensate for the reduction of the pore volume of $ZnWO_4$ triggered by the Dy load. The

crystallinity of doped catalysts provides too important insights. An increase in Dy load diminished the size of the crystallite. Applying the Scherrer equation to the most intense diffraction peaks (Fig. 2a) the following values were obtained: 0.5 mol% Dy (13 nm), 1.0 mol% Dy (9 nm), and 2.0 mol% Dy (7 nm). This effect was attributed to the greater size of the ionic radius of $Dy^{3+}$ ions when compared to the $Zn^{2+}$ cations. The doping of Dy triggers an expansion of the crystalline network of the material, mainly when at higher loads.[32] This lower crystallite size may improve the ability of materials for binding with $H_2O_2$ molecules, which can increase the formation of reactive Oxygen species.[30,31]

Another important factor that may be influencing nerol oxidation is the acidity of the catalysts. According to the results presented by $NH_3$-TPD (Fig. 4), the total acidity is proportional to the amount of Dy, thus, the $ZnWO_4$ catalyst 2.0% Dy, which presented the greatest number of acidic sites (Table 2), was the most active. It is interesting to note that the distinct types of acidic sites (*i.e.*, weak, medium, and strong) can have different effects on the activity of Dy catalysts in the oxidation reactions. Among the used catalysts, those with the highest percentage in medium acidity strength sites were those that showed the best performance in the nerol oxidation. The presence of acidic sites on the catalyst surface can be essential for the interaction of the peroxide oxidant with the substrate.[30]

Scheme 1 describes a probable reaction pathway involving the peroxidation of the Dy-doped Zinc tungstate catalyst (*i.e.*, (Zn, Dy)$WO_4$) and the allylic oxidation assisted by the hydroxyl group.[30,31,38]

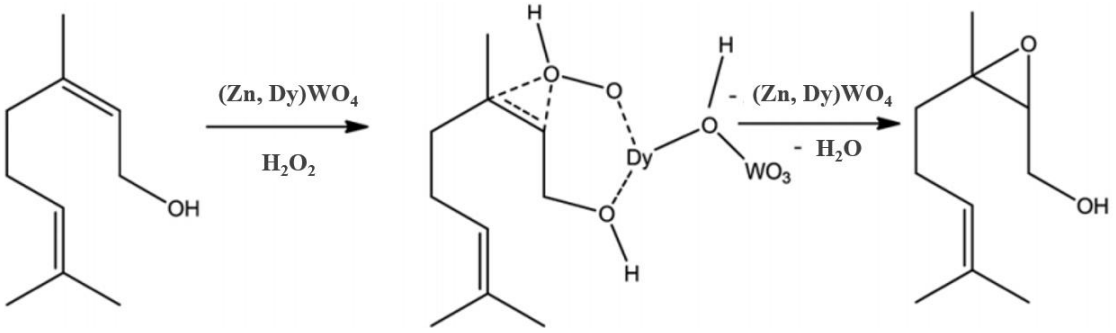


**Scheme 1** Hydroxyl group-assisted allylic oxidation of nerol with Hydrogen peroxide in the presence of $Dy^{3+}$-doped Zinc tungstate catalyst (adapted from ref. 38).

In allylic alcohol oxidation reactions, the active species commonly formed are the metal-peroxide intermediates. The metal acts as a Lewis acid, binding to an Oxygen atom of $H_2O_2$. While an Oxygen atom of the oxidant linked the metal peroxide to the olefin double bond, the Oxygen atom of the allylic hydroxyl group is bonded to the metal. Thus, the O–O

bond cleavage of the peroxide group occurs and, consequently, the epoxide is formed with the release of the catalyst.[31,38]

Fig. 6 shows the conversion and selectivity of the reaction products. Nerol has two potentially oxidizable sites; the carbonyl group which can be oxidized to aldehyde, and a double bond, which may be epoxidized. We have found that regardless of catalyst, nerol epoxide was always the major product, neraldehyde being the minor product. Oligomers, which are not detectable by the GC analysis, were formed in all the reactions, as evidenced by the mass balance of reaction. Once the most active catalyst is selected, we have investigated the effect of the amount of catalyst on the conversion and selectivity of products. Kinetic curves and selectivity of reactions are presented in Fig. 7.

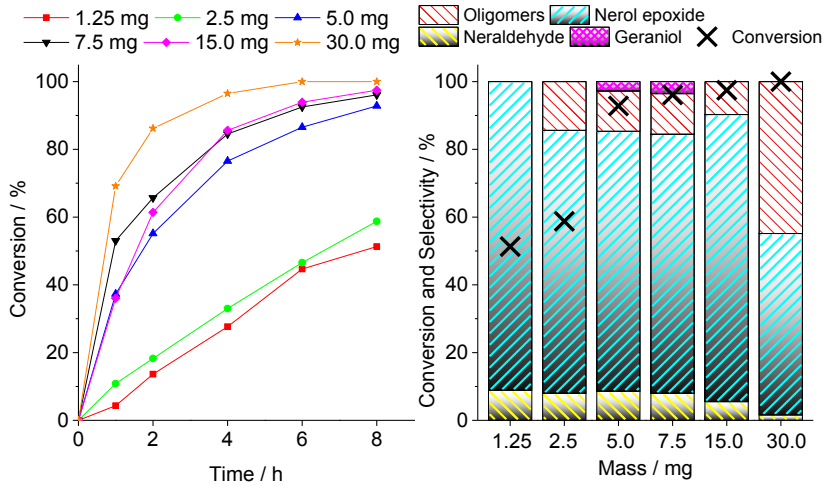


**Fig. 7** Conversion and selectivity of nerol oxidation reactions with $H_2O_2$ in the presence of different amounts of $ZnWO_4$ - 2.0% Dy catalyst. Reaction conditions: nerol (1.375 mmol), $H_2O_2$ (2.750 mmol), temperature (333 K), $CH_3CN$ (10 mL)

An increase in the amount of $ZnWO_4$ 2.0 mol% Dy catalyst enhanced the initial rate and the final conversion of the reactions. This effect can be attributed to the higher number of active sites present in the reaction when a higher mass of catalyst is used. On the other hand, with a load higher than 15.0 mg, the selectivity for oligomers shows a drastic increase. It is a consequence of the noticeable decomposition underwent by the oxidant, diminishing the efficiency of oxidation, a fact that occurred mainly when 30 mg of catalyst was used.

The catalytic performance of $ZnWO_4$ - 2.0 mol% Dy in nerol oxidation reactions with Hydrogen peroxide was compared with various metal oxide and heteropolyacid catalysts (see Fig. SM1, ESI†). It was found that the Dy/$ZnWO_4$ catalyst was more active and selective than other metal oxide catalysts (see ref. ESI†).[36,37] Only the heteropolyacid salt (*i.e.*, $Na_7PW_{11}O_{39}$) was more efficient, however, it was totally soluble in the reaction medium.[19]

The impact of the molar ratio of the oxidant to the substrate was also assessed (Fig. 8). Since the reaction was highly efficient with a low load of the oxidant, this effect was assessed only at three levels. At an equimolar stoichiometric amount (*ca.* 1 : 1), the oxidation was slightly compromised; a lower selectivity toward the main product (*i.e.* nerol epoxide) was achieved. Even an isomerization product (*i.e.*, geraniol) was formed under these conditions, although with a low selectivity (*ca.* 4%). Besides, the highest neraldehyde selectivity was reached with this load of the oxidant. When a 1 : 1.5 or 1 : 2 molar ratio of nerol to the oxidant was used, no significant difference was observed in both conversion and reaction selectivity.

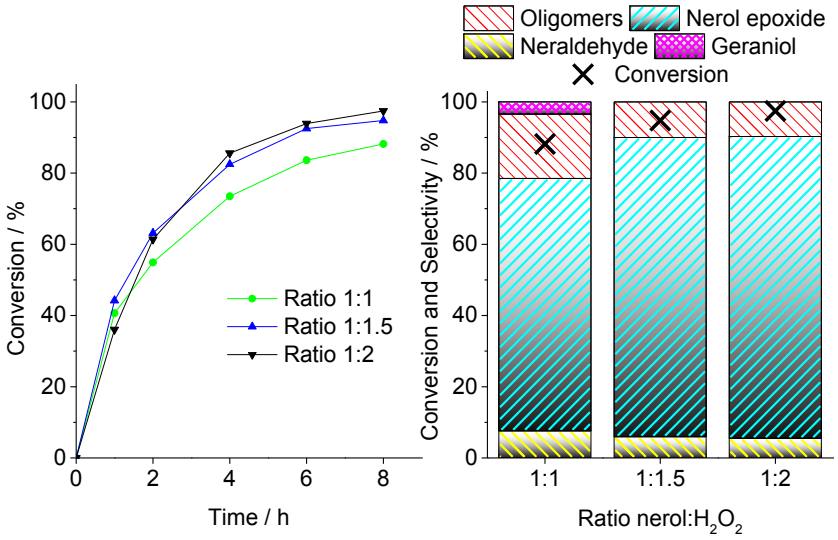


**Fig. 8** Conversion and selectivity of nerol oxidation reactions with different amounts of $H_2O_2$ in the presence of $ZnWO_4$ 2.0 mol % Dy catalyst. Reaction conditions: nerol (1.375 mmol), catalyst (15 mg), temperature (333 K), $CH_3CN$ (10 mL)

The influence of temperature was assessed, without overtaking the boiling point of acetonitrile (Fig. 9). The initial rate of reaction was very sensitive to the increasing temperature, as was also observed for the conversion of the reactions.

Conversely, varying the reaction temperature we noticed that the selectivity of products remained almost untouchable (Fig. 9). Neraldehyde and mainly the nerol epoxide were two oxidation products formed (Scheme 2).

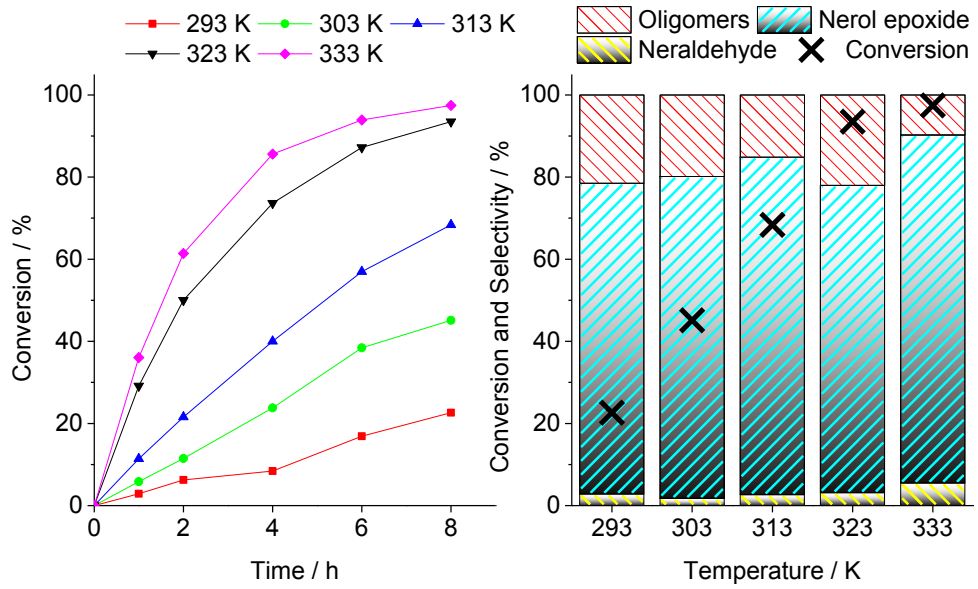


**Fig. 9** Conversion and selectivity of nerol oxidation reactions with $H_2O_2$ in the presence of $ZnWO_4$ - 2.0 mol % Dy catalyst in different temperatures. Reaction conditions: nerol (1.375 mmol), $H_2O_2$ (2.750 mmol), catalyst (15 mg), $CH_3CN$ (10 mL)

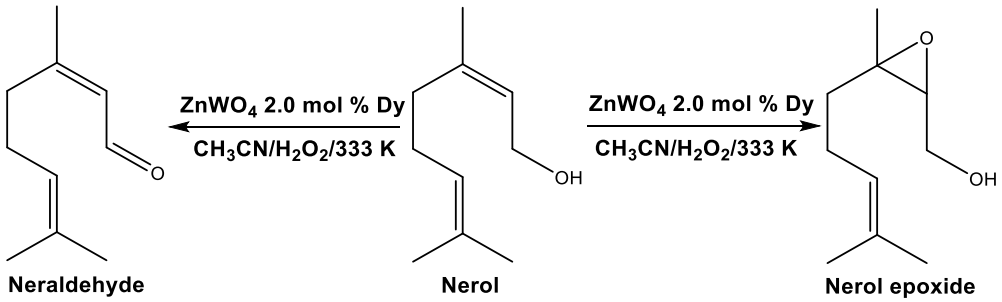


**Scheme 2** Oxidation reaction of nerol to nerol epoxide and neraldehyde

The reaction scope was extended to the other terpenic alcohols and the main results are shown in Fig. 10. The results of the nerol oxidation were compared to those obtained with different alcohols; geraniol (*i.e.*, allylic primary alcohol and geometric isomer of the nerol), borneol (*i.e.*, secondary bicyclic alcohol), and α-terpineol (unsaturated tertiary alcohol) (Fig. 10).

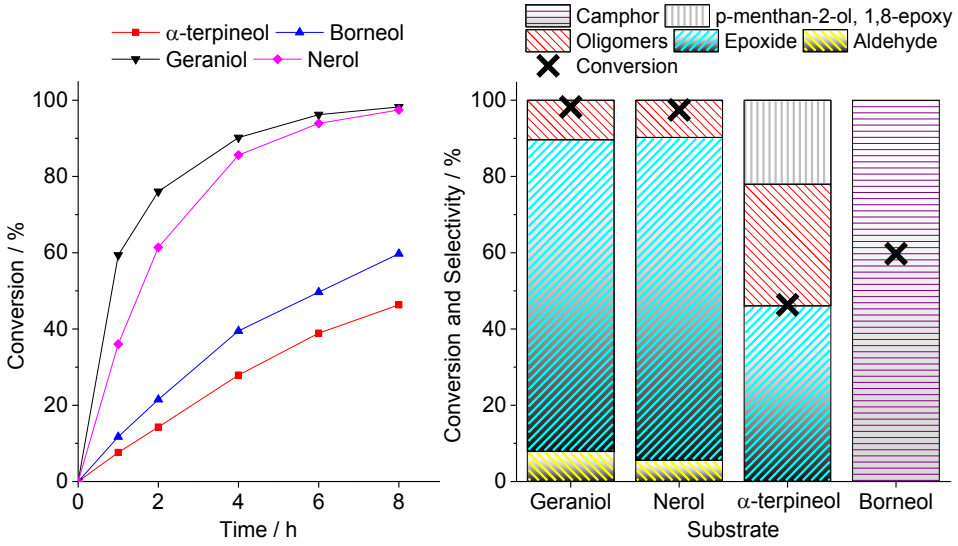


**Fig. 10** Conversion and selectivity of different substrates oxidation reactions with $H_2O_2$ in the presence of $ZnWO_4$ 2.0 mol % Dy catalyst. Reaction conditions: nerol (1.375 mmol), $H_2O_2$ (2.750 mmol), temperature (333 K), catalyst (15 mg), $CH_3CN$ (10 mL)

The substrates were chosen because they have hydroxyl groups and double bonds with different reactivity. The pair (*Z*) nerol and (*E*) geraniol are the *cis* and *trans* isomers, respectively. Although both have been completely consumed (*ca.* 100%, after 8 h), and both have been converted to aldehydes with the same selectivity, their double bonds presented different reactivity, revealing that the reaction selectivity was distinct. While the geraniol provided two epoxide products (*i.e.*, geraniol epoxide and geraniol diepoxide) (Scheme 3), the nerol provided only the epoxide product (Scheme 2).

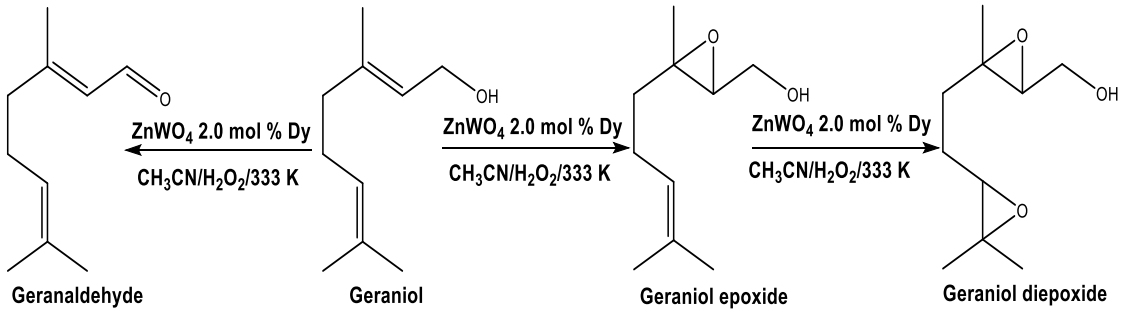


**Scheme 3** Oxidation reaction of geraniol to geranaldehyde, geraniol epoxide and geraniol diepoxide

Firstly, it is important to highlight that although Tatsumi *et al.* previously described that the oxidation reaction of these alcohols toward aldehydes is minimized, attributing it to the presence of the allylic hydroxyl groups.[21] Therefore, the preferential formation of epoxides could be expected. Recently, we have assessed the oxidation of terpenic alcohols over Niobium catalysts and verified the same effect.[38]

On the other hand, the literature describes that epoxidation of this double bond is a hydroxyl group-assisted reaction.[39] In oxidation reactions of the geraniol by Hydrogen peroxide

over Tungsten, Titanium, Niobium or Vanadium oxide catalysts, the coordination of metal oxide catalysts to the olefin double bond, as well as the peroxidation of the metal are always involved.[34,35] The peroxidation step of the Niobium catalyst and the interaction with the organic substrate are attributed to the different species of active sites present in the Niobium catalyst. Lewis acid sites and Brønsted acid sites allow the simultaneous adsorption of the oxidant and the organic substrate even in the presence of water.[40,41] Herein, we suppose that both Tungsten and Dysprosium are active sites for this reaction.

Compared to the geraniol and nerol, the reactivity of α-terpineol was significantly lower; only 35% conversion was achieved. However, even with a tertiary alcohol, two oxidation products were formed. In the presence of $ZnWO_4$ 2.0 mol% Dy catalyst, the double bond of terpineol was epoxidized providing the α-terpineol epoxide (Scheme 4). Even in a lower yield than that achieved in the reactions of nerol and geraniol, an epoxidation product was formed. The lower epoxide formation when compared to the other two terpenic alcohols can be attributed to the absence of the hydroxyl group in the allylic position to the double bond, which assists this kind of epoxidation. In addition, a rare cyclization reaction of this epoxide led to the formation of *p*-mentan-2-ol, 1,8 epoxide (Scheme 4).

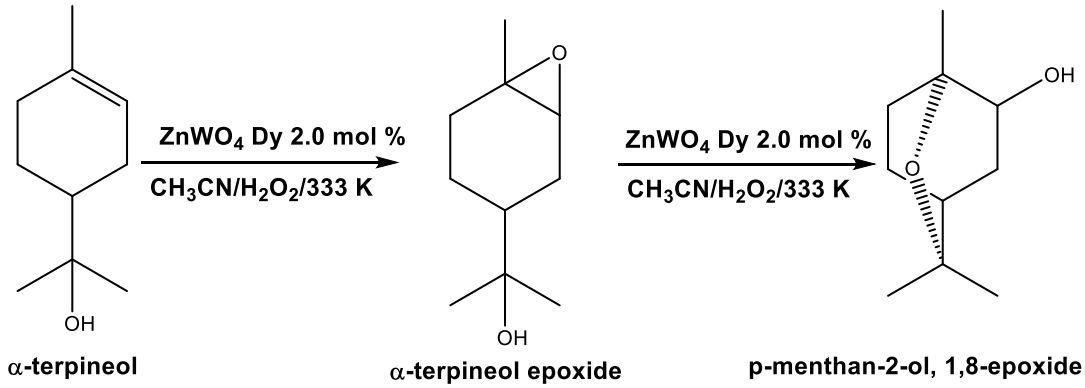


**Scheme 4** Oxidation reaction of α-terpineol to p-menthan-2-ol, 1,8-epoxy and α-terpineol epoxide

The formation of this bicyclic compound can be assigned to the nucleophilic attack of the hydroxyl group on the trisubstituted Carbon of α-terpineol epoxide, which provokes the rupture of the oxirane ring, followed by the prototropism between the hydroxyl group and the Oxygen atom of the epoxide. Previously it was revealed that 1,2-epoxy-cyclohexanes exist in a half-chair conformation, and the hydroxy-substituted isopropyl groups then require this conformation for a nucleophilic attack on the epoxide.[42]

The reaction between borneol and Hydrogen peroxide in the presence of the $ZnWO_4$ – 2.0% Dy catalyst was highly selective toward the carbonylic product (*ca.* 100% selectivity, Fig. 10), exclusively leading to camphor formation (Scheme 5).

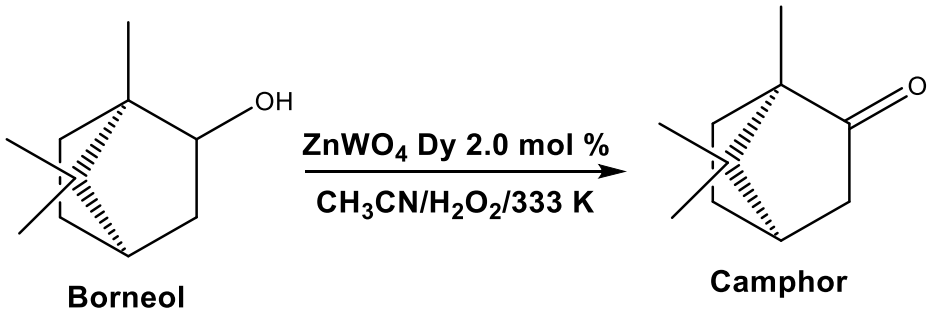


**Scheme 5** Oxidation reaction of borneol to camphor

The lower conversion achieved in borneol oxidation (*ca.* 60%) when compared to the oxidation of other alcohols is a consequence of different reactivity of hydroxyl groups. While geraniol and nerol have primary hydroxyl groups, borneol has the secondary one. The total conversion of the borneol occurred after longer reaction times (*ca.* 20 h).

The reusability of the $ZnWO_4$ 2.0 mol% Dy catalyst was assessed. Kinetic curves and the main results of conversion and selectivity are shown in Fig. 11.

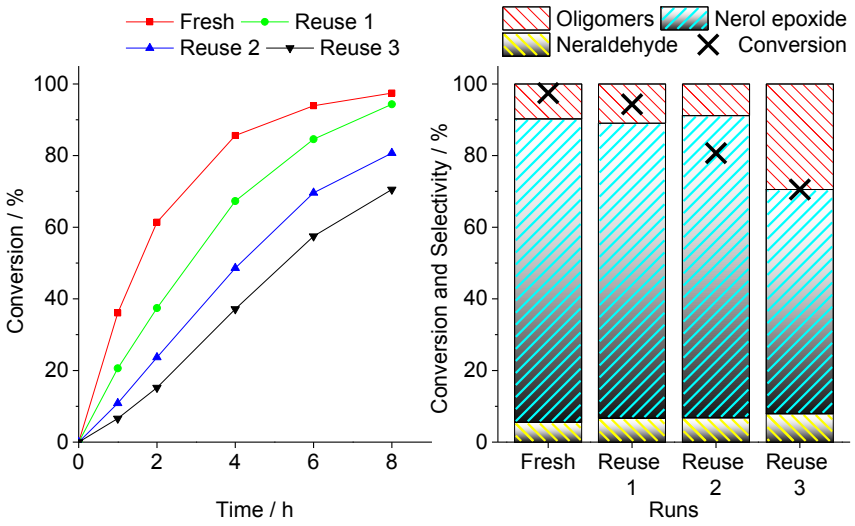


**Fig. 11** Evaluation of the efficiency in the nerol oxidation reaction in recovery and recycling tests of $ZnWO_4$ 2.0 mol % Dy catalyst with $H_2O_2$. Reaction conditions: nerol (1.375 mmol), $H_2O_2$ (2.750 mmol), temperature (333 K), catalyst (15 mg), $CH_3CN$ (10 mL)

Although omitted in Fig. 11, a high recovery rate of the catalyst was achieved in all the recycles, indicating that the procedure used was very efficient. After the first cycle of reuse, there was a gradual decrease in the conversion of reactions, which was followed during three cycles of recovery/reuse. In terms of selectivity, it was noticed that until the second cycle it remained basically constant, however, in the third cycle it was verified that the oxidation became less efficient, with a consequent increase in the formation of oligomers.

Aiming to investigate the reason for the loss in activity of the catalyst after the successive reuses, analyses of XRD patterns and infrared spectroscopy were performed. A comparison of reused and fresh catalyst is shown in Fig. 12 and 13.

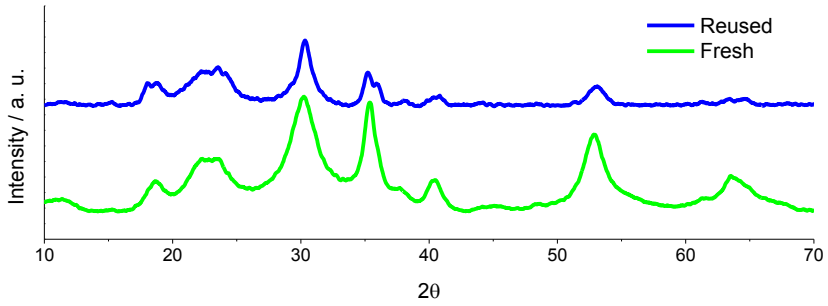


**Fig. 12** Powder XRD patterns of fresh and reused $ZnWO_4$ 2.0 mol % Dy catalyst in nerol oxidation reactions with $H_2O_2$. Reaction conditions: nerol (1.375 mmol), $H_2O_2$ (2.750 mmol), temperature (333 K), catalyst (15 mg), $CH_3CN$ (10 mL)

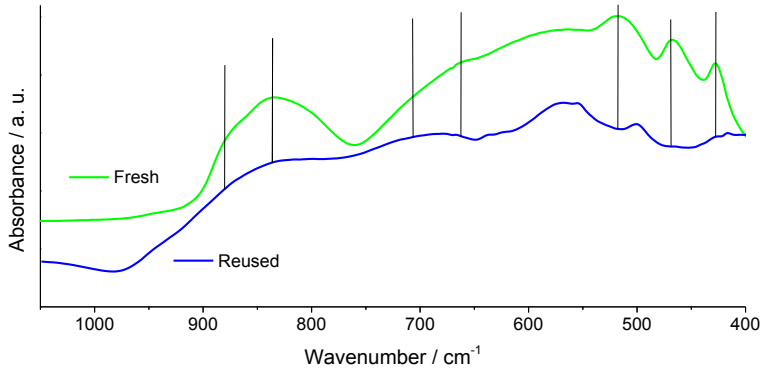


**Fig. 13** Infrared spectra of fresh and reused $ZnWO_4$ 2.0 mol % Dy catalyst in nerol oxidation reactions with $H_2O_2$. Reaction conditions: nerol (1.375 mmol), $H_2O_2$ (2.750 mmol), temperature (333 K), catalyst (15 mg), $CH_3CN$ (10 mL)

As shown in Fig. 12, the diffractogram profile of the reused catalyst showed some differences in relation to the fresh catalyst. With the aid of calculating the crystallite size, it is possible to evaluate the difference between the two materials. The fresh catalyst presents a crystallite size of approximately 7 nm, while after the fourth run this size was increased to 13 nm. Once we had previously demonstrated that the lower the crystallite size, the higher the catalytic activity, which partly explains the loss of activity of the $ZnWO_4$ 2.0 mol% Dy catalyst.

In previously published works, the authors found that crystallinity is a factor that can make the difference in catalytic activity. It was found that in materials with less crystallinity and smaller crystallite size, there is a higher ability to interact more easily with Hydrogen peroxide molecules, which consequently leads to the cleavage of O–O bonds in a greater number of reactive Oxygen species that will directly contribute to the oxidation process.[18,30,34]

On the other hand, comparing the bands referring to the bending of the W–O bonds (*ca.* 463 $cm^{-1}$), and the symmetric and asymmetric stretching modes of the W–O and Zn–O bonds (*ca.* 516 and 425 $cm^{-1}$ wavenumbers), present in the infrared spectrum of the fresh catalyst, and the bands present in the spectrum of the used catalyst, it is possible to see that they were shifted. This suggests that the $ZnO_6$ and $WO_6$ octahedral units, respectively, undergone a distortion, possibly caused by the loss of Dy ions. In addition to this effect, it is possible also that the size of the nanoparticles has undergone an increase, due to heating in the recycling process and due to the coalescence effect caused in the reaction medium.

The leaching of the catalyst was also assessed as reported in the literature.[43–46] Due to the difficulty of detecting the $Dy^{3+}$ ions in solution, two sets of experiments were performed (see Fig. SM2 and SM3, ESI†). The following approaches were used to evaluate the leaching. In the first one, two solutions with only acetonitrile were heated for 30 minutes, one containing the pure Zinc tungstate catalyst and the other containing the $Dy^{3+}$-doped Zinc tungstate catalyst. Afterward, the catalysts were removed, and the reactions proceeded for 8 h. While the first reaction was almost stopped, the second one proceeded to achieve a conversion of 80%. It is suggestive that $Dy^{3+}$ ions truly are being leached to the solution (Fig. 2SM and 3SM, ESI†). Additionally, a second test was performed with the two catalysts; they were heated for 30 minutes in a solution containing the oxidant and substrate, after that, the catalysts were removed (*i.e.*, pure, or doped Zinc tungstate), and the reaction was monitored for 8 h. Once, the results confirmed the $Dy^{3+}$ leaching, indicated by the conversion of 80%. However, different than verified with acetonitrile, there was also leaching of Zinc tungstate, although lower than the leaching of the Dy-doped catalyst. It was revealed that the presence of the aqueous solution of the oxidant increased the leaching of both catalysts (*i.e.*, pure, and doped Zinc tungstate).

## Conclusions

$ZnWO_4$-Dy catalysts were efficiently synthesized by co-precipitation followed by the microwave-assisted hydrothermal heating method, with controlled morphological properties, which demonstrated to be effective catalysts for the selective epoxidation of allylic terpenic alcohols with Hydrogen peroxide. Reactions were carried out in the presence of a Dysprosium-doped Zinc tungstate solid catalyst (*ca.* 0.5; 1.0, 2.0 mol% Dy), and Hydrogen peroxide, a cheap and green oxidant. $ZnWO_4$ 2.0 mol% Dy was the most active and selective catalyst, a consequence of the lowest crystallite size, acidity, the highest surface area, pore volume, and Dy load. As described for Tungsten, Niobium, or Titanium catalysts, the epoxidation of allylic

terpenic alcohols (*i.e.*, nerol and geraniol) with $H_2O_2$ is a hydroxy-assisted reaction. The different stereochemistry of nerol and geraniol revealed that only the geraniol was converted to epoxide and diepoxide products. The reactivity of other terpenic alcohols was also evaluated. Noticeably, the double bond of α-terpineol was epoxidized, and after undergoing a nucleophilic attack of the hydroxyl group led to the formation of a rare product (*i.e.*, *p*-mentan-2-ol, 1,8 epoxide). Borneol was selectively converted to camphor, however, since that it is a secondary alcohol, its total conversion occurred after longer reaction times (*ca.* 20 h). The reusability of the $ZnWO_4$ 2.0 mol% Dy catalyst was investigated. High recovery rates were obtained. After recovery, the solid catalyst was reused without loss of selectivity, however, there was a decrease of conversion after the third run. Infrared spectroscopy analysis and XRD patterns of the reused catalyst showed that the crystallite size of the recovered catalyst was increased, which compromised their activity.

## Conflicts of interest

There are no conflicts to declare.

## Acknowledgements

The authors thank the Federal University of Viçosa, the PPGMQ-MG, and the development agencies CNPq and FAPEMIG. This study was financed in part by the Coordenação de Aperfeiçoamento de Pessoal de Nível Superior – Brasil (CAPES) – Finance Code 001 and PROCAD 2013/2998/2014.

## Notes and references

1 M. Kopečná, M. Macháček, A. Nováčková, G. Paraskevopoulos and J. Roh, K. Vávrová, *Sci. Rep.*, **9**, 2019, 1-12.

2 W. Schwab, C. Fuchs and F. Huang, *Eur. J. Lipid Sci. Technol.*, 2013, **115**, 3-8.

3 M. J. da Silva, A. A. Julio and K. T. dos Santos, *Catal. Sci. Technol.*, 2015, **5**, 1261–1266.

4 M. J. da Silva and J. A. Villarrea, *Catal. Lett.*, 2017, **147**, 1646-1653.

5 C. B. Vilanculo, M. J. da Silva, M. G. Teixeira and J. A. Villarreal, *RSC Adv.*, 2020, **10**, 7691-7697.

6 M. Besson, P. Gallezot and C. Pinel, *Chem. Rev.*, 2013, **114,** 1827-1870.

7 L. A. S. Viana, G. R. N. da Silva and M. J. da Silva, *Catal. Lett.*, 2018, **148**, 374-382.

8 Z. Guo, B. Liu, Q. Zhang and W. Deng, Y. Yang, *Chem. Soc. Rev.*, 2014, **43**, 3480-3524.

9 S. Serra and D. de Simeis, *Catalysts*, 2018, **8**, 362.

10 K. C. Nicolaou, C. V. C. Prasad, P. K. Somers and C. K. Hwang, *J. Am. Chem. Soc.*, 1989, **111**, 5330-5334.

11 P. T. Anastas and M. M. Kirchhoff, *Acc. Chem. Res.*, 2002, **35,** 686-694.

12 W. M. Ventura, D. C. Batalha, H. V. Fajardo, J. G. Taylor, N. H. Marins, B. S. Noremberg, T. Tański and N. L. V. Carreño, *Catal. Commun.*, 2017, **99**, 135-140.

13 J. Piera and J. Baeckvall, *Angew. Chem. Int.*, 2008, **47**, 3506-3523.

14 N. C. Coronel and M. J. da Silva, *J. Cluster Sci.*, 2018, **29**, 195-205.

15 M. J. da Silva and N. A. Liberto, *Curr. Org. Chem.*, 2016, **20**, 1263-1283.

16 M. J. da Silva, L. C. de Andrade Leles, S. O. Ferreira, R. C. da Silva, K. de V. Viveiros, D. M. Chaves and P. F. Pinheiro, *ChemistrySelect*, 2019, **4**, 7665.

17 M. J. da Silva, P. H. S. Andrade, S. O. Ferreira, C. B. Vilanculo and C. M. Oliveira, *Catal. Lett.*, 2018, **148**, 2516-2527.

18 D. C. Batalha, S. O. Ferreira, R. C. da Silva and M. J. da Silva, *ChemistrySelect*, 2020, **5**, 1976-1986.

19 C. B. Vilanculo and M. J. Da Silva, *New J. Chem.*, 2020, **44**, 2813-2820.

20 X. Chai, J. Li, X. Wang, Y. Li and X. Yao, *RSC Adv.*, 2017, **7**, 40046-40052.

21 R. F. Gonçalves, E. Longo, A. P. A. Marques, M. D. P. Silva, L. S. Cavalcante, I. C. Nogueira, I. M. Pinatti, P. F. S. Pereira and M. J. Godinho, *J. Mater. Sci. Mater. Electron.*, 2017, **28**, 15466-15479.

22 Z. Liu, J. Tian, D. Zeng, C. Yu, L. Zhu, W. Huang, K. Yang and D. Li, *Mater. Res. Bull.*, 2017, **94**, 298-306.

23 A. Phuruangrat, P. Dumrongrojthanath, T. Thongtem and S. Thongtem, *J. Ceram. Soc. Japan*, 2017, **125**, 62-64.

24 M. Nishiura and Z. Hou, *Nat. Chem.*, 2010, **2**, 257-268.

25 S. Molaei and M. Ghadermazi, *Solid State Sci.*, 2020, **101**, 106148.

26 K. Thirumalai, M. Shanthi and M. Swaminathan, *Mater. Today Proc.*, 2018, **5**, 15342-15347.

27 M. Thommes, K. Kaneko, A. V. Neimark, J. P. Olivier, F. Rodriguez-Reinoso, J. Rouquerol and K. S. W. Sing, *Pure Appl. Chem.*, 2015, **87**, 1051-1069.

28 V. G. Teixeira, F. M. B. Coutinho and A. S. Gomes, *Quim. Nova*, 2001, **24**, 808-818.

29 L. R. Pizzio and M. N. Blanco, *Microporous Mesoporous Mater.*, 2007, **103**, 40–47.

30 M. Ziolek, I. Sobczak, P. Decyk and L. Wolski, *Catal. Commun.*, 2013, **37**, 85–91.

31 M. Ziolek, I. Sobczak, P. Decyk, K. Sobańska, P. Pietrzyk and Z. Sojka, *Appl. Catal. B Environ.*, 2015, **164**, 288-296.

32 D. P. Dutta and P. Raval, *J. Photochem. Photobiol. A Chem.*, 2018, **357**, 193-200.

33 J. Lu, M. Liu, S. Zhou, X. Zhou and Y. Yang, *Dye. Pigment.*, 2017, **136**, 1-7.

34 P. Manjunathan, S. P. Maradur, A. B. Halgeri and G. V. Shanbhag, *J. Mol. Catal. A: Chem.*, 2015, **396**, 47–54.

35 D. Liu, P. Yuan, H. Liu, J. Cai, D. Tan, H. He, J. Zhu and T. Chen, *Appl. Clay Sci.*, 2013, **80**, 407–412.

36 S. Thanasilp, J.W. Schwank, V. Meeyoo, S. Pengpanich and M. Hunsom, *J. Mol. Catal., A Chem.*, 2013, **380**, 49–56.

37 M. Sun, J. Xia, H. Wang, X. Liu, Q. Xia and Y. Wang, *Appl. Catal., B Environ.*, 2018, **227**, 488–498.

38 F. Zhang, H. Hu, H. Zhong, N. Yan, and Q. Chen, *Dalton Trans.*, 2014, **43**, 6041-6049.

39 D. C. Batalha, N. H. Marins, R. M. Silva, N. L. V. Carreño, H. V. Fajardo and M. J. da Silva, *Mol. Catal.*, 2020, **489**, 110941.

40 R. Kumar, G. C. G. Pais, B. Pandey, and P. Kumar, *J. Chem. Soc., Chem. Commun.*, 1995, 1315-1316.

41 I. W. C. E. Arends and R. A. Sheldon, *Appl. Catal., A*, 2001, **212**, 175-187.

42 W. Adam, A. Corma, T. I. Reddy and M. Renz, *J. Org. Chem.*, 1997, **62**, 3631-3637.

43 R. M. Carman and M. T. Fletche, *Aust. J. Chem.*, 1984, **37**, 1117–1122.

44 S. R. Churipard, P. Manjunathan, P. Chandra, G. V. Shanbhag, R. Ravishankar, P. V. C. Rao, G. S. Ganesh, A. B. Halgeri and S. P. Maradur, *New J. Chem.*, 2017, **41**, 5745–5751.

45 S. R. Churipard, K. S. Kanakikodi, J. R. Choudhuri and S. P. Maradur, *RSC Adv.*, 2020, **10**, 35988–35997.

46 K. S. Kanakikodi, S. R. Churipard, A. B. Halgeri and S. P. Maradur, *Sci. Rep.*, 2020, **10**, 13103–13111.

**Supplemental Material**

**Dysprosium-doped Zinc tungstate nanospheres as highly efficient heterogeneous catalysts in green oxidation of terpenic alcohols with Hydrogen peroxide**

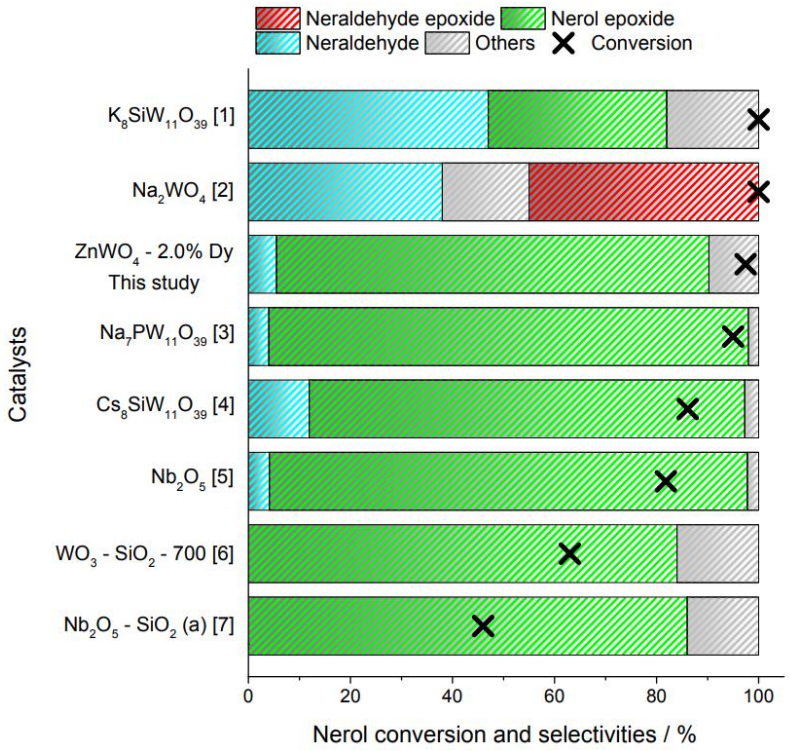


Ref.1 - Nerol:$H_2O_2$ (1:3); Catalyst (1.3 mol %); solvent DMA; 3 h; 363 K
Ref. 2 - Nerol:$H_2O_2$ (1:2); Catalyst (1.3 mol %); solvent DMA; 4 h; 363 K
This study - Nerol:$H_2O_2$ (1:2); Catalyst (3.5 mol %); solvent ACN; 8 h; 333 K
Ref. 3 - Nerol:$H_2O_2$ (1:1); Catalyst (0.3 mol %); solvent ACN; 4 h; 298 K
Ref. 4 - Nerol:$H_2O_2$ (1:2); Catalyst (4.0 mol %); solvent ACN; 8 h; 333 K
Ref. 5 - Nerol:$H_2O_2$ (1:2); Catalyst (4.0 mol %); solvent ACN; 8 h; 333 K
Ref. 6 - Nerol:$H_2O_2$ (1:1); Catalyst (3.4 mol %); solvent - ACN; 2 h; 343 K
Ref. 7 - Nerol:$H_2O_2$ (1:2); Catalyst (4.6 mol %); solvent MeOH; 5 h; 343 K

**Fig. SM1** Comparison of conversion and selectivity of nerol oxidation with Hydrogen peroxide over different solid catalysts

**References used in Fig. SM1:**


1 M. J. Silva, P. H. S. Andrade, S. O. Ferreira, C. B. Vilanculo and C. M. O. Oliveira, *Catal Lett.*, 2018, **148**, 2516-2434.

2 L. A. S. Viana, G. R. N. Silva and M. J. Silva, *Catal Lett.*, 2018, **148**, 374-386.

3 C. B. Vilanculo and M. J. Silva, *New J. Chem.*, 2020, **44**, 2813-2820.

4 D. C. Batalha, S. O. Ferreira, R. C. Silva and M. J. Silva, *ChemSelect*, 2020, **5**, 1976-1986.

5 D. C. Batalha, N. H. Marins, R. C. Silva, N. L. V. Carreño, H. V. Farjado and M. J. Silva, *Mol. Catal.*, 2020, **489**, 110941-110952

6 F. Somma and G. Strukul, *J. Catal.*, 2004, **227**, 344.

7 F. Somma, P. Canton, and G. Strukul, *J. Catal.*, 2005, **229**, 490.

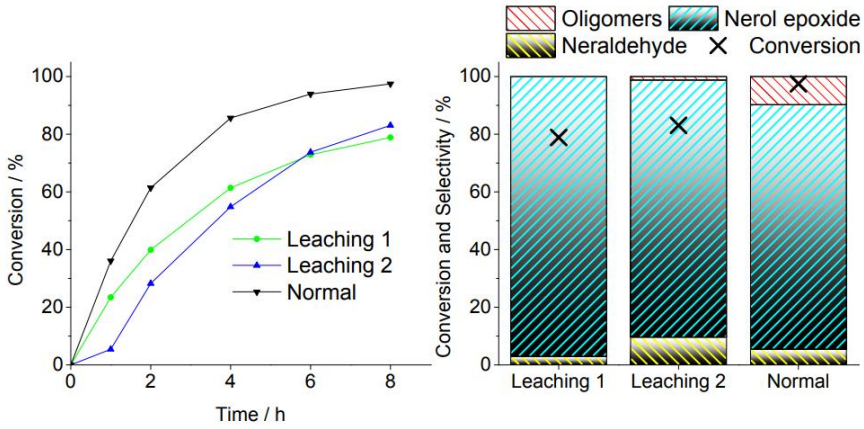


**Fig. SM2** Conversion and selectivity of nerol oxidation reactions with $H_2O_2$ in the presence of $ZnWO_4$ - 2.0% Dy catalyst[a]

[a]Reaction conditions: nerol (1.375 mmol), $H_2O_2$ (2.750 mmol), temperature (333 K), catalyst (15 mg), $CH_3CN$ (10 mL), time (8 h)

*Leaching 1:* Stirring 30 min (catalyst + solvent); after that, the catalyst was removed by centrifugation and the substrate and Hydrogen peroxide were placed in the reaction medium; the reaction was followed for 8 h with aliquots periodically collected.

*Leaching 2:* all components were placed in the reaction medium for 30 min under stirring; after this time, the catalyst was removed by centrifugation and the reaction proceeded normally until 8 h was completed.

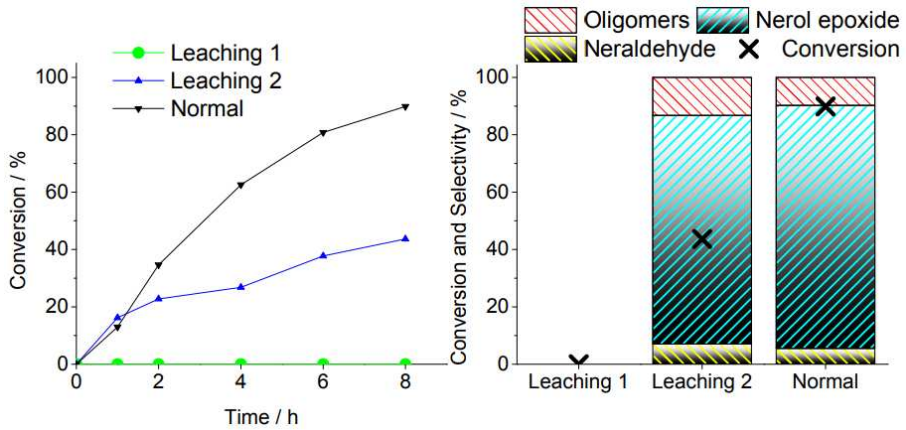


**Fig. SM3** Conversion and selectivity of nerol oxidation reactions with $H_2O_2$ in the presence of $ZnWO_4$ catalyst[a]

[a]Reaction conditions: nerol (1.375 mmol), $H_2O_2$ (2.750 mmol), temperature (333 K), catalyst (15 mg), $CH_3CN$ (10 mL), time (8 h)

*Leaching 1:* Stirring 30 min (catalyst + solvent); after that, the catalyst was removed by centrifugation and the substrate and Hydrogen peroxide were placed in the reaction medium; the reaction was followed for 8 h with aliquots periodically collected.

*Leaching 2:* all components were placed in the reaction medium for 30 min under stirring; after this time, the catalyst was removed by centrifugation and the reaction proceeded normally until 8 h was completed.

## NEROL PRODUCTS

### Nerol epoxide

EIMS 70 eV, m/z (rel. int. %): 170 $[M]^+$ (1), 152 (1), 137 (1), 109 (67), 95 (27), 82 (40), 69 (65), 67 (68), 55 (35), 43 (89), 41 (100).

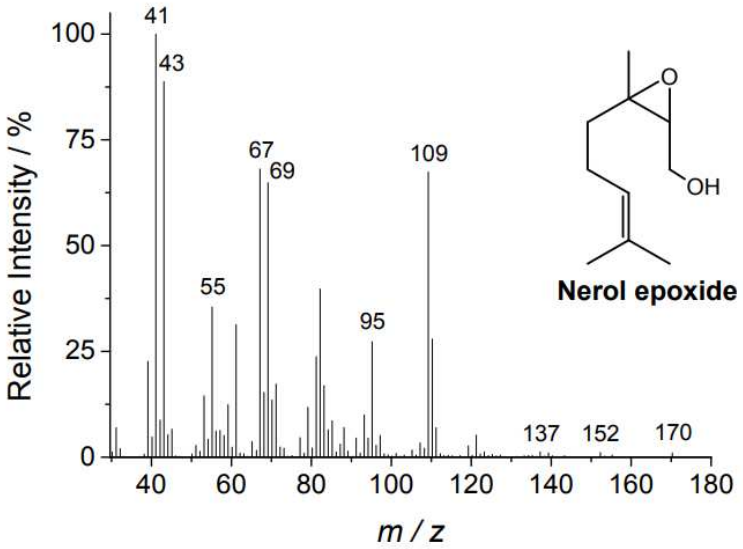


**Fig. SM4** Mass spectrum of nerol epoxide[1]

### Neraldehyde

EIMS 70 eV, m/z (rel. int. %): 152 $[M]^+$ (1), 94 (27), 84 (24), 69 (80), 53 (14), 41 (100), 39 (23).

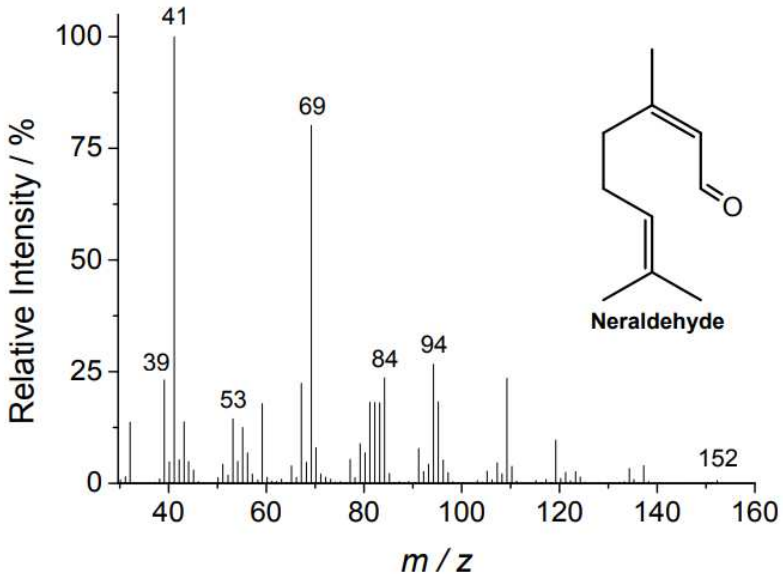


**Fig. SM5** Mass spectrum of neraldehyde[2,3]

## BORNEOL PRODUCT

### Camphor

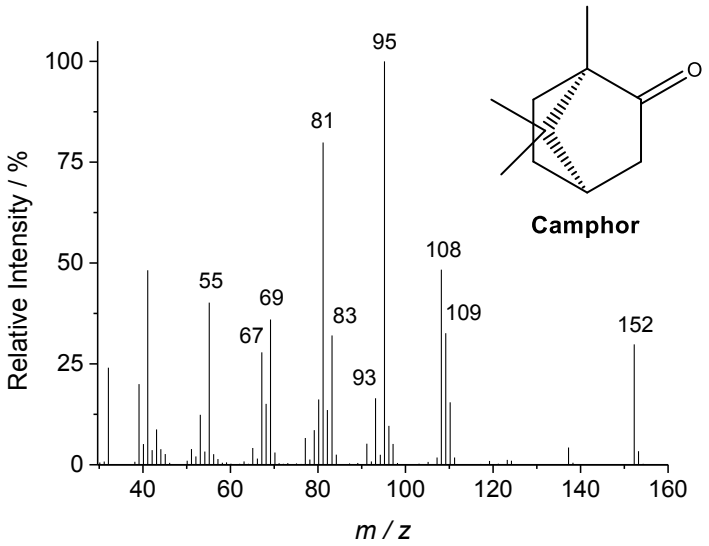


**Fig. SM6** Mass spectrum of camphor[4]

## GERANIOL PRODUCTS

### Geraniol diepoxide

EIMS 70 eV, *m/z* (rel. int. %): 186 $[M]^+$ (1), 155 (1), 125 (9), 111 (10), 93 (7), 84 (29), 71 (30), 59 (22), 43 (100).

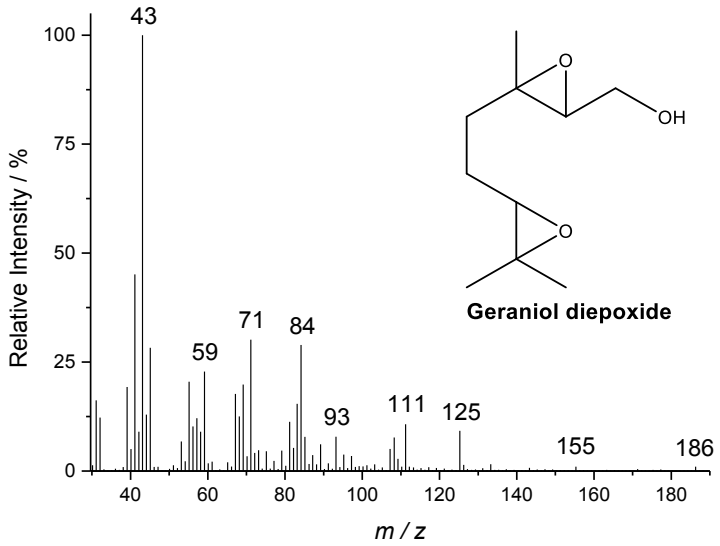


**Fig. SM7** Mass spectrum of geraniol diepoxide[1]

**Geraniol epoxide**

EIMS 70 eV, *m/z* (rel. int. %): 152 $[M-H_2O]^+$ (0.7), 137 (1), 109 (57), 97 (5), 85 (7), 81 (24), 71 (18), 67 (65), 59 (11), 57 (6), 55 (40), 43 (90), 41 (100).

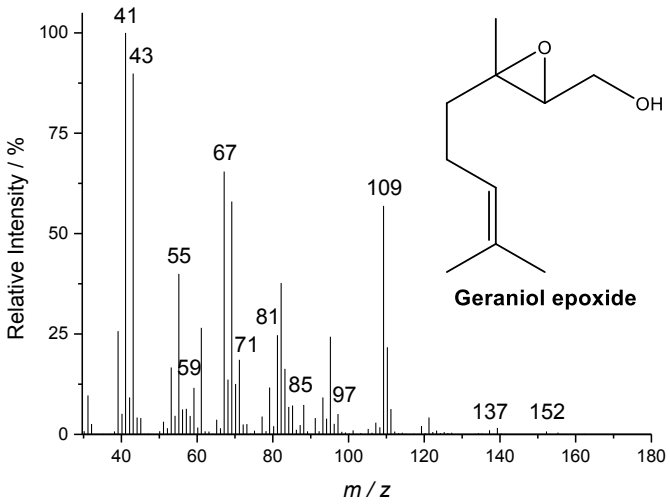


**Fig. SM8** Mass spectrum of geraniol epoxide[1]

**Geranaldehyde**

EIMS 70 eV, *m/z* (rel. int. %): 152 $[M]^+$ (3), 137 (7), 94 (13), 84 (24), 69 (94), 41 (100).

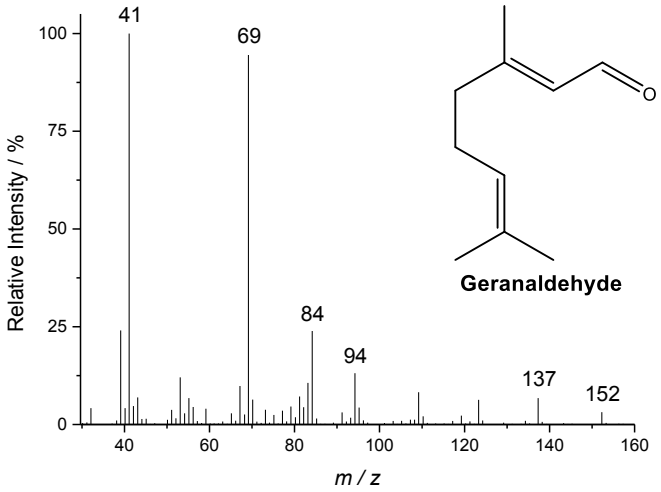


**Fig. SM9** Mass spectrum of geranaldehyde[3]

## α-TERPINEOL PRODUCTS

### p-menthan-2-ol, 1,8-epoxy

EIMS 70 eV, *m/z* (rel. int. %): 170 $[M]^+$ (10), 126 (50), 108 (79), 71 (56), 43 (100), 41 (33).

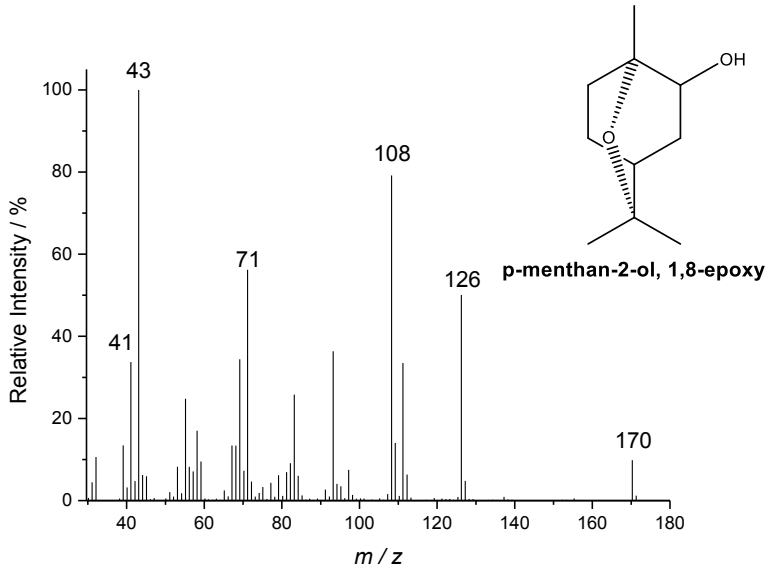


**Fig. SM10** Mass spectrum of p-menthan-2-ol, 1,8-epoxy[5]

### α-Terpineol epoxide

EIMS 70 eV, *m/z* (rel. int. %): 170 $[M]^+$ (0.1), 71 (69), 59 (60), 43 (100), 41 (26).

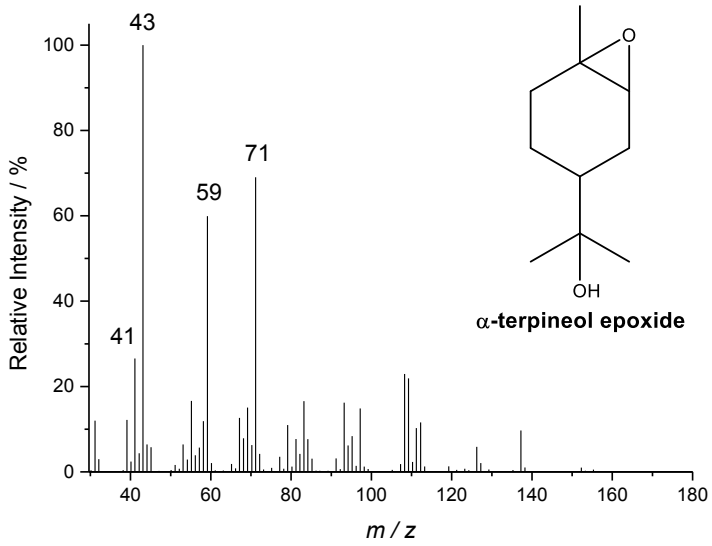


**Fig. SM11** Mass spectrum of α-terpineol epoxide[5]

1 Y. Watanabe, S. Laschat, M. Budde, O. Affolter, Y. Shimada and V. B. Urlacher, *Tetrahedron,* 2007, **63**, 9413-9422.

2 A. Delazar, R. G. Reid, and S. D. Sarker, *Chem. Nat. Compd.*, 2004**, 40,** 24-27

3 D. C. Robacker and L. B. Hendry, *J. Chem. Ecol.*, 1977, **3**, 563-577.

4 P. G. De Pinho, R. F. Gonçalves, P. Valentão, D. M. Pereira, R. M. Seabra, P. B. Andrade, and M. Sottomayor, *J. Pharm. Biomed. Anal.,* 2009, **49**, 674-685.

5 C. W. Wilson III and P. E. Shaw, *Aust. J. Chem.*, 1975, **28**, 2539-2542.

**PAPER 4: Furfural condensation with alkyl alcohols over Niobium catalysts at room temperature**

*Submitted to the Catalysis Letters

Carlos Giovani Oliveira Bruziquesi[a], Daniel Carreira Batalha[b], John Alexander Vergara Torres[b], José Balena G. Filho, Daniele C. Ferreira[c], Márcio José da Silva[b*], Luiz Carlos A. Oliveira[a*]

[a]Chemistry Department, Federal University of Minas Gerais, Belo Horizonte, Minas Gerais, Zip code 31279-201, Brazil
*Corresponding author: Chemistry Department, Federal University of Minas Gerais, e-mail: lcao.ufmg@gmail.com
[b]Chemistry Department, Federal University of Viçosa, Viçosa, Minas Gerais, Zip code 36570-900, Brazil
*Corresponding author: Chemistry Department, Federal University of Viçosa, P.H. Rolfs Avenue, Viçosa, Minas Gerais State, Brazil, Zip code: 36570-900. E-mail: silvamj2003@ufv.br
[c]Department of physics, Federal University of Minas Gerais, Belo Horizonte, Minas Gerais, Zip code 31279-201, Brazil

## Abstract

The production of high value-added chemicals from renewable biomass resources has attracted growing interest due to the environmental and economic reasons. Several platform-molecules like furfural are easily obtained from lignocellulose hydrolysis and has received highlight because can be used as raw material in biorefinery processes to produce biofuels and fine chemicals. In this work, we have developed a process to synthesize furfural acetals at room temperature, using simple commercial Niobium catalysts. The activity of these Niobium catalysts (i.e., pentoxide and phosphate) was evaluated before and after being treated with Hydrogen peroxide, in reactions of furfural condensation with alkyl alcohols to produce acetals at room temperature. All the catalysts commercial and chemically treated were characterized by physical adsorption/ desorption analyses of Nitrogen, infrared, and Raman spectroscopies, scanning electron microscopy, and powder X-ray diffraction analyses. The strength and number of the acidic sites of the catalysts were determined by $NH_3$-Temperature Programmed

Desorption. The effects of main reaction parameters such as temperature, catalyst load, and sort of alcohol were assessed. After being treated with Hydrogen peroxide, phosphate and Niobium pentoxide become less active. Niobium phosphates were the most efficient catalysts, converting almost all the furfural to acetals with various alkyl alcohols. The use of an affordable commercially catalyst, efficient, and solid catalyst (Niobium phosphate) are positive aspects of this process.

Keywords: Niobium phosphate, Niobium pentoxide, furfural, acetalization.

**Graphical Abstract**

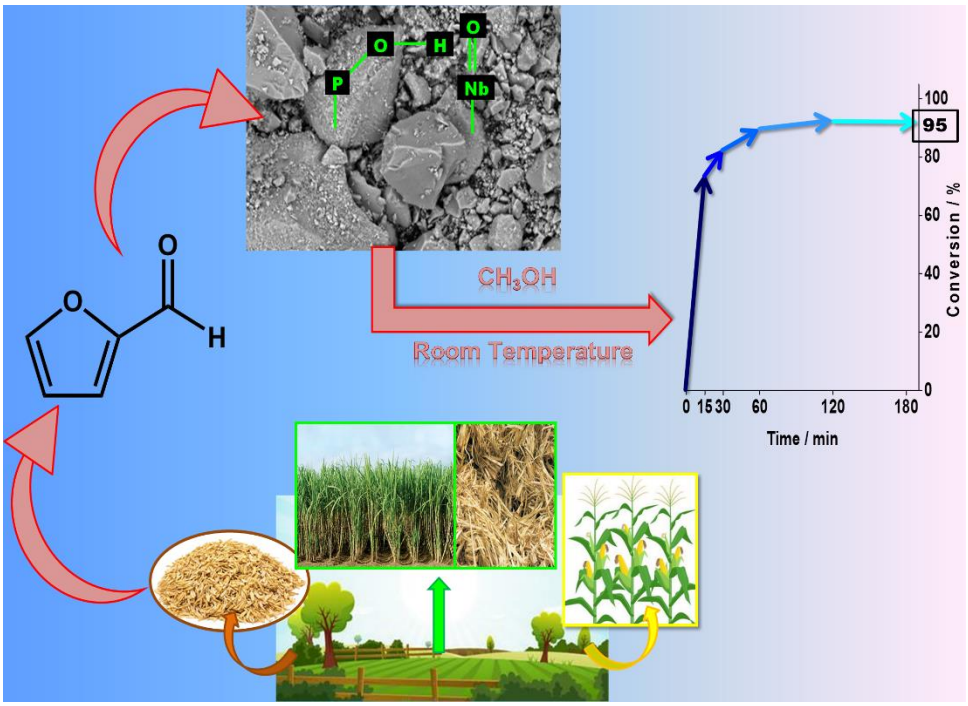


## 1. INTRODUCTION

The conversion of lignocellulosic biomass to chemicals and biofuels may reduce the dependence on fossil fuels, offer a less pollutant renewable energy source and contribute to minimize global warming [1]. Furfural is a versatile platform-molecule obtained from dehydration of xylan present in the lignocellulose residues and can be upgraded to a plethora of chemicals or biofuel compounds [2,3]. Among the several chemical transformations that can valorize the furfural, the acetalization deserves highlight as an attractive synthetic route to obtain valuable furfural derivatives [4]. Acetalization is an efficient approach to yield commercially cost-effective useful fuel additives which have a clean-burning quality with high lubricity, lower sulfur content, enhanced viscosity index, and flashpoint stability [5,6].

Moreover, furfural derivatives are used as ingredients of perfumes, medicines, flavorings, and polymers [7].

The typical routs of furfural acetalization are Brønsted acid-catalyzed reactions, which are carried out in liquid phase in the presence of homogenous catalysts [8]. However, these homogeneous catalytic processes are generally unfriendly to the environment because they have serious drawbacks, such as a large generation of effluents and residues in the steps of neutralization and products, the high corrosiveness of acidic catalysts besides the impossibility to recovery and reuse the catalyst [9].

Alternatively, several acidic solid catalysts have been used in furfural acetalization, due to process more advantageous because there is the possibility of their easier recovery, which is more suitable for industrial processes. Metal salts [10,11], polymers [12], zeolites [13,14], solid supported catalysts [15], and Cesium heteropoly salts are just a few examples [16].

Acetalization of furfural is a promoted reaction by both Lewis or Brønsted acidic sites, which should polarize and protonate the carbonyl group of the furfural, favoring its nucleophilic attack by hydroxyl group of alcohol, leading to a hemi-acetal and further an acetal, after water releasing step. In this regard, Niobium-containing compounds are potential candidate to catalysts, because they have marked acid characteristics, such as the presence of Lewis and Brønsted acid sites [17]. Moreover, they are materials easily obtained with good textural properties, through various processes such as sol-gel, grafting, hydrothermal, coprecipitation, or polymeric precursor methods [18–20], which make them attractive for use as pure, mixed, and supported oxide catalysts [21,22].

Niobium oxide ($Nb_2O_5$) and Niobium phosphate (NbP) are solids that can be considered as bifunctional catalysts due to the presence of Lewis and Brønsted acid sites. However, due to greater thermal stability at high temperatures, Niobium phosphate may be more advantageous than $Nb_2O_5$. The Brønsted acidic sites of the NbP may be better located on the catalyst surface represented by the phosphate groups, while the Lewis acid sites are represented by the unoccupied orbitals of the Niobium atoms [23–25].

The use of metal solid compounds such as Niobium phosphate or oxide excluded the possibility of leaching, avoiding the contamination of products and preserving the catalytic activity [26]. Due to these advantages, Niobium catalysts have been used in various reactions, redox or acid-catalyzed, in the form of nanoparticles, oxides or solid-supported [22,27–30].

In this work, we described the use of Niobium-containing commercial compounds (oxides and phosphates) as catalysts in furfural acetalization reactions with alkyl alcohols. The solid catalysts were characterized by FT-IR and Raman spectroscopy analyses, physical

adsorption/ desorption of Nitrogen, thermogravimetry, powder XRD analyses and electron scanning microscopy. Acidity properties were determined by $NH_3$-Temperature Programed Desorption and Pyridine infrared spectroscopy. The impacts of the Hydrogen peroxide treatment on the physical and structural properties of Niobium catalysts were assessed. The textural and acidic properties of the catalysts were evaluated by different techniques to understand the importance of the different intrinsic characteristics of these materials in the formation of acetals. Different parameters were evaluated, such as nature and mass of the catalyst, temperature, and sort of alcohol used in the reaction. The NbP catalyst showed better performance among all the tested materials, in methyl alcohol, reaching high values of furfural conversion to acetal, with few minutes of reaction in room temperature. The reaction scope was successfully extended to the different alcohols.

## 2. EXPERIMENTAL

### *2.1. Synthesis*

Niobia and Niobium phosphate (respectively named as NA and NbP) were initially treated with Hydrogen peroxide to generate more active surface sites already previously reported [31], leading to the materials T-NA and T-NbP corresponding to their respective Hydrogen peroxide-treated samples. To the treatment with 5 g of the material, 100 mL of deionized water, and 8 mL of $H_2O_2$ (50 % wt) under stirring for 10 min. Past 12 h, the material was centrifuged, washed with distilled water e dried at 80 °C in an oven overnight. The treated niobia and Niobium phosphate were named as T-NA and T-NbP, while for the raw niobia and Niobium phosphate were NA and NbP, respectively.

### *2.2. Characterization*

Powder X-ray data for the catalysts were collected using a SHIMADZU XRD-7000 diffractometer with $CuK_\alpha$ ($\lambda$=1.5418 Å) as radiation source from $2\theta$ = 10-80°, at a 1.0 s step and the generator setting is 30 kV and 30 mA. The textural properties of the samples such as specific surface area, average pore diameter and pore volume were obtained by $N_2$ physical adsorption-desorption assays at 77 K using Quantachrome Autosorb IQ2. Previously, the materials were preheated at 120 °C under the vacuum of $2.0x10^{-9}$ atm.

The acid sites strength was measured by the $NH_3$-temperature programmed desorption technique ($NH_3$-TPD). Initially, 0.2 g of each sample was placed in a U-shaped quartz tube and exposed to the flow of He (40 mL.min$^{-1}$) at 120 °C for 1 hour. This procedure is ordinarily adopted to remove any quantity of water eventually physisorbed. Then, the flux of ammonia (40 mL.min$^{-1}$) occurs for 10 min, thus causing chemisorption through the acid-base reaction. Once again, a flow of He is passed through the sample to remove any amount of physically adsorbed ammonia. CHEMBET-3000 TPR/TPD detector Chemisorption analyzer (Quantachrome instrument) coupled with the TCD detector under heating 200-900 °C (10° C/min) recorded the amount of chemosorbed $NH_3$.

Pyridine chemisorbed FT-IR spectroscopy was used to identify the nature of the acid sites. First, the catalyst surface was cleaned at 200 °C/ 3 h, to eliminating chemi-or physisorbed molecules water. Later, dry pyridine was spread into the samples to the chemisorption. Physisorbed pyridine was driven off by heating the sample at 120 °C for 2 h. Pyr-FTIR spectra of the catalysts were recorded at room temperature using a Spectrum PerkinElmer FT-IR RXI equipment in the range of 1700-1400 cm$^{-1}$. Tablets containing 10 mg of the sample and 80 mg of KBr were pressing under vacuum for 3 minutes.

FT-Raman spectra of the catalysts were recorded on a Witec Alpha 300 equipped with an EMCCD detector. The FT-Raman were excited at 532 nm operated at 150 mW. The morphology of the materials was investigated by scanning electron microscopy (SEM) Hitachi TM 400 Plus.

*2.3. Catalytic tests*

The catalytic tests were conducted in a liquid phase in a glass reactor coupled to a reflux condenser. Typically, furfural (2.5 mmol) was solved in alkyl alcohol (9.4 mL) under magnetic stir, being heated at reaction temperature under room pressure. The addition of solid catalyst (15 mg) started the reaction. Toluene (0.1 mL) was internal standard. All reactions were performed in 180 minutes, being monitored by GC analyses of aliquots collected at regular time intervals to be analyzed in a Shimadzu GC-2010 Plus equipped with an AOC-20i auto-injector and flame ionization detector (FID). Furthermore, reaction aliquots were analyzed by mass spectrometry performed in Shimadzu GCMS-QP2010 Ultra equipment. The correspondent acetal is the unique generated product.

## 3. RESULTS AND DISCUSSION

### *3.1. Characterization of the catalysts*

The diffractograms for all catalysts revealing an amorphous nature for all. It means that the treatment with $H_2O_2$ does not alter the structural nature of the materials. The textural properties of the catalysts from corresponding $N_2$ adsorption-desorption isotherm at 77 K are showed in Figure 1. The amorphous Niobium oxide (NA) sample presents a mesoporous profile characteristic of IV-type (c) isotherms, according to the IUPAC classification. The material also presents a hysteresis profile H2-type, considered as bottle-type pores [32].

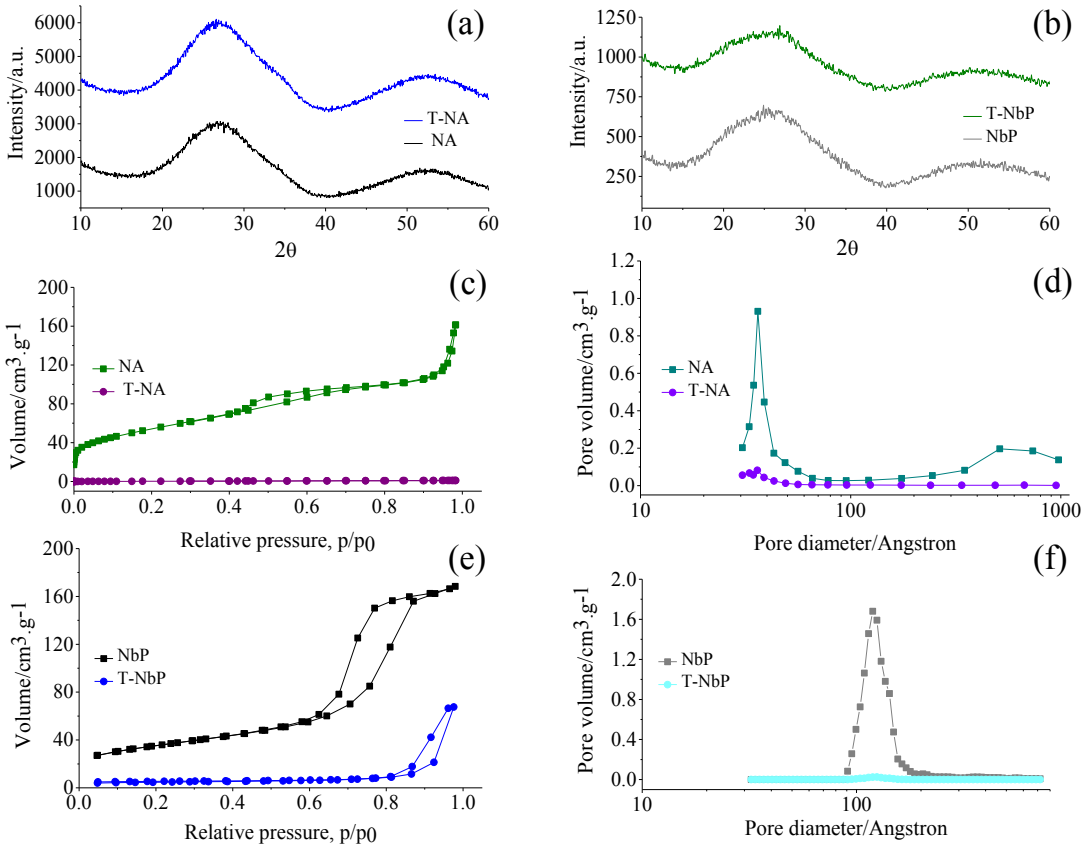


**Figure 1.** X-ray diffraction patterns of the samples (a) and (b), $N_2$ adsorption-desorption curves for the NA, T-NA, NbP and T-NbP (c) and (e), and pore volume distribution of the materials (d) and (f)

The disappearance of its hysteresis (T-NA) may be attributed to the reduction of the mesoporous diameter size. Its specific area value is reduced from 195 $m^2.g^{-1}$ to 83 $m^2.g^{-1}$ after the treatment with Hydrogen peroxide.

In the same way, Nitrogen adsorption/ desorption isotherms and pore size distribution for the materials NbP and T-NbP, obtained by the Functional Density Theory (DFT) (d) and

(f), are shown in Figure 1. NbP isotherm can be classified as type IV (e), which, like the NA material, present mesopores. In addition, the T-NbP isotherm can be classified as type II, a common profile in non-porous or macroporous materials [33]. Here, another method for determining the pore size distribution was adopted, since the conventional BJH method did not allow for a well-defined distribution. The pore size distribution for NbP according to the DFT method showed a broader peak, suggesting a non-homogeneous mesoporosity profile. The treatment with Hydrogen peroxide did not provide the obtaining of uniformly sized pores, as can be seen in Figure 1.

Average pore diameters are centered of 36.16 and 62.24 Å, respectively (see Table 1). Besides, a drastic reduction in the BET surface areas were observed for samples T-NA and T-NbP, which can be attributed to the agglomeration caused by the previous treatment with Hydrogen peroxide [34]. Thus, in face to results, the specific area, pore-volume, and average pore diameter decreased for the T-NA and T-NbP catalysts, which it agrees with XRD diffractograms showing an increase of FWHM (Full width at half maximum) values for the samples [35]. The Table 1 summarizes the area specific, pore size distribution for the catalysts and average pore diameter.

**Table 1.** Textural properties of the Niobium catalysts

| Catalyst | Specific Area ($m^2.g^{-1}$) | Pore Volume ($cm^3.g^{-1}$) | Average Pore Diameter (Å) |
|---|---|---|---|
| **NA** | 195 | 0.20 | 36.16 |
| **T-NA** | 83 | 0.01 | 35.99 |
| **NbP** | 121 | 0.25 | 62.24 |
| **T-NbP** | 16 | 0.09 | 61.13 |

Raman scattering spectroscopy is a technique more sensitive for identification of eventual structural changes, in which case it may relate to the disorder of the bands of the Niobium phosphate catalysts and with the increase in the band intensity, attributed to the distorted $NbO_6$ octahedral [36]. It is due to the spectral change in the symmetrical structure of the $NbO_6$ octahedron or even the Nb-O bond.

For the pure and treated niobic acid, NA and T-NA, Fig. 2a shows bands that exhibit signals between 640-650 $cm^{-1}$, attributed to the vibrational modes of symmetrical stretching of the slightly distorted octahedron $NbO_6$ typically present in the amorphous oxide $Nb_2O_5.nH_2O$ [37-39]. At 200-300 $cm^{-1}$ region is due to the vibrational mode Nb-O-Nb. Band region at 221 $cm^{-1}$ is caused by the octahedron distortion, commonly encountered in hydrated species of

niobates [39]. The asymmetric stretching of the octahedral Nb-O-Nb allows the vibrations at wavenumbers 221 and 651 $cm^{-1}$. The peroxo group formation may be observed through a new signal above 800 $cm^{-1}$ for the T-NA, which suggests the presence of peroxo groups (O-O) on its surface [39].

For the NbP and T-NbP samples, comparing their Raman spectra, there is an increase in band intensity of 590 $cm^{-1}$ compared to 798 $cm^{-1}$. This is attributed to an increase in the degree of lamella disorder caused by the change in the Niobium coordination environment when previously treated with Hydrogen peroxide [40]. Another band, close to 227 $cm^{-1}$, is aligned to the angular deformation mode of Nb-O-Nb. In addition, for this specific region, after treatment with Hydrogen peroxide, there was an increase in the area of the band close to 225 $cm^{-1}$, suggesting an increase in the number of Nb-O-Nb distortions. Thus, the observed spectral change reflects the degree of disorder between the lamellae caused by the change in the Niobium coordination environment when treated with Hydrogen peroxide. At 1014 $cm^{-1}$ it refers to stretching of the $PO_4$ tetrahedrons [41]. In particular, a slight displacement of this band to smaller values is intrinsically linked to the interaction of water molecules with $PO_4$ groups, located between the lamellae [41].

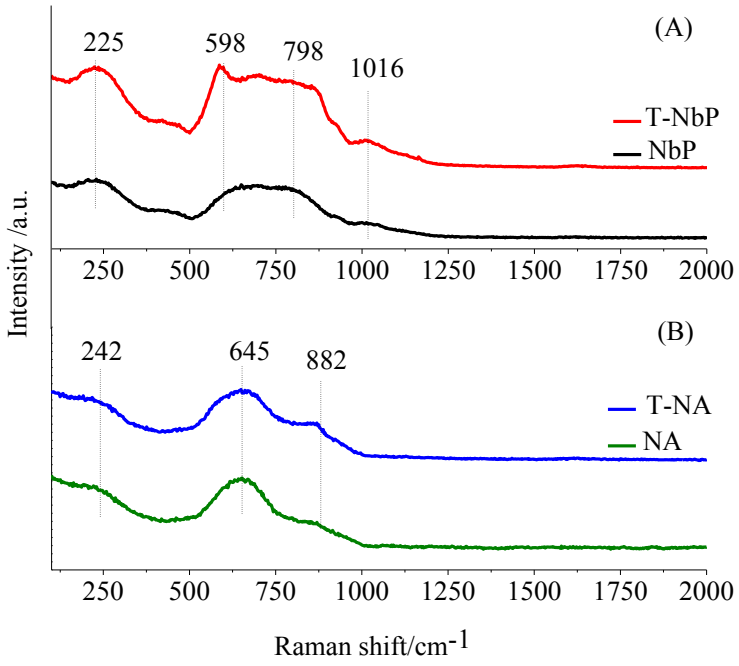


**Figure 2.** Raman profiles of the Niobium catalysts

Pyridine FTIR is commonly used to analyze the Brønsted and Lewis acidic sites over a solid catalyst. The absorption bands at ca.1545 and 1626 $cm^{-1}$ indicate the pyridine adsorption at Brønsted acid sites [42,43]. While the intensity of bands at ca. 1610, 1598, 1578, and 1445

$cm^{-1}$ indicate the effect of coordinatively bonded pyridine sites (Lewis acid sites) [44-47]. In the left of the Fig. 3a it is observed that after the oxidative treatment with Hydrogen peroxide there was no marked change in the profile of acid sites between the samples, NA and T-NA since in all of them there are both Brønsted and Lewis acid sites. An analysis of the B/L ratio intensities of the absorption bands corresponding to the Brønsted and Lewis acidic sites, at the wavenumbers 1634 and 1619 $cm^{-1}$, respectively [46-48], shows a decrease in the B/L ratio, from 0.65 to 0.54. These values suggest the decrease in the Brønsted acid sites after oxidative treatment with $H_2O_2$. On the other hand, in Figure 3b, the infrared absorption profiles of chemisorbed pyridine for NbP and T-NBP samples are shown. A change in acidic sites is observed after $H_2O_2$ treatment. Besides, the band disappears at 1488 $cm^{-1}$, inherent to the Lewis and Brønsted acid sites, simultaneously [44]. Then, the reduction of acidic sites can potentially cause a change, for instance, in the products of the furfural acetalization reaction, since that the acetalization reaction is influenced by acidic properties [49].

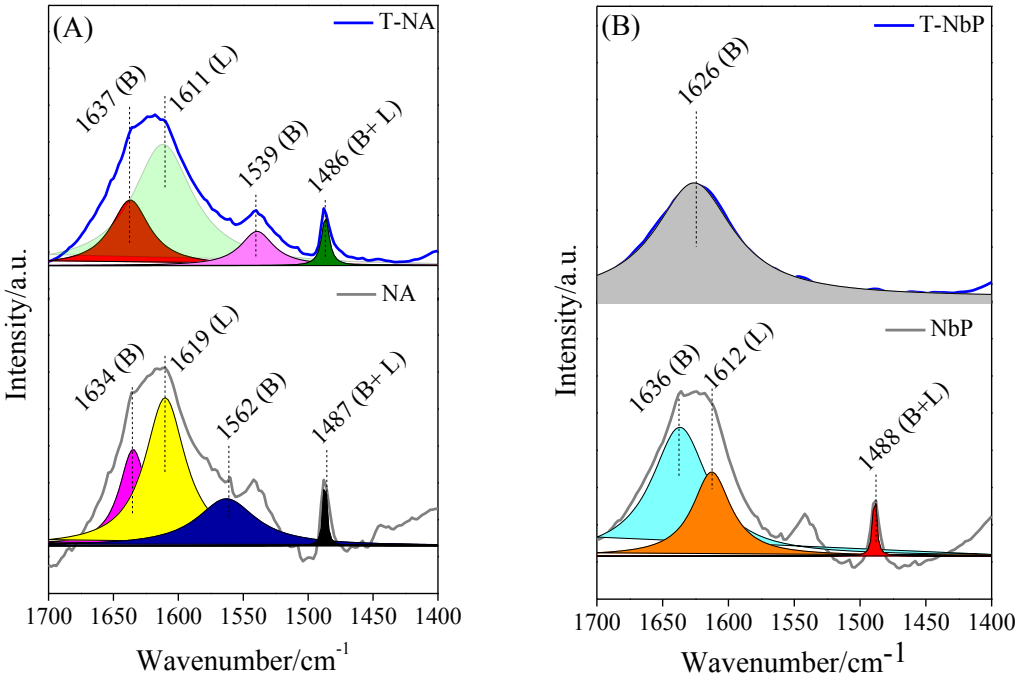


**Figure 3.** Infrared spectra of the Niobium catalysts after pyridine adsorption

The strength of the acidic sites and the total number of these sites, that is, the total acidity, can be determined by the ammonia desorption technique at the programmed temperature. This technique is based on the chemisorption of ammonia in the sample under the constant flow of the gas. In addition, by increasing the temperature at a fixed rate, the ammonia is desorbed from the catalyst and its signal is detected by a TCD detector. As the strength of the acidic sites can be estimated based on the desorption temperature, between 100-200 °C they are

classified as weak; between 200-400 °C as moderate; and above 400 °C as strong [50]. From the profiles shown in Figure 4, it is observed that NbP has substantially greater acidity than NA. In details, NbP has moderate sites between 300 and 400 °C and strong sites from 400 to 900 °C. For NA, there are strong site in the range between 500 and 800 °C.

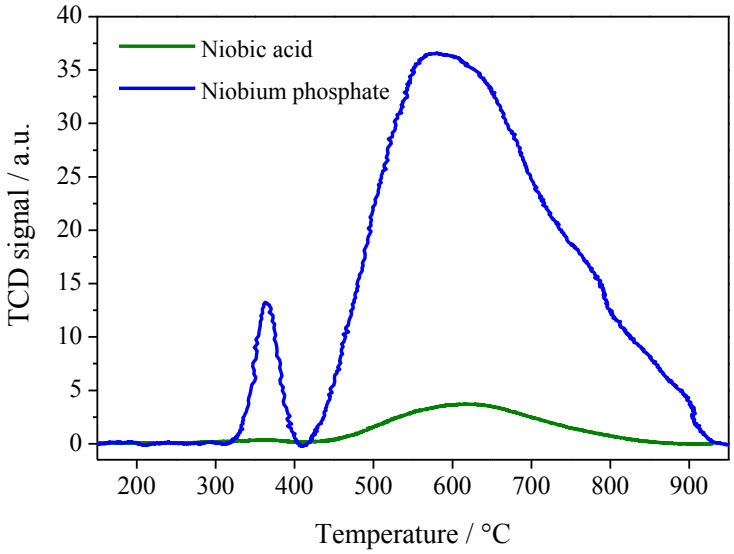


**Figure 4.** TPD-$NH_3$ profiles of the Niobic acid (NA) and Niobium phosphate (NbP) catalysts.

The morphology may be changed with a catalyst that is previously treated with Hydrogen peroxide. Scanning micrographs show changes in their morphologies after oxidative treatment. The images corroborate the information acquired by X-ray diffraction, showing an amorphous character with an irregular surface. In addition, the treatment with $H_2O_2$ suggests an increase in the size of the particles due to a higher incidence of agglomeration. This agglomeration, which results in a rise in the average particle size, also has a strong influence on the specific surface area of the materials, decreasing considerably after agglomeration.

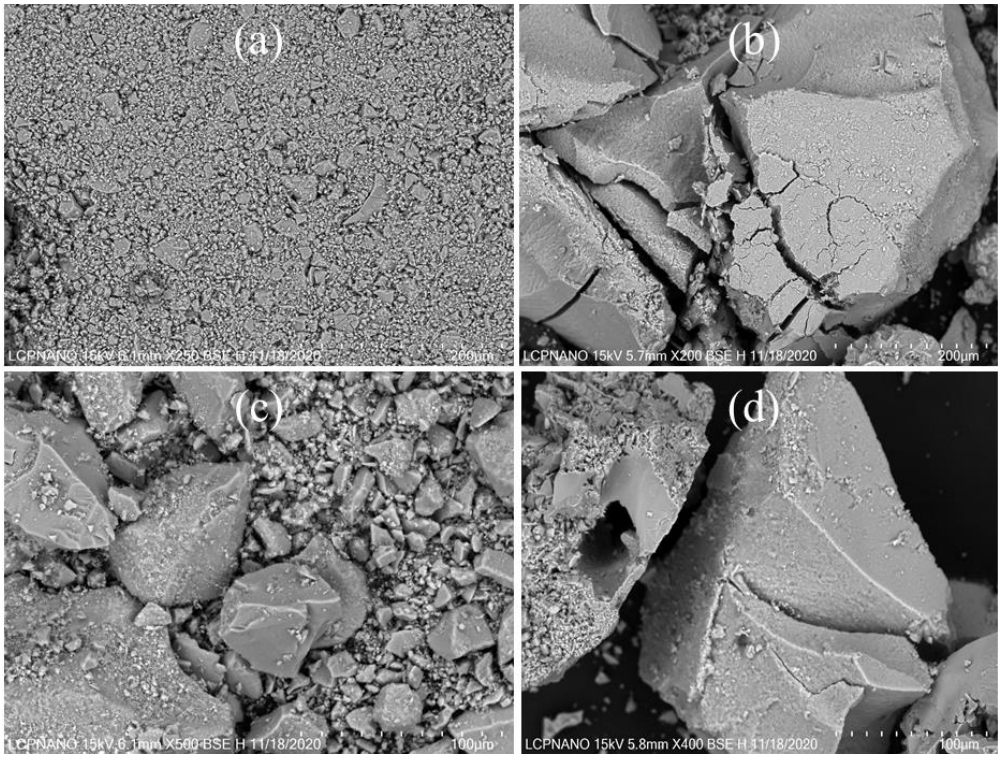


**Figure 5.** Scanning electron micrographs of Niobium phosphates (a) NA (scale of 200 µm); (b) T-NA (scale of 200 µm); (c) NbP (scale of 100 µm); (d) T-NbP (scale of 100µm)

*3.2. Catalytic tests*

The condensation of furfural with alkyl alcohol was performed initially at room temperature (Figure 6). Despite the alcohol excess, in the absence of catalyst no conversion was observed (omitted in Fig. 6).

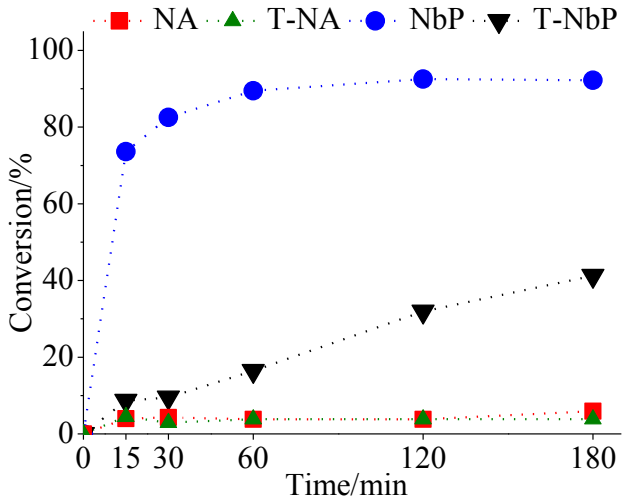


**Figure 6.** Acetalization reaction of furfural in the presence of Niobium catalysts[a]
[a]Reaction conditions: furfural (2.5 mmol), methanol (9.4 mL), catalysts (15 mg), temperature (25 °C), time (180 min), toluene (0.1 mL)

However, when the reaction was carried out in presence of a catalyst, the behavior depended on the type of Niobium compound. Regardless the Hydrogen peroxide treatment, Niobic acid was almost an inactive catalyst (Fig. 6). Conversely, in presence of Niobium phosphate, there was a noticeable increase in the reaction conversion. Remarkably, untreated Niobium phosphate was the most efficient catalyst, reaching 95% of conversion within first hour of reaction. In all these reactions, dimethyl acetal furfural was the only product.

The best performance of Niobium phosphate catalyst can be assigned to its strongest acidity. The total number of acid sites was previously estimated by using $NH_3$-TPD and the results showed that the NbP catalyst presented the highest acidic strength among all catalysts (Figure 3). Undoubtedly, the acidity strength of the catalyst is a key characteristic to its success in acetalization reactions. However, acidity it is not the unique determining factor. When there is a solid catalyzed reaction the size and pore volume can be also playing an essential role on the conversion of substrate. For the NbP and T-NbP catalysts, even drastically decreasing the acidic strength there is a reasonable conversion range for the T-NbP, suggesting that the pore size diameter, with values close to 60 Å, has a beneficial effect on the reaction. In contrast, NA and T-NA present pore diameter size close to 30 Å. Thus, the acidity strength does not seem to be the unique factor for the conversion of furfural. Similar effects have been reported in similar studies [51]. Surprisingly, the surface area has not an essential role in activity of catalysts; even niobic acid presenting the highest surface area, it was almost an ineffective catalyst. It is reinforcing that the strength of acidity and porosity properties are the main aspects herein.

As well as the amount, the nature of acid sites demonstrated also to be important for a good performance of the catalyst. After the Hydrogen peroxide treatment, there was a decrease in the amount of the Brønsted acid sites on Niobium phosphate, consequently, its performance was worse than untreated commercial catalyst.

The role of Brønsted and Lewis acidic sites is to activate the carbonylic Carbon of furfural, favoring its nucleophilic attack by the hydroxyl group of alkyl alcohol. It can occur through the protonation step (Brønsted acidic site) or polarization (Lewis acidic site) of the furfural carbonyl group.

The interaction of empty "*d*" orbitals of the Niobium (HOMO orbitals) with non-ligand electrons of carbonylic Oxygen (LUMO orbitals) remove electronic density from the Carbon, leaving it more susceptible to the attack of the alcohol hydroxyl group. This actuation as a Lewis acid metal catalyst in furfural acetalization was previously described in literature [5,52]. On the other hand, a Lewis acid metal cations such Niobium can also interact with alkyl alcohol releasing $H^+$ ions in alcoholic solutions, which can itself to catalyze the reaction [53,54].

Since the NbP catalyst was the most active it was selected to evaluate the effect of main reaction parameters. In Figures 7a-b are presented the data obtained in reactions where were varied the catalyst load and the reaction temperature, respectively.

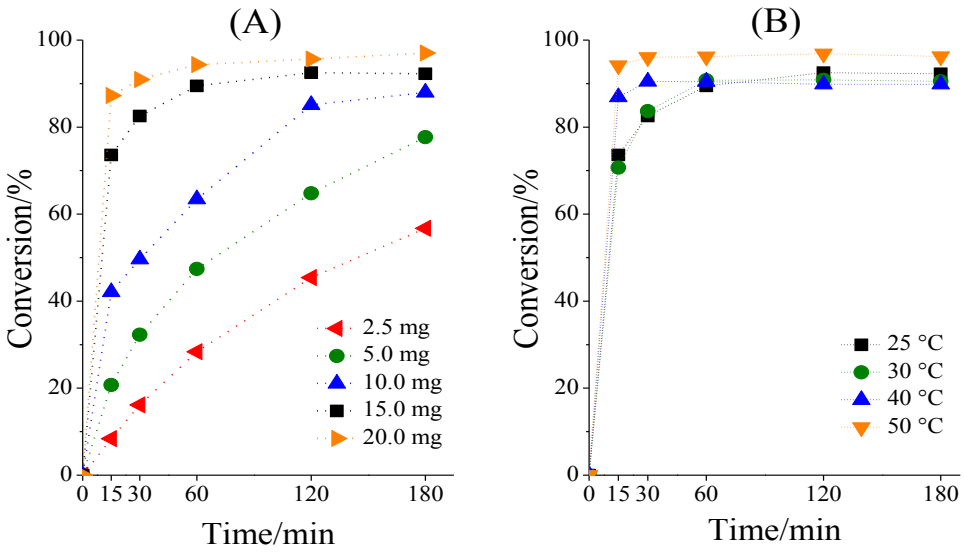


**Figure 7.** Acetalization of furfural with methyl alcohol at different NbP catalyst loadings (A) and reaction temperature (B)[a].
[a]Reaction conditions: furfural (2.5 mmol), methanol (9.4 mL), catalysts (2.5; 5.0; 10.0; 15.0; 20.0 mg), temperature (25 °C), toluene (0.1 mL); In (B) the catalyst load was 15.0 mg and temperatures (25; 30; 40; 50 °C)

An increase in catalyst load enhanced the rate reaction as well as the final conversion (Fig. 7a). This effect can be attributed to the higher number of acidic sites present in the reaction medium when the catalyst load was increased. The reactions carried with the higher loads of catalyst (ca. 15 and 20 mg) achieved the maximum conversion within the first hour of reaction. In all the reactions dimethyl acetal furfural was the only product formed.

Evaluating the effect of the temperature it was possible to conclude the furfural condensation reaction has an endothermic character; an increase in temperature accelerated the reaction; after 30 min of reaction at 50 °C the maximum conversion was reached (Fig.7b). In addition to increase the number of effective collisions between reactants, a higher temperature can be contributing to a better diffusion of reactants into the catalyst pores [52].

The activity of NbP catalyst was also investigated in furfural condensation with different alkyl alcohols (Figure 8). In general, when the size of the alcohols Carbon chain is increased its reactivity in furfural acetalization is reduced [16,52]. This effect was also observed herein, and the reactivity of alcohols obeyed the following trends: methanol > ethanol > propan-1-ol > butan-1-ol (Figure 8).

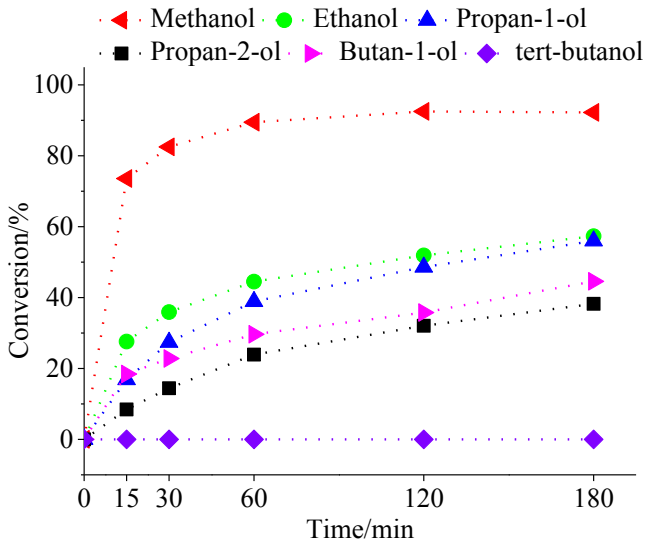


**Figure 8.** Acetalization reaction of furfural with different alkyl alcohols over the NbP catalyst[a]
[a]Reaction conditions: furfural (2.5 mmol), alkyl alcohol (9.4 mL), NbP catalyst (15 mg), temperature (25 °C), time (180 min), toluene (0.1 mL)

On the other hand, it is expected that a higher steric hindrance on hydroxyl group of alcohol compromise its efficiency in the nucleophilic attack of furfural carbonylic Carbon. Indeed, secondary, and tertiary alcohols (i.e., propan-2-ol, *tert*-butanol) were the less reactive alcohols.

## 4. CONCLUSION

Commercial Niobium compounds were evaluated as catalysts on the furfural acetalization reaction with alkyl alcohols at room temperature. The effect of treatment of Niobium catalysts with Hydrogen peroxide was evaluated. Among the catalysts assessed, Niobium phosphate (NbP) was the most active toward the formation of alkyl furfural acetal. The best catalytic performance of NbP catalyst was assigned to its highest Brønsted acidity strength, to greater number of acidic sites as well as the highest volume and pore diameters. The reactivity of other alkyl alcohols was also studied, and we have found that the steric hindrance on the hydroxyl group as well as an increase in size of Carbon chain reduce the alcohol reactivity. In all the reactions, alky furfural acetal was selectively formed. The use of a solid and commercially affordable catalyst, besides the mild reactions are positive aspects of this protocol.

## Conflicts of interest

There are no conflicts to declare.

**Acknowledgements**

The authors are grateful for the financial support from CNPq and FAPEMIG (Brazil). This work was partially financed by the Coordenação de Aperfeiçoamento de Pessoal de Nível Superior - Brasil (CAPES) - Finance Code 001, and Nanonib.

**REFERENCES**

[1] M.M. Antunes, R.F. Mendes, F.A. Almeida Paz, A.A. Valente, R.F.; Paz, F.A.A.; Valente, Versatile Coordination Polymer Catalyst for Acid Reactions Involving Biobased Heterocyclic Chemicals, (2021). doi:10.3390/catal11020190.

[2] J.-P. Lange, E. Van Der Heide, J. Van Buijtenen, R. Price, Furfural-A Promising Platform for Lignocellulosic Biofuels, (n.d.). doi:10.1002/cssc.201100648.

[3] J.J. Bozell, G.R. Petersen, Technology development for the production of biobased products from biorefinery carbohydrates-the US Department of Energy's "Top 10" revisited, (2010). doi:10.1039/b922014c.

[4] L. Filiciotto, A.M. Balu, J.C. Van der Waal, R. Luque, Catalytic insights into the production of biomass-derived side products methyl levulinate, furfural and humins, Catalysis Today. 302 (2018) 2–15. doi:10.1016/J.CATTOD.2017.03.008.

[5] M.J. da Silva, M.G. Teixeira, Assessment on the double role of the transition metal salts on the acetalization of furfural: Lewis and BrØnsted acid catalysts, Molecular Catalysis. 461 (2018) 40–47. doi:10.1016/j.mcat.2018.10.002.

[6] M. Nahavandi, T. Kasanneni, Z.S. Yuan, C.C. Xu, S. Rohani, Efficient Conversion of Glucose into 5-Hydroxymethylfurfural Using a Sulfonated Carbon-Based Solid Acid Catalyst: An Experimental and Numerical Study, ACS Sustainable Chemistry and Engineering. 7 (2019) 11970–11984. doi:10.1021/acssuschemeng.9b00250.

[7] A. Maria, R. Galletti, C. Antonetti, S. Fulignati, D. Licursi, catalysts Direct Alcoholysis of Carbohydrate Precursors and Real Cellulosic Biomasses to Alkyl Levulinates: A Critical Review, (n.d.). doi:10.3390/catal10101221.

[8] M.G. Teixeira, R. Natalino, M.J. da Silva, A kinetic study of heteropolyacid-catalyzed furfural acetalization with methanol at room temperature via ultraviolet spectroscopy, Catalysis Today. 344 (2020) 143–149. doi:10.1016/j.cattod.2018.11.071.

[9] A. Corma, H. García, Lewis acids: From conventional homogeneous to green homogeneous and heterogeneous catalysis, Chemical Reviews. 103 (2003) 4307–4365. doi:10.1021/cr030680z.

[10] C.C. Silveira, S.R. Mendes, F.I. Ziembowicz, E.J. Lenardão, G. Perin, The use of anhydrous CeCl3 as a recyclable and selective catalyst for the acetalization of aldehydes and ketones, Journal of the Brazilian Chemical Society. 21 (2010) 371–374.

doi:10.1590/S0103-50532010000200026.

[11] S. Kanai, I. Nagahara, Y. Kita, K. Kamata, M. Hara, A bifunctional cerium phosphate catalyst for chemoselective acetalization, Chemical Science. 8 (2017) 3146–3153. doi:10.1039/C6SC05642C.

[12] M.X. Tan, L. Gu, N. Li, J.Y. Ying, Y. Zhang, Mesoporous poly-melamine-formaldehyde (mPMF) – a highly efficient catalyst for chemoselective acetalization of aldehydes, Green Chemistry. 15 (2013) 1127–1132. doi:10.1039/C3GC40297E.

[13] H. Li, T. Yang, ] Andersr, S. Saravanamurugan, S. Yang, Chemoselective Synthesis of Dithioacetals from Bio-aldehydes with Zeolites under Ambient and Solvent-free Conditions, (n.d.). doi:10.1002/cctc.201601687.

[14] J.M. Rubio-Caballero, S. Saravanamurugan, P. Maireles-Torres, A. Riisager, Acetalization of furfural with zeolites under benign reaction conditions, Catalysis Today. (2014). doi:10.1016/j.cattod.2014.03.004.

[15] N. Castellanos-Blanco, G. Taborda, M. Cobo, An Efficient Acetalization Method for Biomass-Derived Furfural with Ethanol Using γ-Al 2 O 3-Supported Catalysts, (2020). doi:10.1002/slct.202000410.

[16] M. José Da Silva, · Neide, P.G. Lopes, · Carlos, G. Oliveira Bruziquesi, * Márcio, J. Da Silva, Furfural acetalization over Keggin heteropolyacid salts at room temperature: effect of cesium doping, Reaction Kinetics, Mechanisms and Catalysis. 133 (2021) 913–931. doi:10.1007/s11144-021-02025-5.

[17] P. Carniti, A. Gervasini, F. Bossola, V. Dal Santo, Cooperative action of Brønsted and Lewis acid sites of niobium phosphate catalysts for cellobiose conversion in water, Applied Catalysis B: Environmental. 193 (2016) 93–102. doi:10.1016/J.APCATB.2016.04.012.

[18] A. Esteves, L.C.A. Oliveira, T.C. Ramalho, M. Goncalves, A.S. Anastacio, H.W.P. Carvalho, New materials based on modified synthetic Nb2O5 as photocatalyst for oxidation of organic contaminants, Catalysis Communications. 10 (2008) 330–332. doi:10.1016/J.CATCOM.2008.09.012.

[19] C. Tiozzo, C. Bisio, F. Carniato, M. Guidotti, Grafted non-ordered niobium-silica materials: Versatile catalysts for the selective epoxidation of various unsaturated fine chemicals, Catalysis Today. 235 (2014) 49–57. doi:10.1016/J.CATTOD.2014.02.027.

[20] C. Tiozzo, C. Palumbo, R. Psaro, C. Bisio, F. Carniato, A. Gervasini, P. Carniti, M. Guidotti, The stability of niobium-silica catalysts in repeated liquid-phase epoxidation tests: A comparative evaluation of in-framework and grafted mixed oxides, Inorganica Chimica Acta. 431 (2015) 190–196. doi:10.1016/J.ICA.2015.01.048.

[21] D. Carreira Batalha, N. Hadler Marins, R. Marques e Silva, N. Lenin Villarreal Carreño, H. Vieira Fajardo, M.J. da Silva, Oxidation of terpenic alcohols with hydrogen peroxide promoted by Nb2O5 obtained by microwave-assisted hydrothermal method, Molecular Catalysis. 489 (2020) 110941. doi:10.1016/j.mcat.2020.110941.

[22] J. Wan, P. Yang, X. Guo, R. Zhou, Investigation on the structure-activity relationship of

Nb2O5 promoting CeO2-CrOx-Nb2O5 catalysts for 1,2-dichloroethane elimination, Molecular Catalysis. 470 (2019) 75–81. doi:10.1016/j.mcat.2019.03.010.

[23] J.L. Vieira, M. Almeida-Trapp, A. Mithöfer, W. Plass, J.M.R. Gallo, Rationalizing the conversion of glucose and xylose catalyzed by a combination of Lewis and Brønsted acids, Catalysis Today. 344 (2020) 92–101. doi:10.1016/j.cattod.2018.10.032.

[24] P. Carniti, A. Gervasini, F. Bossola, V. Dal Santo, Cooperative action of Brønsted and Lewis acid sites of niobium phosphate catalysts for cellobiose conversion in water, Applied Catalysis B: Environmental. 193 (2016) 93–102. doi:10.1016/j.apcatb.2016.04.012.

[25] H.G. Bernal, A.M.R. Galletti, G. Garbarino, G. Busca, E. Finocchio, NbP catalyst for furfural production: FT IR studies of surface properties, Applied Catalysis A: General. 502 (2015) 388–398. doi:10.1016/j.apcata.2015.06.031.

[26] E.L. Moreno, K. Rajagopal, Challenges of catalysis acidity in solids, Quimica Nova. 32 (2009) 538–542. doi:10.1590/s0100-40422009000200044.

[27] J. V. Coelho, L.C.A. Oliveira, F.C.C. Moura, P.P. De Souza, C.A. Silva, K.B. Batista, M.J. Da Silva, β-pinene oxidation by hydrogen peroxide catalyzed by modified niobium-MCM, Applied Catalysis A: General. 419–420 (2012) 215–220. doi:10.1016/J.APCATA.2012.01.032.

[28] W.M. Ventura, D.C. Batalha, H. V. Fajardo, J.G. Taylor, N.H. Marins, B.S. Noremberg, T. Tański, N.L.V. Carreño, Low temperature liquid phase catalytic oxidation of aniline promoted by niobium pentoxide micro and nanoparticles, Catalysis Communications. 99 (2017) 135–140. doi:10.1016/J.CATCOM.2017.06.004.

[29] D.C. Batalha, · Sulusmon, C. Luz, J.G. Taylor, H. V Fajardo, B.S. Noremberg, I.J.S. Cherubin, R.M. Silva, M.R.F. Gonçalves, · Carlos, P. Bergmann, A. Valentini, · Neftalí, L. V Carreño, Application of Al 2 O 3 /AlNbO 4 in the oxidation of aniline to azoxybenzene, 74 (2020) 543–553. doi:10.1007/s11696-019-00897-5.

[30] N.K. Gupta, A. Fukuoka, K. Nakajima, Amorphous Nb2O5 as a Selective and Reusable Catalyst for Furfural Production from Xylose in Biphasic Water and Toluene, ACS Catalysis. 7 (2017) 2430–2436. doi:10.1021/acscatal.6b03682.

[31] M. Ziolek, I. Sobczak, P. Decyk, L. Wolski, The ability of Nb2O5 and Ta2O5 to generate active oxygen in contact with hydrogen peroxide, Catalysis Communications. 37 (2013) 85–91. doi:10.1016/j.catcom.2013.03.032.

[32] I.D. Padula, P. Chagas, C.G. Furst, L.C.A. Oliveira, Mesoporous niobium oxyhydroxide catalysts for cyclohexene epoxidation reactions, Applied Sciences (Switzerland). (2018). doi:10.3390/app8060881.

[33] F. Rouquerol, J. Rouquerol, K.S.W. Sing, P. Llewellyn, G. Maurin, Adsorption by powders and porous solids, 2014. doi:10.1017/CBO9781107415324.004.

[34] T.E. Souza, M.F. Portilho, P.M.T.G. Souza, P.P. Souza, L.C.A. Oliveira, Modified niobium oxyhydroxide catalyst: An acetalization reaction to produce bio-additives for sustainable use of waste glycerol, ChemCatChem. 6 (2014) 2961–2969.

doi:10.1002/cctc.201402322.

[35] C. García-Sancho, I. Sádaba, R. Moreno-Tost, J. Mérida-Robles, J. Santamaría-González, M. López-Granados, P. Maireles-Torres, Dehydration of xylose to furfural over MCM-41-supported niobium-oxide catalysts, ChemSusChem. (2013). doi:10.1002/cssc.201200881.

[36] J.M. Jehng, I.E. Wachs, The molecular structures and reactivity of supported niobium oxide catalysts, Catalysis Today. 8 (1990) 37–55. doi:10.1016/0920-5861(90)87006-O.

[37] T. Ikeya, M. Senna, Change in the structure of niobium pentoxide due to mechanical and thermal treatments, Journal of Non-Crystalline Solids. (1988). doi:10.1016/0022-3093(88)90313-4.

[38] K. Nakajima, Y. Baba, R. Noma, M. Kitano, J. N. Kondo, S. Hayashi, M. Hara, Nb2O5•nH2O as a heterogeneous catalyst with water-tolerant lewis acid sites, Journal of the American Chemical Society. (2011). doi:10.1021/ja110482r.

[39] I. Nowak, M. Ziolek, Niobium Compounds: Preparation, Characterization, and Application in Heterogeneous Catalysis, Chemical Reviews. (1999). doi:10.1021/cr9800208.

[40] N.T. do Prado, T.E. Souza, A.R.T. Machado, P.P. Souza, R.S. Monteiro, L.C.A. Oliveira, Enhanced catalytic activity for fructose conversion on nanostructured niobium oxide after hydrothermal treatment: Effect of morphology and porous structure, Journal of Molecular Catalysis A: Chemical. 422 (2016) 23–34. doi:10.1016/j.molcata.2016.01.021.

[41] G.T. Stranford, R.A. Condrate, A raman spectral study of hydrated niobium phosphate (NbPO5) phases, Journal of Solid State Chemistry. 76 (1988) 407–411. doi:10.1016/0022-4596(88)90235-6.

[42] M. Tamura, K.I. Shimizu, A. Satsuma, Comprehensive IR study on acid/base properties of metal oxides, Applied Catalysis A: General. (2012). doi:10.1016/j.apcata.2012.05.008.

[43] Y. Yang, D. Zhou, H. Zhang, B. Yin, Q. Liu, X. Lu, S. Yang, Q. Xia, In-situ construction and catalytic property of highly exposed Lewis acidity on hierarchical Zr-zeolite assisted by K+ cation, Microporous and Mesoporous Materials. (2021) 110898. doi:10.1016/j.micromeso.2021.110898.

[44] B.M. Devassy, S.B. Halligudi, Zirconia-supported heteropoly acids: Characterization and catalytic behavior in liquid-phase veratrole benzoylation, Journal of Catalysis. (2005). doi:10.1016/j.jcat.2005.09.016.

[45] D. Padovan, A. Al-Nayili, C. Hammond, Bifunctional Lewis and Brønsted acidic zeolites permit the continuous production of bio-renewable furanic ethers, Green Chemistry. (2017). doi:10.1039/c7gc00160f.

[46] K.M.A. Santos, E.M. Albuquerque, G. Innocenti, L.E.P. Borges, C. Sievers, M.A. Fraga, The Role of Brønsted and Water-Tolerant Lewis Acid Sites in the Cascade Aqueous-Phase Reaction of Triose to Lactic Acid, ChemCatChem. (2019).

doi:10.1002/cctc.201900519.

[47] G.M. Robb, W. Zhang, P.G. Smirniotis, Acidity of dealuminated β-zeolites via coupled NH3-stepwise temperature programmed desorption (STPD) and FT-IR spectroscopy, Microporous and Mesoporous Materials. (1998). doi:10.1016/S1387-1811(97)00026-7.

[48] C. Ramesh Kumar, K.T.V. Rao, P.S. Sai Prasad, N. Lingaiah, Tin exchanged heteropoly tungstate: An efficient catalyst for benzylation of arenes with benzyl alcohol, Journal of Molecular Catalysis A: Chemical. (2011). doi:10.1016/j.molcata.2011.01.008.

[49] I.A.L. Bassan, D.R. Nascimento, R.A.S. San Gil, M.I.P. Da Silva, C.R. Moreira, W.A. Gonzalez, A.C. Faro, T. Onfroy, E.R. Lachter, Esterification of fatty acids with alcohols over niobium phosphate, Fuel Processing Technology. (2013). doi:10.1016/j.fuproc.2012.09.054.

[50] G.D. Yadav, A.D. Murkute, Preparation of the novel mesoporous solid acid catalyst UDCaT-4 via synergism of persulfated alumina and zirconia into hexagonal mesoporous silica for alkylation reactions, Advanced Synthesis and Catalysis. 346 (2004) 389–394. doi:10.1002/adsc.200303212.

[51] M.J. Climent, A. Corma, S. Iborra, M.C. Navarro, J. Primo, Use of mesoporous MCM-41 aluminosilicates as catalysts in the production of fine chemicals: Preparation of dimethylacetals, Journal of Catalysis. 161 (1996) 783–789. doi:10.1006/jcat.1996.0241.

[52] M.J. da Silva, M.G. Teixeira, R. Natalino, Highly selective synthesis under benign reaction conditions of furfural dialkyl acetal using SnCl2 as a recyclable catalyst, New Journal of Chemistry. 43 (2019) 8606–8612. doi:10.1039/C9NJ01284B.

[53] M.J. da Silva, D.M. Carari, A. Manoel da Silva, Fe(iii)-catalyzed α-terpinyl derivatives synthesis from β-pinene via reactions with hydrogen peroxide in alcoholic solutions, RSC Advances. 5 (2015) 10529–10536. doi:10.1039/C4RA13112F.

[54] M.J. da Silva, C.M. de Oliveira, Metal nitrate-catalyzed one-pot oxidative esterification of benzaldehyde with hydrogen peroxide in alcoholic solutions at room temperature, New Journal of Chemistry. 45 (2021) 3683–3691. doi:10.1039/D0NJ05671E.

## 6. GENERAL CONCLUSIONS OF THE THESIS

For the nerol oxidation reactions, three catalysts of different nature were used, Cesium salts, Niobium oxides and Dysprosium-doped Zinc tungstates. The efficiency of these materials was evaluated with Hydrogen peroxide, a cheap and green oxidant. The lacunar $Cs_8SiW_{11}O_{39}$, $Nb_2O_5$ - 2 h and $ZnWO_4$ 2.0 mol% Dy were the most active and selective catalyst compared with all the solids applied in the presented studies.

For the $Cs_8SiW_{11}O_{39}$ catalyst, it was demonstrated that the presence of Silicon in the Keggin anion, as well as the presence of a vacancy in the heteropolyanion were the main aspects of these reactions, since $Cs_4SiW_{12}O_{40}$ was almost inactive. Also, the activity of the catalyst with Silicon-Tungsten lacunar anion was compared in relation to the counterion effect. The lacunar salt $Na_8SiW_{11}O_{39}$, a soluble catalyst, was also highly active. Nevertheless, the lacunar Potassium silicotungstate catalyst ($K_8SiW_{11}O_{39}$ – partially soluble), showed a lower efficiency. This can be attributed to its lower surface area compared to Cesium salt. It was investigated that the best reaction conditions for the $Cs_8SiW_{11}O_{39}$ catalyst was established with the substrate:oxidant molar ratio of 1:4, 4 mol% of the catalyst and 333 K. The reuse of the main salt was another aspect that was successfully investigated highlighting the recover and reuse without loss of activity or selectivity for five reuse cycles.

The synthesis of Niobium oxide catalysts ($Nb_2O_5$ - 2 h; $Nb_2O_5$ - 4 h; $Nb_2O_5$ - 8 h) through microwave-assisted hydrothermal method enabled the achievement of efficient catalysts in the nerol oxidation. Notably, $Nb_2O_5$ synthesized for two hours was the most efficient among the three Nb solids applied. It was found that the surface area was not the parameter to determine the best activity. Furthermore, other structural properties were crucial for a better activity of $Nb_2O_5$ - 2 h, such as lowest crystallinity, verified by XRD analyses, and highest acidity, checked by the IR and potentiometric titration analyses. It was concluded that catalyst concentrations of 4 mol%, substrate:$H_2O_2$ molar ratio of 1:2, temperature of 333 K and reaction of 8 h were the best conditions for greater efficiency and viability in the oxidation reactions. In all reactions, the epoxides of the alcohols were the major products.

The simple coprecipitation followed by microwave-assisted hydrothermal method, efficient Dysprosium-doped tungstates catalysts were synthesized. All the materials generated substantial results of nerol conversions and nerol epoxide selectivity. The solids, with controlled morphological properties and which demonstrated high selectivity for epoxide with hydrogen peroxide, represented four different materials (ca. 0.0; 0.5; 1.0, 2.0 mol% Dy). Among them, the $ZnWO_4$ 2.0 mol% Dy was the most active and selective catalyst, a

consequence of the lowest crystallite size, the highest surface area, pore volume, Dy load, and acidity. Likewise described for previous catalysts, the epoxidation of allylic terpenic alcohols (i.e., nerol and geraniol) with $H_2O_2$ is a hydroxy-assisted reaction. As the important results found for the other terpenic alcohols oxidation, the α-terpineol was epoxidized followed by the formation of a rare product (i.e., *p*-mentan-2-ol, 1,8 epoxide). It was noticed that the best reaction conditions for the nerol oxidation, together with best nerol epoxide selectivity, comprised 1:2 nerol:$H_2O_2$ molar ratio, 15 mg of catalyst and at 333 K.

Interestingly, these three catalysts, above cited, have in common two distinct properties that stood out: lowest crystallinity and highest acidity, between the catalysts of the same nature. This clue reveals that the crystallinity, that influences in the availability of activating groups on the solid surface, and the acidity, can interfere directly in the performance of these materials in the nerol oxidation.

Regarding to the work presenting the results about acetalization of furfural, four catalysts were evaluated, commercial Niobium compounds and their treated ones with Hydrogen peroxide. Among these solids, the commercial Niobium phosphate was the most active. To this activity, four characteristics can be lifted: highest Brønsted acidity strength, greater number of acidic sites, highest volume and pore diameter. Also, it is important to highlight that the Niobium phosphate was efficient in this reaction in mild conditions.

## 7. OTHER MATERIALS

Besides the prior presented articles, as the results of the work developed in this PhD, two review articles were developed. One of them was recently published in the Energies (Impact Factor 3.004), entitled “Biodiesel Production over Niobium-containing catalysts: A Review”, and other review article is in preparation for quick submission in international scientific journal of high relevance in the academic community.

energies

MDPI

Open Access Review

## Biodiesel Production over Niobium-Containing Catalysts: A Review

by Daniel Carreira Batalha and Márcio José da Silva *

Chemistry Department, Federal University of Viçosa, Viçosa 36570-900, Brazil

* Author to whom correspondence should be addressed.

Academic Editors: Basu Saha and Attilio Converti

*Energies* **2021**, *14*(17), 5506; **https://doi.org/10.3390/en14175506**

**Received: 26 July 2021 / Revised: 27 August 2021 / Accepted: 30 August 2021 / Published: 3 September 2021**

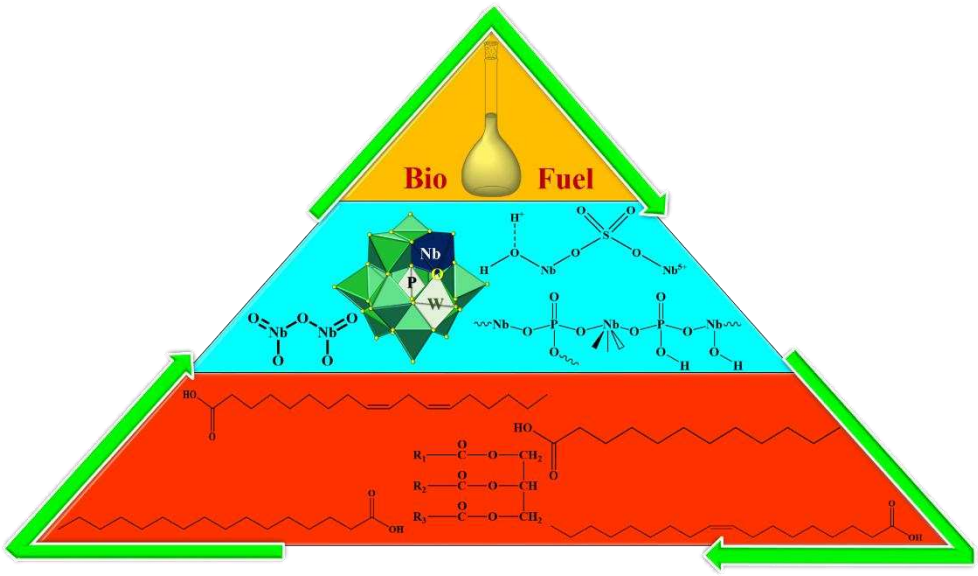


In addition to the aforementioned works, a collaboration article was partially published in the Materials Chemistry and Physics (Impact Factor 4.094), entitled "Influence of $Nb_2O_5$ drown on $SrTiO_3$ nanoseeds in the catalytic oxidation of thioanisole".

Materials Chemistry and Physics

## Influence of Nb2O5 grown on SrTiO3 nanoseeds in the catalytic oxidation of thioanisole

--Manuscript Draft--

Fábio C. Riemke,[a*] Cátia L Ucker,[a] Neftalí L. V. Carreño,[a] Sergio da Silva Cava,[a]

Moisés P. Teixeira,[b] Humberto V. Fajardo,[b] Jason G. Taylor,[b] Márcio J. da Silva,[c]

Daniel C. Batalha,[c] Cristiane W. Raubach[a]

Also, a work was presented in the 20th Brazilian Catalysis Congress, named “Sais heteropoliácidos de Keggin lacunários de Césio: eficientes catalisadores heterogêneos para oxidação do nerol com $H_2O_2$”.